The influence of soil structure on microbial processes in microfluidic models

Arellano, Carlos

2021

The influence of soil structure on microbial processes in microfluidic models

CARLOS ARELLANO CAICEDO
DEPARTMENT OF BIOLOGY | FACULTY OF SCIENCES | LUND UNIVERSITY

The influence of soil structure on microbial processes in microfluidic models

The influence of soil structure on microbial processes in microfluidic models

Carlos Arellano Caicedo

LUND
UNIVERSITY

DOCTORAL DISSERTATION

by due permission of the Faculty of Science, Lund University, Sweden.
To be defended at Blue Hall, Ecology Building, Sölvegatan 37, Lund, Sweden on the 16th of April 2021 at 14.00.

Faculty opponent
Dr. Claire Chenu
AgroParisTech, France

Organization	Document name
LUND UNIVERSITY	Doctoral disertation
Department of Biology	**Date of issue** 2021-04-16
Author(s) Carlos Arellano Caicedo	Sponsoring organization

Title and subtitle
The influence of soil structure on microbial processes in microfluidic models

Abstract

The way microbes behave in nature can vary widely depending on the spatial characteristics of the habitats they are located in. The spatial structure of the microbial environment can determine whether and to which extent processes such as organic matter degradation, and synergistic or antagonistic microbial preocesses occur. Investigating how the different spatial characteristics of microhabitats influence microbes has been challenging due to methodological limitations. In the case of soil sciences, attempts to describe the inner structure of the soil pore space, and to connect it to microbial processes, such as to determine the access of nutrient limited soil microorganisms to soil organic matter pools, has been one of the main goals of the field in the last years. The present work aimed at answering the question of how spatial complexity affects microbial dispersal, growth, and the degradation of a dissolved organic substrate.

Using microfluidic devices, designed to mimic the inner soil pore physical structures, we first followed the dispersal and growth of soil microbes in the devices, using soil inocula or burying the microfluidic devices in the top layer of a soil (**Paper I**). We found that inter-kingdom interactions can play an important role for the dispersal of water-dwelling organisms and that these physically modified their environment. To reveal the effect of the different structures on microbes in more detail we tested the influence of increasing spatial complexity in a porespace on the growth and substrate degradation of bacterial and fungal laboratory strains. The parameters we used to manipulate the pore space's complexity were two: via the turning angle and turning order of pore channels (**Paper II**), and via the fractal order of a pore maze (**Paper III**). When we tested the effect of an increase in turning angle sharpness on microbial growth, we found that as angles became sharper, bacterial and fungal growth decreased, but fungi were more affected than bacteria. We also found that their substrate degradation was only affected when bacteria and fungi grew together, being lower as the angles were sharper. Our next series of experiments, testing the effect of maze fractal complexity, however, showed a different picture. The increase in maze complexity reduced fungal growh, similar to the previous experiments, but increased bacterial growth and substrate consumption, at least until a certain depth into the mazes, contrary to our initial hypothesis. To increase the relevance of our studies, we performed experiments in both microfluidic device designs inoculated with a soil microbial extract and followed the substrate degradation patterns over time (**Paper IV**). We found that as complexity increased, both in terms of angle sharpness and fractal order, substrate consumption also increased. Our results, specially in mazes, might be caused by a reduced competition among bacterial communities and individuals in complex habitats, allowing co-existence of different metabolic strategies and the onset of bacterial biofilm formation leading to a higher degradation efficiency, but further studies are required to confirm this. Our results show that the spatial characteristic of microhabitats is an important factor providing microbes with conditions for a wide variety of ecological interactions that determine their growth and their organic matter turnover.

Key words

Classification system and/or index terms (if any)

Supplementary bibliographical information		**Language** English
ISSN and key title		**ISBN** 978-91-7895-793-4 (print) 978-91-7895-794-1 (pdf)
Recipient's notes	**Number of pages** 63	Price
	Security classification	

Signature 

Date 2021-03-08

The influence of soil structure on microbial processes in microfluidic models

Carlos Arellano Caicedo

LUND
UNIVERSITY

Coverphoto by José Burbano

Faculty of Sciences
Department of Biology

978-91-7895-793-4 (print)
978-91-7895-794-1 (pdf)

Printed in Sweden by Media-Tryck, Lund University
Lund 2021

The Aleph's diameter was probably little more than an inch,
but all space was there, actual and undiminished.

-J.L. Borges, The Aleph

Table of Contents

List of papers

I. Paola Micaela Mafla-Endara, **Carlos Arellano-Caicedo**, Kristin Aleklett, Milda Pucetaite, Pelle Ohlsson, and Edith C. Hammer. Microfluidic chips provide visual access to in situ soil ecology. Submitted.

II. **Carlos Arellano-Caicedo**, Pelle Ohlsson, Martin Bengtsson, Jason P. Beech, Edith C. Hammer. Habitat geometry in artificial microstructure affects bacterial and fungal growth, interactions, and substrate degradation. Submitted.

III. **Carlos Arellano-Caicedo**, Pelle Ohlsson, Martin Bengtsson, Jason P. Beech, Edith C. Hammer. Habitat complexity increases bacterial growth and enzymatic activity while reducing fungal growth in fractal maze model. Manuscript

IV. **Carlos Arellano-Caicedo**, Saleh Moradi, Pelle Ohlsson, Martin Bengtsson, Jason P. Beech, Edith C. Hammer. Microfluidic habitat heterogeneity promotes substrate consumption by soil microbial inoculum. Manuscript.

Author contribution

I. P.M.M. performed the experiments and co-conceived the idea, C.A. did the computer tracking of soil particles, K.A. designed the microfluidic device, M.P. did the spectroscopy analysis of particles inside the microfluidic device, P.O. provided expertise and assistance for the design and fabrication process, and E.H. conceived the idea and contributed to the data analysis. P.M.M. and E.H. wrote the paper with input from all authors.

II. C.A. conceived and performed the experiment and data analysis under the supervision of P.O. and E.H.; M.B. printed the mask used for the experiments. J.B. developed the masters used for the experiments. C.A. wrote the paper with input from all authors.

III. C.A. conceived and performed the experiment and data analysis under the supervision of P.O. and E.H.; M.B. printed the mask used for the experiments. J.B. developed the masters used for the experiments. C.A. wrote the paper with input from all authors.

IV. C.A. conceived the experiment under the supervision of P.O. and E.H. C.A. and S.M. performed the experiment and data analysis; M.B. printed the mask used for the experiments. J.B. developed the masters used for the experiments. C.A. wrote the paper with input from all authors.

Paola Micaela Mafla-Endara - P.M.M.

Carlos Arellano-Caicedo - C.A.

Kristin Aleklett – K.A.

Milda Pucetaite – M.P.

Pelle Ohlsson – P.O.

Edith C. Hammer – E.H.

Martin Bengtsson – M.B.

Jason P. Beech – J.B.

Saleh Moradi – S.M.

Abbreviations and acronyms

SOM	Soil Organic Matter
SOC	Soil Organic Carbon
OM	Organic Matter
PDMS	Polydimethylsiloxane
PP	*Pseudomonas putida*
YMG	Yeast malt glucose medium
CC	*Coprinopsis cinerea*
AMC	Aminopeptidase substrate L-Alanine 7-amido-4-methylcoumarin trifluoroacetate salt
EPS	Extracellular polymeric substances

Popular science summary

We barely stop and think about the life we hold in our hands when we grab a piece of soil. Only one gram of soil can contain more organisms than humans in the entire planet Earth. When we have a closer look, we can find curious facts, such as that the local conditions inside this piece of soil can change drastically over just a few micrometres, that it contains an extraordinarily high diversity of microbes, and that it stores an immense amount of carbon-rich nutrients for those microbes. Microorganisms, such as fungi or bacteria, are found in soils in a state of starvation, which means they are constantly hungry and ready to consume any nutrient that becomes available to them. How is it possible, then, that starving microbes and high amount of nutrients are found simultaneously in soil? What is impeding microbes to access the nutrients? These questions surpass the mere scientific curiosity due to their global relevance. Soils contain the largest reservoir of organic carbon on land on Earth and if, for some reason, anthropological or natural, this carbon becomes available to microbes, large amounts of carbon would be released to the atmosphere, contributing to climate change.

Keeping the carbon buried in soils is therefore crucial if we want to mitigate the effects of climate change. But to do so we need first to understand why and how the carbon is kept in soils, why the starving microbes are not consuming the available nutrients that soil contains. Several theories have been proposed to explain this phenomenon: it has, for instance, traditionally been thought that the nutrients soil contains are composed of too complex, large and amorphous molecules, which surpasses the mechanisms soil microorganisms use for obtaining food. Recent studies, however, show that the majority of nutrients found in soil are small molecules with a high nutritional value for microbes that are consumed immediately when they become available. The idea that microbes and their food are not in reachable contact in the soil, has been brought up in the latest years to explain the accumulation of carbon in soils. The reason why this separation occurs might be the intrinsic nature of soil being a porous system that contains small volumes of countless habitats of different characteristics. Microbes and their food are thus not necessarily located in the same space but separated from one another by a complex labyrinth.

On the other hand, the intrinsic nature of soil, its heterogeneity, that allows it to have so unique properties, also makes it difficult to study. We can manipulate a soil in bulk, measure indirectly how the microbes, nutrients, and other properties, change within it, but we cannot separate its differing microhabitats nor visualize how these processes occur in real time. The fact that we cannot see through soil does not allow us to understand how the labyrinth-like structure of the soil affects the accessibility of microbes to the nutrients contained within it. To tackle this limitation several computer modelling approaches have been tried, which simulate the inner structure of soil to better understand its interaction with microbes. Other attempts are to scan

samples of soils using x-rays to obtain detailed characteristics of its inner porous system. These methods, although valuable and informative, still do not allow us to understand, through visualization, manipulation and quantification, the direct effect of the soil structure on microbes and nutrients.

In the present work, we used microfluidic technology to simulate the inner characteristics of soils. Microfluidics is a technology that allows chemical and physical manipulation at a microscale, allowing us to design our own pore space with fixed characteristics that simulate the inner soil pore space. A microfluidic device is made of Polydimethylsiloxane (PDMS), a transparent rubber-like material, that permits direct visualization of the processes occurring within its microstructures. In this way, we can track how much microbes are growing, how they are moving, competing, and consuming nutrients. Using this technology, we conducted our research in three parts. First, we tested if the method was viable to study real communities of soil microbes and their interactions (**Paper I**); furthermore, we tested how the spatial characteristics of a pore space affected lab microbes (**Paper II** and **Paper III**); and finally, we evaluated if the results obtained with lab microbes can be replicated in natural soil microbes (**Paper IV**). Our initial hypothesis was that a physically complex habitat would limit microbial mobility and growth, leading to an overall reduction in microbial biomass and the nutrients they consume.

First, to test if the microfluidic devices could be used to study soil microbial interactions, their colonization patterns, and the modification they do to their surroundings, we buried microfluidic devices containing structures that mimicked the soil pore space and we studied them in the microscope after two months (**Paper I**). We could find not only that the devices were full of bacteria, fungi, and protozoa, but that air bubbles constitute unsurmountable obstacles for the swimming soil microbes like bacteria or protists, that bacteria and protozoa can use fungal hyphae as a bridge to access deeper regions of the microfluidic device, and that microbes modify their habitat when they colonize it. We then wanted to focus our next studies on the effect of the spatial shape of a soil pore space on microbes and their organic matter degradation in more detail. We used two different concepts to build a pore space with help of geometric structures: one was by looking at the pore space as a conjunction of channels (**Paper II**) or looking at it as a maze with many branching paths which are more or less connected (**Paper III**). When we tested the effect of channels, and how the effect of crooked channels differed from the effect of more straight ones, on a laboratory fungal and bacterial strain, we found that both organisms, as well as their nutrient degradation, are negatively affected in crooked channels, but the effect on fungi is stronger. We then tested the effect of the complexity of mazes on the growth of the lab strains used in the previous study. We found that as maze complexity increased, fungal growth decreased, in accordance with the previous study, but bacterial growth increased. Similarly, the nutrients were degraded more strongly inside the most complex mazes. Finally, we tested the effect

of channel and maze complexity on the nutrient degradation of natural soil microbes (**Paper IV**). We found that nutrient degradation was higher in crooked channels and complex mazes, meaning that as the habitat became more complex, the nutrient consumption was higher.

As it can be seen, our results were the opposite of what we expected in the beginning. We expected to see that complex habitats would decrease the fungi and bacteria inside them, reducing thus the amount of nutrients that were degraded. In turn, we found that while this was true for fungi, it was the opposite for bacteria, which grew more and degraded more nutrients in complex habitats. The explanation of why a more complex habitat promotes higher bacterial biomass and nutrient degradation might be because complex environments offer different advantages. In a complex environment the interaction between individuals is reduced, which means that the competition between them is also reduced, giving the opportunity for a large variety of strategies to emerge and cohabit. Bacteria that prefer to live in association with others, rather than swimming freely, grow better in a complex environment, because they are better protected against predation and high competition. They can then join each other's company and start forming a collective behaviour called "biofilm", where they become more efficient for different processes such as growth and nutrient acquisition.

Even though many parameters that exist in soils, such as air pockets, are not yet included in our later experiments, our approach demonstrates how complex and unintuitive the behaviour of microbes can occur inside microhabitats. The final goal of the approach we use is to be able to replicate as many parameters as possible so that we can evaluate how each one affects soil microbes. Once a clear picture of such effects is drawn, we could be capable of looking at a CT scan of soil and identify what type of microbes, interactions, and functions are happening in each spot and in the entire soil. In this sense, understanding parameter by parameter, how the inner characteristics of soils affect microbes, their interaction, and nutrient consumption, can help us to identify proper strategies to reduce the soil carbon from being consumed, thus reducing thus our contribution to the global climate change.

Introduction

The habitats where microbes grow tend to be patchy and to change over time. These changing habitat characteristics influence not only the way microbes behave, but also the impact they have in ecosystems. Heterogeneous microhabitats can be found inside the human body, in marine sediments, or in soils. In soils, the extreme complex habitat that microbes inhabit is thought to be one of the reasons why the carbon soils contain is preserved and not consumed by microorganisms.

Soil organic matter and the global carbon cycle

It is expected that through the 21st century the global mean temperatures will keep rising if the emissions of greenhouse gases are not decreased(IPCC, 2013). This will likely carry negative effects to the environment, the economy, and human health and safety(Forum, 2009). Since CO_2 emissions from fossil fuels and changes in land use are the main driving forces behind climate change, understanding the global carbon cycle and its dynamics will help us to predict and find possible solutions to such changes.

The carbon cycle describes the transformations carbon undergoes on Earth, which can be part of a long-term geological cycle or a short-term biological cycle (Kasting et al., 1988). While the biggest pools of carbon lay in the long-term geological cycle, it is the biological carbon cycle, the short-term cycle, that human activities impact the most (Lal, 2008). The biological cycle is determined by the balance between photosynthesis and decomposition, and its dominant compounds are CO_2 and CH_4. A theoretical start of the cycle occurs when the atmospheric CO_2 is incorporated in terrestrial biological tissue via photosynthesis. The total amount of carbon incorporated in plant tissues via photosynthesis is known as Gross Primary Productivity. After a portion of this carbon has been respired back to the atmosphere, what remains as death or living biomass is known as Net Primary Productivity. This biomass carbon can later undergo different paths, it can be further consumed by other organisms and be respired as CO_2 back to the atmosphere, or it can enter the soil and be transported later to oceans through rivers, or it can remain in soil forming what is known as soil organic matter (SOM).

The SOM chemical composition is thought to depend on both the initial characteristics of the input material and on the biotic and abiotic processes it is subjected to in the soil (Liang et al., 2017; Stoops et al., 2010). Even though SOM is essential for soil agriculture, water quality and for the resistance a soil can have to erosion (Bot & Benites, 2005; Schmidt et al., 2011), an agreement on the basics of its nature is still lacking(Lehmann & Kleber, 2015). A deeper understanding of SOM might help to clarify why a portion of soil organic carbon is decomposed promptly, while another remains stable in soils for millennia (Schmidt et al., 2011)

Traditional Views on Soil Organic Matter Stability

Three conceptual models that describe the stabilization of OM have been traditionally discussed: The Humification-; the Selective preservation-; and the Progressive decomposition model (Lehmann and Kleber 2015).

The "Humification" perspective is a method-based approach that states that an accumulation of recalcitrant OM due to its chemical properties is the reason why carbon remains in soil. In this approach, SOM is formed of plant material that has been modified by soil microbes into complex lignin-like compounds known as humic substances (Stevenson, 1994). In this process, known as "humification", humic substances increase in size and complexity as they are metabolically processed in soils. However, the methods to extract them from soil consist in harsh alkali extractions which, despite been widely adopted, have not been shown to represent the actual compounds that exist in an undisturbed soil (Lehmann & Kleber, 2015). In this line, recent studies have found that the large molecules, traditionally called humic substances, are rather a product of aggregation of small molecules during the extraction methods (Myneni et al., 1999; Piccolo, 2001; Sutton & Sposito, 2005). It has been, therefore, suggested that the molecular structure of the SOM components does not necessarily determine the long-term persistence of carbon in soils (Schmidt et al., 2011).

Another approach that explains carbon accumulation in soils is the "Selective preservation" model, which assumes that the OM input into soil is, per se, composed of a labile and a stable pool (Lützow et al., 2006). The labile pool is thought to be composed of simple molecules, such as glucose and amino acids, and of macromolecules of high nutritious value for microbes, like polysaccharides or proteins . The stable pool, in contrast, is thought to contain complex molecules of low nutritional value such as amorphous polymers with aromatic rings, which would make this pool less likely to be consumed by soil microbes, and therefore persist in soil (Lützow et al., 2006). Polymers that are part of this pool are lignin and molecules like lipids, waxes, cutin and suberin (Derenne & Largeau, 2001). However, several studies have shown that, given the right conditions, a wide variety of compounds can be mineralized or modified by microbes (Gramss et al., 1999; Hamer et al., 2004; Hazen et al., 2010; Wiesenberg et al., 2004; Yang et al., 2014).

The molecular recalcitrance of a compound plays, therefore, a relative rather than an absolute role in its persistence in soil and might be relevant only in the early stages of decomposition (Lützow et al., 2006)

The "Progressive decomposition" model, on the other hand, is based on the concept of an energetic downhill process where the fauna, plant, and microbial derived compounds, fall into. SOM is here considered as a unstable mixture of different thermodynamic state molecules that tends to fall through a "free energy precipice"(Hedges et al., 2000). In this sense, the SOM would be formed by molecules of different sizes and states of decomposition that accumulate over time. However, as indicated before, molecular structure does not necessarily determine the time a compound would remain in the soil(Schmidt et al., 2011). Thus, factors, other than the chemical properties of SOM compounds, might be preventing its mineralization.

Emergent views on soil organic matter persistence

Recent advances in SOM research indicate that none of the presented concepts suffice to explain the nature of SOM. There are still phenomena that cannot be answered with the traditional views on SOM. It is possible to find, for instance, high concentrations of supposedly labile OM in soils such as free amino acids (Gallet-Budynek et al., 2009; Jones et al., 2009; McDowell et al., 2006; Van Hees et al., 2008; Yu et al., 2002) On the other hand, the addition of low molecular weight compounds to soils resulting in a rapid mineralization rate, reveals the starving nature of soil microbes (Hobbie & Hobbie, 2013). This paradox supports the idea that a part of the SOM, in natural conditions, is not accessible to microbes and that the high concentration of low molecular weight compounds extracted from soil might be sample-induced (Hobbie & Hobbie, 2013). To explain this lack of accessibility, new models have been proposed (Lehmann & Kleber, 2015), where the accessibility of microbes to SOM is the driver of OM decomposition. Accessibility is defined in terms of both physiochemical interactions of the OM with mineral surfaces, where the attachment of organic molecules to mineral surfaces limits their availability, and in terms of the physical protection of SOM within the inner soil structure (Lehmann & Kleber, 2015).

Soil structure

Soil is considered the most complex biomaterial known, which is in part due to the interaction of soil microbes with its heterogeneous microenvironments, forming a self-organized system that sustains its functionalities over time (Young & Crawford, 2004). The way particles and voids are distributed in the soil matrix, regardless

chemical heterogeneities, is known as soil structure (Rabot et al., 2018). This property of soils has been traditionally studied because it can help to descre some soil physical aspects like hydraulic and solute transport properties (Bejat et al., 2000; Vogel, 2000), soil water retention curves (Vogel, 2000), hysteresis, or dependence of the soil media on its previous phenomena (Jerauld & Salter, 1990), or the relationship between capillary pressure and saturation based on the heterogeneity of the pores (Ferrand & Celia, 1992).

But soil structure does not only alter soil physical parameters, it also influences the living organisms inside it. Plants, for instance, adjust their root colonization showing a preference to pores generated by organisms such as earthworms (Stirzaker et al., 1996). For microorganisms, soil structure is considered to have a major impact due to the diversity of microenvironments it provides (Young & Crawford, 2004). It can, for instance, promote differences in the abundance of different microbial communities (Negassa et al., 2015), affect local denitrification and intra-aggregate anoxia patterns (Arah & Vinten, 1995), affect the decomposition rate of freshly added plant residues depending on the pore connectivity (Negassa et al., 2015). On the other hand, microorganisms can in turn also affect the soil structure: It has e.g. been shown that microbial decomposition activity inside artificial soil aggregates caused micro-cracks that changed their inner porosity and morphology (De Gryze et al., 2006).

The study of the structure of soil can be approached by either looking at the matter it is composed of, or, in contrast, at the empty spaces this matter creates. Thus, the approaches to study soil structure consist mainly of two perspectives: the soil physical approach and the soil pore approach.

Soil physical approach

The physical approach or aggregate approach is a method-based characterization of the soil structure and it is defined by the stability of the soil particles after a certain separation treatment. It has been established a three-state organization of the soil solid phase: macroaggregate, mesoaggregate, and microaggregate (J. Six et al., 2004).

The aggregate properties of soils have been suggested to be determinant for the SOM dynamics inside them. The SOM inside soil aggregates is thought to be protected from microbial degradation due to the inaccessibility of degrading enzymes and the reduced oxygen diffusion inside of them (J. Six et al., 2002). Poorly stable macroaggregates have been shown to offer little protection to SOM in the long term when compared to more stable microaggregates (J. Six et al., 2002). Therefore, the amount of carbon contained in microaggregates-within-macroaggregates as a ratio of the total SOC is proposed as indicator of the physical stabilization of SOM in soils(Johan Six & Paustian, 2014).

Pore space perspective

The pore space perspective, as opposed to the aggregate perspective, focuses on the soil architecture, or the properties of the soil pore space(Ritz & Iain, 2012). The physical part is, however, not completely disregarded, for the composition of the pore forming particles is also studied inside this approach. Parameters such as distance between different pores, their sizes, shapes, conditions, are studied for determining the involvement they have in the soil functions.

The methods for characterizing the pore space of a soil can be divided into indirect methods and direct methods. A, third and theoretical way of studying the soil pore structure is with the use of network models, which are an idealized representation of the geometrical characteristics of porous media (Vogel, 2000).

Indirect Methods for studying pore space

The indirect methods refer to the study of the pore space without a direct visualization of it, but with the use of probe molecules to infer its bulk characteristics. Mercury porosimetry has been used for decades for this purpose and it consists in the introduction of mercury into the soil sample, followed by a pressure application so that the mercury penetrates the pores of the soil. The characteristics of the pore space are then calculated based on the pressure applied and the volume of mercury introduced (Van Brakel et al., 1981). One of the advantages of this system is the wide range of pore sizes that can be covered in a single run (Rabot et al., 2018). However, facts such as the drying of the soil before analysis likely changes the original pore space, or that the largest entrance toward a pore is measured instead of the actual size of the pore, are some drawbacks to this method (Rabot et al., 2018; Van Brakel et al., 1981).

The correlation between the soil water content and its matric potential can also be used as a method for inferring the pore space characteristics of a soil. This method is based on the water retention curve of a soil and the different indicators derived from it. A soil with many large pores will show a retention curve that drops rapidly its volumetric water contents under high matric potentials, whereas a soil with fine pores retains water even at high matric potentials (Nimmo, 2013). However, when the water retention curve is in the dry range of a soil, this method is prone to errors that can be partly compensated by considering the relative humidity or osmotic equilibrium of the soil (Rabot et al., 2018).

Using gases is another way to study indirectly the pore space of a soil. This can be done by using gas as the mobile phase to determine the pore space properties of a soil derived from isotherm or model applications (Zachara et al., 2016). The gases used are generally dinitrogen (N_2), carbon dioxide (CO_2), or water vapor, which are introduced in a small soil sample (between 1 to 5 mm columns) (Rabot et al., 2018). After being degassed, the samples are subjected to a fixed pressure of the gas in use. The introduced gas forms monolayers at first and then multilayers against the pore

walls. Micropores are the first pores to be filled because the interaction between the gas and the pore walls is higher (Lowell et al., 2004). Mesopore and macropore filling needs more pressure because multilayers need to be formed, thus relying not only on the interaction of gas to pore walls but also on interaction of the gas with itself(Sing, 1985). The amount of adsorbed gas is calculated using the difference in pressures before and after equilibrium. The range of pores that can be characterized in size are between 1 and 200 nm in diameter (Darbyshire et al., 1993).

Direct Methods for studying pore space

Direct methods are the ones that allow the characterization of the pore space by direct visualization of it. The strength of these techniques is that they allow a characterization of the morphological and topological features of the pore space. Among the direct methods are the optical (electron) microscopes, which can visualize the pore space directly in thin sections of a sample (Bruand & Cousin, 1995; Pagliai et al., 2004). Other methods allow characterization of the soil pore space without thin sectioning, by using radiation that passes through the sample followed by a digital 3D reconstruction. These methods are, namely, X-ray tomography, gamma-ray tomography, neutron tomography, and nuclear magnetic resonance imaging (Cnudde & Boone, 2013; Pires et al., 2005; Pohlmeier et al., 2008; Schaap et al., 2008). The studied pore size limit depends on the resolution of the scan (Wildenschild et al., 2002). A further segmentation, using the obtained image contrast, allows identification of the different phases, namely: air, water, soil matrix, roots, gravel.

These approaches have nonetheless some drawbacks such as the necessity of expensive equipment, possible introduction of artifacts during sample preparation, and lack of standard protocol for digital segmentation. This last one produces significant differences in the proportion of the phases of the soil depending on the type of segmentation used (Baveye et al., 2010).

Pore space and soil organic matter

The pore space characteristics of a soil have been suggested to be crucial for the fate of the SOM. The challenge is, however, to know what type of spatial arrangements or characteristics influence SOM and soil functions. An example of this challenge is the unclear and sometimes contradictory role of the bulk soil porosity in determining soil functions. Experiments using medical X ray scans suggest that it is more important to know parameters that describe connectivity or presence of obstacles, rather than bulk porosity when describing air, water, and solute transport through soil (Katuwal et al., 2015). In the same line are the results of Larsbo et al., (2016) and of Paradelo et al., (2016), that show that SOM content was not correlated with the total imaged porosity. Also, bulk macroporosity measurements derived from CT images could not predict spatial characteristics of a pore space, such as its tortuosity, which is thought to be relevant for soil processes(Katuwal et al., 2015).

Therefore, bulk porosity per se seems not to provide enough information about soil functions and SOC turnover.

The pore size distribution of a soil, rather than its bulk porosity, has also been studied in relation to SOM fate. Concentrations of SOM have been found to be linked to the volume of the pores that surround it, especially the smaller ones. For instance, the SOM content of a soil was found to be correlated with the volume of the pores below 0.6 mm, but not with the pores bigger than 1.2 mm(Larsbo et al., 2016). Complementary, Ananyeva et al., (2013)found that the correlation between porosity and total carbon content in studied soil aggregates was positive for pores between 15 and 37.5 μm and negative for pores between 37.5 and 67.5 μm. Also, Toosi et al., (2017)found in soils of different land management that the abundance of pores below 32 and above 136 μm was positively correlated with FTIR indicators of low decomposable OM. There seems to be, thus, a link between SOC stabilization and the number of small pores in the soil.

The correlation between pore space of a soil and SOM is likely to go on both directions, meaning that SOM can also have a feedback on soil porosity. For instance, high concentrations of organic carbon in soils were linked to an increase in the arrival time of a tracer through those soils, indicating the presence of weak preferential transports(Larsbo et al., 2016). This correlation might be occurring because having weak preferential transports allows new nutrients to be distributed through the whole pore space, preserving the carbon concentrations inside it.

Not only the pore size has been under scrutiny when studying the link of pore space and SOC, but soil aeration, or the access of pores to air, has also been pointed as a crucial factor for soil processes related to SOM. For instance, Naveed et al., (2014) found that fertilized soils have a better aeration compared to non-fertilized soils, which could be attributed to a higher number of macropores, higher gas diffusivity and air permeability, and the higher connectivity between pores in fertilized soils compared to non-fertilize ones. This has been supported by analysis of soils that show a positive correlation between connectivity of the pore network and macro porosity which might promote aeriation(Paradelo et al., 2016). Aeriation, or the access of pores to the atmosphere has been shown to be crucial for organic matter mineralization. This was evidenced by Kravchenko et al., (2015)who found that pores connected to atmosphere tend to lose more particulate organic matter compared to other pores. It seems, thus, that the access of the pores to air is a crucial factor that might promote SOM mineralization, if well connected, or SOM preservation if not connected to air.

Microfluidic models

One of the challenges with studying soil is the difficulty of visualizing the processes that occur inside it in real time. A way to tackle this challenge is by studying such processes with the use of micro models that simulate soil. These models allow us to test specific soil parameters and follow the processes inside them in real time. An emerging approach of models that simulate the pore space are the microfluidics systems.

Microfluidics are defined as the manipulation of fluids within structures at the micrometre scale (Beebe et al., 2002). Due to its unique characteristics, regarding control of flows, chemical gradients, structures, among others, it has been widely used in fundamental and applied research of several fields such as soft-matter physics, chemical engineering, disease diagnostics and biomedicine (Rusconi et al., 2014).

One of the main characteristics of microfluidics is the change of hydrodynamics that occur when the fluid transport system is small, as its dynamics become different than the ones experienced at the macroscale: Fluids in channels smaller than 100 μm and fluid velocities in the μm/s order enter a low Reynolds number regime which means that flow becomes exclusively laminar (Brody et al., 1996) instead of turbulent, which is the common condition at macroscale. Laminar flow, as opposed to the chaotic state of the turbulent one, occurs orderly and in parallel to the surface of flow (Beebe et al., 2002). This occurs because in small compartments, viscous forces become dominant over inertial forces, turbulence is thus neglectable, and the role capillary forces play is significantly higher than in large dimension processes (Beebe et al., 2002). Also, since diffusion time is proportional to the square of the diffusion distance, it becomes the main mixing mechanism at the microscale (Brody et al. 1996). Additionally, surface tension as well as evaporation play a more important role in small volumes as opposed to macro scale ones (Brody et al., 1996). All these characteristics of the microscale are likely to be dominant as well in the soil pore space, specially in the mores below 50 μm, where most microbial activity is thought to happen, being thus of high relevance the application of microfluidics to study soil microbial processes.

Fabrication

There are currently several methods for the fabrication of microfluidic devices. The efficacy of each one of them depends on the type of experiment performed.

The fabrication method that is mostly used for biological and biomedical purposes nowadays is soft photolithography since its fast, less expensive, and needs less specialized techniques(Beebe et al., 2002). Soft photolithography consists in the moulding of a polymer called polydimethylsiloxane (PDMS), formed by an

elastomer and a curing agent, onto a photoresist master. The use of soft photolithography for biological research has been widely reviewed before (Whitesides et al., 2001).

There are, nonetheless, other methods for the fabrication of microfluidic devices. In situ construction, for instance, is based on photopolymerizable liquids, lithography (Beebe et al., 2002), where the walls of the device are formed by 3D printed material or by polymerized material, which was exposed to UV light, and the non-exposed part that remains unpolymerized is washed away (Khoury et al., 2002). Since it does not need the use of a clean room or other expensive equipment, it is a fast and simple process. However, in situ construction is limited in its dimensions by the resolution of the mask and the polymerization effect of the polymer(Beebe et al., 2002)). Other promising techniques, such as micro moulding (Choi et al., 2001), or laser ablation (Roberts et al., 1997)have shown limitations, especially due to their low resolution and low throughput.

Microfluidics in Microbial Ecology

Microfluidics have been used to investigate a wide range of microbial phenomena at the micrometre scale, which include processes such as microbial chemotaxis, the effect of fluid flows in microbes, microbial navigation and their effect on flows, surface-microbe interactions, among others.

Chemotaxis

Before microfluidics, chemotaxis, which is the property of organisms that allows them to adjust their motility based on the chemical gradient around them, was traditionally characterized with chemotaxis assays. These assays include protocols such as stopped flow diffusion chambers, continuous-flow capillary assays, two chamber glass capillary arrays, swarm plate assays, and tethered cell assays(Ahmed et al., 2010). The main challenges in these traditional methods were related to the control of experimental factors, such as chemical gradients, at the relevant scale for microbes. With the use of microfluidics and its accurate control over channel geometries and fluid flows, some of the pitfalls that are traditionally encountered can be potentially solved. , allowing a revision of the previously stablished knowledge by chemotaxis assays. Mao et al., (2003), for instance, showed with a microfluidic gradient generator composed of two continuous laminar flows that the chemotactic sensitivity of *E. coli* is 1000-fold higher than previously described with traditional capillary-based methods.

The main advantage of microfluidics when it comes to chemotaxis studies is the possibility of a direct control of the created gradients. Masson et al., (2012), for example, produced a controllable gradient by connecting reservoirs through a microfluidic channel. To get even more controllable gradients, it is also possible to

separate the test channels from the chemical gradient using membranes of porous materials like nitrocellulose (Diao et al., 2006) or hydrogel agarose(Cheng et al., 2007), which prevents direct interaction between cells with the gradient. Stable gradients have also been produced with oxygen by using a two-layer microfluidic device creating a gradient from aerobic to microaerobic conditions(Adler et al., 2012), and with temperature to test the confound effect between chemotaxis and thermotaxis in *E. coli* (Salman et al., 2006).

Unsteady gradients have also been part of experimental designs inside microfluidics to mimic more realistic conditions. An unsteady gradient of α-methylaspartate, for example, was used to obtain a detailed map of the chemotactic velocity of *E. Coli* (Ahmed & Stocker, 2008). Unsteady gradients have also been shown to be produced by the organisms themselves as an effect of bacterial nutrient consumption(Saragosti et al., 2011).

Flows

Microbes in nature are exposed to flow regimes that determine their life cycles. To simulate the effect of flows on microbial communities, different microfluidic approaches have been optimized to expose microbes to controlled flow regimes. Marcos et al., (2009)for instance, used a microfluidic device to study the effect of a shear flow in the alignment of helically shaped, non-motile bacteria, showing how bacteria align according to flows as a mean of adaptation. Flows in nature do not occur only in one direction but rather can be of a wide variety of types. In this sense microfluidic approaches have been developed to study extensional flows, hyperbolic flows and vortex flows, that serve to test the response of microorganisms to different types of flows (Hudson et al., 2004; Marcos & Stocker, 2006).

Motility effects on fluids

Microbial motility itself can also affect chemical diffusion and fluid properties. Using a microfluidic flow cell, (Kim & Breuer, 2004)showed that the presence of motile *E. coli* increased the effective diffusion coefficient of Dextran. Also, it has been shown, using bacterial surface arrays (carpets), that the temperature and nutrient conditions in which bacteria grow determine their mixing performance of their culturing liquid. (Kim & Breuer, 2007). Moreover, Gachelin et al., (2013) showed, by changing the shear rate of a fluid, that the viscosity of the fluid changed due to the mixing effect created by *E. coli* motility inside it.

Interaction with surfaces

In every type of environment, microbes encounter surfaces that affect their behaviour and life cycles. However, the study of the biophysical mechanisms behind microbe-surface interactions are still underexplored (Rusconi et al., 2014). Some attempts have been done to explore these interactions using microfluidics. Lauga et al., (2006), for instance, showed that *E. coli* swim in a circular motion when they

are near a solid boundary, which causes a hydrodynamic trapping of the cells close to the surface. Also, by letting bacteria move on an agar substrate and confined in PDMS microchannels, (DiLuzio et al., 2005)found that bacteria swam mainly to their right along the right wall of the channels. These results highlight the importance of studying microbial processes occurring at surfaces, for they seem to be different than the ones performed in traditional plate studies.

It has also been shown that bacteria can get trapped when encountering dead ends or funnel like structures. Galajda et al., (2007)managed to concentrate motile bacteria in certain regions of the microfluidic device, and to separate them from non-motile ones by using funnel like structures. Even with the presence of flow against the orientation of the funnel structures in a channel, contra intuitively concentrates more bacteria in the section of the channel after the funnel than before it (Altshuler et al., 2013). This shows the importance of corners for bacterial accumulations in absence of gradients. However, it seems that when a density threshold of bacteria is reached, enough substrate consumption causes the formation of an attractant gradient that allows bacteria to escape from a barrier of funnels (Lambert et al., 2010).

Bacterial attachment to surfaces is of great importance for different fields of research like biomedical or environmental sciences. Microfluidic approaches have revealed that there might be bacterial attachment mechanisms to surfaces that we are still not aware of. Lecuyer et al., (2011), for instance, showed that mutant strains of *Pseudomonas aeruginosa* lacking surface organelles or extracellular matrix could still present a shear-enhanced attachment to the surface of the channels. These results indicate that not only extra cellular matrix and surface organelles are involved in bacterial attachment to surfaces, but that other mechanisms might also play an important role. A similar phenomenon was seen when comparing wild type *Xilella fastidiosa* with mutants lacking type I and type IV pili under different flow regimes (De La Fuente et al., 2007). Also, mechanisms like bacterial alignment, can as well be used by bacteria to perdure in surfaces. Shen et al., (2012)showed that *Pseudomonas aeruginosa*, besides using attachment mechanisms, also oriented themselves upstream against the flow direction. This mechanism, according to the authors, could be beneficial for bacterial persistence under flow regimes.

Not only the bacterial physiology determines surface attachment but also the chemical and the topographical properties of a surface play a crucial role in the adhesion of bacteria to them. By testing the effect of having lipid membranes on a surface, Holz et al., (2009) showed that the size of the membrane patches and the number of bacteria determine whether *Neisseria gonorrhoeae* presents a clustering or a spreading behaviour when attaching to surfaces. On the other hand, studies concerning the interactions between cells and different topographic features at the nanoscale have been widely reviewed, and the importance of elucidating such interactions with bacteria has been particularly pointed out(Anselme et al., 2010)). An example of the effect of surface topography on bacteria was shown by

Hochbaum & Aizenberg, (2010)when different surfaces characteristics promoted specific orientation patterns in gram negative and gram-positive bacteria.

Microfluidics for studying soil microbial processes

The advantages of microfluidics for soil studies are the transparency it provides for real time visualization and the versatility at manipulating its internal parameters, both of which are key for understanding soil phenomena. Over the last years there has been increasing interest in the use of microfluidics in soil sciences (Aleklett et al., 2018; Karadimitriou & Hassanizadeh, 2012; Stanley et al., 2014, 2016; Stanley & van der Heijden, 2017). Microfluidic devices have been applied to answer a wide variety of research questions ranging from the effect of extracellular polymeric substances (EPS) on the drying dynamic of soils (Deng et al., 2015), to the role soil unicellular eukaryotes play on transporting nanoparticles(Rubinstein et al., 2015). Microfluidics allow also the incorporation of optodes (sensor device to optically measure the concentration of a substance) to measure indirectly some of the properties inside the device, such as pH and redox potential, that could not be measure in real time at the pore scale in real soil (Pedersen et al., 2015; Rubol et al., 2016)).

The production of EPS is crucial for the survival of many microbes and is considered a key advantage for EPS forming microorganisms over their planktonic counterparts Rusconi et al., (2014). Researchers have used microfluidics for studying the formation of bacterial EPS in flows(Rusconi et al., 2010), the effect of a channel curvature in EPS formation(Rusconi et al., 2011), clogging of channels due to EPS and biomass accumulation(Drescher et al., 2013), EPS forming dynamics in a wide variety of geometric features (Kumar et al., 2013; Marty et al., 2012; Valiei et al., 2012). As mentioned before, Deng et al.,(2015)used a CT-based soil chip to show that the presence of EPS strongly increased the water retention potential of the artificial pore space.

However, as Baveye et al., (2018)mentioned, two main challenges remain for the application of microfluidic models in soil research. The first one is related to the connectivity of the pore space which is limited by the 2D structure of the microfluidics (often referred to as pseudo-3D since it has a constant and low height) and does not resemble the real 3D nature of soils. Moreover, designs based on μCT images miss “sub resolution” pores, which are not detected due to CT limitations in resolution (currently at 10 μm) Baveye et al., (2018) and ,thus, it is difficult to know how those pores, that are crucial for biological activities, are arranged in an undisturbed state.

Aims

The aim of my PhD project was to reveal the effect soil structure has on microbial processes. For this purpose, I used microfluidic techniques that simulated different soil parameters and its effect on lab and natural microbial populations. The present work focuses on the following questions:

- Can microfluidics be a tool for studying the influence of soil structure on microbial interactions at inter-kingdom level? What is the effect of the liquid phase, pore geometry on microbial colonization? To what degree do microbes and physical forces modify the microhabitats? **(Paper I)**
- We then moved to a more specific question of influence of pore geometry on microbial biomass. Thus, if we see the inner soil pore space as a conjunction of channels, what is the impact of the turning angle on the growth of microbes and substrate degradation? (**Paper II)** The initial thought was that sharper turning angles would reduce fungal and bacterial growth since channels become less accessible. This reduction in growth would also be translated into a reduced substrate degradation. Hence, sharper angles would lead to low microbial biomass and low substrate degradation. For this question, a fungal and a bacterial fluorescent lab strains were used to detect biomass and a fluorogenic peptide was used to detect enzymatic activity.
- If we consider the soil pore space as a maze with branching paths of different connectivity where microbes grow, what is the effect of maze complexity in microbial growth and substrate degradation? (**Paper III)** We expected that an increase in maze complexity, obtained by an increase in the maze fractal order, would lead to a reduction of bacterial and fungal biomass and the substrate degraded. The lab strains used in this question were the same as in the previous question.
- Finally, how similar are the obtained results when the effect of angle sharpness and the maze fractal order are tested in a soil inoculum containing natural microbial communities? (**Paper IV)** Nutrient degradation was followed by using the same fluorogenic substrate that was used in the two previous questions.

Main results and conclusions

Microfluidics for studying soil structure

One of the main challenges when studying soil microbial ecology is that microbial processes cannot be seen, and their activity must be measured indirectly. Hence, by having a methodology to study soil microbial functions that allows a direct visualization of processes in real time, can be a powerful tool to investigate longstanding knowledge gaps in the field. In this first project we tested microfluidic techniques for studying soil microbial processes, and more specifically, we tested broad questions on microbial exploration of a pristine pore space. To do this, we performed a series of experiments with soil microbial communities inside microfluidic devices where we could test the effect of pore geometry, the distribution of the liquid phase, and interaction of fungal hyphae with swimming microorganisms, as well as the habitat modification microbes and particles do to their surroundings (**Paper I**).

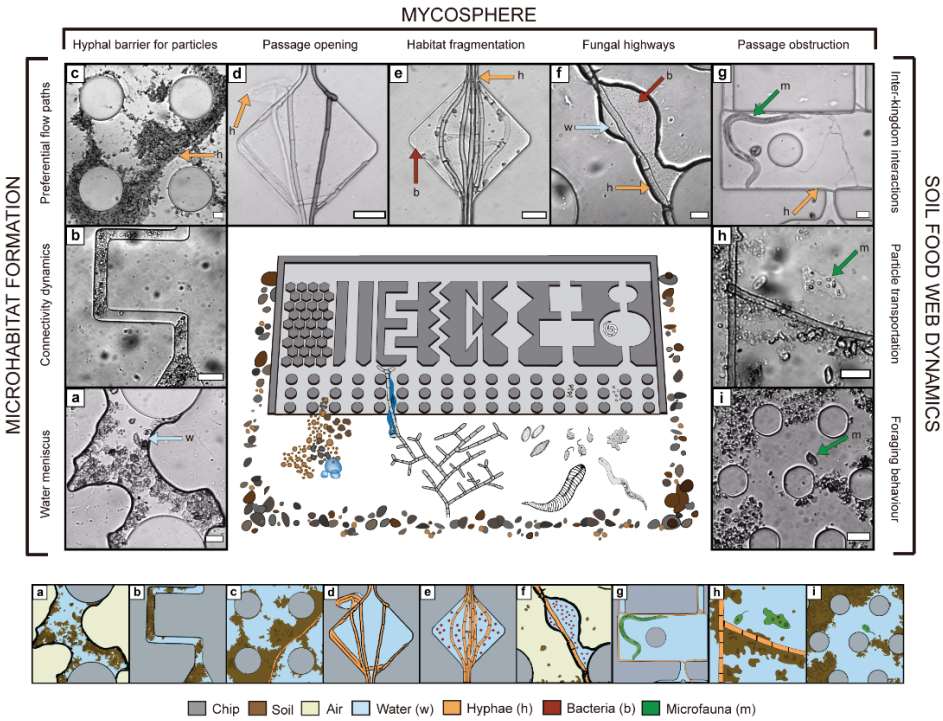

Figure 1. Types of soil organisms and processes studied in the microfluidic device. The devices were colonized by soil microorganisms when buried in the field. The inner section shows a schematic drawing of the types of structures contained (dimensions are enlarged for didactic purposes). Bright field microscopy images indicate the types of processes observed in the study: a, Water meniscus connecting soil particles and structures. b, Mobile soil particles blocking connectivity of the artificial pore spaces. c, Preferential water flow paths developing among soil particles sedimenting at the bottom of hyphal structures. d, Passage opening by hyphae: hyphae broke through the borders of an artificial pore space, creating a new micropore. e, Habitat fragmentation by hyphae clogging a pore neck. f, Fungal highways: hypha-facilitated bacterial dispersal across air gaps. g, Passage obstruction: a hypha blocking the entrances to a rectangle pore occupied by a nematode. h, Particle transport: amoeba transporting ingested bacteria and particles. i, Foraging behaviour: flagellated protozoa foraging around and in soil aggregates. Images a, d, and e derive from air filled chips; b, f, g, and i derive from malt medium-filled chips; c and h derive from water filled chips.

The microfluidic device design was made in AutoCAD 2015 and it consisted of a series of pillars as entry to a treatment area. The treatments had channels with varying width and shapes and were either filled with air, water, or nutrient medium to test the effect of a liquid or air interphase in microbial colonization. The inner part of the microfluidic device contained channels of different geometry with increasing complexity so that it could be tested the effect of these on microbial colonization. Additionally, other two aspects were tested: the effect of fungal hyphae of the advancement of swimming organisms, and the habitat modification organisms did to the structures in the microfluidic device. The microfluidic devices were buried under a soil plot for a period of two months, after which they were recovered and analysed in the microscope. In a parallel approach we incubated

microfluidic devices containing soil in the laboratory, so that we could follow the changes inside over time.

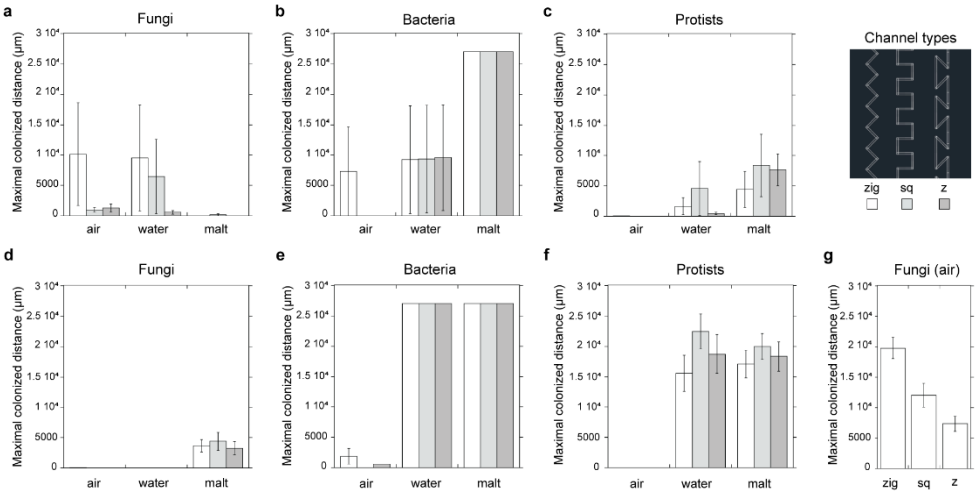

Figure 2. Maximum dispersal extent of different soil microbial groups. Colonization distances of the three microbial groups, fungi, bacteria, and protists, recorded in soil chips incorporated into soil (a, b, c, Expt. 1, n=3) and incubated with soil in the laboratory (d, e, f, Expt. 2, n=3 chips x 12 channels). g, Fungal colonization distance in Expt. 3 (air-filled chips, n=2 chips x 12 channels). The channels analysed are 10 µm wide, shaped with corners of different angles (see legend: zigzag (white bars), square (light grey bars), z-shaped (dark grey bars), under dry =air-filled, water-filled, or malt extract-filled conditions, error bars denote the standard error of the mean. The maximum extent of the channels was 2700 µm and thus the maximum possible colonization extent of this experiment.

The data analysis indicated that bacteria and protozoa were strongly dependent on connected liquid phases for their colonization of the microfluidic devices. Fungi, on the other hand showed variable results, indicating that other factors than liquid or air phases influence their colonization. At the same time, the presence of fungal hyphae did not enhance the colonization of bacteria and protozoa, although fungal hyphae increased the wettability of dry spaces by, putatively, exudate secretion. Channel geometry did not affect the colonization of the channels at this level of replication, except for fungi in one of the experiments which grew better when the deviation from a straight path was minimum. Finally, microbes also altered their habitat by growing in it, especially fungi, which dragged and modified the arrangement of mineral particles inside the microfluidic device.

In conclusion, microfluidic devices can act as a connection between lab and field experiments as we can insert a controllable device into a natural ecosystem, which will become thus a part of the ecosystem, and test parameters that could not be tested with traditional techniques. It is possible to internally replicate experimental sampling points to a very high number which allows us to make rough estimates on the relevance of processes as well.

Effect of angles in a pore space

It has been hypothesized that one of the reasons why SOM is not consumed by microbes is because they are not co-located in space and time. What separates, thus, microbes from decomposers to be co-located is the soil matrix around them. In this sense, our initial thought was that a complex set of structures that separate microbes and substrate would decrease the interaction between them, slowing down the substrate degradation rate. For this purpose, we tested how the turning angle sharpness in a geometrical, channel-shaped pore space affected fungal and bacterial growth inside a microfluidic device. Our hypothesis was that as a channel's turning angle sharpness increased, bacterial and fungal growth would decrease, due to the elevated energy investment needed to find their path in sharp angled channels. This biomass reduction would thus lead to a reduction of substrate degradation in sharper angled channels (**Paper II**).

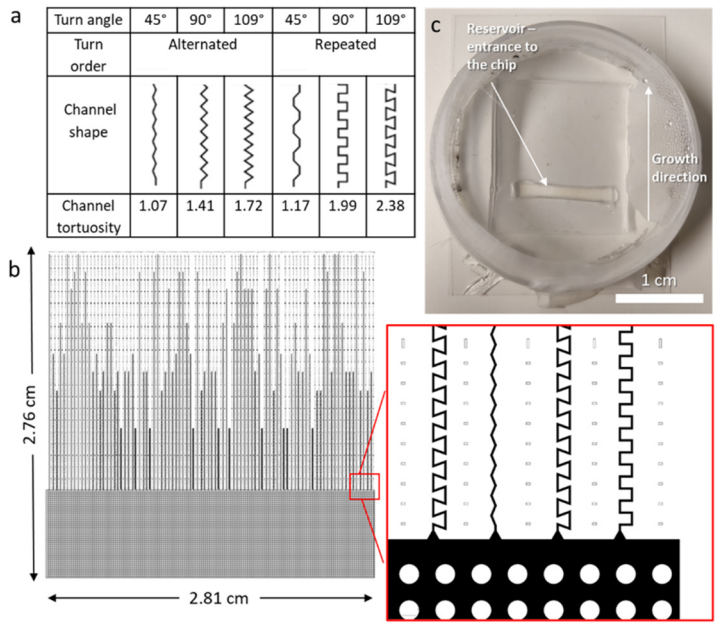

Figure 1. Microfluidic device design containing different channel treatments. (a) Channel types used. Each channel had a bending angle (45°, 90°, and 109°) and a turn order (alternated or repeated). (b) Entire design, consisting of a pillar system as entrance to the channels, and thesix type of channels in six variations distributted randomly. The design dimensions were: 281 mm x 276 mm. (c) The PDMS microfluidic device bonded to a glass bottom Petri dish.

Using AutoCAD 2019 we designed a microfluidic device that contains a series of channels with different turning angle. The tested channel types had turning angles of 45, 90, or 109 degrees, and for each angle two turning orders were tested: an alternated turning order, where a right turn was followed by a left turn, or a repeated

turning order, where each turn direction was followed by a turn of the same direction (two to the left, followed by two to the right). The volume of the channels was normalized so that all channels would contain the same volume of medium. After the microfluidic device was filled with nutrient medium M9, it was inoculated with either the bacterial strain *Pseudomonas putida* (PP), the fungal strain *Coprinopsis cinerea* (CC), or with both of strains together. In this way we could test the effect of the structures on each strain and in the interaction of both. A fluorogenic substrate, the amino peptidase substrate L-Alanine 7-amido-4-methylcoumarin trifluoroacetate salt (AMC), was added to the growing medium so that enzymatic activity inside the microfluidic structures could be followed in time. The inoculated microfluidic devices were imaged using epifluorescence microscopy every 24 hours for 14 days. At the end of the experiment the obtained images were subjected to a process of background subtraction, alignment, and measurement. In this way, we obtained the bacterial and fungal biomass, as well as the substrate degradation inside each type of treatment channel.

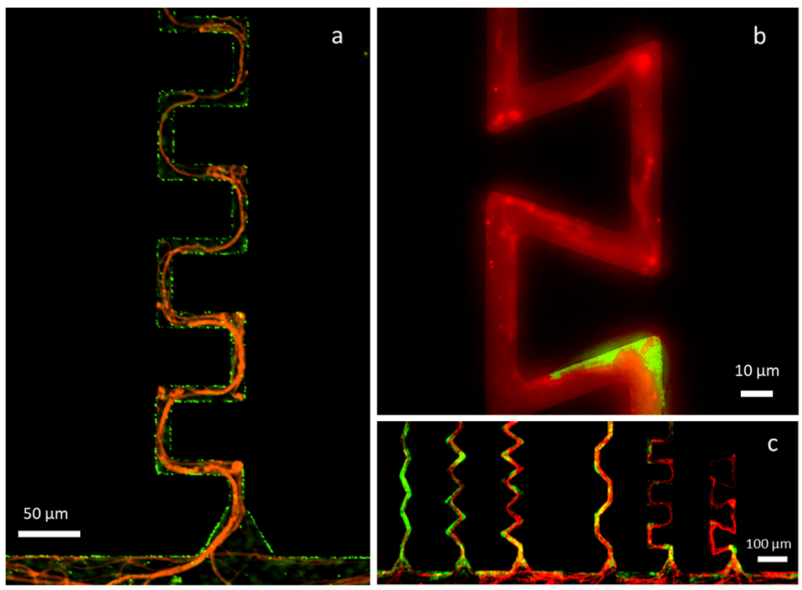

Figure 2. Fluorescence images of the bacterial strain *P. putida* mt-2 (green) together with the fungal strain *C. cinerea* AmutBmut PMA412 (red) with M9 liquid medium inside the PDMS microfluidic device on day 2 after inoculation. (a) 90°-angled channel with repeated turn order colonized by bacteria and fungi. (b) 109°-angled channel with repeated turn order where accumulations of fungal hyphae block do not allow bacteria to advance further inside the channel. (c) All the type of channels studied colonized by both strains (from left to right: 45°, 90°, and 109°, with alternated turning order, and 45°, 90° and 109°, with repeated turning order) taken at 4x magnification.

The image analysis revealed that the growth of both PP and CC were negatively affected in sharper turning angle channels. This negative effect was stronger when the turning order of the angles was repeated than when it was alternated. When grown together, the negative effect of angle sharpness continued for both strains but

became stronger for bacteria when growing together with fungi. Substrate degradation was not different between channels when PP and CC grew separated, but when both strains were together substrate degradation was lower in sharper angles.

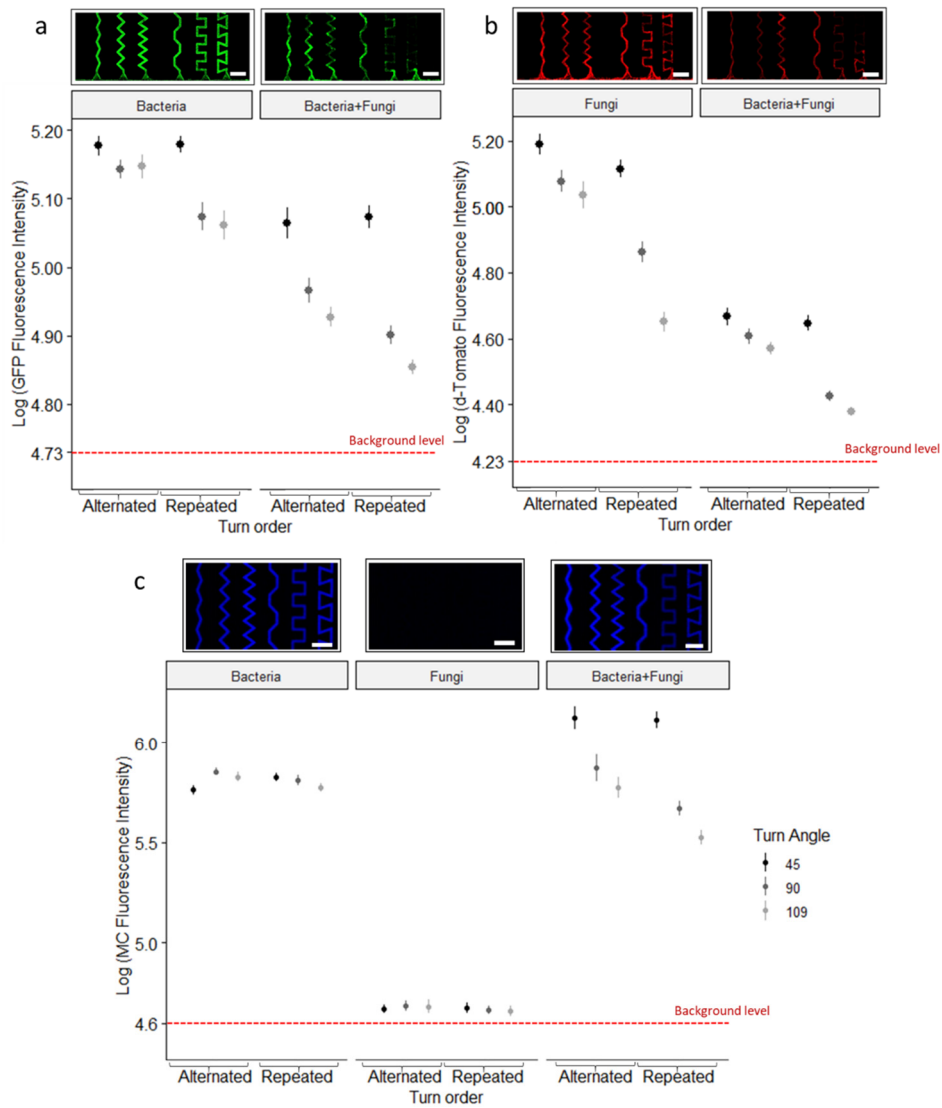

Figure 3. Bacterial and fungal biomass and substrate degradation in the different conditions. Upper pannels of each graph show examples of the initial part of the channels colonized by *P.putida* expressing GFP *C. Cinerea* expressing d-tomato, or AMC (scale bar=100 µm) in conditions of absence (left) and presence (right) of competitor. Bottom panels show the three-way analysis of the response of bacterial biomass (a) fungal biomass (b) or substrate degradation (c) to the different channel types and competition conditions at the day of maximum fluorescence signal. The symbols represent the mean log-transformed fluorescence of each fluorophore for each treatment and the error bars represent the ±SE based on ANOVA for all the channel types (n=50).

These results were according to our initial expectations that angle sharpness would reduce biomass and substrate degradation. Both, fungal and bacterial biomass, were reduced in sharper angles due to the increased difficulty to access them. Bacteria could be limited in their dispersal because the sharp turning angles are higher than the angles they naturally turn while swimming in a free medium, and thus repeatedly hit walls or make detours before finding their way to the next channel segment. In the case of fungi, when hitting a wall at 90 degrees or more, the mechanism that keeps growth directionality loses direction, followed by a branching event. The habitat modification caused by fungal hyphae strengthened the effect of structures on bacterial growth, meaning that the habitat for bacteria became more difficult to access when fungi were present. This did not occur vice versa, meaning that the presence of bacterial biomass did not affect the response of fungi to the structures. Finally, the reduction in substrate degradation in sharper angled channels seem to be occasioned by the limited access bacteria had in those channels, which limited the amount of enzymatic degradation they could perform, while fungi did not degrade the substrate in significant levels.

Our findings confirmed our hypothesis that an increase in turning angle sharpness reduces microbial biomass and nutrient degradation. They also reveal that the effect structures have on microbes are of different magnitude depending on the microbial group we studied. Overall, this study shows the relevance of considering multi species and multi-kingdom organisms in experimental designs so that we can draw a clear picture of how these interactions might be occurring in nature.

Effect of fractal order

The results found in the previous project followed a certain factor of habitat complexity, which was turning angle and order. In the present project, we wanted to evaluate the effect of another parameter of habitat complexity by looking at the pore space as a maze instead of a conjunction of channels. In this sense, the selected parameter that defined complexity was the fractal order of a series of mazes inside a microfluidic device (**Paper III**).

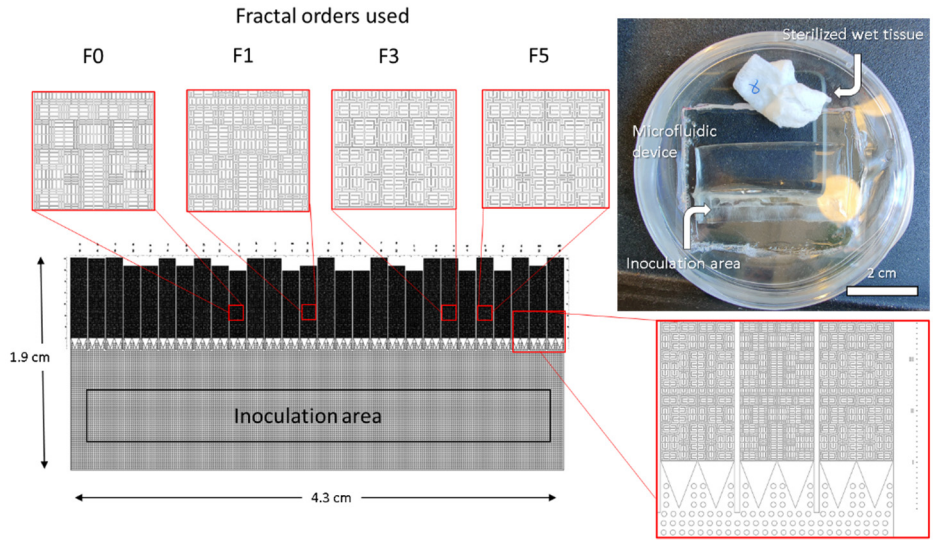

Figure 4. Fractal microfluidic device design, containing the 4 types of mazes studied with different fractal order: order 0 (F0), order 1 (F1), order 3 (F3), and order 5 (F5). 7 replicates of each maze type with a standarized volume were included in the. The microfluidic device was molded in PDMS and bonded to a glass-bottom Petri dish. The device containes a pillar system as entrance to the structures. A sterile wet tissue was placed inside the Petri dish to prevent humidity losses.

The design of the microfluidic device was done in AutoCAD 2019 and comprehended four types of mazes replicated 7 times each one, distributed randomly inside the design. Each maze contained the same volume and was filled with structures that followed a Hilbert curve pattern. The simplest of the mazes corresponded to the order 0 of the fractal, meaning that none of its inner structures were connected with each other, giving a complete accessibility to the space inside. The rest of the mazes were of order 1, 3 and 5, which means that the forming unit of the maze was 1, 3 or 5 iterations of the basic Hilbert curve unit, respectively. The microfluidic devices, previously filled with M9 medium containing AMC, were inoculated with PP and CC separately and together, and were followed for 10 days. Every 24 hours the microfluidic devices were imaged with epifluorescence microscopy so that data on fungal and bacterial biomass, and substrate degradation could be measured. The obtained images were subjected to alignment, background subtraction and measurement as a post processing step. Also, with the purpose of measuring how biomass and substrate degradation changed within the mazes, a spatial analysis of the fluorescence within the fractal mazes was performed, where fluorescence intensity was obtained as a function of the accessibility of each region of the maze.

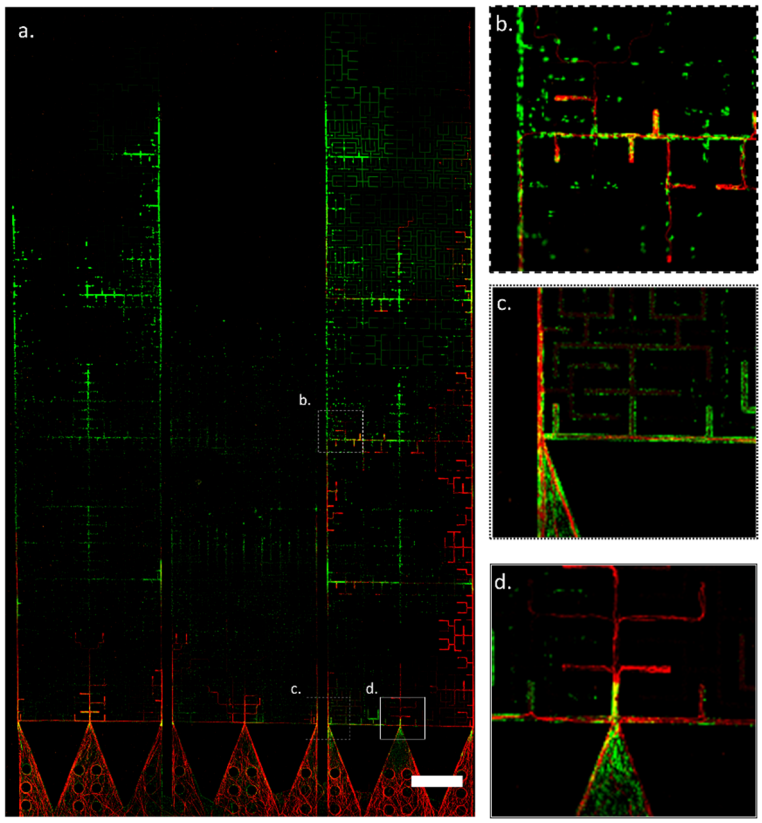

Figure 2. Fractal microfluidic device colonized by the fungal strain *Coprinopsis cinerea* expressing d-tomato (red) and the bacterial strain *Pseudomonas putida* expressing GFP, 24 hours after inoculation (a). Dead-ends colonized either by fungi or bacteria (b). Dead ends colonized by bacteria (c). Dead-ends colonized by fungi (d). Pictures were taken with 20x magnification. Scale bar represents 500 µm.

The data obtained indicates that the effect of the maze fractal order was different for bacteria and for fungi. Bacteria, contrary to our initial thought, had a higher biomass in the complex mazes, F3 and F5, compared to the lower order ones, F0 and F1. This phenomenon was stronger when looking at the substrate degradation (caused by bacteria mainly) which was consistently higher as maze fractal order increased. Fungi, on the other hand, were negatively affected as fractal order of the mazes increased, which was in line with our hypothesis. When both organisms, PP and CC, grew together, the biomass pattern of fungi was similar to when CC grew alone; whereas bacterial distribution pattern was changed, as the two complex mazes, F3 and F5, were colonized first, followed by a higher colonization in the following days in mazes F0 and F1. Substrate degradation, however, was similar to the bacterial treatment when both organisms were cultivated together, meaning that higher fractal order mazes showed the highest enzymatic activity.

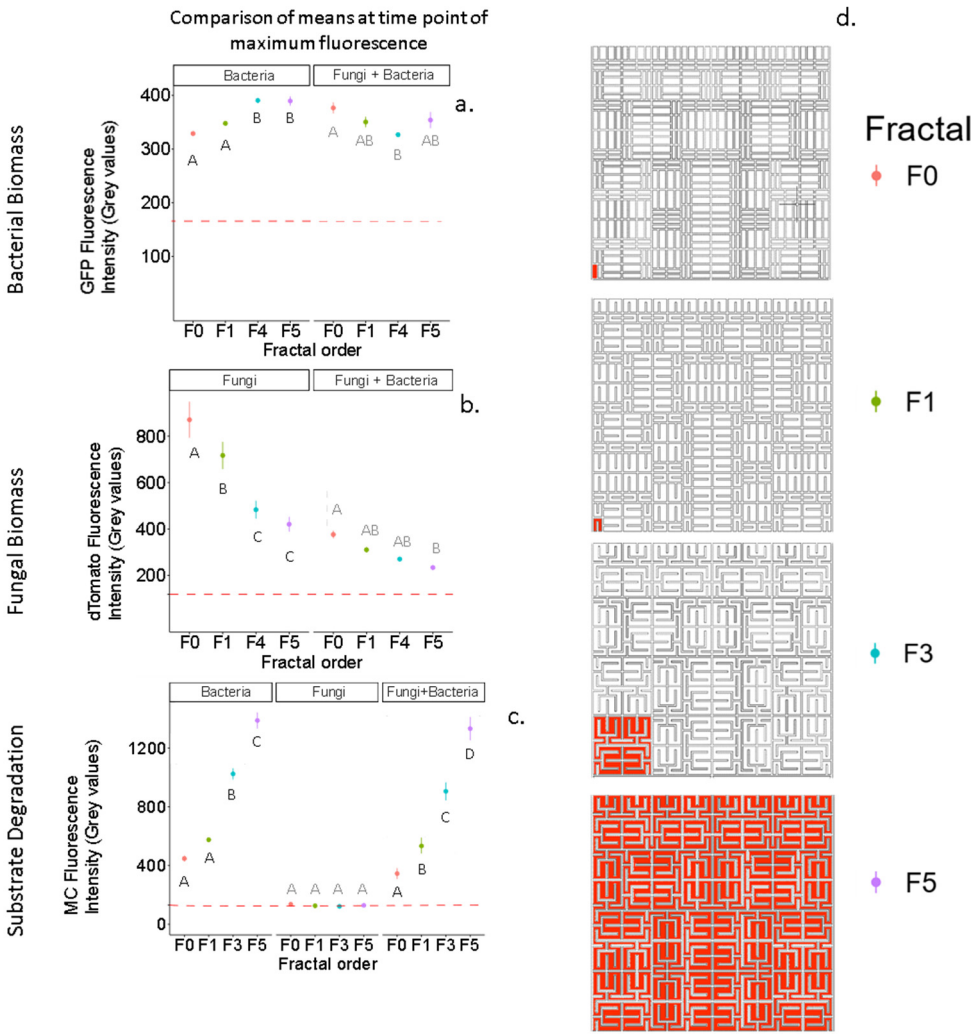

Figure 3 comparison of mean values of bacterial biomass (a), fungal biomass (b), and substrate degradation (c), between treatments on the day of maximum fluorescence signal. Capital letters under themean values indicate weather significant difference was found between means ($p<0.05$). The dashed red line shows the background fluorescence level for each fluorescence channel. The maze representation (d) indicates the basic structure of each maze. As mazes increase fractal order, the building block of the maze increases in size, and the overall connectivity of the maze decreases.

The spatial analysis of the mazes, which show how the fluorescence changed within the mazes, revealed that bacterial biomass decreased towards the innermost regions of the maze when growing alone. When growing with CC, however, bacterial biomass was especially affected in the most accessible regions, where it was lower, and increased towards the inner regions of the maze. This increase in bacterial biomass occurred until a certain region of the maze, after which it decreased. Fungal

biomass, on the other hand, always followed the same pattern, meaning it was high in the most accessible regions of the maze and decreased towards the inner regions. Substrate consumption, both in bacterial and in bacterial with fungal conditions, increased as accessibility of the maze decreased until a certain point of accessibility, after which substrate degradation decreased.

The reason why bacteria seem to benefit by habitat fragmentation is that an increase of obstacles, which limit or reduce interactions and competition, results in a wider variation of metabolic strategies that can co-occur even within the same clonal population. While a connected habitat favours only fast growers, which outcompete individuals with lower metabolic rates but higher nutrient acquisition efficiency, a fragmented habitat allows both strategies to survive, leading to a higher population and a jointly higher enzymatic activity. Also, the presence of dead ends and corners in the most complex mazes favours the accumulation of quorum sensing molecules which attract more bacteria that could be eventually forming biofilms with a higher nutrient acquisition efficiency. This did not occur in the fungal treatment, where the fungi, in order to colonize complex habitats, need to do more turns, and branch less, in comparison with a simpler habitat. Branching in open spaces mean that the mycelium exploration capacity would be doubled after every branching event. When one of the new branches encounters a dead end instead of an open space, the advantage that branching offers for space explorations is reduced. The same occurs with the turns that are necessary for exploring the maze. While growing in an open space does not demand turning or directional changes, encountering obstacles such as the studied mazes, forces fungi to turn, branch, and loose directionality, which occasions a reduction in the overall biomass.

These results as well indicate the importance of considering different microbial groups when trying to understand the role of habitat structure on soil processes. Also, it shows that the characteristics of the pore space can determine which microbes will be favoured, and the way those microbes would behave. In this sense, a well-connected habitat might be dominated by fungi, whereas a fragmented habitat would be dominated by bacteria, and would promote a higher bacterial growth with a wider variety of metabolic strategies and a higher substrate degradation efficiency

.

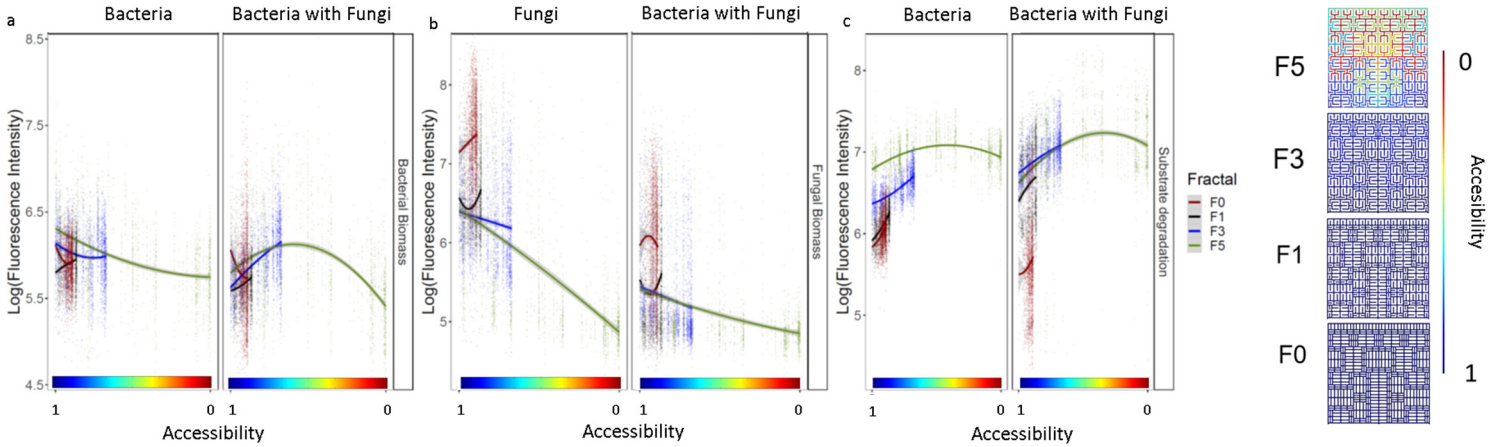

Figure 4. Distribution of bacterial (a) and fungal biomass (b), and substrate degradation (c) along the mazes. The x axis represents the accesibility region within each maze, being 1 the most acccesible regions located at the entrance of the maze, and 0 the regions with the lowest accesibility being the deepest region of the highest fractal order maze F5. Each dot represents the mean fluorescence of a specific region within the maze. The level of accesibility of each region of the maze was calculated using a COMSOL simulation of difussion. The lines in each pannel correspond to curve fittings using a quadratic model. The right pannels show how accesibility changes for each type of maze.

Effect of habitat complexity on a natural soil inoculum

The two previous studies analysed the effect of microhabitat structures on a bacterial and a fungal strain. A question remained whereas the obtained data could be relevant for a natural microbial community. Thus, a new set of experiments was performed in which the parameters of turning angle sharpness, as well as maze fractal order, were tested on a microbial inoculum extracted from soil (**Paper IV**).

The microfluidic devices containing the channels with different turning order and angle, and the ones containing mazes with different fractal orders, were first filled with M9 medium containing the fluorogenic aminopeptidase substrate AMC. The soil inoculum was obtained by suspending soil in water, followed by a sonication and a sedimentation step. The suspended liquid phase was then centrifuged, and the supernatant removed and replace by M9 medium. A small volume of this suspension was added to the microfluidic devices, which were imaged for 12 days using epifluorescence microscopy. The images obtained were aligned, their background subtracted to minimize autofluorescence noise, and measured to quantify fluorescence intensity inside each treatment. Fluorescence profiles were obtained from both, channels, and mazes, in order to see how substrate degradation changed in space within the studied structures.

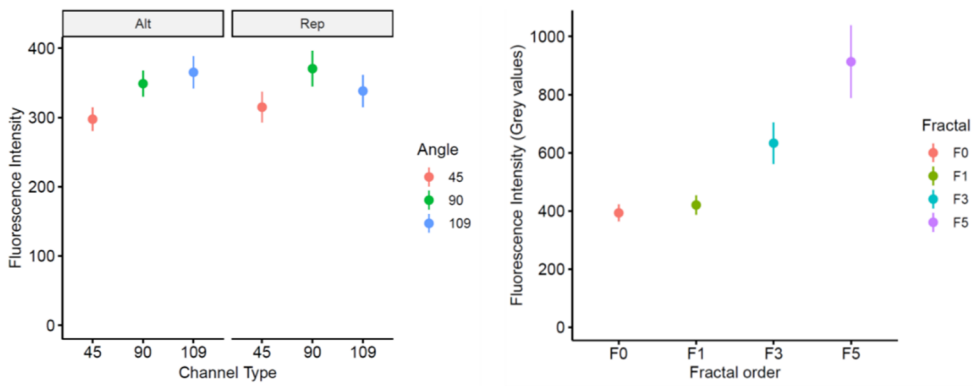

Figure 1. comparison of mean values of substrate AMC degradation within channels (left) and mazes (right). Data points correspond to the day of maximum fluorescence signal for each treatment type.

The image analysis showed that the substrate degradation generally was higher as the complexity of the structures increased. Sharper angles and higher fractal order mazes showed the highest enzymatic activity in the twelve days of experiment. DIC images indicate that the microfluidic devices were mainly colonized by bacteria and fungi while fungi were absent, and protozoa started growing only after the

experiment was over. Within the structures, spatial analysis indicated that the substrate degradation became higher towards the deeper regions of the channels and mazes until a specific point were degradation started to decrease.

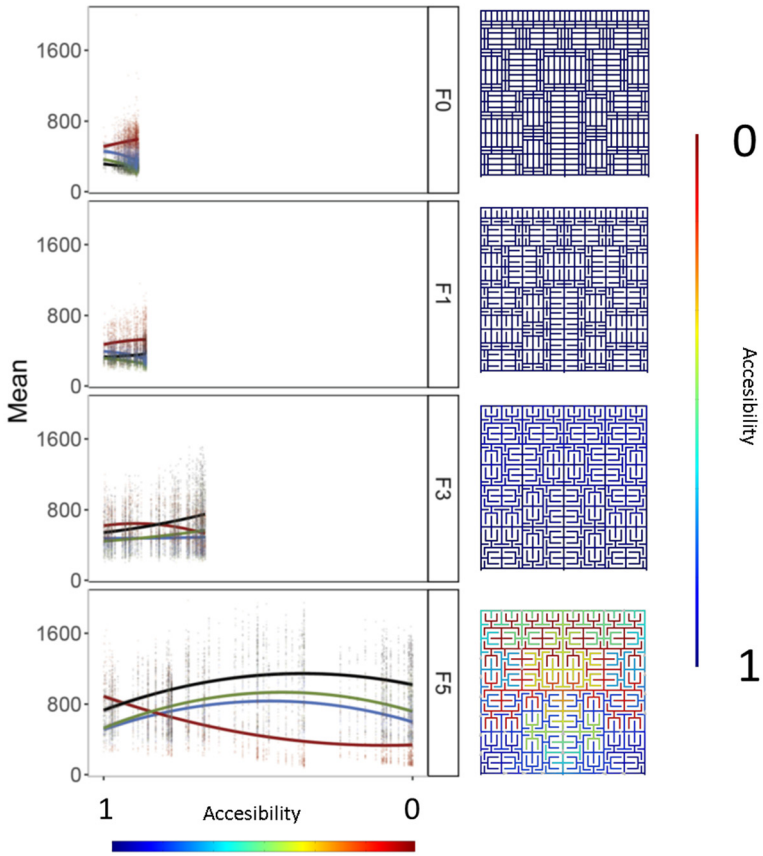

Figure 2. Distribution of substrate degradation along the studied mazes. The x axis shows the accesibility region within each maze, being 1 the most acccesible regions located at the entrance of the maze, and 0 the regions with the lowest accesibility being the deepest region of the highest fractal order maze F5. Different colors represent different time points: day 2 (red), day 5 (black), day 8 (green), and day 12 (grey). Each dot represents the mean fluorescence of AMC degradation in a specific region within the maze. The level of accesibility of each region of the maze was calculated using a COMSOL simulation of difussion. The lines in each pannel correspond to curve fittings using a quadratic model. The right pannels show how accesibility changes for each type of maze.

These results might be explained with the fact that a fragmented or a complex habitat reduced the interactions that exist between individuals of a microbial community. This occasions that the competition or the selection pressure inside fragmented habitats is lower, leading to a wider variety of metabolic strategies and species to coexist. As a result, communities, species, or individuals, typically slow growers but efficient at substrate acquisition, are not outcompeted by inefficient fast grower ones, leading to higher enzymatic degradation in complex habitats.

Synthesis and outlook

This project started with the idea that physical complexity in soil is a responsible factor for the soil carbon protection from microbial decomposers. In this sense, we first tested the effect of physical parameters on the dispersion of soil microorganisms and how these in turn modified their environment (**Paper I**). Then, we focused on studying the effect of complexity of a channel-like pore space on the growth on lab microbes and on substrate degradation (**Paper II**). We continued by evaluating the effect of complexity of a maze-like pore space on microbial growth of lab strains and nutrient degradation (**Paper III**). Finally, we tested the effect of channel and maze complexity on substrate degradation using a soil microbial inoculum (**Paper IV**). We found different and at first glance opposing results on the effect of increasingly complex structures on bacterial growth and substrate degradation. This, we think, is because we look at different aspects of spatial complexity that seem to affect bacterial growth in different was.

The way structures interact with microbes seem to depend, thus, on which of the microbial processes is affected. The two main processes that are being affected in our experiments are, to the best of our knowledge, accessibility and scale of competition. Channels with increasingly sharper turning angles seem to mainly affect the accessibility of the structures to the organisms by obstructing their navigation, whether they are bacteria or fungi. Fungi are more affected in this regard because a loss in directionality by one hypha in a certain region implies that the fungi would stop growing further at that specific point. Bacteria, however, are capable to find their ways through sharp turns because the directionality loss of an individual would not stop the growth of many more that would come after. The spatial shapes of the mazes, on the other hand, affect both accessibility of the structures and the possible interactions occurring inside them. The increasing number of dead-end paths and the decreasing connectivity of the channels create compartments where both, molecules, like enzymes, nutrients, or quorum sensing molecules, and cell movements are increasingly confined. This seems to be affecting fungi negatively but bacteria positively, which might be having a reduced competition with each other in complex habitats, which allow a wider range of metabolic strategies to emerge and cohabit. The lowered competition (or increased cooperation) seems to be happening at species level (intraspecific competition) and at community level (interspecific competition), which is reflected in the higher

substrate degradation inside complex habitats. Our results open up a variety of other questions:

- What is the role of surface properties in microbial and substrate accumulation? The experiments we performed were done using a silicone-based polymer, PDMS, which surface properties differ from the minerals that are the building blocks in the soil pore space. A closer approach to simulate these surfaces is thus crucial to increase our understanding of the impact of soil structure on microbial processes.
- How can the presence of a controlled air interface interact with physical properties of the pore space? Our experiments, beside our first one, consisted of a saturated interface where microbes could navigate freely. This scenario is possible to be found in the soil pore space under water-saturated conditions, but the upper layers of a soil are commonly found in a constant change, switching from being saturated to being filled with air gaps. Thus, including air gaps is crucial for a wider understanding of microbial processes at the pore scale.
- Are we seeing biofilm formation in our devices? Another crucial phenomenon seeing in microbes is the formation of biofilms or collective behaviour facilitated by quorum sensing. The impact of these processes in our experiments still remain as a hypothesis for we have not yet measured to what extent collective behaviour due to quorum sensing is occurring. And since these type of processes have been shown to determine the lifecycle of microbes in other areas, such as for pathogens studied in medicine, they might be occurring as well in soils.
- What occurs in the long term? Our experiments in the lab did not last more than 14 days. However, having a longer experiment would allow to study metabolic and genetic changes, having the proper methodology, inside microbial communities that could shed light on the long effect impact of structure on soil processes.

Of course, our methodology relies on a simplification of conditions in relation to real soils, but the fact that founding unintuitive results, sometimes contrary to our initial hypothesis, in such a simplified system, indicates that a more complex system becomes even more unpredictable and challenging to study. We hope that this study can thus serve as milestone for future soil microbial ecology studies where more parameters and even more complex conditions are tested.

Methodology used

Microfluidic device fabrication

Designs

The microfluidic devices used in the present work were design using AutoCAD. Three designs were created for the different studies which had different geometrical characteristics. The first design was used for **Paper I**, the second design for **Paper II** and **Paper IV**, and the third design for **Paper III** and **Paper IV**.

For **Paper I**, a design that contained different structure type was needed since we needed to test different aspects of microbial colonization. Hence, the structures inside comprehended a series of channels with different geometry in their angle, to test how microbial navigation could be influenced by them; it also contained a series of channels with diamonds along them to facilitate microbial dispersion measurements. The diameter of the channels used was 10 μm so that it would allow the entrance of all types of soil microorganisms.

The second design, used for **Paper II** and **Paper IV**, consisted of a series of channels connected to a common entrance. The channels were of 6 different types that varied in two parameters: turning angle (45°, 90°, or 109°) and turning order (alternated, or repeated). These three angles were selected so that they represent broadly the types of turning angles that exist in soil: obtuse, right, acute; and the turning orders were selected so that we could see if the impact of angles in the channels depends on how previous turns were, or if the effect were merely local. The width and height of the channels was 10 μm and 12 μm respectively so that they allow the entrance of fungal hyphae. Each microfluidic device contained 10 channels of each type distributed randomly along a rectangular pillar system that served as a common entrance.

In **Paper III** and **Paper IV** we used a third design that consisted of a series of mazes of different fractal order. The type of fractal used as a base unit for the mazes was the space-filling curve Hilbert curve. This fractal type was selected because it did not produce variation in channel size inside its structure, but rather it kept it homogeneous, with a fixed width of 10μm, independently of the fractal order used. Four fractal orders were tested: 1, 3, and 5, which corresponded to the number of iterations of the basic fractal unit. Also, as a way of testing the absence of any dead

end in the mazes, a 0-order fractal was included in the design, which differ from the order 1 fractal in that the middle wall of the basic unit, which produces a dead end, was removed, leaving only two opposed, non-connected walls, as the basic unit of the maze. The basic unit of each fractal order was multiplied until its structures filled the entire maze and produce the same normalized volume for all treatments. Each microfluidic device of this design contained seven replicates of each fractal order maze distributed randomly along a rectangular pillar system that served as entrance.

Mask and master fabrication

The Auto Cad designs were printed on photomasks to be later used for making the masters. The photomasks were made of soda lime glass with a thin layer of chromium (Nanofilm, CA, USA). The shapes of the designs were patterned with a dwl66+ mask writer (Heidelberg Instruments, Germany). A NdYag laser, 532 nm, was used to draw the patterns on a photoresist, AZ1500. The patterns were subsequently developed in AZ 351B positive developer and the chromium etched in TechniEtchCr01 (Microchemicals GmbH, Ulm Germany).

For the master fabrication, SU-8 2015 (MicroChem, Newton, MA, USA) was dispensed onto a previously heat-dried (90 degrees 30 minutes) 3- inch silicon wafer (Siegert Wafer, Aachen, Germany) and spun at 4000 rpm to obtain a 12 μm thick layer. The SU-8 was exposed to UV-light using a mask aligner that contained the mask (Karl Suss MJB4 soft UV, Munich, Germany). The photoresist that was not crosslinked after UV exposure was developed (MrDev600) and rinsed with isopropanol. To prevent PDMS from sticking to the master, the wafer was activated in an oxygen plasma for 60 seconds (ZEPTO, Diener Plasma-Surface Technology, Germany) and exposed overnight to a vapor of trichloro (1H,1H,2H,2H-perfluorooctyl) silane (PFOTS, Sigma Aldrich, Saint Louis, MO, USA) at 180 degrees during which a monolayer is formed.

PDMS and microfluidic device obtention

SYLGARDTM 184 PDMS (Dow Chemicals Company, Midland, Michigan) was obtained by mixing the elastomer with the curing agent in a mass proportion of 10:1, poured on the master, degassed at -15 kPa for one hour and polymerized in an oven at 60 ˚C for two hours.

The PDMS labyrinths were removed from the master and an entrance was opened in the pillar system. Depending on the design, the entrance had different dimensions. For the first design, a cut that covered the entire pillar system was done and the remaining PDMS was removed to leave the pillar system exposed to the exterior. For the second and third design, a rectangular portion of 2.5 cm x 0.5 cm and 3 cm x 0.5 cm respectively was cut out in the middle of the pillar system, approximately

0.5 cm away from the entrance of every channel or maze. This cut was made to create the reservoir that served as entrance to the labyrinth. The PDMS labyrinths and an object glass for the first design or a glass bottom Petri dish for the second and third design were activated using a Zepto Plasma System (Diener Plasma Surface Technology, Germany; negative polarity; 1 min for cover slips and 10 seconds for PDMS labyrinths). Directly after activation, the surfaces were put together, forming a tight, irreversible bond, and the treatment medium was introduced through the pillar system to keep the channels hydrophilic.

Inoculation process

Belowground inoculation

The inoculation was done differently depending on the project. For **Paper I**, two conditions were used: one with the microfluidic devices buried in the soil, and the other having a portion of soil at the microfluidic device entrance.

Fungal inoculation

For **Paper II** and **Paper III**, the inoculation was done with the fungal strain Coprinopsis cinerea that expressed constitutively the fluorescent protein d-tomato. The mother culture of each experiment was precultured for 2 weeks on YMG medium at 21°C. A rectangular portion of the outer colony part was cut out and placed at the pillar system entrance of the microfluidic device.

Bacterial inoculation

Bacterial inoculation for **Paper II** and **Paper III** was done using the bacterial strain *Pseudomonas putida* mt-2 that expressed constitutively the fluorescent protein GFP. For inoculation, an overnight culture of PP was prepared in M9 medium with PH 6.5 at 28°C and 150 rpm. On the day of the experiment, overnight culture was centrifuged at 5000 rpm for 10 min and the supernatant was disposed. The obtained pellet was resuspended in fresh M9 medium with PH of 6.5 containing the fluorogenic substrate AMC. The bacterial concentration was measured as optical density and a volume was added to the microfluidic device so that the final concentration of bacteria inside the device was 0.2 OD_{600}. In experiments were bacteria was cultivated together with fungi, in order to avoid priority effects, the inoculation of bacteria was done after fungal hyphae had grown sufficiently inside the pillar system.

Natural inoculum

For the inoculation with a natural soil microbial community, a soil sample taken from the sample plot of the Ecology Building was mixed with water and vortexed for three minutes. The mix was let to repose for one minute so that coarse sand particles could precipitate. The liquid phase was later centrifuged at 5000 rpm for 10 minutes and the supernatant was removed. Fresh M9 medium containing the AMC substrate was added to the pellet and resuspended. Centrifugation and resuspension allowed us to have a more homogeneous inoculum and helped to avoid priority effects in the experiments.

Microscopy

Two main microscopy techniques were used in the experiments: DIC and epifluorescence microscopy. DIC was used in experimental conditions were fluorescent microbial populations were not present.

For the visualization of the fluorescent strains and the AMC degradation, epifluorescence microscopy was performed using a fully motorized Nikon Ti2-E inverted microscope with PFS4 hardware autofocus, full 25 mm field-of-view, CoolLED pE300-White MB illumination connected via a 3 mm liquid light guide (LLG). Grey scale pictures were taken with a Nikon Qi2 camera with 1x F-mount adapter. The filters used in the experiments were a LED-DAPI-A- 2360A Semrock Filter Cube (Ex: 380-405 nm, Em: 413-480 nm) for measuring AMC degradation, GFP-4050B Semrock Filter Cube (Ex: 444-488 nm, Em: 498-553 nm) for PP biomass, and mCherry-C Semrock Filter Cube (Ex: 520-585 nm, Em: 600-680 nm) for CC biomass. Entire microfluidic device images for overall fluorescence quantification were obtained using a (MRH00041) CFI Plan Fluor 4X, N.A. 0.13, W.D. 17.1 mm objective, with an exposure time of 20 ms for GFP, 100 ms for DAPI, and 100 ms for mCherry. For high magnification picture acquisition, a (MRD31905) CFI Plan Apochromat DM Lambda 100X Oil N.A. 1.45, W.D. 0.13mm and a (MRD30405) CFI Plan Apochromat DM Lambda 40X, N.A. 0.95, W.D. 0.21mm objectives were used. The JOBS package included in the NIS-Elements software was used for coordination of the multipoint imaging. Pictures were taken for every chip every 24 hours for the entire duration of each experiment. The days selected for analysis were the ones of maximum fluorescent signal.

Image analysis

DIC images from **Paper I** were studied visually to detect the presence of fungal hyphae, bacterial cells, or protozoa. Measurement rulers that were part of the design were used to indicate distance inside each channel type.

Fluorescence images obtained for **Paper II**, **Paper III**, and **Paper IV**, were post-processed in order to have them aligned in the same fashion and background subtracted before measurements could be performed in them. Background subtraction was done using the rolling ball algorithm with a rolling ball radius of 7 pixels which corresponded to the width of the microfluidic channels in the 4x images. Measurements of fluorescence intensity were done using a ROI measurement which calculated the mean fluorescence intensity of all the pixels contained in a rectangular ROI that contained either a channel or a maze depending on the microfluidic device. The software used for the image analysis was Image J.

For profile measurements of fluorescence along channels, the multiline measurement tool of Image J was used. In the case of fluorescence profiles for mazes a diffusion model for accessibility estimation was used. Using COMSOL we evaluated the necessary time of each region of the maze to reach half the concentration of a given particle, assuming a concentration 0 at the beginning of the simulation and a source of the particle located in the entrance of the mazes. The level of accessibility was given from 1 to 0, being 1 the most accessible regions of the maze, and 0 the regions that took the longest to reach half the concentration of the simulated particle in the most complex maze. The accessibility of each region of the mazes was compared to the fluorescence measured using the ROI measurement of the second fractal unit of each maze type, located approximately in the middle section of each maze, to obtain the fluorescence profiles as a function of the accessibility.

Statistics

For statistical analysis, data from the day showing maximum fluorescence was chosen. One, two- and three-way ANOVA were used depending on the number of factors considered in the experiments.

The experiments had a full-factorial design were all the structure conditions were tested for all culture conditions. Each chip had all the structures tested, either channels or mazes. Multilevel model fitting correcting for random effects was used to test the influence of every factor on the variables. Additionally, for testing significant differences in variances three-way or two-way multivariate ANOVA correcting for random effects was conducted using R. Random effects were

attributed to each microfluidic device as a physical replicate of the experiments. Fluorescence data was log-transformed when necessary to obtain normality of the residuals and homogeneity of variances. The significance threshold used for all statistical tests was $p < 0.05$. When significant differences were found in ANOVA, interactions were analysed separately using Dunn's method for multiple comparison of means. Pairwise comparisons were performed with t-tests, using Holm corrected p-values.

Also, linear regressions were done using R, with bacterial biomass, fungal biomass, and substrate consumption as dependent variables and tortuosity of the channels as independent variables.

References

Adler, M., Erickstad, M., Gutierrez, E., & Groisman, A. (2012). Studies of bacterial aerotaxis in a microfluidic device. *Lab on a Chip*. https://doi.org/10.1039/c2lc21006a

Ahmed, T., Shimizu, T. S., & Stocker, R. (2010). Microfluidics for bacterial chemotaxis. In *Integrative Biology*. https://doi.org/10.1039/c0ib00049c

Ahmed, T., & Stocker, R. (2008). Experimental verification of the behavioral foundation of bacterial transport parameters using microfluidics. *Biophysical Journal*. https://doi.org/10.1529/biophysj.108.134510

Aleklett, K., Kiers, E. T., Ohlsson, P., Shimizu, T. S., Caldas, V. E., & Hammer, E. C. (2018). Build your own soil: Exploring microfluidics to create microbial habitat structures. In *ISME Journal* (Vol. 12, Issue 2, pp. 312–319). https://doi.org/10.1038/ismej.2017.184

Altshuler, E., Miño, G., Pérez-Penichet, C., Río, L. Del, Lindner, A., Rousselet, A., & Clément, E. (2013). Flow-controlled densification and anomalous dispersion of E. coli through a constriction. *Soft Matter*. https://doi.org/10.1039/c2sm26460a

Ananyeva, K., Wang, W., Smucker, A. J. M., Rivers, M. L., & Kravchenko, A. N. (2013). Can intra-aggregate pore structures affect the aggregate's effectiveness in protecting carbon? *Soil Biology and Biochemistry*. https://doi.org/10.1016/j.soilbio.2012.10.019

Anselme, K., Davidson, P., Popa, A. M., Giazzon, M., Liley, M., & Ploux, L. (2010). The interaction of cells and bacteria with surfaces structured at the nanometre scale. In *Acta Biomaterialia*. https://doi.org/10.1016/j.actbio.2010.04.001

Arah, J. R. M., & Vinten, A. J. A. (1995). Simplified models of anoxia and denitrification in aggregated and simple-structured soils. *European Journal of Soil Science*. https://doi.org/10.1111/j.1365-2389.1995.tb01347.x

Baveye, P. C., Laba, M., Otten, W., Bouckaert, L., Dello Sterpaio, P., Goswami, R. R., Grinev, D., Houston, A., Hu, Y., Liu, J., Mooney, S., Pajor, R., Sleutel, S., Tarquis, A., Wang, W., Wei, Q., & Sezgin, M. (2010). Observer-dependent variability of the thresholding step in the quantitative analysis of soil images and X-ray microtomography data. *Geoderma*. https://doi.org/10.1016/j.geoderma.2010.03.015

Baveye, P. C., Otten, W., Kravchenko, A., Balseiro-Romero, M., Beckers, É., Chalhoub, M., Darnault, C., Eickhorst, T., Garnier, P., Hapca, S., Kiranyaz, S., Monga, O., Mueller, C. W., Nunan, N., Pot, V., Schlüter, S., Schmidt, H., & Vogel, H. J. (2018). Emergent properties of microbial activity in heterogeneous soil microenvironments: Different research approaches are slowly converging, yet major challenges remain. In *Frontiers in Microbiology*. https://doi.org/10.3389/fmicb.2018.01929

Beebe, D. J., Mensing, G. A., & Walker, G. M. (2002). Physics and Applications of Microfluidics in Biology. *Annual Review of Biomedical Engineering*. https://doi.org/10.1146/annurev.bioeng.4.112601.125916

Bejat, L., Perfect, E., Quisenberry, V. L., Coyne, M. S., & Haszler, G. R. (2000). Solute transport as related to soil structure in unsaturated intact soil blocks. *Soil Science Society of America Journal*. https://doi.org/10.2136/sssaj2000.643818x

Bot, A., & Benites, J. (2005). The importance of soil organic matter. *FAO Soils Bulletin*. https://doi.org/10.1080/03650340214162

Brody, J. P., Yager, P., Goldstein, R. E., & Austin, R. H. (1996). Biotechnology at low Reynolds numbers. *Biophysical Journal*. https://doi.org/10.1016/S0006-3495(96)79538-3

Bruand, A., & Cousin, I. (1995). Variation of textural porosity of a clay-loam soil during compaction. *European Journal of Soil Science*. https://doi.org/10.1111/j.1365-2389.1995.tb01334.x

Cheng, S. Y., Heilman, S., Wasserman, M., Archer, S., Shuler, M. L., & Wu, M. (2007). A hydrogel-based microfluidic device for the studies of directed cell migration. *Lab on a Chip*. https://doi.org/10.1039/b618463d

Choi, J.-W., Kim, S., Trichur, R., Cho, H. J., Puntambekar, A., Cole, R. L., Simkins, J. R., Murugesan, S., Kim, K., Lee, J.-B. J. B., Beaucage, G., Nevin, J. H., & Ahn, C. H. (2001). A Plastic Micro Injection Molding Technique Using Replaceable Mold-Disks for Disposable Microfluidic Systems and Biochips. In *Micro Total Analysis Systems 2001: Proceedings of the micro-TAS 2001 Symposium, held in Monterey, CA, USA 21--25 October, 2001*. https://doi.org/10.1007/978-94-010-1015-3_181

Cnudde, V., & Boone, M. N. (2013). High-resolution X-ray computed tomography in geosciences: A review of the current technology and applications. In *Earth-Science Reviews*. https://doi.org/10.1016/j.earscirev.2013.04.003

Darbyshire, J. F., Chapman, S. J., Cheshire, M. V., Gauld, J. H., McHardy, W. J., Paterson, E., & Vaughan, D. (1993). Methods for the study of interrelationships between micro-organisms and soil structure. *Geoderma*. https://doi.org/10.1016/0016-7061(93)90097-5

De Gryze, S., Jassogne, L., Six, J., Bossuyt, H., Wevers, M., & Merckx, R. (2006). Pore structure changes during decomposition of fresh residue: X-ray tomography analyses. *Geoderma*. https://doi.org/10.1016/j.geoderma.2005.09.002

De La Fuente, L., Montanes, E., Meng, Y., Li, Y., Burr, T. J., Hoch, H. C., & Wu, M. (2007). Assessing adhesion forces of type I and type IV pili of Xylella fastidiosa bacteria by use of a microfluidic flow chamber. *Applied and Environmental Microbiology*. https://doi.org/10.1128/AEM.02649-06

Deng, J., Orner, E. P., Chau, J. F., Anderson, E. M., Kadilak, A. L., Rubinstein, R. L., Bouchillon, G. M., Goodwin, R. A., Gage, D. J., & Shor, L. M. (2015). Synergistic effects of soil microstructure and bacterial EPS on drying rate in emulated soil micromodels. *Soil Biology and Biochemistry*. https://doi.org/10.1016/j.soilbio.2014.12.006

Derenne, S., & Largeau, C. (2001). A review of some important families of refractory macromolecules: Composition, origin, and fate in soils and sediments. In *Soil Science*. https://doi.org/10.1097/00010694-200111000-00008

Diao, J., Young, L., Kim, S., Fogarty, E. A., Heilman, S. M., Zhou, P., Shuler, M. L., Wu, M., & DeLisa, M. P. (2006). A three-channel microfluidic device for generating static linear gradients and its application to the quantitative analysis of bacterial chemotaxis. *Lab on a Chip*. https://doi.org/10.1039/b511958h

DiLuzio, W. R., Turner, L., Mayer, M., Garstecki, P., Weibel, D. B., Berg, H. C., & Whitesides, G. M. (2005). Escherichia coli swim on the right-hand side. *Nature*. https://doi.org/10.1038/nature03660

Drescher, K., Shen, Y., Bassler, B. L., & Stone, H. A. (2013). Biofilm streamers cause catastrophic disruption of flow with consequences for environmental and medical systems. *Proceedings of the National Academy of Sciences*. https://doi.org/10.1073/pnas.1300321110

Ferrand, L. A., & Celia, M. A. (1992). The effect of heterogeneity on the drainage capillary pressure-saturation relation. *Water Resources Research*. https://doi.org/10.1029/91WR02679

Forum, G. H. (2009). The Anatomy of a Silent Crisis. *Chief Executive*.

Gachelin, J., Miño, G., Berthet, H., Lindner, A., Rousselet, A., & Clément, É. (2013). Non-newtonian viscosity of escherichia coli suspensions. *Physical Review Letters*. https://doi.org/10.1103/PhysRevLett.110.268103

Galajda, P., Keymer, J., Chaikin, P., & Austin, R. (2007). A wall of funnels concentrates swimming bacteria. *Journal of Bacteriology*. https://doi.org/10.1128/JB.01033-07

Gallet-Budynek, A., Brzostek, E., Rodgers, V. L., Talbot, J. M., Hyzy, S., & Finzi, A. C. (2009). Intact amino acid uptake by northern hardwood and conifer trees. *Oecologia*. https://doi.org/10.1007/s00442-009-1284-2

Gramss, G., Voigt, K. D., & Kirsche, B. (1999). Degradation of polycyclic aromatic hydrocarbons with three to seven aromatic rings by higher fungi in sterile and unsterile soils. *Biodegradation*. https://doi.org/10.1023/A:1008368923383

Hamer, U., Marschner, B., Brodowski, S., & Amelung, W. (2004). Interactive priming of black carbon and glucose mineralisation. *Organic Geochemistry*. https://doi.org/10.1016/j.orggeochem.2004.03.003

Hazen, T. C., Dubinsky, E. A., DeSantis, T. Z., Andersen, G. L., Piceno, Y. M., Singh, N., Jansson, J. K., Probst, A., Borglin, S. E., Fortney, J. L., Stringfellow, W. T., Bill, M., Conrad, M. E., Tom, L. M., Chavarria, K. L., Alusi, T. R., Lamendella, R., Joyner, D. C., Spier, C., … Mason, O. U. (2010). Deep-sea oil plume enriches indigenous oil-degrading bacteria. *Science*. https://doi.org/10.1126/science.1195979

Hedges, J. I., Eglinton, G., Hatcher, P. G., Kirchman, D. L., Arnosti, C., Derenne, S., Evershed, R. P., Kögel-Knabner, I., De Leeuw, J. W., Littke, R., Michaelis, W., & Rullkötter, J. (2000). The molecularly-uncharacterized component of nonliving organic matter in natural environments. In *Organic Geochemistry*. https://doi.org/10.1016/S0146-6380(00)00096-6

Hobbie, J. E., & Hobbie, E. A. (2013). Microbes in nature are limited by carbon and energy: The starving-survival lifestyle in soil and consequences for estimating

microbial rates. *Frontiers in Microbiology*, *4*(NOV), 1–11. https://doi.org/10.3389/fmicb.2013.00324

Hochbaum, A. I., & Aizenberg, J. (2010). Bacteria pattern spontaneously on periodic nanostructure arrays. *Nano Letters*. https://doi.org/10.1021/nl102290k

Holz, C., Opitz, D., Mehlich, J., Ravoo, B. J., & Maier, B. (2009). Bacterial motility and clustering guided by microcontact printing. *Nano Letters*. https://doi.org/10.1021/nl903153c

Hudson, S. D., Phelan, F. R., Handler, M. D., Cabral, J. T., Migler, K. B., & Amis, E. J. (2004). Microfluidic analog of the four-roll mill. *Applied Physics Letters*. https://doi.org/10.1063/1.1767594

IPCC. (2013). Working Group I Contribution to the IPCC Fifth Assessment Report, Climate Change 2013: The Physical Science Basis. In *IPCC* (Vol. AR5).

Jerauld, G. R., & Salter, S. J. (1990). The effect of pore-structure on hysteresis in relative permeability and capillary pressure: Pore-level modeling. *Transport in Porous Media*. https://doi.org/10.1007/BF00144600

Jones, D. L., Kielland, K., Sinclair, F. L., Dahlgren, R. A., Newsham, K. K., Farrar, J. F., & Murphy, D. V. (2009). Soil organic nitrogen mineralization across a global latitudinal gradient. *Global Biogeochemical Cycles*. https://doi.org/10.1029/2008GB003250

Karadimitriou, N. K., & Hassanizadeh, S. M. (2012). A Review of Micromodels and Their Use in Two-Phase Flow Studies. *Vadose Zone Journal*. https://doi.org/10.2136/vzj2011.0072

Kasting, J. F., Toon, O., & Pollack, J. B. (1988). How climate evolved on the terrestrial planets. *Scientific American*. https://doi.org/10.1038/scientificamerican0288-90

Katuwal, S., Norgaard, T., Moldrup, P., Lamandé, M., Wildenschild, D., & de Jonge, L. W. (2015). Linking air and water transport in intact soils to macropore characteristics inferred from X-ray computed tomography. *Geoderma*. https://doi.org/10.1016/j.geoderma.2014.08.006

Khoury, C., Mensing, G. A., & Beebe, D. J. (2002). Ultra rapid prototyping of microfluidic systems using liquid phase photopolymerization. *Lab on a Chip*. https://doi.org/10.1039/b109344d

Kim, M. J., & Breuer, K. S. (2004). Enhanced diffusion due to motile bacteria. *Physics of Fluids*. https://doi.org/10.1063/1.1787527

Kim, M. J., & Breuer, K. S. (2007). Use of Bacterial Carpets to Enhance Mixing in Microfluidic Systems. *Journal of Fluids Engineering*. https://doi.org/10.1115/1.2427083

Kravchenko, A. N., Negassa, W. C., Guber, A. K., & Rivers, M. L. (2015). Protection of soil carbon within macro-aggregates depends on intra-aggregate pore characteristics. *Scientific Reports*. https://doi.org/10.1038/srep16261

Kumar, A., Karig, D., Acharya, R., Neethirajan, S., Mukherjee, P. P., Retterer, S., & Doktycz, M. J. (2013). Microscale confinement features can affect biofilm formation. *Microfluidics and Nanofluidics*. https://doi.org/10.1007/s10404-012-1120-6

Lal, R. (2008). Carbon sequestration. *Philosophical Transactions of the Royal Society of London. Series B, Biological Sciences*, *363*(1492), 815–830. https://doi.org/10.1098/rstb.2007.2185

Lambert, G., Liao, D., & Austin, R. H. (2010). Collective escape of chemotactic swimmers through microscopic ratchets. *Physical Review Letters*. https://doi.org/10.1103/PhysRevLett.104.168102

Larsbo, M., Koestel, J., Kätterer, T., & Jarvis, N. (2016). Preferential Transport in Macropores is Reduced by Soil Organic Carbon. *Vadose Zone Journal*. https://doi.org/10.2136/vzj2016.03.0021

Lauga, E., DiLuzio, W. R., Whitesides, G. M., & Stone, H. A. (2006). Swimming in circles: Motion of bacteria near solid boundaries. *Biophysical Journal*. https://doi.org/10.1529/biophysj.105.069401

Lecuyer, S., Rusconi, R., Shen, Y., Forsyth, A., Vlamakis, H., Kolter, R., & Stone, H. A. (2011). Shear stress increases the residence time of adhesion of Pseudomonas aeruginosa. *Biophysical Journal*. https://doi.org/10.1016/j.bpj.2010.11.078

Lehmann, J., & Kleber, M. (2015). The contentious nature of soil organic matter. In *Nature*. https://doi.org/10.1038/nature16069

Liang, C., Schimel, J. P., & Jastrow, J. D. (2017). The importance of anabolism in microbial control over soil carbon storage. In *Nature Microbiology*. https://doi.org/10.1038/nmicrobiol.2017.105

Lowell, S., Shields, J. E., Thomas, M. A., & Thommes, M. (2004). Characterization of Porous Solids and Powders-Surface Area, Pore Size and Density. *Particle Technology Series*. https://doi.org/10.1007/978-1-4020-2303-3

Lützow, M. V., Kögel-Knabner, I., Ekschmitt, K., Matzner, E., Guggenberger, G., Marschner, B., & Flessa, H. (2006). Stabilization of organic matter in temperate soils: Mechanisms and their relevance under different soil conditions - A review. In *European Journal of Soil Science*. https://doi.org/10.1111/j.1365-2389.2006.00809.x

Mao, H., Cremer, P. S., & Manson, M. D. (2003). A sensitive, versatile microfluidic assay for bacterial chemotaxis. *Proceedings of the National Academy of Sciences*. https://doi.org/10.1073/pnas.0931258100

Marcos, Fu, H. C., Powers, T. R., & Stocker, R. (2009). Separation of microscale chiral objects by shear flow. *Physical Review Letters*. https://doi.org/10.1103/PhysRevLett.102.158103

Marcos, & Stocker, R. (2006). Microorganisms in vortices: A microfluidic setup. *Limnology and Oceanography: Methods*. https://doi.org/10.4319/lom.2006.4.392

Marty, A., Roques, C., Causserand, C., & Bacchin, P. (2012). Formation of bacterial streamers during filtration in microfluidic systems. *Biofouling*. https://doi.org/10.1080/08927014.2012.695351

Masson, J.-B., Voisinne, G., Wong-Ng, J., Celani, A., & Vergassola, M. (2012). Noninvasive inference of the molecular chemotactic response using bacterial trajectories. *Proceedings of the National Academy of Sciences*. https://doi.org/10.1073/pnas.1116772109

McDowell, W. H., Zsolnay, a., Aitkenhead-Peterson, J. a., Gregorich, E. G., Jones, D. L., Jödemann, D., Kalbitz, K., Marschner, B., & Schwesig, D. (2006). A comparison of

methods to determine the biodegradable dissolved organic carbon from different terrestrial sources. *Soil Biology and Biochemistry*, *38*, 1933–1942. https://doi.org/10.1016/j.soilbio.2005.12.018

Myneni, S. C. B., Brown, J. T., Martinez, G. A., & Meyer-Ilse, W. (1999). Imaging of humic substance macromolecular structures in water and soils. *Science*. https://doi.org/10.1111/j.0022-1856.2004.00144.x

Naveed, M., Moldrup, P., Vogel, H. Jö., Lamandé, M., Wildenschild, D., Tuller, M., & de Jonge, L. W. (2014). Impact of long-term fertilization practice on soil structure evolution. *Geoderma*. https://doi.org/10.1016/j.geoderma.2013.12.001

Negassa, W. C., Guber, A. K., Kravchenko, A. N., Marsh, T. L., Hildebrandt, B., & Rivers, M. L. (2015). Properties of soil pore space regulate pathways of plant residue decomposition and community structure of associated bacteria. *PLoS ONE*. https://doi.org/10.1371/journal.pone.0123999

Nimmo, J. R. (2013). Porosity and Pore Size Distribution. In *Reference Module in Earth Systems and Environmental Sciences*. https://doi.org/10.1016/B978-0-12-409548-9.05265-9

Pagliai, M., Vignozzi, N., & Pellegrini, S. (2004). Soil structure and the effect of management practices. *Soil and Tillage Research*. https://doi.org/10.1016/j.still.2004.07.002

Paradelo, M., Katuwal, S., Moldrup, P., Norgaard, T., Herath, L., & de Jonge, L. W. (2016). X-ray CT-Derived Soil Characteristics Explain Varying Air, Water, and Solute Transport Properties across a Loamy Field. *Vadose Zone Journal*. https://doi.org/10.2136/vzj2015.07.0104

Pedersen, L. L., Smets, B. F., & Dechesne, A. (2015). Measuring biogeochemical heterogeneity at the micro scale in soils and sediments. In *Soil Biology and Biochemistry*. https://doi.org/10.1016/j.soilbio.2015.08.003

Piccolo, A. (2001). The supramolecular structure of humic substances. In *Soil Science*. https://doi.org/10.1097/00010694-200111000-00007

Pires, L. F., Bacchi, O. O. S., Reichardt, K., & Timm, L. C. (2005). Application of γ-ray computed tomography to analysis of soil structure before density evaluations. *Applied Radiation and Isotopes*. https://doi.org/10.1016/j.apradiso.2005.03.019

Pohlmeier, A., Oros-Peusquens, A., Javaux, M., Menzel, M. I., Vanderborght, J., Kaffanke, J., Romanzetti, S., Lindenmair, J., Vereecken, H., & Shah, N. J. (2008). Changes in Soil Water Content Resulting from Root Uptake Monitored by Magnetic Resonance Imaging. *Vadose Zone Journal*. https://doi.org/10.2136/vzj2007.0110

Rabot, E., Wiesmeier, M., Schlüter, S., & Vogel, H. J. (2018). Soil structure as an indicator of soil functions: A review. In *Geoderma*. https://doi.org/10.1016/j.geoderma.2017.11.009

Ritz, K., & Iain, Y. (2012). The Architecture and Biology of Soils: Life in Inner Space - by Ritz, K. & Young, I. *European Journal of Soil Science*. https://doi.org/10.1111/j.1365-2389.2012.01454.x

Roberts, M. A., Rossier, J. S., Bercier, P., & Girault, H. (1997). UV laser machined polymer substrates for the development of microdiagnostic systems. *Analytical Chemistry*. https://doi.org/10.1021/ac961038q

Rubinstein, R. L., Kadilak, A. L., Cousens, V. C., Gage, D. J., & Shor, L. M. (2015). Protist-facilitated particle transport using emulated soil micromodels. *Environmental Science and Technology*. https://doi.org/10.1021/es503424z

Rubol, S., Dutta, T., & Rocchini, D. (2016). 2D visualization captures the local heterogeneity of oxidative metabolism across soils from diverse land-use. *Science of the Total Environment*. https://doi.org/10.1016/j.scitotenv.2016.06.252

Rusconi, R., Garren, M., & Stocker, R. (2014). Microfluidics Expanding the Frontiers of Microbial Ecology. *Annual Review of Biophysics*. https://doi.org/10.1146/annurev-biophys-051013-022916

Rusconi, R., Lecuyer, S., Autrusson, N., Guglielmini, L., & Stone, H. A. (2011). Secondary flow as a mechanism for the formation of biofilm streamers. *Biophysical Journal*. https://doi.org/10.1016/j.bpj.2011.01.065

Rusconi, R., Lecuyer, S., Guglielmini, L., & Stone, H. A. (2010). Laminar flow around corners triggers the formation of biofilm streamers. *Journal of the Royal Society Interface*. https://doi.org/10.1098/rsif.2010.0096

Salman, H., Zilman, A., Loverdo, C., Jeffroy, M., & Libchaber, A. (2006). Solitary modes of bacterial culture in a temperature gradient. *Physical Review Letters*. https://doi.org/10.1103/PhysRevLett.97.118101

Saragosti, J., Calvez, V., Bournaveas, N., Perthame, B., Buguin, A., & Silberzan, P. (2011). Directional persistence of chemotactic bacteria in a traveling concentration wave. *Proceedings of the National Academy of Sciences*. https://doi.org/10.1073/pnas.1101996108

Schaap, J. D., Lehmann, P., Kaestner, A., Vontobel, P., Hassanein, R., Frei, G., de Rooij, G. H., Lehmann, E., & Flühler, H. (2008). Measuring the effect of structural connectivity on the water dynamics in heterogeneous porous media using speedy neutron tomography. *Advances in Water Resources*. https://doi.org/10.1016/j.advwatres.2008.04.014

Schmidt, M. W. I., Torn, M. S., Abiven, S., Dittmar, T., Guggenberger, G., Janssens, I. A., Kleber, M., Kögel-Knabner, I., Lehmann, J., Manning, D. A. C., Nannipieri, P., Rasse, D. P., Weiner, S., & Trumbore, S. E. (2011). Persistence of soil organic matter as an ecosystem property. In *Nature*. https://doi.org/10.1038/nature10386

Shen, Y., Siryaporn, A., Lecuyer, S., Gitai, Z., & Stone, H. A. (2012). Flow directs surface-attached bacteria to twitch upstream. *Biophysical Journal*. https://doi.org/10.1016/j.bpj.2012.05.045

Sing, K. S. W. (1985). Reporting physisorption data for gas/solid systems with special reference to the determination of surface area and porosity (Recommendations 1984). *Pure and Applied Chemistry*. https://doi.org/10.1351/pac198557040603

Six, J., Bossuyt, H., Degryze, S., & Denef, K. (2004). A history of research on the link between (micro)aggregates, soil biota, and soil organic matter dynamics. In *Soil and Tillage Research*. https://doi.org/10.1016/j.still.2004.03.008

Six, J., Conant, R. T., Paul, E. A., & Paustian, K. (2002). Stabilization mechanisms of soil organic matter: Implications for C-saturation of soils. In *Plant and Soil*. https://doi.org/10.1023/A:1016125726789

Six, Johan, & Paustian, K. (2014). Aggregate-associated soil organic matter as an ecosystem property and a measurement tool. *Soil Biology and Biochemistry*. https://doi.org/10.1016/j.soilbio.2013.06.014

Stanley, C. E., Grossmann, G., Casadevall i Solvas, X., & DeMello, A. J. (2016). Erratum: Soil-on-a-Chip: microfluidic platforms for environmental organismal studies (Lab Chip (2016) 16 (228-241)). In *Lab on a Chip*. https://doi.org/10.1039/c6lc90011a

Stanley, C. E., Stöckli, M., Van Swaay, D., Sabotič, J., Kallio, P. T., Künzler, M., Demello, A. J., & Aebi, M. (2014). Probing bacterial-fungal interactions at the single cell level. *Integrative Biology (United Kingdom)*. https://doi.org/10.1039/c4ib00154k

Stanley, C. E., & van der Heijden, M. G. A. (2017). Microbiome-on-a-Chip: New Frontiers in Plant–Microbiota Research. In *Trends in Microbiology*. https://doi.org/10.1016/j.tim.2017.05.001

Stevenson, F. . (1994). Humus chemistry. *Genesis, Composition, Reactions*, 443. https://doi.org/10.1038/245109a0

Stirzaker, R. J., Passioura, J. B., & Wilms, Y. (1996). Soil structure and plant growth: Impact of bulk density and biopores. *Plant and Soil*. https://doi.org/10.1007/BF02257571

Stoops, G., Marcelino, V., & Mees, F. (2010). Interpretation of Micromorphological Features of Soils and Regoliths. In *Interpretation of Micromorphological Features of Soils and Regoliths*. https://doi.org/10.1016/C2009-0-18081-9

Sutton, R., & Sposito, G. (2005). Molecular structure in soil humic substances: the new view. *Environmental Science & Technology*. https://doi.org/10.1021/es050778q

Toosi, E. R., Kravchenko, A. N., Mao, J., Quigley, M. Y., & Rivers, M. L. (2017). Effects of management and pore characteristics on organic matter composition of macroaggregates: evidence from characterization of organic matter and imaging. *European Journal of Soil Science*. https://doi.org/10.1111/ejss.12411

Valiei, A., Kumar, A., Mukherjee, P. P., Liu, Y., & Thundat, T. (2012). A web of streamers: Biofilm formation in a porous microfluidic device. *Lab on a Chip*. https://doi.org/10.1039/c2lc40815e

Van Brakel, J., Modrý, S., & Svatá, M. (1981). Mercury porosimetry: state of the art. *Powder Technology*. https://doi.org/10.1016/0032-5910(81)85001-2

Van Hees, P. A. W., Johansson, E., & Jones, D. L. (2008). Dynamics of simple carbon compounds in two forest soils as revealed by soil solution concentrations and biodegradation kinetics. *Plant and Soil*. https://doi.org/10.1007/s11104-008-9623-3

Vogel, H. J. (2000). A numerical experiment on pore size, pore connectivity, water retention, permeability, and solute transport using network models. *European Journal of Soil Science*. https://doi.org/10.1046/j.1365-2389.2000.00275.x

Whitesides, G. M., Ostuni, E., Takayama, S., Jiang, X., & Ingber, D. E. (2001). Soft Lithography in Biology and Biochemistry. *Annual Review of Biomedical Engineering*. https://doi.org/10.1146/annurev.bioeng.3.1.335

Wiesenberg, G. L. B., Schwarzbauer, J., Schmidt, M. W. I., & Schwark, L. (2004). Source and turnover of organic matter in agricultural soils derived from n-alkane/n-carboxylic acid compositions and C-isotope signatures. *Organic Geochemistry*. https://doi.org/10.1016/j.orggeochem.2004.03.009

Wildenschild, D., Vaz, C. M. P., Rivers, M. L., Rikard, D., & Christensen, B. S. B. (2002). Using X-ray computed tomography in hydrology: Systems, resolutions, and limitations. *Journal of Hydrology*. https://doi.org/10.1016/S0022-1694(02)00157-9

Yang, J., Yang, Y., Wu, W. M., Zhao, J., & Jiang, L. (2014). Evidence of polyethylene biodegradation by bacterial strains from the guts of plastic-eating waxworms. *Environmental Science and Technology*. https://doi.org/10.1021/es504038a

Young, I. M., & Crawford, J. W. (2004). Interactions and self-organization in the soil-microbe complex. In *Science*. https://doi.org/10.1126/science.1097394

Yu, Z., Zhang, Q., Kraus, T. E. C., Dahlgren, R. A., Anastasio, C., & Zasoski, R. J. (2002). Contribution of amino compounds to dissolved organic nitrogen in forest soils. *Biogeochemistry*. https://doi.org/10.1023/A:1020221528515

Zachara, J., Brantley, S., Chorover, J., Ewing, R., Kerisit, S., Liu, C., Perfect, E., Rother, G., & Stack, A. G. (2016). Internal Domains of Natural Porous Media Revealed: Critical Locations for Transport, Storage, and Chemical Reaction. In *Environmental Science and Technology*. https://doi.org/10.1021/acs.est.5b05015

Acknowledgments

Edith. I do not know what my expectations were before I started my PhD, but certainly, whatever they were, the experience I had surpasses them. Thank you very much for your support, for seeing me as a human being first, and as a scientist later. Your support, feedback, and kindness contributed undoubtedly to finishing this work. Thank you for trusting in me and my capabilities since the first day, for choosing me to be your first PhD student. It has been a pleasure working with you.

Pelle. Thank you for being supportive all these years. All your feedback, comments, advice, have been incredibly valuable and essential for finishing this thesis. Thank you for believing in me, even though I had no previous experience with this method, for always giving value to my work, for being positive even when the experiments were not working yet.

Johannes. We have discussed about science, philosophy, and literature, and almost always disagree, but those disagreements are from where I have learned the most these years. Thank you for always having positive energy and transmitting it to all of us who work with you. Being part of your lab meetings helped me to have a broader perspective, not only regarding our topic, but of science in general. You certainly inspire those around you to do our best and to always aim higher. Thank you for your support during my last months of PhD, for your advice on the experimental set-up, on the data analysis, and on how to handle the hectic final stage of the thesis.

Jason and Martin, thank you very much for helping me with the fabrication of the microfluidic devices and for sharing your expertise with me. It has truly been a pleasure working with you.

Katarina. The way you guided me as an examiner helped me to keep track of my studies and my goals. I am sure this PhD would have been a lot more difficult to accomplish without your expertise. Thank you for that.

Anders. Thank you for giving me the chance to start working at the Microbial Ecology unit. Even though my background was not in microbial ecology, you trusted in my eagerness to learn new topics. Your constant support of my work motivated me and keeps motivating me every day.

Erland. Thank you for your advice on my experiments and for helping me to get the bacterial strain I ended up using in my experiments. It is always a pleasure to discuss with you and to listen to your opinions on all matters. Certainly, your knowledge in microbial ecology is vast and, at times, overwhelming, but it is precisely that what keeps inspiring me to learn more and more every day.

Håkan. Thank you for letting me work with you in the mesh bag project, which ended up being my beginning in the Microbial Ecology group. The smile and cheerfulness you show to everyone in the unit makes us feel welcome and at home even though we might be far away from it.

Ainara, como nos dijo una vez un sabio literato, tu nombre nos recuerda a Ariadna, que entregó un hilo a Teseo para que encontrase la salida del laberinto. Creo que al final fuiste eso para mí, y aún más. Fuiste no solamente la guía, sino que estuviste dentro del laberinto conmigo, en el oscuro pasaje del que solo se puede salir con la verdadera amistad. Muchas gracias por confiar en mí y por hacer que confiara en mí. Tu prudencia, tu amistad, la alegría con que ves la vida, es algo que llevaré conmigo para siempre.

Carles, moltes gràcies per la teva amistat, per els teus consejs, que hi anavan desde com hauria de fer un model amb l'ordinador, fins com ahuría de pronunciar apropiadament el catalá de la profunditat del teu país. Moltes gracias per mostrarme la grandeza que pot alcanzar la amistat, la humilitat i el carinyo, i per sobre tot, el amor per les coses simples, com fer unes birres al sol, anar a pescar o acampar, o nomes parlar de la vida i de com sortirem de aquest laberinto.

Dimitrios. Thank you for your friendship and for your support, for making me feel welcome and comfortable since my first days at the department. The passion you have for what you do, for the mysterious world of fungi, is something that inspired me and keeps inspiring me to do science. Discussing my results with you always helped me to understand how much I still ignore, and that motivates me to learn more every day.

Micaela, muchas gracias por tu amistad, por tus consejos, por las conversaciones y por el apoyo constante que siempre me has dado. Juan Pablo, gracias por tu amistad, por las largas charlas de lo misteriosa que es la vida a veces. Muchas gracias a los dos por ser una parte de mi amado país aquí en Suecia.

Daniel. My friend, thank you for being supportive during the last days of my PhD and for being such a good friend since the first day I met you. The moments we have spent together are stored in the bottom of my heart. Thank you for reading my thesis and for the invaluable comments you gave me.

Michiel. The way I approach experiments or data analysis is still the very way you showed me years ago. Discovering how science is done and the meticulous procedure it demands is something I learned from you and for which I will be

forever thankful. You taught me not only how to handle laboratory equipment, how to do an experiment, and how fungi grow and function, but you also taught me the most important thing a scientist needs to know: constancy, thoroughness, and passion for what you do.

Milda. All the times we spent, either in meetings, at the coffee table, dinners, or camping, have been a pleasure. The passion for what you do and the enthusiasm you have when facing challenges is something I have tried to learn from you all these years.

Lettice. Thank you for the good energy and the smile you always show to all of us around you. You truly inspire me with your passion for science, and with the ferocity and humbleness you face all obstacles that might come in front of you.

To all Rousk Lab members, Meng, Mingyue, Qinmei, Carla, Blandine, Sara, Alex, Garazi, Sandra, Kristin R., thank you for giving me the chance to share lab meetings with you. Discussing articles, bringing figures, having breakfast together, were the best way to learn about science, how to discuss articles, how to see critically others and our own results.

Muchas gracias a mis amigos Jesús, David, Violeta, Rodrigo, Hamid, Leidys, Pedro, por los momentos compartidos dentro y fuera de la universidad. Los planes de todos los viernes durante el verano con ustedes definitivamente fueron un combustible imprescindible para mis últimos meses de doctorado.

Martin, Raphael, Margarida. Thank you for the incredible moments we spent together, for being such a nice crew and bringing joy to my life every time we met. I hope many poster sessions await us in the future.

Thank you to all the Microbial Ecology group, Per P., Tomas, Eva, Tao, Lelde, Cesar, Gry, Saeed, Kristin A., Anna, Lokesh, Johan, Shakil, Per B., Cristina, Molly. I have learned so much from every single one of you these years and I could not wish for a better group to have done my PhD thesis in.

Emily. Thank you for the nice talks and the constant support. Learning Swedish, either in courses or in our fika på Svenska, has been, without a doubt, the most fun way to learn a language. Having your friendship is a true privilege and has been crucial for making my time in the Ecology building one of the best in my life.

Sam, Saleh, Arah, Stephanie. All this work would not have been possible to accomplish without you. The exactness and motivation you had in every single experiment we did together contributed enormously to the finalization of this project.

Miguel. Muchas gracias por todo tu apoyo, por enseñarme a usar R, por ayudarme a interpretar mis datos, por tenerme paciencia y, por sobre todo, por ser un amigo incondicional. Mucho de lo que está escrito en este trabajo no hubiese sido posible sin tu ayuda.

Thank you very much to all my friends from the Biology Department, Linus, Ann-Kathrin, Utku, Pierre, John, Humberto, Judith, Veronica, Groa, Elsa, Vinardas, Arne, Inga, Hanna, Philip, Julian, Qinyang, Kristaps, Yesbol, Charlie, Aivars, Jacob, Arne, María, Tristan, Katja, Franca, Elsie, Kath, Suvi, Maarit, Romain, Mara. The times spent with you in the Pub, football, Christmas dinners, BLAM, BBQs, made this PhD one of the most exciting and fun experiences of my life. I will keep all and each one of you in my heart wherever I go.

Pablo. Estuviste conmigo en los momentos más difíciles, cuando empecé mi doctorado, y cuando lo acabé. Siempre has sido un apoyo incondicional y una inspiración para mí, para seguir adelante sin importar lo oscuro que sea el camino, y para siempre ver el lado positivo de las cosas. Compartir contigo mis dudas, mis alegrías, mis momentos difíciles, ha sido un regalo que me ha ayudado a que esta experiencia sea una de las mas hermosas de mi vida.

Finalmente, muchas gracias a mi familia, mi papi, mi mami, mi ñaña, Joaquina, Benja, por el apoyo incondicional durante todo mi doctorado. Gracias por siempre confiar en lo que puedo lograr, por dejarme ser libre de elegir y de, muchas veces, cometer mis propios errores. La vida entera no me alcanzaría para agradecerles lo que son conmigo y lo que significan para mí. La tristeza de estar lejos de ustedes durante tanto tiempo se compensa con el hecho de saberlos dentro de mi corazón, y de saberme yo dentro del suyo. Este trabajo es fruto de ustedes y de su amor.

Paper I

Microfluidic chips provide visual access to in situ soil ecology

Paola Micaela Mafla-Endara[1,2], Carlos Arellano-Caicedo[1], Kristin Aleklett[1,3], Milda Pucetaite[1], Pelle Ohlsson[4], and Edith C. Hammer[1,2]*

[1] Department of Biology, Lund University, SWEDEN

[2] Centre for Environmental and Climate Science, CEC, Lund University, SWEDEN

[3] Department of Plant Protection Biology, Swedish University of Agricultural Sciences, SWEDEN

[4] Department of Biomedical Engineering, Lund University, SWEDEN

*corresponding author: Edith Hammer, Microbial Ecology, Department of Biology, Lund University, Ecology Building, Sölvegatan 37, 223 62 Lund, Sweden, +46 (0)732 44 1968, edith.hammer@biol.lu.se

Abstract

Microbes govern most soil functions, but investigation of these processes at the scale of their cells has been difficult to accomplish. Here we incubate microfabricated, transparent ‘soil chips’ with soil, or bury them directly in the field. Both soil microbes and minerals enter the chips, which enables us to investigate diverse community interdependences, such as inter-kingdom and food-web interactions, and feedbacks between microbes and the pore space microstructures. The presence of hyphae (‘fungal highways’) strongly and frequently increases the dispersal range and abundance of water-dwelling organisms such as bacteria and protists across air pockets. Together with physical forces such as water movements, fungi form new microhabitats by altering the pore space architecture and distribution of soil minerals in the chip. We show that soil chips hold a large potential for studying in-situ microbial interactions and soil functions, and to interconnect field microbial ecology with laboratory experiments.

Introduction

Soil microorganisms are essential for nutrient cycling, soil aggregation, and regulation of soil carbon storage. Their home, the soil, consists of matrices of mineral particles that harbour partly interconnected pores. These pore spaces are full of contrasting microhabitats of varying size and chemical condition, in which microbes live, and which they constantly re-shape1,2. The physical microstructure of soil is a strong determinant of soil functions and ecological interactions3. It makes the soil habitat unique, extraordinarily species rich4, and allows for the accumulation of organic matter despite the presence of many substrate-limited microorganisms5,6. The arrangement and structure of soil aggregates and pore spaces define the connectivity between microhabitats and thus the soil microorganisms' access to or restriction from different resources (e.g., food sources, water, and oxygen) based on their dispersal potential7,8. The system is highly dynamic in space and time: solid particles are moved by both physical processes and biota, and additional barriers for diffusion and mass flow occur when pores dry out, inhibiting the dispersal of microorganisms such as bacteria and protists that are reliant on hydraulic connectivity for relocation8–10.

Despite the continuous effort to understand how communities of soil microbes function and contribute to soil processes, current techniques have not been able to completely address the complexity of their spatiotemporal organization at the microscale1,11–13. For organisms living inside the minuscule, solid, soil microstructures, it is expected that most of the cell-to-cell interactions take place over short distances, generally no more than a few tens of micrometres14. Identifying and studying these microhabitats is challenging as their spatial organization is easily destroyed and lost during sample processing12,15. As a result, the capacity for addressing fundamental knowledge gaps in the field of soil science has been limited, including the impact of spatial microstructures on biogeochemical processes like nutrient cycling, feedbacks between microbes and soil physical processes, inter-kingdom interactions, and biodiversity-function relationships16–18. We have now developed a microfluidic system that allows us to experimentally address these questions in situ and with higher spatial control than previously possible. Natural microbial communities can be inoculated into these systems, selected only by their ability to pass through the entrance of limited size.

Microfluidic chips have already demonstrated their usefulness in controlling and shaping micro-environments for the study of cell-to-cell interactions, and revolutionized biomedical research with, e.g., organ-on-a-chip devices19. Even within soil science and microbial ecology, chips have been used to address important questions20,21 such as how to increase the number of culturable bacteria from the environment22, how bacteria spatially organize in a pore space along chemical gradients23, and how intracellular signals propagate in fungal networks24. In most cases, chips have been inoculated with one or two microbial species at a

time, exposed to very controlled spatial and/or chemical conditions. In this study, we used a whole-soil inoculum for microfluidic chips to investigate interactions within multi-species microbial communities including physical soil components. We studied the early microbial colonization of the chip's pristine, soil-like habitat by (I) burying it directly into the soil habitat in the field, or (II) inoculating it with soil and incubating it in the laboratory. We expect the first approach to allow us to study conditions most closely resembling those in nature, while the second approach allows us to follow processes over time. We asked whether the dispersal capability of three functional microbial groups—fungi, bacteria and protists—into a pristine pore space environment is influenced by pore space characteristics such as their geometric shape and chemical conditions, and by interactions with other microbes. We further examined how the microhabitats themselves are affected by abiotic and biotic factors such as drying and rewetting of the soil, and by the microorganisms themselves.

The chip design contained different experimental sections with distinct geometrical patterns25 (Supplementary Fig. 1a, Sections A-E), which we used to address the following specific questions: a) How is microbial dispersal influenced by the pore spaces being filled with air, water, or nutrient medium? b) How does pore space geometry affect microbial dispersal, such as channels angled in zigzag patterns, forcing the microbes to navigate through increasingly sharper turns? c) Are bacteria and protists influenced in their dispersal capabilities to new pore spaces by the presence of a fungal hypha? and d) How does drying and rewetting soil, and the moving and growing microorganisms, affect the spatial arrangement of the chips' pore space?

In summary, our experiments show that water and nutrient conditions mainly affect water-dwelling organism groups of bacteria and protists, while the shape of the microstructures has an effect on fungal dispersal. Fungal hyphae strongly enhance the colonization success for both bacteria and protists in an initially dry pore space via increased pore wetting. The chips also reveal spatiotemporal changes of microhabitats: hyphae both open up new passages in the pore space system and block them for both organisms and abiotic soil components. Water movements, triggered by drying and rewetting the soil, lead to the development of preferential water pathways that differentiate microhabitats further.

Results

All major groups of soil microorganisms (bacteria, fungi, protists), as well as invertebrates such as nematodes and microarthropods, colonized the chips and explored their internal structures, both when the chips were incorporated into soil (Expt. 1) and when they were incubated with soil in the laboratory (Expt. 2 & 3). Soil mineral particles (Supplementary Fig. 2) and soil solution also entered the chips via water movements. The transparency of the chips allowed us to observe the

primary colonization of a pristine pore space and soil microbial interactions in real time (Fig. 1): microhabitat formation (Fig. 1a-c, Supplementary Movies 1-2), interactions of fungal hyphae with other soil organisms and components (Fig. 1c-h, Supplementary Movies 3-7), and microbial food web interactions (Fig. 1g-i, Supplementary Movies 7-8).

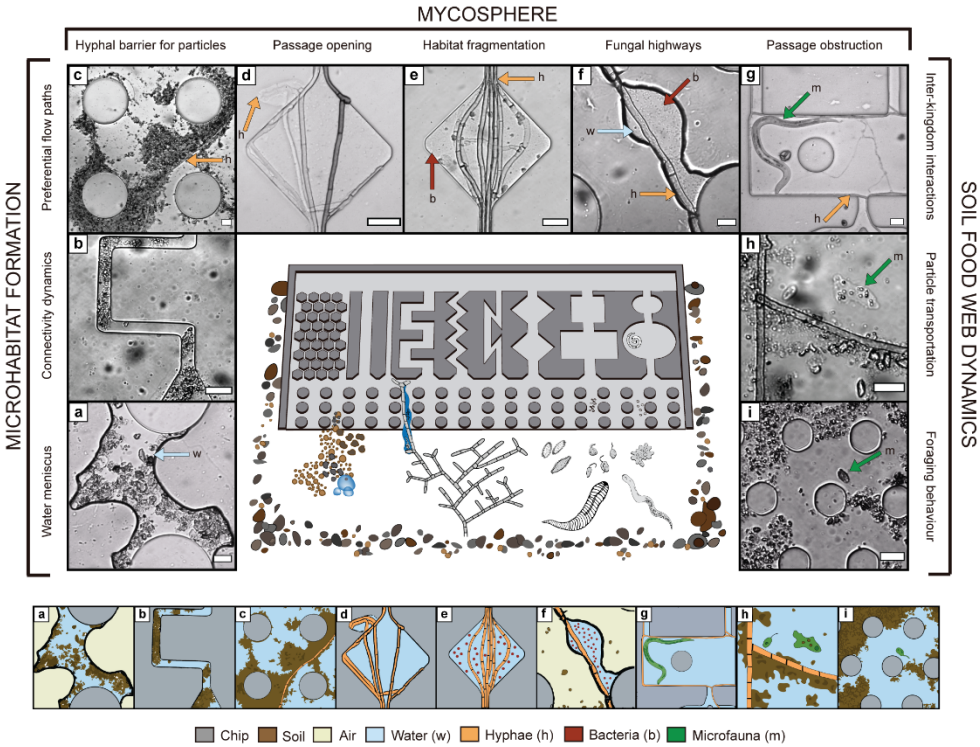

Figure 1. Soil organisms and processes recorded in micro-engineered soil chips. The chips were colonized in situ from a natural soil when buried in the field. The inner section shows a schematic drawing of the design of the silicone and glass chip (dimensions exaggerated for clarity) and indicates the 7 µm high opening from where soil components and organisms can enter. Bright field microscopy images are grouped into the research fields of microhabitat formation, the mycosphere, and soil food web dynamics. A graphic legend below the chip explains content of the microscope images. a, Water meniscus connecting soil particles and chip structures. b, Mobile soil particles blocking connectivity of the artificial pore spaces. c, Preferential water flow paths developing among soil particles sedimenting at the bottom of hyphal structures. d, Passage opening by hyphae: hyphae broke through the borders of an artificial pore space, creating a new micropore. e, Habitat fragmentation by hyphae clogging a pore neck. f, Fungal highways: hypha-facilitated bacterial dispersal across air gaps. g, Passage obstruction: a hypha blocking the entrances to a rectangle pore occupied by a nematode. h, Particle transport: amoeba transporting ingested bacteria and particles. i, Foraging behaviour: flagellated protozoa foraging around and in soil aggregates. Images a, d, and e derive from air-filled chips; b, f, g, and i derive from malt medium-filled chips; c and h derive from water-filled chips. Each type of observation was recorded at least 3 times. Figure panels a, b, and d-i are supported by Supplementary Videos 1-8, resp. Scale bars, 20 µm (a-i).

Pore space geometrical characteristics and filling

To assess the influence of growth medium conditions in the pore spaces on the dispersal of soil microbes, we filled the chips with either malt extract medium, water, or left them empty prior to incubation in or with soil. Bacteria and protists colonized the chips filled with malt extract medium or water to a much larger extent than air-dry ones in-situ (Expt. 1, Fig. 2b, c; $F= 26.8$, $p<0.0001$ and $F= 9.03$, $p=0.005$, resp.; $n=3$, $DF=8$), and in the laboratory-controlled setups, both liquid-filled chips were colonized to a significantly larger extent by bacteria and protists than in the air-filled chips (Expt. 2, Fig. 2e, f; $F=1075$; $F=157$, resp; $p<0.0001$ for both; $n=12$ x 2 channels x chip, $DF=8$). In contrast, fungal hyphae showed variable results, with strong or weak growth without a consistent effect of chip filling in both the field- and lab incubated settings (Fig. 2a, d). The lab-incubated chips (Expt. 2) enabled us to investigate the colonization of pore spaces in a time-resolved manner (Supplementary Fig. 3; Supplementary GIFs 1-3). The organisms entered the liquid filled chip from within hours (bacteria) to days (fungi, protists and nematodes). Generally, cell numbers in the malt treatment were immediately higher than in the water treatment and maintained larger population sizes, especially for protists, throughout the experiment. We found a high turnover of fungal hyphae in the malt treatment (Supplementary GIF 3).

We further analysed the influence of channel-shape geometries on the dispersal ability of the different soil microorganisms, both in the in situ-chips (Fig. 2a-c) and in the laboratory incubations (Fig. 2d-g). Water-dwelling organisms such as bacteria (Fig. 2b, e) and protists (Fig. 2c, f) were not affected in their dispersal by the three investigated channel shapes. Fungi preferred, at sufficient colonization, to grow through ‘zigzag’ channels, deviating 45° from the main growth direction in alternating 90° angles, over ‘square’ 90° angles alternating perpendicularly to the growth direction, or ‘z’-channel angles of 135° (Fig. 2g. Expt. 3, air-filled chips; $F=21.7$, $p>0.0001$, $n=12$x2 channels per type x chip; no significant effects found during Expt. 1 and 2, Fig 2a, d).

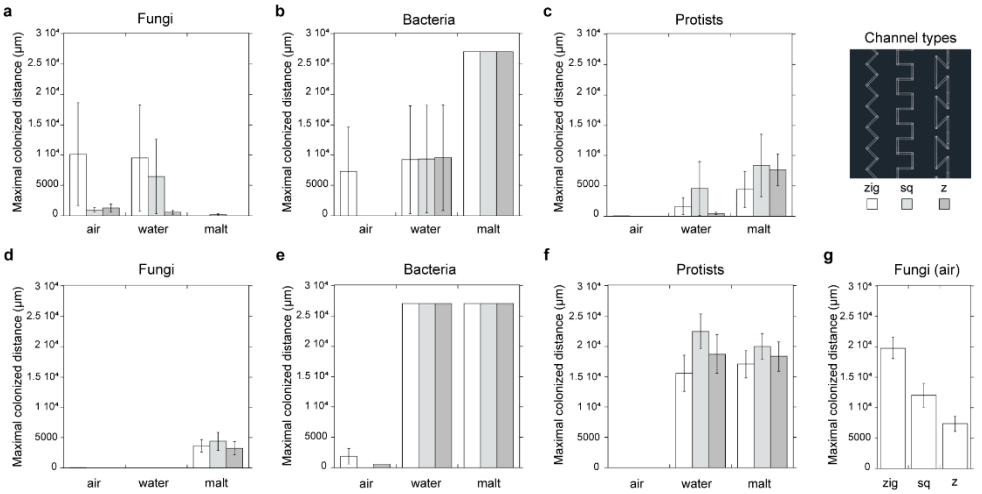

Figure 2. Maximum dispersal extent of different soil microbial groups. Colonization distances of the three microbial groups, fungi, bacteria, and protists, recorded in soil chips incorporated into soil (a, b, c, Expt. 1, n=3) and incubated with soil in the laboratory (d, e, f, Expt. 2, n=3 chips x 12 channels). g, Fungal colonization distance in Expt. 3 (air-filled chips, n=2 chips x 12 channels). The channels analysed are 10 µm wide, shaped with corners of different angles (see legend: zigzag (white bars), square (light grey bars), z-shaped (dark grey bars), under dry =air-filled, water-filled, or malt extract-filled conditions, error bars denote the standard error of the mean. The maximum extent of the channels was 2700 µm and thus the maximum possible colonization extent of this experiment.

The influence of fungal hyphae on microbial dispersal

To study the impact of fungal hyphae on the dispersal of other soil organisms, we used sets of air-filled chips where air pockets constitute obstacles for water-dwelling organisms in Expt. 1. After two months buried in the soil, those chips were no longer exclusively dry, as condensation water and soil solution had been dragged into the chip space, resulting in a patchy distribution of air and water in the pore space, and a subsequent colonization of its crevasses. We measured the dispersal and abundance of bacteria in the repeated widenings (Fig. 3a) in initially air-filled channels colonized by hyphae compared to directly adjacent hypha-free channels. Results showed that the presence of hyphae, coming directly from the surrounding soil into the chip, facilitated bacterial dispersal deeper into the chip interior by enabling their passage across air pockets (Figs. 1f, 3b, d-f; Supplementary Movie 5), which resulted in a more than six-fold increase in bacterial abundance in channels with a hypha ($F= 45.6$, $p<0.0001$; n=33 x 4; or paired t-test $p=0.0008$, n=4, DF=3 Fig. 3b). Hyphal presence changed the pore space hydrology, as 80% of the pores containing hyphae filled up with liquid, in contrast to only 40% of the widenings without hyphae (Fig. 3c, ChiSquare 42.5, $p<0.0001$, n=264, DF=1). Bacterial cell abundance commonly peaked at two different areas near the hyphal frontier: close to the tip (Fig. 3e) or further behind (Fig. 3f).

While the chips embedded in-situ in a natural outdoor soil ecosystem experienced the most realistic environmental influences, the chips that were incubated with soil in the laboratory enabled us to follow processes in a time-resolved manner (Expt. 3, Fig. 4, Supplementary GIFs 4-6). In air-filled pore spaces connected to soils with intermediate humidity, hyphae were commonly the first to enter the channels, shortly followed by water films and then bacteria (Fig. 4a). The presence of hyphae increased the water saturation of the pore spaces (between days 6-20; $F=44.6$, $p<0.0001$, see Fig. 4b), increased the bacterial populations colonizing the chips' pores during the first 20 days by more than 8-fold ($F=23.9$, $p<0.0001$, largest enhancement at day 12, 170-fold), and the extent of bacterial dispersal into the channels ($p=0.033$; Fig. 4c). At day 12, already 46% of the 108 channels were colonized by hyphae, and 10% of all channels contained bacteria growing along hyphae, compared to 3% of the channels colonized by bacteria alone (Supplementary Fig. 4a).

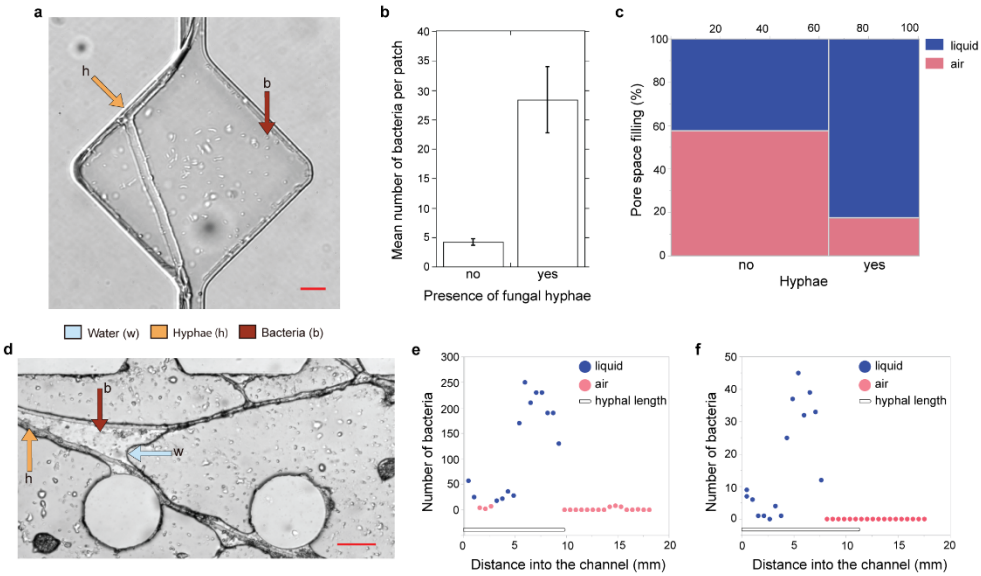

Figure 3. Fungal hyphae influence the dispersal of bacteria. a, Example of a diamond-shaped widening along the channels which served as the basic entity to calculate bacterial abundance depending on the presence of a hypha. b, Abundance of bacteria in diamond-shaped openings depending on presence of a fungal hypha. n=4x33 in a paired ANOVA, error bars denote the standard error of the mean. c, Contingency diagram showing the occurrence of air or water in diamond-shaped openings depending on the presence of a fungal hypha. Along the x-axis the frequency of channels containing hyphae, and along the y-axis the frequency of channels containing liquid or water, is shown, 264 observations in total. d, Example of fungal highways developed within the soil chip's pillar system, where hyphae drag water films with them, allowing bacterial transgression. e, f, Bacterial abundance along a fungal hypha protruding into an initially air-filled channel. Bacteria were quantified per diamond-widening, each dot represents a diamond. Red dots represent diamonds that remained air-filled after two months in the soil, blue dots represent soil-solution filled diamonds at examination. The line beneath the data curve represents the extent of the hypha in the chip. Scale bars, 10 µm (a), 50 µm (d). Data derives from chips of Expt. 1 that were buried in soil and initially air-filled.

Protist colonization of the pore spaces (in total 261 encounters, dominated by flagellates and some amoebae) was also enhanced when fungal hyphae were present in the pore spaces during the first 20 days after inoculation, until the artificial waterlogging event ($F=5.1$, $p=0.02$, Fig. 4b). Protists were almost five times more abundant in the pores containing hyphae, and their colonization depth into the channels was increased 4-fold. After 20 days, 23% of the channels contained protists, in 68% of those together with hyphae (Supplementary Fig. 4b).

Bacterial and protist dispersal increased over time until we performed the waterlogging event before measurement at day 28, equalizing water levels in channels with and without hyphae, and consecutively also their bacterial colonization (Fig. 4b). After the waterlogging event, we let the chips dry out and found, contradicting our expectations, that channels containing fungal hyphae did not retain water better than the ones without hyphae. We also investigated the dynamics of hyphal influence on bacterial dispersal using a third approach, by quantifying the colonization of droplets of condensed water that spontaneously and frequently formed within the pillar system, analysed in one chip (Fig. 4e, Supplementary Movie 9). Initially, most water droplets were sterile, and ca. 25% of them started to form along hyphae. The first water droplets colonized by bacteria were almost exclusively those containing hyphae. Over time, drying and rewetting events caused droplets to unite or split so that bacteria-only droplets started to occur more frequently.

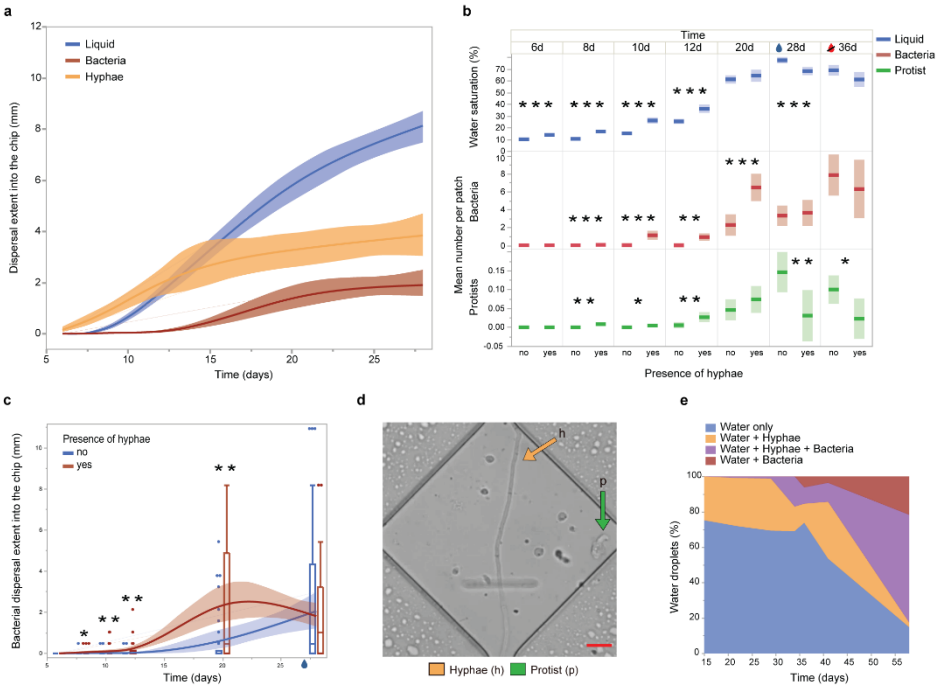

Figure 4. The influence of fungal hyphae on pore wetting and microbial dispersal recorded in Expt. 3, soil incubated on initially air-filled chips in the laboratory, monitored over time. a, Dispersal extent of fungal hyphae, water films, and bacteria into the 'diamond' channels, mean and 95%-confidence interval, n=3x36. b, Presence of water and abundance of bacteria and protists in diamond shape widenings over time, depending on the presence of a fungal hypha, mean and 95%-confidence interval, n=3x1188. c, Bacterial dispersal extent into channels with diamond-shape widenings, depending on the presence of fungal hyphae, boxplot combined with curve of the means and 95%-confidence interval, n=3x36. Prior to day 28, we performed a waterlogging treatment to the inoculation soil that saturated most parts of the chips' pore spaces, indicated by the blue droplet in b and c. Between days 29 and 36, chips were exposed to drying without any additional watering, indicated by the strikethrough red droplet in b. d, Example of a diamond-shaped widening along the channels with a protist along a hypha. e, Quantification of the presence of hyphae and bacteria contained within spontaneously formed water droplets within the entry system of an initially air-filled chip. Humidity of the inoculation soil was kept equable, no waterlogging or drying was applied. Stars in b and c denote statistically significant differences at * p<0.05; ** p<0.01; *** p<0.0001. Scale bar, 10 µm.

Microhabitat formation

In addition to microorganisms, abiotic components also entered the chips: mineral particles, identified with in-situ Raman scattering microspectroscopy as quartz (Supplementary Fig. 2), as well as soil solution. This enabled us to study how microorganisms interact with soil particles and contribute to shaping the dynamic soil pore space. We observed the formation of new microhabitats inside and around newly formed soil aggregates (Fig. 1a-c, h-i, Supplementary Movies 1-2, 7-8), changing the original pore connectivity and pore size distribution.

We recorded particles being dragged along with moving water inside the chip in evolving meandering stream patterns, and bacteria being strongly displaced (Supplementary Movie 10). As a result of the water mass flow, stream channels in

between the mineral particles developed and were re-shaped over time. Particle movement in the streams was quantified via automated particle tracking (Fig. 5, Supplementary Movies 11, 12; tracked particles and original video, resp.). Particles in the presented video (recorded at a minimum displacement distance of 20 µm per frame) moved with an average speed of 65 µm/s. The average speed of the fastest 10% of these particles was 138 µm/s, most of which moved through one of the two clearly visible water flow paths in Fig. 5a, while the largest part of the recorded area showed little or no water movements.

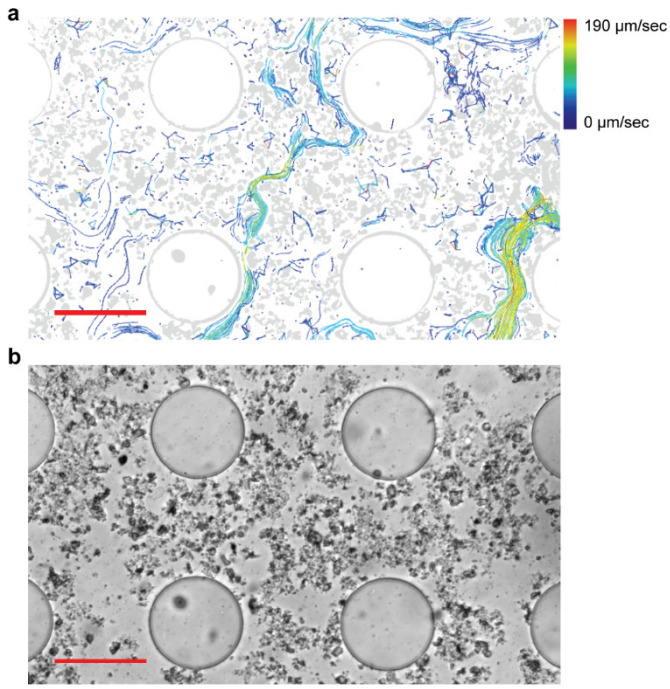

Figure 5. Preferred water flow paths in the soil matrix within the chip, revealed by tracking of displaced particles. a, Threshold image and tracked particle visualization of a 45s long real-time movie sequence (ImageJ plug-in TrackMate version 3.8.0.; Supplementary Movie 10). Colours of the lines following the tracked paths indicate the mean velocity of the particles. The large round structures are pillars of the chip, smaller particles are soil minerals that were dragged into the chip. The recorded water flow was caused by drying of the chip through the adjacent soil layer. b, Original bright field image (Supplementary Movie 11), recorded from an initially air-filled chip buried in soil of Expt. 1. Scale bar,100 µm (a, b).

We also recorded effects of biota on the soil physical structure: fungal hyphae directly changed the pore space shape by breaking up solid structures with help of hyphal tip forces (Fig. 1d), or by blocking passages in the chips' pore spaces themselves (Fig. 1e, g), and indirectly, by constituting barriers for mineral particles that accumulated along the hyphae during water movement of drying and rewetting events (Fig. 1c, h). Hyphal colonization restricted microbial dispersal of larger

organisms such as protists and nematodes by occupying and obstructing the access to free pore spaces (Fig. 1g, Supplementary Movies 6, 13). Both nematodes and larger protists were frequently observed having difficulties passing hyphae in the chip with its low height of 7 µm, especially if the hyphae occupied narrow constrictions in the solid pore matrix of the chip. Phagotrophic ciliates displayed an active hunting behaviour, pushed into aggregates and moved them, thus also creating new passages (Supplementary Movie 14). During drying processes, we saw a distinct development of water menisci connecting structures (Fig. 1a), especially around fungal hyphae (Fig. 1f, Fig. 3d), which increased hydraulic connectivity and maintained the potential for bacterial motility. The cells that died inside the chip laid the base for an initial organic matter build-up, and necromass inside the system was recycled within the food web which was clearly visible when bacteria accumulated around fractured cells and organisms (Supplementary Movie 15, Supplementary GIF 3).

Discussion

Despite the infinite number of pores present in soil, soil microbes usually occupy only a fraction of them26, and they need to navigate across these in search of food and suitable environmental conditions. Investigating the soil microhabitats at a relevant scale will give deeper insights into soil processes such as carbon cycling. The soil chips, colonized by a rich microbial community, constitute literal windows into the soil, allowing us to monitor soil processes in real time, and multi-level interactions among and between microorganisms and their habitat (Fig. 1). We examined the effect of principal pore space characteristics (Fig. 2) and showed that fungal hyphae frequently increased pore connectivity and dispersal of water dwelling organisms (Figs. 3, 4), which is likely of high relevance for their colonization success in an ever-changing pore space system. We demonstrated that the dynamics of changing microhabitats are caused by both physical forces and biological activity (Fig. 5).

The pore space geometry inside the soil chips affected the colonizing capacity of fungi, showing that fungi experience difficulties navigating through acute angles and geometries that are not in line with their initial growth direction. This confirms previous results from laboratory experiments25,27, which we here extend to species from complex natural inocula. The variation found in our results suggests however that fungal reactions to microspaces can depend on factors not specifically tested in this study, such as priority effects by the order in which individual species entered the channels25, or seasonal variation. It has been suggested that fungal hyphae prefer growing in air-filled pore spaces28, but our study did not confirm this to be generally true. However, we did find that water dwelling organisms are strongly restricted in their dispersal ability in air-filled pore spaces (Fig. 2). Under these dry

soil pore conditions the phenomenon of ‘fungal highways’ becomes important, where hyphae facilitate dispersal of motile bacteria along them29,30.

While fungal highways have previously been demonstrated in laboratory settings31,32 and indirectly in-situ33, we have produced direct microscopic footage of hypha-mediated bacterial dispersal proceeding from natural conditions into a pristine pore space, quantified that footage, and elucidated the sequence of processes and causes over time (Fig. 3, 4). The presence of fungal hyphae facilitated the dispersal and population growth of water-dwelling soil microbes, including protists, severalfold. Our results suggest that enhanced pore filling with soil solution, rather than newly created elongated liquid films along the hyphae, is the responsible mechanism (Supplementary GIFs 4-6), and single remaining air bubbles were observed to be insurmountable obstacles for bacteria (Supplementary Movie 16). The higher levels of wettability in channels containing fungal hyphae could be explained by the fungi producing exudates, in a manner similar to how bacterial extracellular polymeric substances have been shown to be responsible for increased water retention in micropore spaces34. Dispersal via fungal hyphae is hypothesized to explain the maintenance of costly flagella for soil-dwelling bacteria, even in soil with generally low water content35. In this study, bacteria were found to colonize even channels without hyphae, but in fewer cases, and cell numbers commonly remained lower in those channels (Fig. 4c, 4b, Supplementary GIF 6). Bacterial abundance is known to be generally higher in the mycosphere than in bulk soil32. Laboratory experiments have shown how mycosphere bacteria are likely to have greater access to nutrients36–38, both in the form of exudates and nutrients released during fungal degradation of organic matter. The pore spaces of the air-filled chips were initially nutrient void, and at least part of the increased bacterial abundance along hyphae in our experiment may be explained by hyphal-fed population growth inside the chip, rather than solely by means of dispersal via the hyphae.

The potential importance of fungal hyphae for dispersal of other soil organisms, such as protists, has previously been hardly recognized, and our results are the first to bring attention to this unexplored field of research. The larger eukaryotic cells would not be able to travel in water films along hyphae, but they can take advantage of the increased water filling in larger pores that hyphae generate. The influence of fungal hyphae on general microbial dispersal dynamics is thus greater than previously acknowledged. Especially important, our data can demonstrate that this phenomenon is not a rare, anecdotal event but rather, under intermediate humidity conditions in the pores, occurred in up to 32% (bacteria) resp. 16% (protists) of 108 examined channels. In a real soil pore system, this priority dispersal should exhibit a large competitive advantage, as freshly opened soil spaces (e.g., via bioturbation39) likely contain free nutrients and degradable necromass.

Soil-inoculated chips hold an especially high potential for future studies involving protists, such as their involvement in trophic networks. Although it is well known that many protists feed on bacteria and control microbial populations40, the details

of dietary requirements of most soil protists, and their functions in soil processes, have been difficult to study directly41. Our soil chips create new possibilities for visual and time-resolved monitoring of food web structures, and may in the future identify food web members via single cell genomics on extracted material, increasing our understanding of protists' involvement in soil nutrient cycles.

Both macro- and microaggregates are in permanent turnover42, and much of the soil pore space is permanently being reshaped. The largest effects on microhabitat modification are usually caused by physical forces. Preferential flow paths are the main channels for water movement in soil, and their chemical composition can be very different from the soil matrix located in smaller pores, because only a fraction of water and solutes passes from the preferential flow path to the surrounding matrix43–45. Our results illustrate that microbes will experience very local levels of habitat stability and nutrient supply, and the need for anchorage or biofilm formation. To the best of our knowledge, our results constitute the first record of water movements in and around mobile and realistic soil microaggregates1 which result in the development of distinctly different characteristics in microhabitats located only a few micrometres away from one another. Other current studies are commonly performed at spatial scales larger than soil micropores, since most of the methods used (e.g., magnetic resonance imaging (MRI), neutron computed tomography (NCT), and X-ray tomography (XRT)) produce insufficient image resolution46–48, and are often incompatible with live imaging of undisturbed biota activity during measurements. This leaves crucial knowledge gaps regarding flows and solute transport in soils at the low micrometre and nanometre scale where microbial activity is confined.

Visualizing how flows influence the microbial environment can help us predict the way microbes react to and interact with different flow movements in the soil. Chip studies on time-resolved microbe-habitat interactions constitute a valuable addition to studies in 2-D thin sections of soil microbe distribution14, e.g., for investigations of bacterial biofilm settlement in relation to different shear forces in a simulated sand pore space49. Aufrecht et al. (2019) successfully identified the spatial distribution of fluorescent bacterial strains when inhabiting a microfluidic chip with water flows around a fixed solid PDMS matrix, while we here use a pore space combining fixed and mobile solids (the PDMS structures and the soil particles, resp.) which allow us to record spatial changes in the pore space as a response of water flows. However, it must be considered that the measurements and observations of the present study correspond to flow properties around microaggregates formed inside a synthetic porous medium with surface roughness and charges that might differ from those found in natural soils. This could be improved by harbouring more soil material and having a longer stabilization phase, allowing organic coatings to form on the chip surfaces. Despite the simplifications of this experiment, we believe that the knowledge obtained will be of great significance for an increased understanding of water flows, such as during drying

and rewetting inside soil aggregates, and their impact on soil biota and their functions.

Bioturbation of soil is commonly ascribed to larger soil fauna50, while insufficient data is available on the role of microorganisms51. The strong influence of fungal hyphae on both opening and blocking of passages in soil makes them important 'ecosystem engineers' for microbial microhabitats. Hyphae are able to exert considerable pressure at their tips52, and when many hyphal tips join they can vigorously open passages in their surrounding (Fig. 1d)25. Hyphae blocking pore space passages for both soil components and organisms, as recorded in the soil chips, is a likely overestimation of their occurrence in real 3-D pore systems, because of their uniform and low height (7 μm), but our results illustrate the principle that hyphae can influence pore connectivity at necks and constrictions. We found, unexpectedly, not only hyphae but even protists forcing new passages through aggregated soil in their hunt for food (Supplementary Movie 13). This demonstrates the importance of the interplay of the microbial community with their fluctuating microenvironment, at different scales, for important large-scale processes such as nutrient cycling.

We see microfluidic chips as a promising tool to deepen insights into soil ecology by observing biological processes in a transparent and geometrically realistic environment, making it possible to track large numbers of individual cells in real time, including traditionally unculturable species22, and as an optimal platform for connecting research frontiers in the fields of soil physics and soil ecology at relevant scale. Nevertheless, soil ecologists should remain aware of the limitations of these highly artificial systems, where current technology only provides a pseudo-3-dimensional space, and the fabrication material lacks many properties of soil minerals: the chips are unnatural in terms of their chemical composition (silicone-based polymer) and surface properties (smooth, inert, and either homogenously hydrophilic when wet, or homogenously hydrophobic when dry), but represent an improvement in realism in terms of their physio-spatial properties because they fragment the microbial habitat. Their miniscule channels generate a large surface structure with strong surface tension, capillary forces, adhesion, and viscous drag; and liquids moving through the structures exhibit a laminar flow, just like real soil solution in small pores20.

Compared to the more frequently used lab-strain inoculation of microfluidic chips, soil inocula contain many organisms that interact with each other, as well as solutes and mineral particles diffusing into the chips. This can thus add several layers of complexity into controlled laboratory experimental systems, and may become an important link between field and laboratory experiments in microbial ecology. We present two different ways of using soil as ecosystem inoculum, either in-situ incubation in a natural soil ecosystem, or else taking soil inoculum into the laboratory. Combining these two approaches may yield the most comprehensive results for many questions: the most realistic picture may be drawn from in-situ

inoculation, where chips are exposed to natural oscillations in humidity, temperature, plant photosynthate inputs, and changes in the microbial species pool. Fungi can interconnect the natural soil with the chips' interior and move nutrients into it, especially in mycorrhizal symbiosis with surrounding plants. On the other hand, experiments using soil inoculum in the laboratory are easier to accomplish, control, and manipulate, and may be monitored with time resolution. To combine advantages of both, microcosms could be constructed with larger amounts of soil, including vegetation, placed around the chip in a large Petri dish.

Micro-engineered chips could be successfully combined in the future with other techniques (e.g., microspectroscopy, epifluorescence microscopy, single-cell sequencing) to incorporate high-resolution information about the chemical and genetic characteristics of the different soil components53. Future studies may investigate, e.g., directly and at microscale how abiotic components (e.g., pH or toxic compounds) affect different microbial groups; how the diversity of microbial communities is linked to different soil ecosystem functions such as soil carbon sequestration; and the ecophysiology of important but understudied organism groups such as soil fungi and protists. We even see a high potential in microfluidic chips to bring soils closer to society, as visual experience may increase interest and concern for an ecosystem in need of protection.

Material and methods

Chip design

We constructed a proxy of a soil pore space system in a micro-engineered silicone chip containing different sets of microstructures, termed the "Obstacle chip"25. The chip consists of an artificial pore system open on one side for inoculum, and it was designed to investigate the growth and dispersal behaviour of soil microbes (Supplementary Fig. 1a, b). The chip's pore-space dimensions were optimized to match the dimensions of fungal hyphae, with structure widths ranging between 4 and 100 µm, and a uniform height of approximately 7 µm to aid microscopy, since cells are located in the same focal plane and rarely overlay. It contained five different geometric sections accessible by soil microbes via a common entry area (Supplementary Fig. 1a). The entry area consists of an open area with round pillars of 100 µm diameter at a separation of 100 µm, holding up the chip's ceiling. It was cut open longitudinally with a scalpel prior to bonding (see below, section 'Chip fabrication'), ensuring direct contact of the soil with the chip's interior. The inner section comprises a combination of differently shaped channels and obstacles constituting five experimental sections, of which two were systematically examined in this study: 1) Section C: A set of channels with sharp corners of three different types (n=12, randomly distributed): zigzag channels (90° turns with all channel sections at ±45° angle from the main growth direction), meandering square channels

(90° turns with each section oriented in either the main growth direction or perpendicular to it), 'z'-shaped channels (sharp corners diverting 135° from the previous growth direction, with channel sections in the main growth direction and at angles of 45° and 135° from it); 2) Section D: So-called 'diamond channels,' with a repeated combination of 10 µm wide and 400 µm long straight channels alternating with 140 µm wide diamond-shaped widenings. This channel type was replicated in 36 channels, each containing 33 diamond widenings. The widenings were used as quantification units to count bacteria and protist cell numbers, and for determination of liquid ingression, for the experiments on dispersal via fungal hyphae. Section A of the chip contained systems of hexagonal pillars of different diameters, Section B consisted of straight channels with different widths, and Section E contained two types of obstacle courses comprised of complex structures. Those and the entrance system provided space for general observations. The design was constructed in AutoCad 2015 (Autodesk), in which patterns within experimental Sections A and C were randomized using a custom script from UrbanLISP (http://www.urbanlisp.com).

Chip fabrication

The microfluidic chips were moulded in polydimethylsiloxane (PDMS) on a photoresist master defined by UV lithography and bonded to glass slides, according to Aleklett et al.25. The master was made by spin coating a thick negative photoresist (SU-8 5, MicroChem Corp, USA) on a glass plate for 60 seconds at 1250 rpm. This generated a photoresist layer of approximately 7µm. The photoresist was soft baked for 5 minutes at 90°C on a hot plate, patterned by UV exposure (Karl-Suss MA4 mask aligner) and post-exposure baked. It was then developed for 3 minutes in mr-Dev 600 (MicroChem) and finally rinsed with isopropanol (VWR International).

The PDMS slabs were produced by thoroughly mixing a PDMS base and a curing agent (both Sylgard 184, Dow Corning, USA) in a 10:1 ratio, followed by pouring the mix onto the master in a 4 mm-thick layer, and degassing it in a vacuum chamber at -25 kPa for 45 minutes. Then the PDMS was cured in an oven for 2.5 h at 60 °C. Once cooled, the PDMS was cut into pieces covering an area (about 40×65 mm) slightly larger than the designed pattern, creating a lateral opening to the chip along the pillar system.

The PDMS slabs were bonded to glass slides. Twelve glass slides, 55×75 mm and 1 mm thick (Thermo Scientific), were first cleaned with acetone, 75% ethanol and deionized water, and then dried under an air-blower to enhance the bonding strength. The pieces of PDMS and the glass slides were treated separately in an oxygen plasma chamber (Diener Electronic Zepto). A glass slide was exposed to oxygen plasma under UV light for one minute, followed by exposure of a PDMS piece for 10 seconds. Once both samples were plasma-treated, they were immediately brought in contact with their activated surfaces facing each other, and gently pressed

to each other in the centre parts of the chip. To avoid collapse of the ceiling of the entrance, none of the chip edges were pressed, but heated for approximately 15 seconds at 100°C to ensure a proper bonding. After another 15 seconds, the chips with liquid treatments were filled with different media using a micropipette, taking advantage of the PDMS's temporary hydrophilia following plasma treatment so that liquids were readily drawn into its structures. The chips were filled with one of the following three treatments: (1) deionized water, (2) liquid malt medium, a complex medium to provide a nutrient-rich environment including reduced sugars such as disaccharide maltose and in lower proportion nitrogenous components such as peptides, amino acids purines and vitamins (malt extract for microbiology, Merck KGaA), or (3) chips were left empty, i.e., air-filled. The eight chips filled with liquid were then placed in a vacuum chamber for 30 minutes at -25kPa to remove any bubbles. Finally, the chips were kept in sterile Petri dishes, sealed with Parafilm and stored overnight in a cold room before being dug down into the soil.

Expt. 1: In situ incubation of chips

To evaluate the effect of different nutritional conditions on colonization of the soil chips by microbes, we evaluated three pore space filling treatments: (1) deionized water, (2) malt extract medium, or (3) air; n=3.

The experimental site was a small grove of deciduous trees in the city of Lund, Sweden (55° 42′ 49.5″ N, 13° 12′ 32.5″ E; Supplementary Fig. 1c). The season chosen for burial of the chips was the early autumn (October 2017) to guarantee a moist soil during the experiment. Groups of replicates of all three chip treatments were buried randomly within the inner parts of the grove (n=4). The litter layer was removed, and 20×20 cm holes were carefully dug into the ground with a spade. The chips were placed horizontally in the soil at a depth of 10 cm in which the PDMS chip was facing up and the glass slide down. Horizontal placement was chosen to probe a single stratum of the soil, serving as a comparable inoculum to the whole of the entry system, and to aid non-destructive recovery. The soil was carefully placed back in its original orientation, and the litter layer was placed back. A string attached to each chip was placed with its opposite end above the soil surface and attached to a pin, to guide future retrieval. There was a minimum distance of one meter between each chip replicate.

Preliminary experiments had shown that a two-month incubation period would grant the colonization of different types of soil microorganisms and minerals, and a stabilization of the inner environmental conditions between the soil chip and the surrounding soil. Thus, after 64 days (December 2017), the chips were collected by carefully removing soil around the string leading to each chip. We carefully kept the adjacent soil atop the glass slide along the opening of the chip, to keep our artificial pore system connected to the real soil pore system, and to avoid such disturbances as hyphal tearing or evaporation of the liquid inside the chips (Supplementary Fig. 1d). We cleaned the chip windows by softly wiping them with

a clean wipe and deionized water. Samples were carefully transported to the microscopy facilities, located adjacent to the burial site. The chips were harvested one at a time and analysed under the microscope immediately after collection and cleaning.

We recorded the presence or absence of the main soil microbial groups in the entry systems and in the different channels, including their furthest extent into the chips, with help of the internal rulers (n=3 per treatment).

To analyse the effect of fungal hyphae on bacterial abundance, we recorded real-time videos slowly scanning along the whole length of the diamond-shaped opening channels (each 33 diamonds, section D in Supplementary Fig. 1a; Fig. 3). The rather sparse hyphal colonization allowed us to select pairs of channels where in the first channel a hypha had proliferated far into the channel, combined with a directly adjacent channel without hyphae, n=4. We then counted the number of bacterial cells in diamond-shaped widenings, the presence or absence of fungal hyphae, and the presence or absence of liquid inside each diamond. After measurements, the chips were left uncovered at room temperature for 60 minutes to initiate air drying in the adjacent soil, in order to observe the real-time effects of drying on organisms and particles in the pore space system of the chips. The adjacent soil was re-wetted by adding 400 µl of water. The water inside the chips corresponded to the adjacent soil pore water, regressed upon evaporation, and refilled the chip structures upon rewetting of the adjacent soil.

Expt. 2-3: Laboratory incubation of soil on chips

In a complementary approach, we collected soil from a lawn in Lund, Sweden, at 10 cm depth, and placed 5g of this soil in front of the entry system of the chip. Chips received the three nutrient condition treatments as described above, air, water or malt medium (n=2, Expt. 2); an additional set of air-filled chips was studied to quantify fungal highways (n=3, Expt. 3). Chips were monitored under the microscope after inoculation, after 6 hours, after 24 hours, and thereafter every second day. Observation was documented with images and videos. Chips were kept in sealed Petri dishes with wet cotton cloths to maintain high humidity and were taken out for analysis only. The soil inoculum on the chips and the interior of the chips were kept moist with 500µl of water added to the soil once a week. The artificial waterlogging event in the chips of Expt. 3 (‘fungal highways’) was achieved by adding a total of 2 ml of water to the inoculum soil over the course of a week, and the drying event was achieved by discontinuing the watering.

During Expt. 2, we recorded the abundance and the furthest extent of bacteria, protists (including the morpho-groups ciliates, flagellates and amoeboids), and the extent of hyphal colonization into the diamond section over time. After two month of incubation we measured the furthest extent of colonization into the angled channels for the organism groups bacteria, fungi and protists. During Expt. 3, we

recorded the presence and the furthest extent of hyphae, liquid, bacteria and protists in the diamond channels over time.

Microscopy and image analysis of the chips

All visual inspection and imaging were done with an inverted microscope (Nikon Diaphot 300) with 40-400× magnification. Cells down to a size of circa 0.4 µm were recordable in movement. The real cell number may be underestimated in a few cases, since small cells may have remained undetected at rest. The absence/presence of the main soil microbiota groups (fungi, bacteria, protists, nematodes, and microarthropods) was recorded in the entry system and in the different channels. Where present, the maximum individual extent of each soil biota group into the chip was recorded in the straight and turning channels. Videos and images of particles and microbial interactions were recorded in the entry system and in the channels and pillar systems of the chip. Bright field images and real-time videos were recorded through the microscope with a digital camera (USB29 UXG M). All images shown in Figure 1, except for 1c and 1h, were extracted from videos (Supplementary Videos 1-6, 8) using Adobe Premiere Pro CS6. All images shown in Figs. 1and 3 were cropped in Adobe Photoshop CC (v. 20.0) and the image from Fig. 4 was cropped in Adobe Photoshop 2020 (v.21.2.4); contrast and brightness were adjusted to obtain optimal visual data. Scale bars were added with ImageJ Software (v. 1.56h, NIH). False-colour image legends were produced in Adobe Photoshop CC (v. 20.0). The central illustration and the final assembly of other elements of Figure 1 were performed in Adobe Illustrator 2020. Images shown in Figure 5 were captured using the ImageJ plug-in TrackMate version 3.8.0.

Velocity analysis of particles in water flow paths

The velocity analysis of soil particles in soil solution streams was performed in ImageJ version 1.52i. A 48-second video clip of the drying event inside the chip was converted to an 8-bit file and subjected to a threshold of grey values from 0 to 175. This range was selected because it showed to be optimal in the number of moving particles captured. Particles were tracked with the Image J plug-in TrackMate version 3.8.0. A LoG detector, which applies a Laplacian of Gaussian filter to the image, was used to detect the particles. The parameter 'Estimated blob diameter,' which should have approximately the same size as the analysed particles, was set to 2.76 µm. The radius of the particles considered by the software then ranged from one-tenth to two times the radius. This value represents the quality of the detection, and must be a positive number with higher numbers representing higher quality. This size range was chosen because particles smaller than 2 µm were frequently lost in the tracking algorithm, and particles larger than 6 µm commonly were aggregates that could break apart and move in parts. The quality histogram threshold was set above 37. The particles were tracked using the simple Linear Assignment Problem (LAP) tracker function, with linking and gap-closing conditions of 30 and 40 pixels respectively, and a maximum frame gap of 0 frames

(frame rate: 18.3 frames per second). Velocity tracking in Fig. 5 is visualized as colour-coded mean velocity tracking lines, showing individual velocities of the particles.

Raman scattering microspectroscopy in the chips

Raman scattering spectra of particles in the chips were recorded using a long working distance ×50/0.5 objective of a LabRAM HR Evolution confocal Raman microscope, equipped with 785 nm diode excitation laser, 600 gr/mm diffraction grating, and front-illuminated thermoelectrically deep-cooled CCD camera Sincerity (Horiba Scientific). The confocal mode of the microscope was used, employing 50 μm diameter pinhole. Spectra in the spectral region 200-970 cm-1 were acquired with an acquisition time of 30 s and 32 accumulations, at full excitation laser power (neutral density filter T =100 %, P785 = 100 mW). Spectra of the particles in the chip were compared with mineral reference spectra and identified as quartz. Other peaks in the spectra are assigned to the PDMS (Supplementary Fig. 2).

Statistical analyses

Data was statistically evaluated in JMP Pro 15.0 (SAS Institute Inc., Cary, USA) with the significance level set to α=0.05, two-sided tests. Analysis was performed on log-transformed data if necessary to meet normal distribution of the residuals.

Expt. 1: The influence of the chip-filling treatment and the different channel shapes on the maximum colonization distances of fungal hyphae, bacteria, and protists was evaluated via a restricted maximum likelihood ANOVA model, with the full-factorial combination of the two factors 'channel type' (three levels: zigzag/square/z-shaped; maximum extent per channel type) and 'nutrient treatment' (three levels: air/water/malt medium), and the factor 'chip replicate'/location (n=3) as a random attribute. The influence of the presence of fungal hyphae on the presence of bacteria in Expt. 1 was investigated in a paired set of channels with a hypha, against directly adjacent channels without hypha, n=4. Data of four channel pairs from one air-filled chip were evaluated by a paired two-way t-test. In an alternative approach, individual pores were used as a replication base, n=33 in 4 pairs in a restricted maximum likelihood ANOVA model depending on the presence/absence of a hypha and with pairs as random attribute factor, which produced similar results. The influence of the presence of fungal hyphae on the presence of water in the diamond widenings of the initially air-filled chips was analysed with a 2×2 contingency analysis and evaluated for dependency with Pearson's Chi-squared test.

Expt. 2: A restricted maximum likelihood ANOVA model with the full-factorial combination of the two factors 'channel type' (three levels: zigzag/square/z-shaped; 12 of each channel types per chip) and 'nutrient treatment' (three levels: air/water/malt medium), and the factor 'chip replicate' (n=2) as a random attribute,

was used to test the influence of nutrient condition and channel shape on fungal, bacterial, and protist dispersal.

Expt. 3: A restricted maximum likelihood ANOVA model, with a full-factorial combination of the factors 'time' and 'presence of hyphae', and with the factor 'chip replicate' (n=3) as a random attribute, was used to test the influence of fungal hyphae on water ingression, bacterial, and protist dispersal over time both on pore space (n=1188 x 3 chips) and at channel replication (n=36 x 3 chips).

The datasets generated and analyzed during the current study presented in Figures 2-5, and image and video documentations are available from the corresponding author upon reasonable request.

Acknowledgements

We thank Martin Bengtsson for expertise and assistance during the design and production of the chips. EH acknowledges funding from the Foundation of Strategic Research (Future research leader grant SSF FFL18-0089), EH and PO acknowledge funding from the Swedish research council (VR-621-2014-5912), PO from the Sten K Johnsson foundation, EH and KA from the Crafoord foundation, the Wallenberg foundation and the strategic research environment for Biodiversity and Ecosystem Services in a Changing Climate (BECC).

Statement of authorship: EH and PM developed of the idea and concept of the study. KA designed and fabricated the soil chip master, PO provided technical assistance and expertise for the design and fabrication process. PM fabricated chips, recorded and analysed microbial growth inside the chips. EH statistically analysed the data from the chips. PM and EH prepared figures and movies. CA analysed particle velocities. MP performed spectroscopic analysis of minerals in the chips. PM and EH wrote the first version of the manuscript. PM, CA, KA, MP, PO and EH contributed to interpretations of the data, the revisions and the finalization of the manuscript.

References

1. Totsche, K.U. et al. Microaggregates in soils. J. Plant Nutr. Soil Sci. 181, 104–136 (2018).
2. Nunan, N. The microbial habitat in soil: Scale, heterogeneity and functional consequences. J. Plant Nutr. Soil Sci. 180, 425–429 (2017).
3. Erktan, A., Or, D. & Scheu, S. The physical structure of soil: Determinant and consequence of trophic interactions. Soil Biol. Biochem. 148, 107876 (2020).
4. Tecon, R. & Or, D. Biophysical processes supporting the diversity of microbial life in soil. FEMS Microbiol. Rev. 41, 599–623 (2017).

5. Schmidt, M. W. I. et al. Persistence of soil organic matter as an ecosystem property. Nature 478, 49–56 (2011).
6. Hobbie, J. E. & Hobbie, E. A. Microbes in nature are limited by carbon and energy: The starving-survival lifestyle in soil and consequences for estimating microbial rates. Front. Microbiol. 4, 1–11 (2013).
7. Yang, P. & van Elsas, J. D. Mechanisms and ecological implications of the movement of bacteria in soil. Appl. Soil Ecol. 129, 112–120 (2018).
8. Ebrahimi, A. N. & Or, D. Microbial dispersal in unsaturated porous media: Characteristics ofmotile bacterial cell motions in unsaturated angular pore networks. Water Resour. Res. 50, 7406–7429 (2014).
9. Geisen, S. et al. The soil food web revisited : Diverse and widespread mycophagous soil protists. Soil Biol. Biochem. 94, 10–18 (2016).
10. Schimel, J. P. Life in Dry Soils: Effects of Drought on Soil Microbial Communities and Processes. Annu. Rev. Ecol. Evol. Syst. 49, 409-432 (2018).
11. Hol, F. J. H. & Dekker, C. Zooming in to see the bigger picture: Microfluidic and nanofabrication tools to study bacteria. Science (80-.). 346, (2014).
12. Baveye, P. C. et al. Emergent properties of microbial activity in heterogeneous soil microenvironments: Different research approaches are slowly converging, yet major challenges remain. Front. Microbiol. 9, 1–48 (2018).
13. Fierer, N. Embracing the unknown: Disentangling the complexities of the soil microbiome. Nat. Rev. Microbiol. 15, 579–590 (2017).
14. Raynaud, X. & Nunan, N. Spatial ecology of bacteria at the microscale in soil. PLoS One 9, (2014).
15. Rovira, A. D. & Greacen, E. L. The effect of aggregate disruption on the activity of microorganisms in the soil. Aust. J. Agric. Res. 8, 659–673 (1957).
16. Brose, U. & Scheu, S. Into darkness: unravelling the structure of soil food webs. Oikos 123, 1153–1156 (2014).
17. Wilpiszeski, R. L. et al. Soil Aggregate Microbial Communities: Towards Understanding Microbiome Interactions at Biologically Relevant Scales. Appl. Environ. Microbiol. 85, 1–18 (2019).
18. Vos, M., Wolf, A. B., Jennings, S. J. & Kowalchuk, G. A. Micro-scale determinants of bacterial diversity in soil. FEMS Microbiol. Rev. 37, 936–954 (2013).
19. Whitesides, G. M. The origins and the future of microfluidics. Nature 42, 368-373 (2006).
20. Aleklett, K. et al. Build your own soil: Exploring microfluidics to create microbial habitat structures. ISME J. 12, 312–319 (2018).
21. Stanley, C. E., Grossmann, G., Casadevall i Solvas, X. & DeMello, A. J. Soil-on-a-Chip: microfluidic platforms for environmental organismal studies. Lab Chip 16, 228–241 (2016).
22. Nichols, D. et al. Use of ichip for high-throughput in situ cultivation of "uncultivable microbial species▽. Appl. Environ. Microbiol. 76, 2445–2450 (2010).

23. Borer, B., Tecon, R. & Or, D. Spatial organization of bacterial populations in response to oxygen and carbon counter-gradients in pore networks. Nat. Commun. 9, 769 (2018).
24. Schmieder, S. S. et al. Bidirectional Propagation of Signals and Nutrients in Fungal Networks via Specialized Hyphae. Curr. Biol. 29, 217-228.e4 (2019).
25. Aleklett, K., Ohlsson, P., Bengtsson, M. & Hammer, E. C. Fungal foraging behaviour and hyphal space exploration in micro-structured Soil Chips. ISME J. 1–12 doi:10.1038/s41396-020-00886-7
26. Kuzyakov, Y. & Blagodatskaya, E. Microbial hotspots and hot moments in soil: Concept & review. Soil Biol. Biochem. 83, 184–199 (2015).
27. Held, M., Kaspar, O., Edwards, C. & Nicolau, D. V. Intracellular mechanisms of fungal space searching in microenvironments. Proc. Natl. Acad. Sci. U. S. A. 116, 13543–13552 (2019).
28. Soufan, R. et al. Pore-scale monitoring of the effect of microarchitecture on fungal growth in a two-dimensional soil-like micromodel. Front. Environ. Sci. 6, 68 (2018).
29. Zhang, Y., Kastman, E. K., Guasto, J. S. & Wolfe, B. E. Fungal networks shape dynamics of bacterial dispersal and community assembly in cheese rind microbiomes. Nat. Commun. 9, 1–12 (2018).
30. Kohlmeier, S. et al. Taking the fungal highway: Mobilization of pollutant-degrading bacteria by fungi. Environ. Sci. Technol. 39, 4640–4646 (2005).
31. Ingham, C. J., Kalisman, O., Finkelshtein, a. & Ben-Jacob, E. Mutually facilitated dispersal between the nonmotile fungus Aspergillus fumigatus and the swarming bacterium Paenibacillus vortex. Proc. Natl. Acad. Sci. 108, 19731–19736 (2011).
32. Warmink, J. A. & Van Elsas, J. D. Selection of bacterial populations in the mycosphere of Laccaria proxima: Is type III secretion involved? ISME J. 2, 887–900 (2008).
33. Simon, A., Hervé, V., Al-Dourobi, A., Verrecchia, E. & Junier, P. An in situ inventory of fungi and their associated migrating bacteria in forest soils using fungal highway columns. FEMS Microbiol. Ecol. 93, 1–9 (2017).
34. Deng, J. et al. Synergistic effects of soil microstructure and bacterial EPS on drying rate in emulated soil micromodels. Soil Biol. Biochem. 83, 116–124 (2015).
35. Pion, M. et al. Gains of Bacterial Flagellar Motility in a Fungal World. Appl. Environ. Microbiol. 79, 6862–6867 (2013).
36. de Menezes, A. B., Richardson, A. E. & Thrall, P. H. Linking fungal–bacterial co-occurrences to soil ecosystem function. Curr. Opin. Microbiol. 37, 135–141 (2017).
37. Deveau, A. et al. Bacterial-fungal interactions: Ecology, mechanisms and challenges. FEMS Microbiol. Rev. 42, 335–352 (2018).
38. Worrich, A. et al. Mycelium-mediated transfer of water and nutrients stimulates bacterial activity in dry and oligotrophic environments. Nat. Commun. 8, 15472 (2017).
39. Koestel, J. & Schlüter, S. Quantification of the structure evolution in a garden soil over the course of two years. Geoderma 338, 597–609 (2019).

40. Clarholm, M., Bonkowski, M. & Griffiths, B. Protozoa and Other Protista in Soil. Mod. soil Microbiol. 147–175 (2007).
41. Geisen, S. & Bonkowski, M. Methodological advances to study the diversity of soil protists and their functioning in soil food webs. Appl. Soil Ecol. 123, 328–333 (2018).
42. De Gryze, S., Six, J. & Merckx, R. Quantifying water-stable soil aggregate turnover and its implication for soil organic matter dynamics in a model study. Eur. J. Soil Sci. 57, 693–707 (2006).
43. Ali, G., Macrae, M., Walker, M., Laing, J. & Lobb, D. Preferential Flow in Vertisolic Soils with and without Organic Amendments. Agric. Environ. Lett. 3, 1800180 (2018).
44. Bundt, M., Widmer, F., Pesaro, M., Zeyer, J. & Blaser, P. Preferential flow paths: Biological 'hot spots' in soils. Soil Biol. Biochem. 33, 729-738 (2001).
45. Weiler, M. & Flühler, H. Inferring flow types from dye patterns in macroporous soils. Geoderma 120, 137–153 (2004).
46. Luo, L., Lin, H. & Halleck, P. Quantifying Soil Structure and Preferential Flow in Intact Soil Using X-ray Computed Tomography. Soil Sci. Soc. Am. J. 72, 1058-1069 (2008).
47. Koestel, J. & Larsbo, M. Imaging and quantification of preferential solute transport in soil macropores. Water Resour. Res. 50, 4357-4378 (2014).
48. Sammartino, S. et al. Identifying the functional macropore network related to preferential flow in structured soils. Vadose Zo. J. 14, (2015).
49. Aufrecht, J. A. et al. Pore-scale hydrodynamics influence the spatial evolution of bacterial biofilms in a microfluidic porous network. PLoS One 14, e0218316 (2019).
50. Six, J., Bossuyt, H., Degryze, S. & Denef, K. A history of research on the link between (micro)aggregates, soil biota, and soil organic matter dynamics. Soil Tillage Res. 79, 7–31 (2004).
51. Lehmann, A., Zheng, W. & Rillig, M. C. Soil biota contributions to soil aggregation. Nat. Ecol. Evol. 1, 1828–1835 (2017).
52. Tayagui, A., Sun, Y., Collings, D. A., Garrill, A. & Nock, V. An elastomeric micropillar platform for the study of protrusive forces in hyphal invasion. Lab Chip 17, 3643–3653 (2017).
53. Pucetaite, M., Ohlsson, P., Persson, P. & Hammer, E. Shining new light into soil systems: Spectroscopy in microfluidic soil chips reveals microbial biogeochemistry. Soil Biol. Biochem. 153, 108078 (2021).

Supplementary material

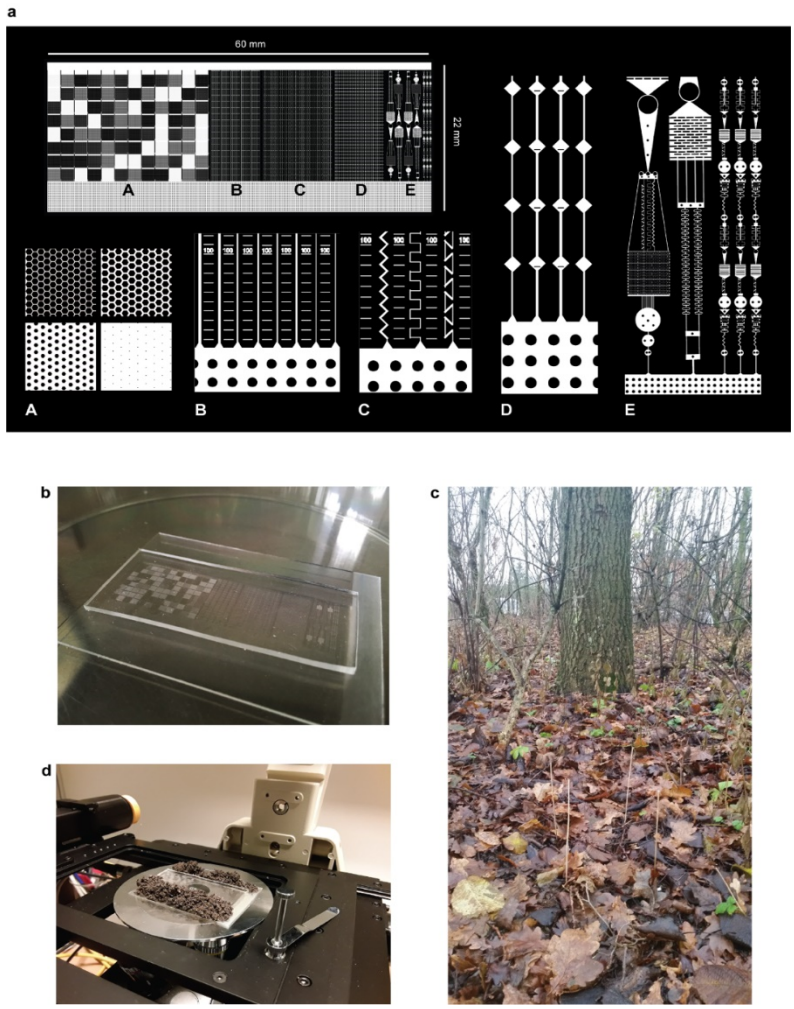

Supplementary Figure 1. The soil chip and its use in soil. a, Overview over the design of the chip's internal structures. b, Photograph of a newly produced chip. c, Burial site where a chip remained in the soil at 10 cm depth for two months. d, Microscopy analysis of the chip with adjacent soil after unearthing.

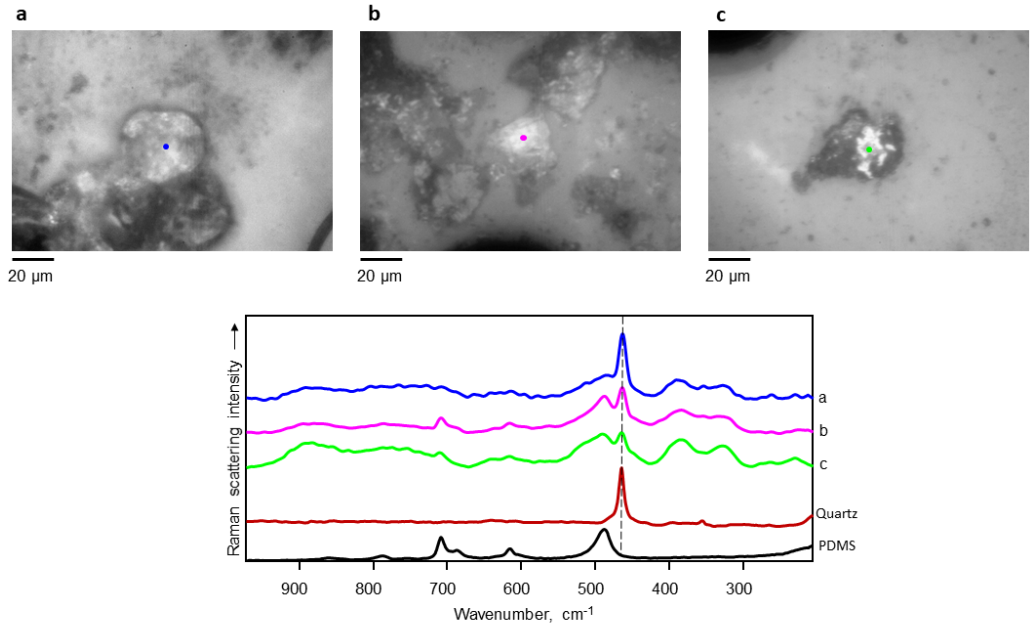

Supplementary Figure 2. Raman scattering microscopic analysis of mineral particles inside the chip. Examples of measured minerals (a-c), and their corresponding spectra over the reference spectra for quartz and PDMS.

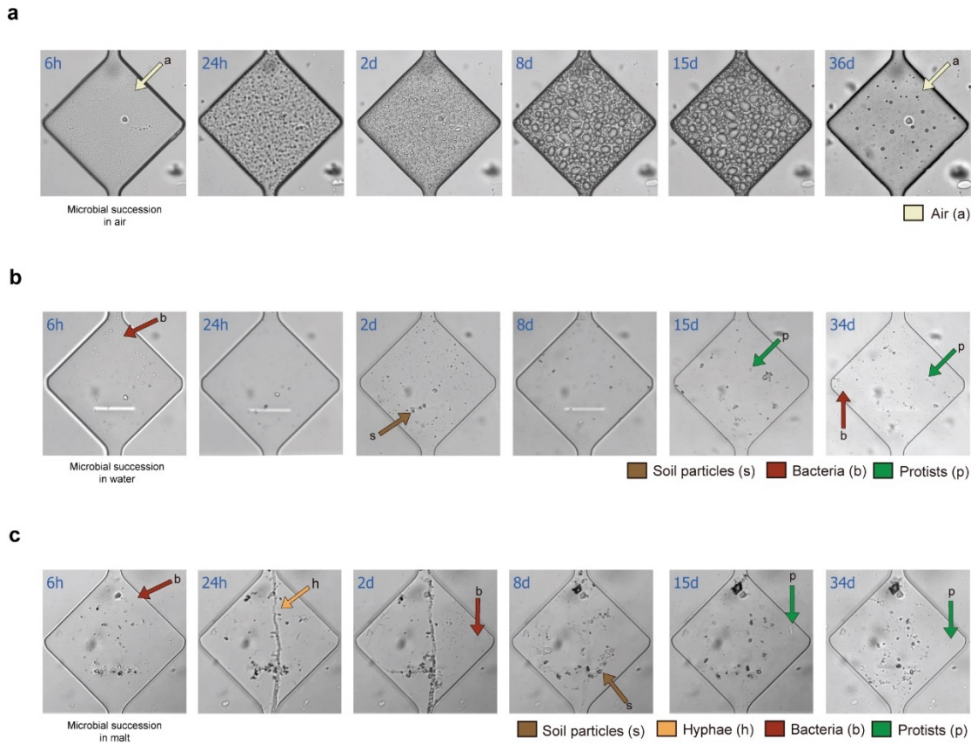

Supplementary Figure 3. Microbial succession in the soil chips incubated with soil in the laboratory. Image sequences of the time-resolved changes in microbial colonization of a diamond-shaped widening along the channels used to calculate the presence of major soil microbial groups and water films in chips filled with air (a), water (b) and malt (c) (GIFs 3-5, resp.).

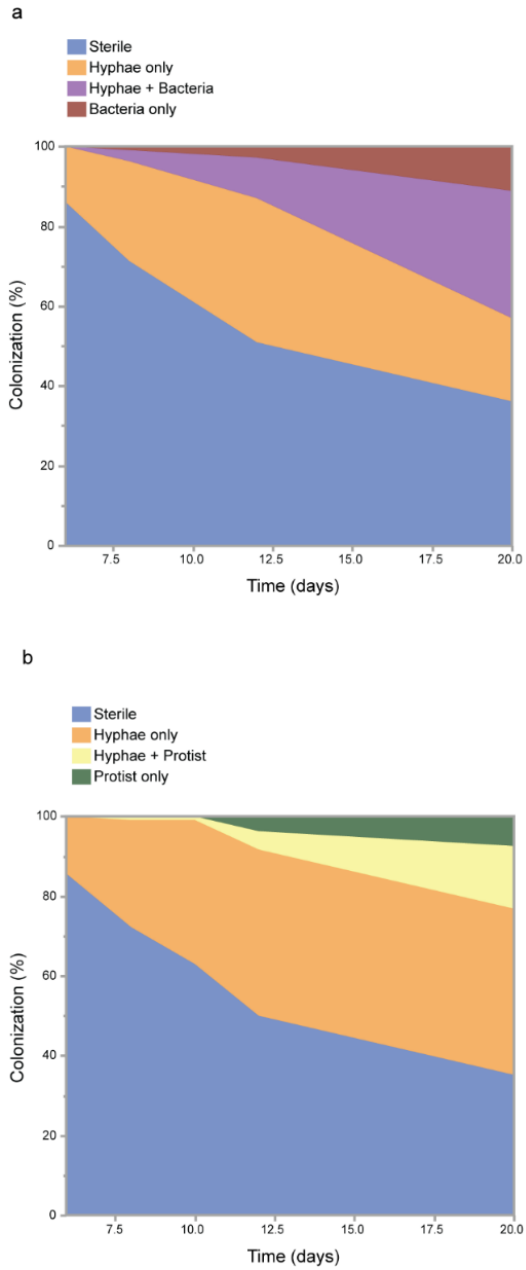

Supplementary Figure 4. Frequency of co-dispersal of bacteria and protists with fungal hyphae. Percentage of the 108 examined channels of three initially air-filled chips without any microorganism (sterile), with hyphae only, with bacteria or both (a), and with protists or both (b).

Paper II

Habitat geometry in artificial microstructure affects bacterial and fungal growth, interactions, and substrate degradation

Running Title: Habitat geometry affects decomposers

Authors:

Carlos Gustavo Arellano Caicedo[1,*]

Pelle Ohlsson[2]

Martin Bengtsson[2]

Jason P. Beech[3]

Edith C. Hammer[1]

Afiliations:

[1.] Department of Biology, Lund University, Lund, Sweden

[2.] Department of Biomedical Engineering, Lund University, Sweden

3. Division of Solid State Physics, Lund University, Sweden

*Corresponding author. E-mail address: carlos.arellano@biol.lu.se

Key words:

microhabitat, bacteria, fungi, bacterial-fungal interactions, organic matter stabilization, soil pore space, physical carbon stabilization, organic matter occlusion, microfluidics, micromodel, *Pseudomonas putida, Coprinopsis cinerea*

Abstract

Microhabitat conditions determine the magnitude and speed of microbial processes but have been challenging to investigate. In this study we used microfluidic devices to determine the effect of the spatial distortion of a pore space on fungal and bacterial growth, interactions, and substrate degradation. The devices contained channels differing in bending angles and order. Sharper angles reduced fungal and bacterial biomass, especially when angles were repeated in the same direction. Substrate degradation was only decreased by angles when fungi and bacteria were grown together. Investigation at the cellular scale suggests that this was caused by fungal habitat modification, which branched in sharp and repeated turns, blocking the dispersal of bacteria and the substrate.

Our results demonstrate how the geometry of microstructures can influence microbial activity. This can be transferable to soil pore spaces, where spatial occlusion and microbial feedback on microstructures is thought to explain organic matter stabilization.

Introduction

Spatial confinement affects microbial behavior, interactions and the chemical processes they drive [1]–[5]. The need to include spatial explicitness into microbial studies has recently been pointed out in research related to biofilm formation [6], host-pathogen interactions in microenvironments [7], the coexistence of bacteria with bacteriophages [8], and competing bacteria in gut microbiomes [9]. Spatially defined microhabitats are especially relevant in soils and can explain many of its unique properties [10]–[12], where the heterogeneous distribution of pores, nutrients, air and gas in soils enhances microbial diversity and functions [13].

Microbes determine the biogeochemical cycles across all ecosystems [14], where changes in microbial metabolism can lead to an acceleration or a delay of such cycles. It has been hypothesized that spatial restriction plays an important role in preventing microbial access to soil organic matter (SOM) [15], which could explain the persistence of large amounts of SOM despite being largely composed of simple and highly nutritious molecules [16]. Since SOM constitutes a carbon stock that is larger than the combined stocks of the atmosphere and global vegetation [17], changes in its carbon cycling rates will have consequently large effects on atmospheric CO2 levels. However, our understanding of how physical microstructure of soils affects microbes and their ecosystem functions, such as SOM turn over, is limited [18].

Morphology and topology of the soil pore space have been characterized using direct methods of visualization, such as electron microscopy and X-ray tomography [19]–[22]. X-ray tomography studies have revealed correlations between pore size and SOM losses, feedback of SOM decay on the porous space, and an influence of pore heterogeneity, and their connection to the atmosphere as determinants of SOM fate [23]–[27]. Studies using these techniques have, however, limitations such as the lack of a controlled and manipulatable environment, the lack of real-time measurement of processes in the inner space, disturbance of natural conditions during sample preparation, subjectivity when thresholding greyscale images, and a current resolution limit of a few tens of micrometres which does not allow the study of smaller micropores [28].

A complementary approach that solves these issues is to study soil pore space using model systems. Such model systems include the use of a controlled assembly of different soil materials [29], transparent materials [30], or 3D-printed soil structure proxies [30]. A particularly promising approach is micro-engineered or microfluidic devices [31].

Microfluidics is defined as the manipulation of fluids within structures at the micrometre scale [32]. The use of microfluidics opens up the possibility of studying a wide range of microbial phenomena at the micrometre scale in a higher level of detail than with other methods. Some of the microbial processes studied with microfluidics include chemotaxis [33]–[36], bacterial motility [34], the effect of

EPS in soil drying processes [37], transport of nanoparticles by unicellular eukaryotes [38], and fungal-bacterial interactions [39]. These systems can also be powerful tools to investigate the effect of soil physical characteristics on soil microbial communities [31].

In the present study we have developed a microfluidic approach to explore the effect of a simulated pore space, consisting of differently angled channels, on fungal and bacterial biomass distribution and organic matter degradation. We chose to use the geometrical structures of long channels differing in their deviation from a straight, undisturbed passage that could represent major patterns found in the soil pore space. The studied channels differed in their bending angle, and the turning direction of the angles, which resulted in different tortuosities (the ratio of the channel length to the straight distance between the beginning and the end of it). Angles were selected to represent the three main types of angles that can exist within a range of 180 degrees (acute, right, and obtuse). To track substrate degradation, we used a fluorogenic peptide that becomes fluorescent after enzymatic cleavage. The selected substrate is degraded only by the bacterial and not the fungal strain used, which allows us to estimate how bacterial substrate degradation is affected through the experiment. Our hypotheses were: (1) Bacterial and fungal biomass will be most strongly reduced in channels with sharp turning angles and repeated turn order. This, we thought, would occur because obstacles reduce fungal growth, according to models based on tomography images [40], as well as because sharp angles require sharper turns than the natural turns of free swimming bacteria [41]. (2) When growing together, we expected an enhancing effect of the angle and turn order on bacteria and fungi respectively, because the presence of the other organism's biomass contributes to the solid physical structure, thus increasing the complexity of the spatial structures. Finally, we hypothesized that (3) bacterial substrate degradation would follow bacterial biomass patterns and thus be higher in channels with smooth angles and alternated turns.

Materials and methods

Chip design

The chip design was drawn in AutoCad 2018 (Autodesk) and consists of six kinds of treatment channels and a pillar system that served as an entrance to the channels (Figure 1). The pillar system is formed by pillars of 100 micrometers in diameter, separated by 100 micrometers, and allows bacteria and fungi to penetrate the full width of the chip before entering the treatment channels. The treatments consist of dead-end channels of six different geometries (n=10/per chip) with the same internal volume. The channels are randomly distributed in parallel orientation along the chip.

The parameters assigned to the channels were "Angle" and "Turn order". The angles used were 45˚, 90˚, 109˚, measured as the deviation from a continued straight line

and thus the turning angle an organism in this channel needs to perform (Figure 1). Channels of each angle had two types of arrangements, one with an alternated turn order, and one with a repeated turn order. Channel types with an alternated turn order followed a pattern of alternating right and left bends, while channels with repeated turn order followed a pattern of two right turns followed by two left turns. The channels dimensions were adjusted so that every type of channel would contain the same volume (2.42 nL) with a width of 10 µm and a height of 12 µm. Each channel segment was 50 µm long before the next turn.

Chip fabrication

The chip was molded in polydimethylsiloxane (PDMS) silicone rubber and bonded onto a glass bottom Petri dish [31]. The master that served as mold for the PDMS was in turn fabricated through photolithography using a photomask.

The photomask was made of soda lime glass with a thin layer of chromium (Nanofilm, CA, USA). The shapes were patterned with a dwl66+ mask writer (Heidelberg Instruments, Germany). A NdYag laser, 532 nm, was used to draw patterns on a photoresist, AZ1500. The pattern was subsequently developed in AZ 351B positive developer and the chromium etched in TechniEtchCr01 (Microchemicals GmbH, Ulm Germany). For master fabrication, SU-8 2015 (MicroChem, Newton, MA, USA) was dispensed onto a heat-dried (90 degrees 30 minutes) 3-inch silicon wafer (Siegert Wafer, Aachen, Germany) and spun at 4000 rpm to achieve a 12 µm thick layer. The SU-8 was exposed with UV-light in a contact mask aligner (Karl Suss MJB4 soft UV, Munich, Germany). After UV exposure, the non-crosslinked photoresist was developed (MrDev600) and rinsed with isopropanol. To prevent PDMS from sticking to the mold, the wafer was activated in oxygen plasma for 60 seconds (ZEPTO, Diener Plasma-Surface Technology, Germany) and exposed overnight to a vapor of trichloro (1H,1H,2H,2H-perfluorooctyl) silane (PFOTS, Sigma Aldrich, Saint Louis, MO, USA) at 180 degrees during which a monolayer is formed. SYLGARDTM 184 PDMS (Dow Chemicals Company, Midland, Michigan) was made by mixing the elastomer with the curing agent in a mass proportion of 10:1, poured on top of the master, degassed at -15 kPa for one hour and polymerized in an oven at 60 ˚C for two hours.

The PDMS labyrinths were removed from the master and a rectangular portion of 2.5 cm x 0.5 cm was cut out in the middle of the pillar system, approximately 0.5 cm away from the entrance of every channel. This cut was made to create the reservoir that served as entrance to the labyrinth (Figure 1b). The PDMS labyrinths and a glass bottom Petri dish were activated using a Zepto Plasma System (Diener Plasma Surface Technology, Germany; negative polarity; 1 min for cover slips and 10 seconds for PDMS labyrinths). Directly after activation, the surfaces were put together, forming a tight, irreversible bond [42], and 150 µl of the treatment medium was introduced through the reservoir to keep the channels hydrophilic.

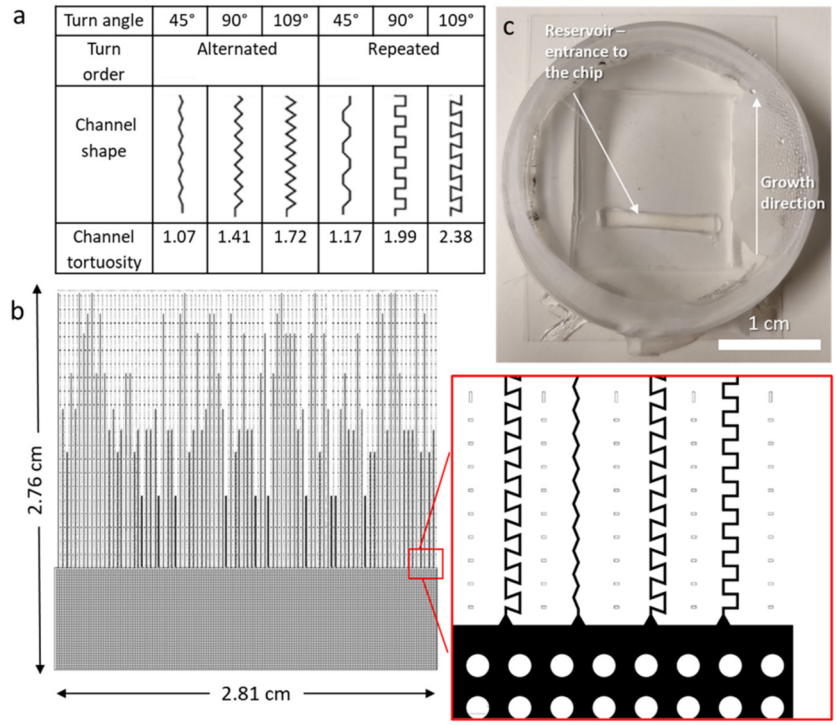

Figure 1. Chip design and arrangement of channels. (a) Channel geometries used in the Channel chip. Each channel has one type of bending angle (45°, 90°, and 109°) and one turn order (alternated or repeated). The channel tortuosity is shown in the last row, which is the ratio between the distance inside the channel between two points and the distance between the same points in a straight line. (b) Chip design, consisting of a pillar system serving as the entry area to the channels, and the array of channels in six variations, randomly distributed along the chip. The chip design dimensions were: 281 mm x 276 mm. (c) The PDMS chip bonded to a custom-made glass bottom Petri dish, containing the growth medium and microbial cultures introduced via the rectangular reservoir opening.

Bacterial strains and growth conditions

The bacterial strain used in the experiment was Pseudomonas putida mt-2 carrying plasmid-borne msfGFP-reporter constructs. Bacteria were pre-cultured overnight in M9 minimal medium (12.8 g/L NaHPO4.7H2O, 3 g/L KH2PO4, 0.5 g/L NaCl, 100 mg/L NH4Cl, 0.12 g/L MgSO4, 4 g/L d-Glucose, 11.66 mg/L CaCl2, 13.5 mg/L FeCl2, 125 mg/L MgCl2.6H2O, 1 mg/L MnCl2.4H2O, 1.7mg of ZnCl2, 0.43mg CuCl2.2H2O, 0.6 mg CoCl2.6H2O, 0.6mg Na2MoO4.2H2O, pH 6.5) [43] with pH 6.5 at 28°C and agitated at 150 rpm.

The experiments with Pseudomonas putida mt-2 were conducted as follows: 2 ml of overnight cultures were pelleted by centrifugation (5000 g for 10 min at 21 °C), and cells were resuspended in 0.5 ml of fresh M9 medium. L-Alanine 7-amido-4-methylcoumarin (AMC, 160 mg/L) was added to the medium to determine substrate consumption inside the chips. AMC is a fluorogenic substrate that becomes fluorescent when it is enzymatically hydrolyzed by aminopeptidase enzymes [44].

The fluorescence from the AMC shows the extent of enzymatic activity that the bacteria have, which can be quantified within each structure. 1.5 µl of the bacterial suspension was added to the entrance of the chip to obtain a final optical density at 600 nm of 0.2 OD600 [45], [46].

Fungal strains and growth conditions

The fungal strain used was Coprinopsis cinerea AmutBmut PMA412, expressing constitutively the cytoplasmic fluorescent dTomato protein [47]. Pre-incubation was done in 1.5% agar plates containing Yeast Malt Glucose medium [39]. A rectangular plug of the mycelium sized 1 mm x 25 mm was placed upside down in the reservoir inside the chip. Care was taken to separate the fungal mycelium from the top of the agar plug so that no extra nutrients would be added to the medium. The inner part of the labyrinth was filled beforehand with M9 medium containing 160 mg AMC/L (pH 6.5) by capillary forces directly after bonding. After 48 hours, once the hyphae had arrived at the entrance of the channels, the medium from the reservoir was extracted and replaced with fresh medium. In the fungal-bacteria treatment, an inoculum of Pseudomonas putida was introduced in the reservoir after the medium replacement to a final concentration of OD600 0.2. Sterile wet tissues were placed inside the Petri dishes to preserve humidity. The plates were sealed with Parafilm to prevent water from evaporating and kept in the dark at room temperature.

In total, 15 chips were used for the experiment, 5 containing Pseudomonas putida and 5 with Coprinopsis cinerea (absence of competitor), and 5 containing both (presence of competitor).

Microscopy

Epifluorescence microscopy was used for visualization of P. putida, C. Cinerea, and AMC using a fully motorized Nikon Ti2-E inverted microscope with PFS4 hardware autofocus, full 25 mm field-of-view, CoolLED pE300-White MB illumination connected via a 3 mm liquid light guide (LLG), and a Nikon Qi2 camera with 1x F-mount adapter. The filters used were LED-DAPI-A-2360A Semrock Filter Cube (Ex: 380-405 nm, Em: 413-480 nm), GFP-4050B Semrock Filter Cube (Ex: 444-488 nm, Em: 498-553 nm), mCherry-C Semrock Filter Cube (Ex: 520-585 nm, Em: 600-680 nm). The entire chip images for overall fluorescence quantification were captured using a (MRH00041) CFI Plan Fluor 4X, N.A. 0.13, W.D. 17.1 mm objective, with an exposure time of 20 ms for GFP, 100 ms for DAPI, and 100 ms for mCherry. For high magnification pictures a (MRD31905) CFI Plan Apochromat DM Lambda 100X Oil N.A. 1.45, W.D. 0.13mm and a (MRD30405) CFI Plan Apochromat DM Lambda 40X, N.A. 0.95, W.D. 0.21mm objectives were used. NIS-Elements software was used for coordination of the multipoint imaging. Pictures were taken for every chip for 14 days. The days selected for analysis were the ones of maximum biomass, namely day 2 for Pseudomonas putida biomass and

its AMC consumption, and day 6 for Coprinopsis cinerea biomass, its AMC consumption, and the AMC consumption of the fungal+bacterial conditions.

Image Analysis

The fluorescence intensity was quantified using ImageJ 1.52n [48]. Background was subtracted using the ImageJ rolling ball algorithm [49] using 7 pixels as radius of rolling ball for images taken with 4x objective. The rolling ball radius was given based on the size of the biggest fluorescent object, which was the width of a channel. After the subtraction, the mean florescence intensity per pixel was quantified inside each channel using the ROI manager tool. The rectangular ROIs were of the same size and covered every individual channel of the experiment.

To attain a deeper understanding of the fluorescence distribution along the channels, fluorescent profiles were obtained for every type of channel. For this purpose, the segmented line tool and the measure tool were used to cover manually the entire length of the channels.

Besides the images obtained with the 4x objective, the 40x and the 100x objectives were used to obtain higher magnification images to facilitate overall result interpretation. The time-lapse videos of colonizing hyphae were obtained with a 40x objective every 5 minutes for a total period of 12 hours.

Statistical Analysis

For in-depth statistical analysis, the data from the day typically showing maximum biomass (indicated by maximum fluorescence, Supplementary Figure 1) was chosen, namely day 2 for bacteria and day 6 for fungi. Day 6 was also selected for substrate consumption comparison.

The experiment had a full-factorial design with the factors Angle (45°, 90°, 109°), Turn order (alternated or repeated), and Competition (presence or absence of the other organism). Each chip had 10 channels of each type (with all the angle-turn order combinations), and five chips of each inoculation type were analyzed: 5 with bacteria (bacteria in absence of competitor), 5 with fungi (fungi in absence of competitor), and 5 with bacteria and fungi (presence of competitor). Multilevel model fitting correcting for random effects was used to test the influence of every factor on the variables. Additionally, a three-way multivariate ANOVA correcting for random effects was conducted using R [50] for testing significant differences in variances. Random effects were attributed to each microfluidic device as a physical replicate of the experiment. Angle, turn order, and competition were considered fixed factors for bacterial and fungal biomass, while angle, turn order, and organism (fungi, bacteria, fungi+bacteria) were the fixed factors for substrate consumption. Fluorescence data was log-transformed to obtain normality of the residuals and homogeneity of variances. The significance threshold used for all statistical tests was $p < 0.05$. When significant differences were found in the ANOVA, interactions

were analyzed separately using Dunn's method for multiple comparison of means [51]. Pairwise comparisons were performed with t-tests, using Holm corrected p-values [52].

Also, linear regressions were done using R, with bacterial biomass, fungal biomass, and substrate consumption as dependent variables and tortuosity of the channels as independent variables.

Results

We inoculated the chips with either a fungal (Coprinopsis cinerea), a bacterial (Pseudomonas putida), or a fungi+bacteria inoculum. The chips contained six types of channels that varied in two parameters: bending angle (45°, 90°, 109°) and bending order (alternated, repeated). Bacterial and fungal growth, together with substrate consumption (L-Alanine 7-amido-4-methylcoumarin trifluoroacetate salt), were followed over time using fluorescence microscopy. During the 14 days the experiment lasted, the organisms successfully colonized all chip channels of all tested turn angles and turn orders (**Fel! Hittar inte referenskälla.**, Supplementary Figure 1) and caused measurable substrate consumption along the channels (Supplementary Figure 2).

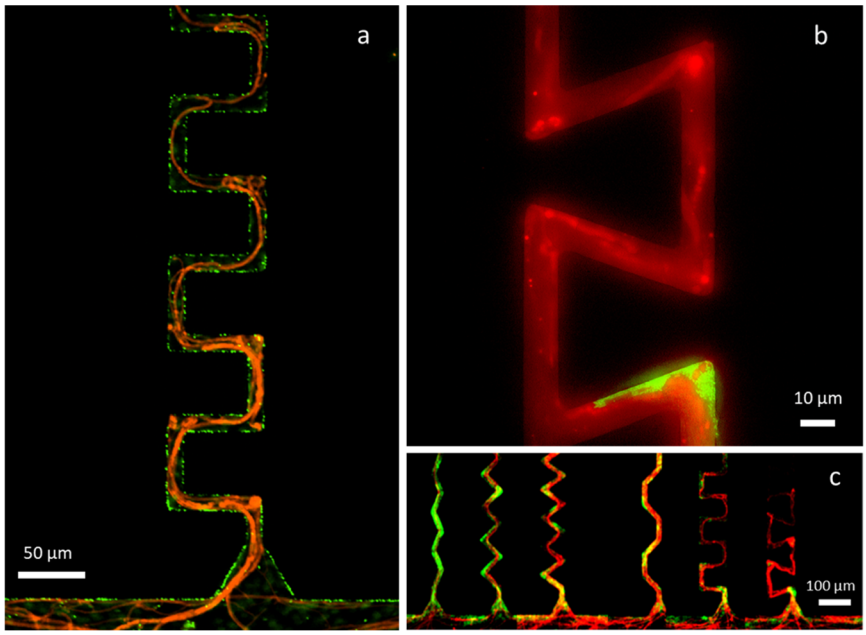

Figure 2. Epifluorescence images of the bacterial strain P. putida mt-2 (green) grown together with the fungal strain C. cinerea AmutBmut PMA412 (red) on M9 liquid medium inside the PDMS chip on day 2 after inoculation. (a) 90°-angled channel with repeated turn order. (b) 109°-angled channel with repeated turn order where fungal hyphae block the channel and do not allow bacteria to advance further. (c) All the type of channels studied (from left to right: 45°, 90°, and 109°, with alternated turning order, and 45°, 90° and 109°, with repeated turning order) at 4x magnification.

Bacterial biomass

While all channels were colonized over their whole length (Figure 5), there were significant differences in the amount of bacterial biomass depending on the angle and order of their turns (Figure 3a). Angles reduced bacterial biomass as they became sharper. However, their effect was stronger when the bending order was repeated and when the fungus was present (Figure 3a, Supplementary Table 1, Supplementary Table 2, Supplementary Table 3). Repeated bending order lowered bacterial biomass, independently of whether the fungus was present or not. Alternated and repeated turn order channels differed significantly from each other in their impact on bacterial biomass only at angles of 90 and 109 degrees (Supplementary Figure 3) while they did not differ at angles of 45 degrees.

When the fungus was present, the effect of channel turning angles on bacterial biomass was increased, producing significantly lower bacterial biomass as angles became sharper. Such reduction occurred regardless of their angle turn order. b shows an example of fungal hyphae blocking the access of bacteria to the deeper part of the channel.

Bacterial biomass was also negatively correlated with channel tortuosity (Supplementary Figure 4a, Supplementary Table 4), increasingly when fungi were present.

Fungal biomass

Angles reduced fungal biomass in general as they became sharper, but their impact was significantly higher when their turn order was repeated b, Figure 5, Supplementary Table 5, Supplementary Table 6, Supplementary Table 7). The presence of bacteria caused a reduction of the overall fungal biomass independently of the structures. The fungal biomass was distributed heterogeneously along the different types of channels, where typically most of the hyphae concentrated in the first parts of the channels, while fewer, if any, hyphae progressed towards the deep interior of the channels. The dispersal distance into the channels was especially decreased in sharp angle and repeated turn order channels (Figure 4). Supplementary videos 1-6 and Figure 4 show the effect of every type of angle and turn order on the fungal growth.

Fungal biomass was negatively correlated with channel tortuosity (Supplementary Figure 4b, Supplementary Table 8) and had a steeper slope when regressed against tortuosity in the absence of bacteria.

Substrate consumption

Bacteria caused degradation of the AMC substrate detectable within 24 hours, while fungi did not cause significant degradation during the experiment. The effect that the structures had on bacterial substrate degradation depended on the interactions with the fungi present in the chip (Figure 3c). Bacteria alone had a generally higher substrate consumption than fungi alone in all types of channels and was not affected by the turn angles or the turn order of the channels (Supplementary Table 9, Supplementary Table 10, Supplementary Table 11).

Only when bacteria were cultivated with fungi the AMC degradation was significantly affected by both the turn angle and turn order (Supplementary Figure 6), generally showing decreasing substrate degradation as turn angles became sharper, and when turn order was repeated.

Substrate degradation was distributed differently along the channels depending on the treatment conditions (Figure 5), being highest in the middle of the channel and decreasing towards the ends for bacteria only. This effect was less strong in the sharper angled channels and changed to a gradual increase with increasing channel depth when fungi were present. Substrate degradation was negatively correlated with channel tortuosity only when bacteria and fungi grew together (Supplementary Figure 4c, Supplementary Table 12).

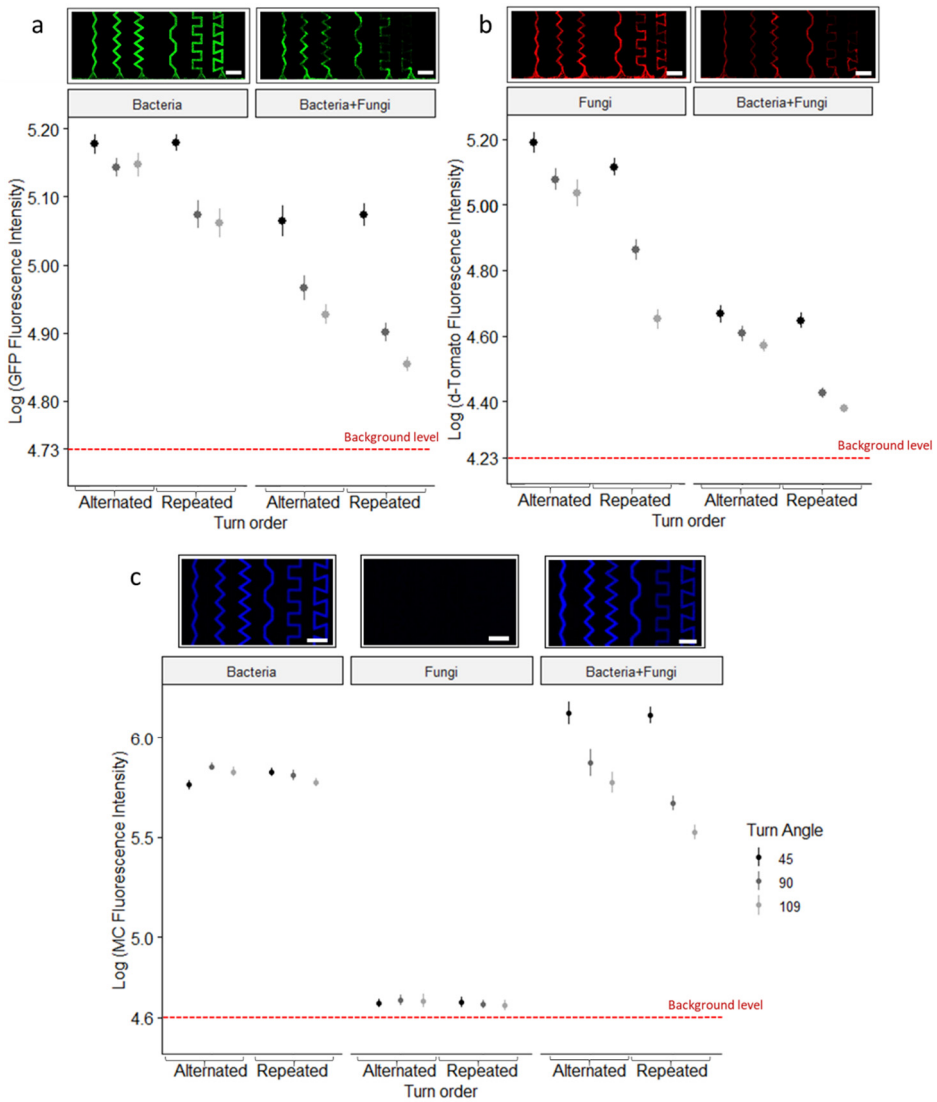

Figure 3. Bacterial and fungal biomass and their substrate consumption in differently angled channels. Upper pannels show examples of the initial part of the microfluidic channels colonized by P.putida expressing GFP constitutively inside the microfluidic chip, on day 2 after inoculation, growing without (left) and with (right) the competitor C. cinerea (scale bar=100 µm). Bottom panels show the three-way analysis of the response of bacterial biomass to the different channel types at day 2, in absence (left) and in presence (right) of the fungal competitor C. cinerea, as quantified via bacterial GFP fluorescence expression. (b) Upper pannels show examples of the initial part of the microfluidic channels colonized by C.cinerea expressing d-Tomato constitutively, on day 6 after inoculation, growing in absence (left) and presence (right) of the competitor P. putida. Below shows the three-way analysis plot of the d-Tomato fluorescence intensity of C. cinerea inside the channels on day 6, without (left) and with (right) the competitor P. putida. (c) Upper panels show the substrate consumption represented by fluorescence of released 4-methylcoumarin in the initial part of the microfluidic channels, at day 6 after inoculation with the bacterial strain P. Putida ("bacteria"), the fungal strain C. cinerea ("fungi"), and the combined experiment containing P. putida and C. cinerea ("bacteria+fungi"; Scale bars = 100 µm). The symbols represent the mean log-transformed fluorescence of the respective fluorophore for each treatment and the error bars represent the ±SE based on ANOVA for all the channel types (n=50).

Discussion

Channel shapes similarly affected C. cinerea and P. putida when they had been grown alone. But when grown together, the effect of shapes on bacteria increased, whereas it remained similar on fungi. The pore space habitat inside the chip was dynamic and evolved over time as both strains grew. When both strains were together, fungi changed the physical environment so much that it resulted in a reduction in bacterial growth. Bacterial habitat modification, on the other hand, did not affect fungal foraging, which was only affected by the (solid) chip obstacles. The effect of the habitat modification was also reflected on the substrate consumption, which was affected by structures only when bacteria and fungi grew together.

Bacterial biomass

Bacterial biomass was reduced as the turning angle became sharper. The effect of the angles was enhanced when their turn order was repeated. This interaction occurred, however, only at sharp angles, 90° and 109°. This result might be explained by the fact that a 45° turning angle is still inside the range of angles that P. putida tumble (randomly change direction) in a free-swimming environment [41]. Therefore, bacteria can swim through these channels without being significantly affected by the corners and the way they are arranged. On the other hand, in 90° and 109° angle channels, repeated turn order reduced the motility of bacteria more strongly. This suggests that bacteria not only keep a tumble frequency memory [53] but also a tumble direction memory, which seems to be affected by the repeated turn order angles, leading to an increased time to cover a distance [54]. Bacterial biomass at 45°, however, was similar for both angle arrangements, suggesting that before the critical point (90°), turning directions do not affect the dispersal and growth of bacteria. Bacterial accumulation has been modeled to occur in 90° corners [55], and similar accumulations seem to be occurring in the present experiment at 90° and 109°, which can block additional parts of the void pore space and by this impede further bacterial dispersal. It has been shown that the mean distance bacteria run before tumbling for bacterial strains such as E. coli is approximately 19 μm [56], which is lower than the distance between channel turns in our experiment (50 μm). Having a shorter distance between the channel turns could, thus, produce a higher cell accumulation and thus a stronger effect on bacterial colonization of the channels.

The way structures affected bacterial biomass was stronger when fungi were present. In general, there was less bacterial biomass when cultivated together with the fungus. Since antibiotic production by C. cinerea has been reported to affect exclusively gram-positive bacteria [57], we believe that the main reason for this must be competition for nutrients and space [58].

Interestingly, when fungi were present, hyphae increased the effect that structures had on bacterial biomass, where sharper angles and repeated turn order reduced bacterial biomass more than when they were not present. Such findings, together with high magnification pictures (Figure 2b), suggest that the habitat modification caused by fungi – by blocking the pore space with their hyphae – increased the complexity of the habitat where bacteria grew. In nature, fungi might act not only as bridges or networks [59] [60], and "highways" for bacterial dispersal [61], but also as barriers that prevent bacteria from advancing further inside the soil pores. The interaction between the effect of structures and the presence of competitor in bacterial biomass indicates that competition does not only occur for nutrients but also for space.

Fungal biomass

Turns in the channels reduced fungal biomass as angles became sharper, the effect increased when turn order of the angles was repeated. Thus, the effect of an angle in a pore space depends on how it is positioned, similar to what has been suggested by models based on tomography images [40]. When fungal hyphae hit a wall, their Spitzenkörper shifts towards the wall and stays near the wall as hyphae grow [62]. Spitzenkörper seems to be responsible for the reorientation of hyphae after hitting an obstacle because it remains in the part of the hyphae that is close to the wall, in a phenomenon known as thigmotropism [63], as a way to maintain its original directionality after the obstacle is circumvented. In alternated turns channels, hyphae seem to maintain the original directionality regardless of the contact angle reducing the effect of the angles on fungal biomass. The explanation can be as follows: once a hypha encounters an obstacle, the Spitzenkörper shifts towards the wall and stays near the wall as hyphae grow [62], where it remains close to the wall, in line with the direction of its growth. When hitting the next wall in a channel with alternating turns, both directions would help hyphae to find the right path. This contrasts with channels with repeated turn order, where during every second turn, one of the two directions does not point towards the right path and instead hit a wall. Such findings can be corroborated by high-magnification analysis of single hyphal tip growth, showing that frequent hyphal branching occurred only at angles of 90° and 109° (Figure 4, Supplementary Video1-6), and that hyphae suffered loss of direction in corners of repeated turn order (with 90° and 109°).

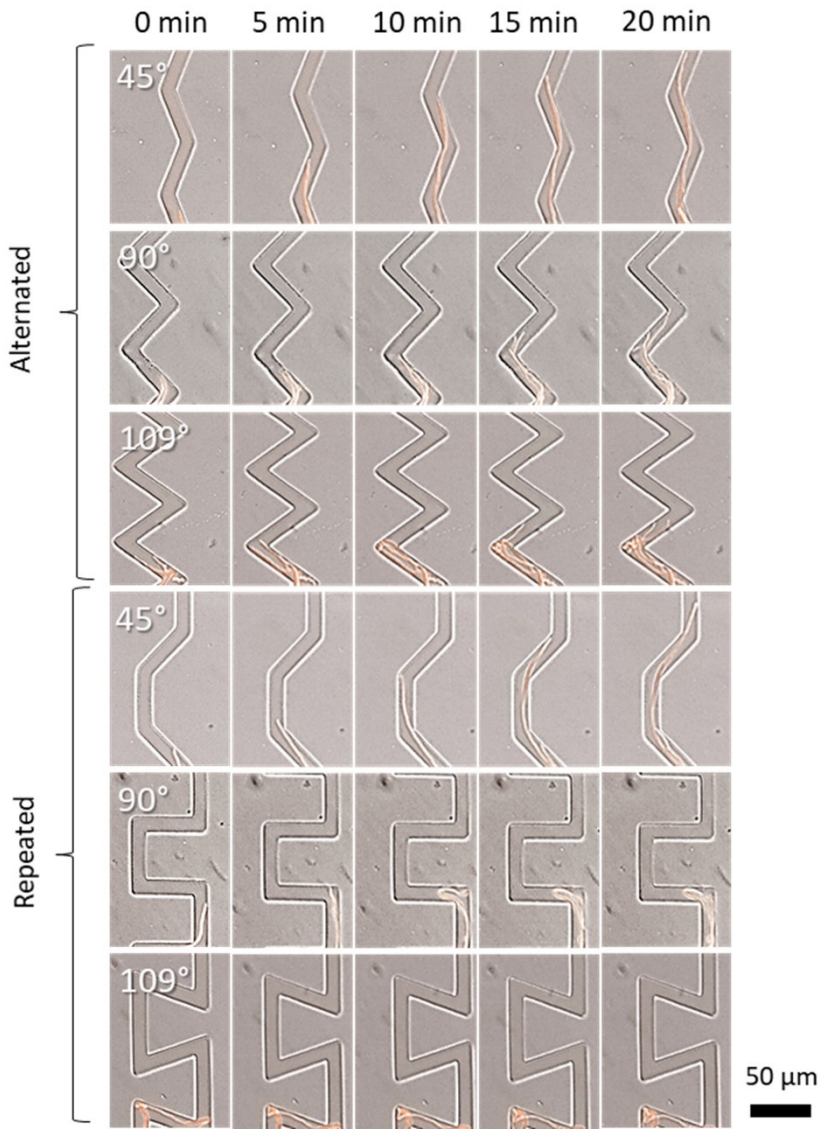

Figure 4. Time lapse images of *C. cinerea* passing through the different types of channels in absence of a competitor at day 1. Pictures were taken with a 40x objective at a time interval of 5 minutes in brightfield with DIC overlayed with the red fluorescence channel.

The fluorescent profiles (Figure 5) show that the fungal biomass distribution along the channels was indeed affected by the angle sharpness. Hyphae covered longer distances in the 45° channels, but in the channels with angles of 90° and 109°, the fluorescent profile locally reached higher levels of fluorescence, specifically in the first parts of the channels. This could be explained by the fact that when hyphae hit

a wall at an angle of 90° and 109° the Spitzenkörper shrinks [62] and leads to a branching event that initiates growth towards both sides. Eventually, one of the sides would reach the continuation of the path, whereas the other grows towards its origin or gets trapped between two corners. Such branching leads eventually to a localized accumulation of biomass in the beginning of the 90° and 109°-angled channels, even though their total biomass is lower than the 45°-angled channels. (Figure 5, Figure 4 and Supplementary video 1-6). Branching events can be observed after hyphae encounter walls, but this does not generally stop the hyphal advancement in alternated turn orders as it was found for repeated turn order. The importance of branching for a successful fungal colonization in microstructures has been explored previously [64]; the present study suggests that the higher hyphal branching rates produced by encountering 90° and 109° corners lead to a different fungal biomass distribution along the different microstructures.

Applied to a situation in real soil, this would mean that pore space passages forcing fungi to bend at a certain angle could be prone to cause a local accumulation of fungal biomass, where joint forces of several hyphal tips may support its effort to penetrate the pore wall. Models performed on soil derived from micro-computed tomography images consider that pore volume, pore connectivity, and presence of water bubbles affect fungal growth inside the pore space [40], [65]. Although it remains to investigate exactly how much of the pore space can be protruded by fungal hyphae, the current study adds passage turning angle and the way they are arranged (turn order) to the characteristics that should be considered when evaluating the effect of soil architecture on fungal growth.

The effect that the studied angles had on fungi did not depend on the presence of bacteria but occurred similarly when the fungus grew alone. The same is observed in the linear regression of fungal biomass vs channel tortuosity in absence and in presence of bacteria (Supplementary Figure 4, Supplementary Table 8). Therefore, the only effect of bacterial presence on fungal biomass seems to be an overall reduction of hyphae across all the angle profiles. This reduction can be mainly attributed to competition for nutrients. This seems to suggest that bacteria, as opposed to fungi, do not alter the spatial habitat in a way that would interfere with fungal foraging. Even though bacteria grow faster [66], bacterial biomass did not change the effect structures had on fungal growth, as hyphae can easily push through bacterial colonies using protrusive forces [67], [68]. Besides nutrient competition, other explanations of importance when studying polymicrobial interactions, such as quorum sensing signaling, which could change bacterial or fungal metabolisms [58], might also play a role in the reduction of fungal biomass.

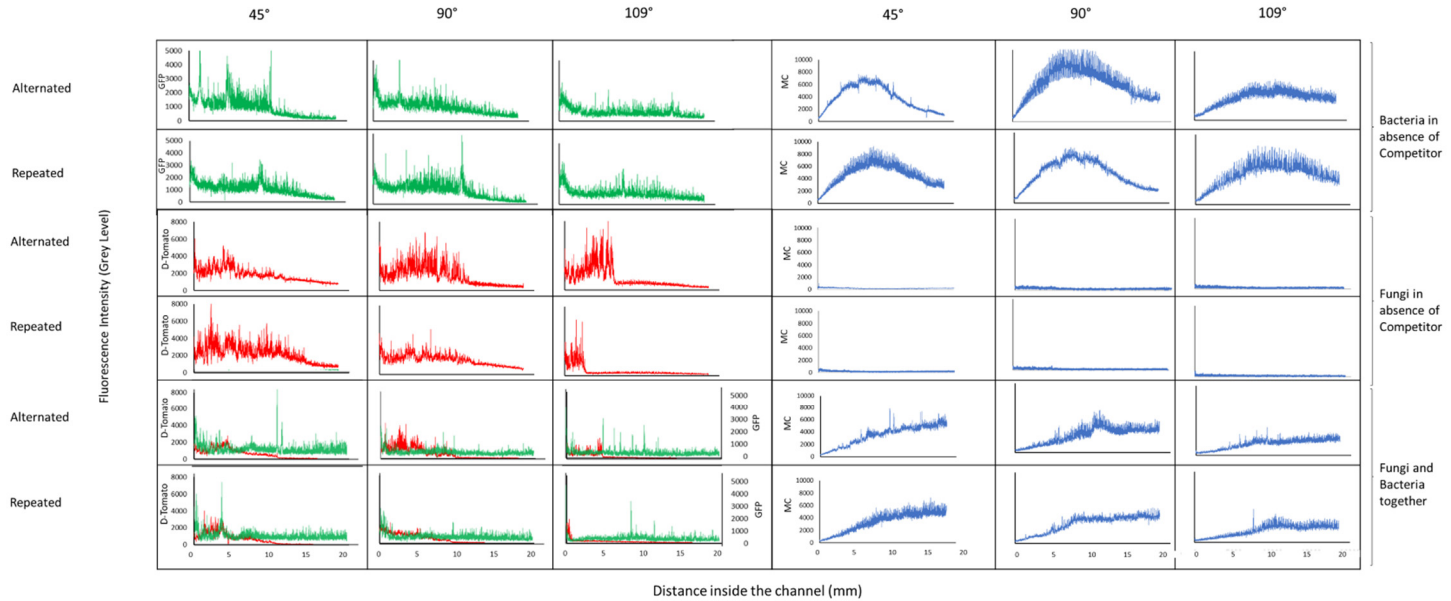

Figure 5. Examples of fluorescent profiles of *P. putida* expressing GFP constitutively, *C. cinerea* expressing d-Tomato constitutively, and 4-methylcoumarin inside the microfluidic channels, on days 2 for *P. putida* and 6 for *C. cinerea* and 4-methylcoumarin, after inoculation inside the microfluidic channels. The fluorescent profiles show the changes in fluorescence along the length of every type of channel studied under the two competitor conditions. The beginning of the channel is located on the left side of each plot.

Effect of structures on substrate degradation

Substrate degradation did not differ across angles and angle arrangements when bacteria and fungi grew by themselves. The two structure parameters only affected substrate degradation when bacteria and fungi grew together.

P. putida alone degraded the AMC through the different channels even though mineral nitrogen was provided. Regardless of the different biomass levels encountered in the channels, the substrate cleavage of the cells did not differ between channel type, which means that cells had a higher enzyme activity rate (Supplementary table 13) in channels with sharper turning angle and repeated turn order. Fungi did not degrade the peptide when grown alone, which gives us the advantage that we could measure bacterial substrate degradation exclusively, even in the presence of the fungus. Since fungi have generally a higher nitrogen use efficiency than bacteria [69]–[71], the mineral nitrogen provided in the medium could have sufficed for a much longer growth period than for bacteria. Nonetheless, C. cinerea did not show enzymatic activity that cleaves AMC in trials with an order of magnitude lower nitrogen levels (data not shown).

When C. cinerea and P. putida were incubated together, the substrate degradation was different across angle and turn order types, following a similar pattern as bacterial and fungal biomass in those chips. While in co-cultured chips, bacterial and fungal biomasses were lower than when they grew alone, indication competition for nutrients, substrate degradation was higher in both channels with 45° angles. The increase of substrate consumption in low-angled channels may be caused by the onset of fungal peptide degradation under competition, an over-proportional increase in bacterial degradation under competition, or both. However, substrate degradation was lower in those with 109° angles compared to substrate degradation in chips with only one of the organisms (Fig 3, supplementary Fig 4c). The decreasing levels of substrate consumption in sharper-angled channels may partly be explained by the lowering biomass of both bacteria and fungi, but the same decrease in biomass did not affect substrate consumption in bacteria-only and fungi-only systems. Thus, the lowered substrate consumption in the 90° and 109°-angled channels is presumably due to the habitat modification produced by hyphae, as they block the channels and restrict passage for bacteria, and substrate and fluorophore exchange via diffusion between the channels and the pillar system.

Our results show that the geometry of the pore space significantly affected how much bacteria and fungi grew. They also show that bacteria are affected by the habitat modification by fungal hyphae, whereas fungi were not affected by the habitat modification by bacteria. It has been suggested that spatial heterogeneity in substrate distribution can reduce respiration from soils [72]. In the present study, we do not see that structure itself could reduce substrate consumption of single cultures of bacteria, but the interaction of fungal biomass with structure allowed such a reduction to occur. Further experiments could address the factors influencing fungal

degradation activity, or focus on tracking how much of a common substrate is accessed by bacteria and fungi, and how much of it is assimilated into their biomass and consecutively into their necromass. To extrapolate our findings to the fate of organic matter in soil pore spaces there is the need to continue work with more diverse and more complex substrates that require subsequent attack by a wide variety of enzymes or radicals. However, our experiments address general effects of microstructures on fungal and bacterial growth, as well as bacterial enzymatic activity. Our findings highlight the fact that functions of different microbial groups can neither be assessed accurately when studied isolated without interactions, nor without considering the habitat where interactions occur, as brought forward in [73]. In the present study we can witness that microbial functions and competition can differ across space at micrometre scale, and can be influenced by habitat modification of the involved organisms.

Although real soil pore space physical parameters differ in more parameters than turning angle, this study succeeded in isolating this factor and showing how it influences the biomass distribution and substrate consumption of soil microbes. Further soil pore geometrical properties could be identified using the information provided from micro-computed tomography to include these parameters into microfluidic devices. In the present setup we used a saturated system where liquid was filling the whole of the microfluidic device pore system, where both bacteria and substrates could freely move within the limits of the pore walls. In nature, under non-saturated conditions, water films alternate with air bubbles in soil pore spaces, hampering diffusion of substrates and creating barriers for swimming organisms [74]–[76]. Thus, air barriers and gas mobility should also be considered since they will likely influence outcomes of substrate availability. It would also be relevant to have a constant flow of nutrient medium inside the system, and thus avoid microbial starvation. It has been shown that when starvation initiates, the strength of pore clogging due to bacterial accumulation diminishes, increasing the permeability of the porous system [77]. Also, adding flows to the experimental system would elucidate how these structures affect the hydraulic properties of the bacterial colonization and possible biofilm formation. Flows and the location of the pores with respect to the flow have been shown to be crucial when predicting bacterial accumulation in porous systems [78] [79].

The habitat where microbes grow and interact is not stable over time, but it changes as a result of the microbial processes inside it. The need to better understand how microenvironments co-evolve with microorganisms has been pointed out previously [18], [73]. In this study, we have only analysed the interaction of two parameters of structure on the degradation of a specific substrate by two lab strains. We found that sharper angles and repeated turns reduced bacterial and fungal growth, as well as bacterial enzymatic activity. In nature, needless to say, soils contain many more parameters of structure [80], countless substrate types [81], and countless microbial species interactions [82], [83]. Despite the necessary simplifications, this study

suffices to demonstrate the importance of microhabitats and to initiate a closer way of studying the complex role of physical structure on soil microbial ecology and on soil nutrient occlusion, leading ultimately to a better understanding of the laws of soil carbon storage. A deeper understanding of how microbes behave in microhabitats will give us the possibility to comprehend their role across all the environments in which they are present, from soil microbiology, to gut microbiome and biofilm-forming pathogens.

Acknowledgements

The authors acknowledge funding by the Swedish Research Council (VR-621-2014-5912), the Foundation for Strategic Research (Future research leader grant SSF FFL18-0089), and the strategic research environment BECC. We thank Johannes Rousk, Miguel Gómez, and Maarit Mäenpää for their expertise and assistance in data analysis and statistics, and Sam Bengtsson Gartner and Stephanie Casey for their assistance in the device fabrication, microscopy, and image analysis.

Contributions

EH and CGAC conceived the idea, developed the study design, interpreted the data, and wrote the manuscript. CGAC designed and manufactured the chips, performed the experiments, and analysed the data. PO assisted in the chip design, data interpretation, and manuscript writing. MB developed an adjusted protocol for the mask design and manufacturing. JB developed an adjusted protocol for the master manufacturing. All authors contributed with exchange of ideas and reviewed the manuscript.

Conflict of interest

The authors declare no conflict of interest.

References

[1] E. M. Bach, R. J. Williams, S. K. Hargreaves, F. Yang, and K. S. Hofmockel, “Greatest soil microbial diversity found in micro-habitats,” *Soil Biol. Biochem.*, vol. 118, no. January, pp. 217–226, 2018, doi: 10.1016/j.soilbio.2017.12.018.

[2] G. Wang and D. Or, “Hydration dynamics promote bacterial coexistence on rough surfaces,” *ISME J.*, vol. 7, no. 2, pp. 395–404, 2013, doi: 10.1038/ismej.2012.115.

[3] R. B. Franklin and A. L. Mills, “Importance of spatially structured environmental heterogeneity in controlling microbial community composition at small spatial scales

in an agricultural field," *Soil Biol. Biochem.*, vol. 41, no. 9, pp. 1833–1840, 2009, doi: 10.1016/j.soilbio.2009.06.003.

[4] M. Vos, A. B. Wolf, S. J. Jennings, and G. A. Kowalchuk, "Micro-scale determinants of bacterial diversity in soil," *FEMS Microbiol. Rev.*, vol. 37, no. 6, pp. 936–954, 2013, doi: 10.1111/1574-6976.12023.

[5] J. Zhou *et al.*, "Spatial and resource factors influencing high microbial diversity in soil," *Appl. Environ. Microbiol.*, vol. 68, no. 1, pp. 326–334, 2002, doi: 10.1128/AEM.68.1.326-334.2002.

[6] R. S. Friedlander, H. Vlamakis, P. Kim, M. Khan, R. Kolter, and J. Aizenberg, "Bacterial flagella explore microscale hummocks and hollows to increase adhesion," *Proc. Natl. Acad. Sci. U. S. A.*, 2013, doi: 10.1073/pnas.1219662110.

[7] J. Barrila *et al.*, "Modeling host-pathogen interactions in the context of the microenvironment: Three-dimensional cell culture comes of age," *Infect. Immun.*, 2018, doi: 10.1128/IAI.00282-18.

[8] M. Lourenço *et al.*, "The Spatial Heterogeneity of the Gut Limits Predation and Fosters Coexistence of Bacteria and Bacteriophages," *Cell Host Microbe*, 2020, doi: 10.1016/j.chom.2020.06.002.

[9] H. P. Lu, Y. C. Lai, S. W. Huang, H. C. Chen, C. H. Hsieh, and H. T. Yu, "Spatial heterogeneity of gut microbiota reveals multiple bacterial communities with distinct characteristics," *Sci. Rep.*, 2014, doi: 10.1038/srep06185.

[10] C. A. Guerra *et al.*, "Blind spots in global soil biodiversity and ecosystem function research," *Nat. Commun.*, vol. 11, no. 1, pp. 1–13, 2020, doi: 10.1038/s41467-020-17688-2.

[11] K. Nagy, Á. Ábrahám, J. E. Keymer, and P. Galajda, "Application of microfluidics in experimental ecology: The importance of being spatial," *Front. Microbiol.*, vol. 9, no. MAR, 2018, doi: 10.3389/fmicb.2018.00496.

[12] R. Tecon and D. Or, "Biophysical processes supporting the diversity of microbial life in soil," *FEMS Microbiol. Rev.*, vol. 41, no. 5, pp. 599–623, 2017, doi: 10.1093/femsre/fux039.

[13] R. Tecon and D. Or, "Biophysical processes supporting the diversity of microbial life in soil," *FEMS Microbiology Reviews*. 2017, doi: 10.1093/femsre/fux039.

[14] P. G. Falkowski, T. Fenchel, and E. F. Delong, "The microbial engines that drive earth's biogeochemical cycles," *Science*. 2008, doi: 10.1126/science.1153213.

[15] J. E. Hobbie and E. A. Hobbie, "Microbes in nature are limited by carbon and energy: The starving-survival lifestyle in soil and consequences for estimating microbial rates," *Front. Microbiol.*, vol. 4, no. NOV, pp. 1–11, 2013, doi: 10.3389/fmicb.2013.00324.

[16] P. W. Hill, J. F. Farrar, and D. L. Jones, "Decoupling of microbial glucose uptake and mineralization in soil," *Soil Biol. Biochem.*, 2008, doi: 10.1016/j.soilbio.2007.09.008.

[17] IPCC, "Climate change 2007: the physical science basis," 2007. doi: 10.1260/095830507781076194.

[18] P. C. Baveye *et al.*, “Emergent properties of microbial activity in heterogeneous soil microenvironments: Different research approaches are slowly converging, yet major challenges remain,” *Frontiers in Microbiology*. 2018, doi: 10.3389/fmicb.2018.01929.

[19] A. Bruand and I. Cousin, “Variation of textural porosity of a clay-loam soil during compaction,” *Eur. J. Soil Sci.*, 1995, doi: 10.1111/j.1365-2389.1995.tb01334.x.

[20] V. Cnudde and M. N. Boone, “High-resolution X-ray computed tomography in geosciences: A review of the current technology and applications,” *Earth-Science Reviews*. 2013, doi: 10.1016/j.earscirev.2013.04.003.

[21] M. Pagliai, N. Vignozzi, and S. Pellegrini, “Soil structure and the effect of management practices,” 2004, doi: 10.1016/j.still.2004.07.002.

[22] L. F. Pires, O. O. S. Bacchi, K. Reichardt, and L. C. Timm, “Application of γ-ray computed tomography to analysis of soil structure before density evaluations,” *Appl. Radiat. Isot.*, 2005, doi: 10.1016/j.apradiso.2005.03.019.

[23] M. Larsbo, J. Koestel, T. Kätterer, and N. Jarvis, “Preferential Transport in Macropores is Reduced by Soil Organic Carbon,” *Vadose Zo. J.*, 2016, doi: 10.2136/vzj2016.03.0021.

[24] K. Ananyeva, W. Wang, A. J. M. Smucker, M. L. Rivers, and A. N. Kravchenko, “Can intra-aggregate pore structures affect the aggregate’s effectiveness in protecting carbon?,” *Soil Biol. Biochem.*, 2013, doi: 10.1016/j.soilbio.2012.10.019.

[25] E. R. Toosi, A. N. Kravchenko, J. Mao, M. Y. Quigley, and M. L. Rivers, “Effects of management and pore characteristics on organic matter composition of macroaggregates: evidence from characterization of organic matter and imaging,” *Eur. J. Soil Sci.*, 2017, doi: 10.1111/ejss.12411.

[26] S. Katuwal, T. Norgaard, P. Moldrup, M. Lamandé, D. Wildenschild, and L. W. de Jonge, “Linking air and water transport in intact soils to macropore characteristics inferred from X-ray computed tomography,” *Geoderma*, 2015, doi: 10.1016/j.geoderma.2014.08.006.

[27] W. C. Negassa, A. K. Guber, A. N. Kravchenko, T. L. Marsh, B. Hildebrandt, and M. L. Rivers, “Properties of soil pore space regulate pathways of plant residue decomposition and community structure of associated bacteria,” *PLoS One*, 2015, doi: 10.1371/journal.pone.0123999.

[28] E. Rabot, M. Wiesmeier, S. Schlüter, and H. J. Vogel, “Soil structure as an indicator of soil functions: A review,” *Geoderma*. 2018, doi: 10.1016/j.geoderma.2017.11.009.

[29] G. J. Pronk *et al.*, “Interaction of minerals, organic matter, and microorganisms during biogeochemical interface formation as shown by a series of artificial soil experiments,” *Biology and Fertility of Soils*. 2017, doi: 10.1007/s00374-016-1161-1.

[30] H. Downie, N. Holden, W. Otten, A. J. Spiers, T. A. Valentine, and L. X. Dupuy, “Transparent Soil for Imaging the Rhizosphere,” *PLoS One*, 2012, doi: 10.1371/journal.pone.0044276.

[31] K. Aleklett, E. T. Kiers, P. Ohlsson, T. S. Shimizu, V. E. Caldas, and E. C. Hammer, “Build your own soil: Exploring microfluidics to create microbial habitat structures,” *ISME Journal*, vol. 12, no. 2. pp. 312–319, 2018, doi: 10.1038/ismej.2017.184.

[32] D. J. Beebe, G. A. Mensing, and G. M. Walker, “Physics and Applications of Microfluidics in Biology,” *Annu. Rev. Biomed. Eng.*, 2002, doi: 10.1146/annurev.bioeng.4.112601.125916.

[33] T. Ahmed, T. S. Shimizu, and R. Stocker, “Microfluidics for bacterial chemotaxis,” *Integrative Biology*. 2010, doi: 10.1039/c0ib00049c.

[34] T. Ahmed and R. Stocker, “Experimental verification of the behavioral foundation of bacterial transport parameters using microfluidics,” *Biophys. J.*, 2008, doi: 10.1529/biophysj.108.134510.

[35] H. Mao, P. S. Cremer, and M. D. Manson, “A sensitive, versatile microfluidic assay for bacterial chemotaxis,” *Proc. Natl. Acad. Sci.*, 2003, doi: 10.1073/pnas.0931258100.

[36] J. Saragosti, V. Calvez, N. Bournaveas, B. Perthame, A. Buguin, and P. Silberzan, “Directional persistence of chemotactic bacteria in a traveling concentration wave,” *Proc. Natl. Acad. Sci.*, 2011, doi: 10.1073/pnas.1101996108.

[37] J. Deng *et al.*, “Synergistic effects of soil microstructure and bacterial EPS on drying rate in emulated soil micromodels,” *Soil Biol. Biochem.*, 2015, doi: 10.1016/j.soilbio.2014.12.006.

[38] R. L. Rubinstein, A. L. Kadilak, V. C. Cousens, D. J. Gage, and L. M. Shor, “Protist-facilitated particle transport using emulated soil micromodels,” *Environ. Sci. Technol.*, 2015, doi: 10.1021/es503424z.

[39] C. E. Stanley *et al.*, “Probing bacterial-fungal interactions at the single cell level,” *Integr. Biol. (United Kingdom)*, 2014, doi: 10.1039/c4ib00154k.

[40] R. Falconer, A. Houston, W. Otten, and P. Baveye, “Emergent behavior of soil fungal dynamics: Influence of soil architecture and water distribution.,” *Soil Sci.*, vol. 177, no. 2, pp. 111–119, 2012.

[41] K. J. Duffy and R. M. Ford, “Turn angle and run time distributions characterize swimming behavior for Pseudomonas putida,” *J. Bacteriol.*, vol. 179, no. 4, pp. 1428–1430, 1997, doi: 10.1128/jb.179.4.1428-1430.1997.

[42] J. C. Mcdonald, D. C. Duffy, J. R. Anderson, and D. T. Chiu, “Review General Fabrication of microfluidic systems in poly (dimethylsiloxane),” *Electrophoresis*, vol. 21, no. 1, pp. 27–40, 2000, [Online]. Available: http://www.ncbi.nlm.nih.gov/pubmed/10634468.

[43] M. C. M. Smith, “Molecular biological methods for bacillus,” *FEBS Lett.*, 1991, doi: 10.1016/0014-5793(91)80059-c.

[44] B. S. Razavi, X. Zhang, N. Bilyera, A. Guber, and M. Zarebanadkouki, “Soil zymography: Simple and reliable? Review of current knowledge and optimization of the method,” *Rhizosphere*, vol. 11, no. June, p. 100161, 2019, doi: 10.1016/j.rhisph.2019.100161.

[45] M. Nicodème, J. P. Grill, G. Humbert, and J. L. Gaillard, “Extracellular protease activity of different Pseudomonas strains: Dependence of proteolytic activity on culture conditions,” *J. Appl. Microbiol.*, 2005, doi: 10.1111/j.1365-2672.2005.02634.x.

[46] I. Güll, P. M. Alves, F. Gabor, and M. Wirth, “Viability of the human adenocarcinoma cell line Caco-2: Influence of cryoprotectant, freezing rate, and storage temperature,” *Sci. Pharm.*, 2009, doi: 10.3797/scipharm.0810-07.

[47] C. Burns *et al.*, “Efficient GFP expression in the mushrooms Agaricus bisporus and Coprinus cinereus requires introns,” *Fungal Genet. Biol.*, 2005, doi: 10.1016/j.fgb.2004.11.005.

[48] J. Schindelin *et al.*, “Fiji: An open-source platform for biological-image analysis,” *Nature Methods*. 2012, doi: 10.1038/nmeth.2019.

[49] M. A. Kneen and H. J. Annegarn, “Algorithm for fitting XRF, SEM and PIXE X-ray spectra backgrounds,” *Nucl. Instruments Methods Phys. Res. Sect. B Beam Interact. with Mater. Atoms*, 1996, doi: 10.1016/0168-583X(95)00908-6.

[50] R. C. Team, “R: A Language and Environment for Statistical Computing,” *Vienna, Austria*, 2019.

[51] O. J. Dunn, “Multiple Comparisons Among Means,” *J. Am. Stat. Assoc.*, 1961, doi: 10.2307/2282330.

[52] S. Holm, “A simple sequentially rejective multiple test procedure,” *Scand. J. Stat.*, 1979.

[53] S. Rashid, Z. Long, S. Singh, M. Kohram, H. Vashistha, and S. Navlakha, “Adjustment in tumbling rates improves bacterial chemotaxis on obstacle-laden terrains,” vol. 116, no. 24, 2019, doi: 10.1073/pnas.1816315116.

[54] K. J. Duffy, P. T. Cummings, and R. M. Ford, “Random walk calculations for bacterial migration in porous media,” *Biophys. J.*, vol. 68, no. 3, pp. 800–806, 1995, doi: 10.1016/S0006-3495(95)80256-0.

[55] H. Shum and E. A. Gaffney, “Hydrodynamic analysis of flagellated bacteria swimming in corners of rectangular channels,” *Phys. Rev. E - Stat. Nonlinear, Soft Matter Phys.*, vol. 92, no. 6, pp. 1–11, 2015, doi: 10.1103/PhysRevE.92.063016.

[56] Ò. Guadayol, K. L. Thornton, and S. Humphries, “Cell morphology governs directional control in swimming bacteria,” no. March, pp. 1–13, 2017, doi: 10.1038/s41598-017-01565-y.

[57] A. Essig *et al.*, “Copsin, a novel peptide-based fungal antibiotic interfering with the peptidoglycan synthesis,” *J. Biol. Chem.*, vol. 289, no. 50, pp. 34953–34964, 2014, doi: 10.1074/jbc.M114.599878.

[58] E. F. Dixon and R. A. Hall, “Noisy neighbourhoods: Quorum sensing in fungal-polymicrobial infections,” *Cell. Microbiol.*, vol. 17, no. 10, pp. 1431–1441, 2015, doi: 10.1111/cmi.12490.

[59] T. Banitz, I. Fetzer, K. Johst, L. Y. Wick, H. Harms, and K. Frank, “Assessing biodegradation benefits from dispersal networks,” *Ecol. Modell.*, vol. 222, no. 14, pp. 2552–2560, 2011, doi: 10.1016/j.ecolmodel.2010.07.005.

[60] S. Furuno, K. Päzolt, K. Rabe, T. R. Neu, H. Harms, and L. Y. Wick, “Fungal mycelia allow chemotactic dispersal of polycyclic aromatic hydrocarbon-degrading bacteria in water-unsaturated systems,” *Environ. Microbiol.*, vol. 12, no. 6, pp. 1391–1398, 2010, doi: 10.1111/j.1462-2920.2009.02022.x.

[61] S. Kohlmeier, T. H. M. Smits, R. M. Ford, C. Keel, H. Harms, and L. Y. Wick, "Taking the fungal highway: Mobilization of pollutant-degrading bacteria by fungi," *Environ. Sci. Technol.*, vol. 39, no. 12, pp. 4640–4646, 2005, doi: 10.1021/es047979z.

[62] M. Held, O. Kaspar, C. Edwards, and D. V. Nicolau, "Intracellular mechanisms of fungal space searching in microenvironments," *Proc. Natl. Acad. Sci. U. S. A.*, vol. 116, no. 27, pp. 13543–13552, 2019, doi: 10.1073/pnas.1816423116.

[63] R. Soufan *et al.*, "Pore-Scale Monitoring of the Effect of Microarchitecture on Fungal Growth in a Two-Dimensional Soil-Like Micromodel," *Front. Environ. Sci.*, vol. 6, no. July, 2018, doi: 10.3389/fenvs.2018.00068.

[64] K. L. Hanson, D. V. Nicolau, L. Filipponi, L. Wang, A. P. Lee, and D. V. Nicolau, "Fungi use efficient algorithms for the exploration of microfluidic networks," *Small*, vol. 2, no. 10, pp. 1212–1220, 2006, doi: 10.1002/smll.200600105.

[65] R. Pajor, R. Falconer, S. Hapca, and W. Otten, "Modelling and quantifying the effect of heterogeneity in soil physical conditions on fungal growth," *Biogeosciences*, vol. 7, no. 11, pp. 3731–3740, 2010, doi: 10.5194/bg-7-3731-2010.

[66] A. Varma, L. Abbott, D. Werner, and R. Hampp, *Plant surface microbiology*. 2008.

[67] R. R. Lew, "How does a hypha grow? the biophysics of pressurized growth in fungi," *Nat. Rev. Microbiol.*, vol. 9, no. 7, pp. 509–518, 2011, doi: 10.1038/nrmicro2591.

[68] A. Tayagui, Y. Sun, D. A. Collings, A. Garrill, and V. Nock, "An elastomeric micropillar platform for the study of protrusive forces in hyphal invasion," *Lab Chip*, vol. 17, no. 21, pp. 3643–3653, 2017, doi: 10.1039/c7lc00725f.

[69] R. D. Bardgett and E. McAlister, "The measurement of soil fungal:bacterial biomass ratios as an indicator of ecosystem self-regulation in temperate meadow grasslands," *Biol. Fertil. Soils*, vol. 29, no. 3, pp. 282–290, 1999, doi: 10.1007/s003740050554.

[70] G. B. De Deyn, J. H. C. Cornelissen, and R. D. Bardgett, "Plant functional traits and soil carbon sequestration in contrasting biomes," *Ecol. Lett.*, vol. 11, no. 5, pp. 516–531, 2008, doi: 10.1111/j.1461-0248.2008.01164.x.

[71] L. D. J. Kuijper, M. P. Berg, E. Morriën, B. W. Kooi, and H. A. Verhoef, "Global change effects on a mechanistic decomposer food web model," *Glob. Chang. Biol.*, vol. 11, no. 2, pp. 249–265, 2005, doi: 10.1111/j.1365-2486.2005.00898.x.

[72] R. E. Falconer, G. Battaia, S. Schmidt, P. Baveye, C. Chenu, and W. Otten, "Microscale Heterogeneity Explains Experimental Variability and Non-Linearity in Soil Organic Matter Mineralisation," *PLoS One*, vol. 10, no. 5, p. e0123774, 2015, doi: 10.1371/journal.pone.0123774.

[73] A. Deveau *et al.*, "Bacterial-fungal interactions: Ecology, mechanisms and challenges," *FEMS Microbiol. Rev.*, vol. 42, no. 3, pp. 335–352, 2018, doi: 10.1093/femsre/fuy008.

[74] M. Ecology, "Habitable Pore Space and Survival of Rhizobium leguminosarum biovar trifolii Introduced into Soil Author (s): J . Postma and J . A . van Veen Published by : Springer Stable URL : https://www.jstor.org/stable/4251110," vol. 19, no. 2, pp. 149–161, 1990.

[75] G. L. Grundmann, “Spatial scales of soil bacterial diversity - The size of a clone,” *FEMS Microbiol. Ecol.*, vol. 48, no. 2, pp. 119–127, 2004, doi: 10.1016/j.femsec.2004.01.010.

[76] Y. Kuzyakov and E. Blagodatskaya, “Microbial hotspots and hot moments in soil: Concept & review,” *Soil Biol. Biochem.*, vol. 83, pp. 184–199, 2015, doi: 10.1016/j.soilbio.2015.01.025.

[77] D. S. Kim and H. S. Fogler, “Biomass evolution in porous media and its effects on permeability under starvation conditions,” *Biotechnol. Bioeng.*, vol. 69, no. 1, pp. 47–56, 2000, doi: 10.1002/(SICI)1097-0290(20000705)69:1<47::AID-BIT6>3.0.CO;2-N.

[78] H. J. Dupin and P. L. McCarty, “Mesoscale and microscale observations of biological growth in a silicon pore imaging element,” *Environ. Sci. Technol.*, vol. 33, no. 8, pp. 1230–1236, 1999, doi: 10.1021/es981146p.

[79] J. A. Aufrecht, J. D. Fowlkes, A. N. Bible, J. Morrell-Falvey, M. J. Doktycz, and S. T. Retterer, “Pore-scale hydrodynamics influence the spatial evolution of bacterial biofilms in a microfluidic porous network,” *PLoS One*, vol. 14, no. 6, pp. 1–17, 2019, doi: 10.1371/journal.pone.0218316.

[80] R. W. Vervoort and S. R. Cattle, “Linking hydraulic conductivity and tortuosity parameters to pore space geometry and pore-size distribution,” *J. Hydrol.*, vol. 272, no. 1–4, pp. 36–49, 2003, doi: 10.1016/S0022-1694(02)00253-6.

[81] I. Kögel-Knabner, “The macromolecular organic composition of Plant and microbial residues as inputs to soil organic matter,” *Soil Biol. Biochem.*, vol. 34, no. 2, pp. 139–162, 2002, doi: 10.1016/S0038-0717(01)00158-4.

[82] M. T. Hoffman and A. E. Arnold, “Diverse bacteria inhabit living hyphae of phylogenetically diverse fungal endophytes,” *Appl. Environ. Microbiol.*, vol. 76, no. 12, pp. 4063–4075, 2010, doi: 10.1128/AEM.02928-09.

[83] L. R. Thompson *et al.*, “A communal catalogue reveals Earth’s multiscale microbial diversity,” *Nature*, vol. 551, no. 7681, pp. 457–463, 2017, doi: 10.1038/nature24621.

Supplementary material

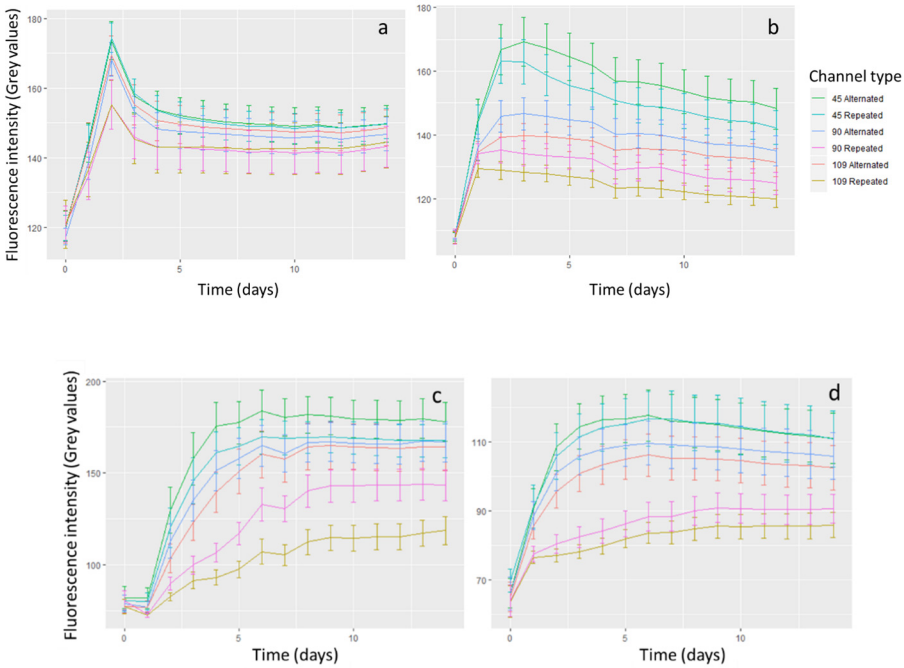

Supplementary Figure 1. Bacterial biomass of Pseudomonas putida estimated via its constitutive expression of GFP inside the microfluidic channels, during the 14 days after inoculation, growing without (a), and with the competitor Coprinopsis cinerea (b). The Y-axis represents the fluorescence intensity, quantified as grey value, of GFP corresponding to each type of channel (n=50). Fungal biomass of Coprinopsis cinerea expressing d-Tomato constitutively inside the microfluidic channels, during the 14 days after inoculation, growing without (c), and with the competitor Pseudomonas putida (d). The Y-axis represents the fluorescence intensity of d-Tomato corresponding to each type of channel (n=50).

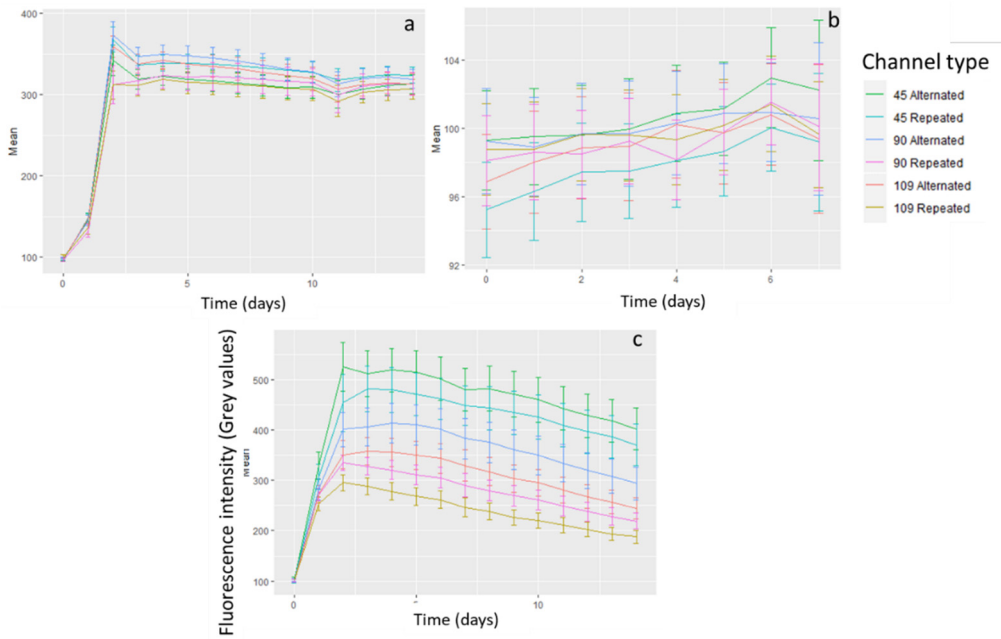

Supplementary Figure 2. Substrate consumption of L-Alanine 7-amido-4-methylcoumarin trifluoroacetate salt inside the microfluidic channels, during the 14 days after inoculation. The panels show bacterial experiment with Pseudomonas putida (a), Coprinopsis cinerea (b) and together both organisms together (c). The Y-axis represents the fluorescence intensity of 4-methylcoumarin corresponding to each type of channel (n=50).

Supplementary Table 1. Output of three-way ANOVA of the variable log-transformed bacterial biomass measured via their GFP fluorescence, with chip as random effect and Angle, Turn order, and Competition as fixed factors. Contrasts ngle*Turn order and Angle*Competition were analyzed separately using the Dunn's method for multiple comparison of means. Pairwise comparisons were done with t-tests with p values adjusted using Holm corrections.

	Sum of squares	Mean Square	Degrees of freedom	Density degrees of freedom	F value	P value	
Angle	1.797	0.899	2	580	98.737	<2.2e-16	***
Turn order	0.328	0.328	1	580	36.028	3.43e-09	***
Competition	0.104	0.104	1	8	11.409	0.01	**
Angle*Turn order	0.212	0.106	2	580	11.627	1.12e-05	***
Angle*Competition	0.279	0.14	2	580	15.332	3.25e-07	***
Competition*Turn order	0.002	0.002	1	580	0.249	0.618	
Angle*Competition*Turn order	0.0004	0.0002	2	580	0.024	0.977	
Angle*Turn order							
Angle @Alternated TO	0.388	0.194	2	288	2.066	0.09962	.
Angle @Repeated TO	1.620	0.810	2	288	8.618	1.1e-4	***
Angle*Competition							
Angle @Absence	0.343	0.172	2	293	1.829	0.1406	
Angle @Presence	1.732	0.866	2	293	9.226	7e-5	*

Pairwise comparison:

Turn order = Repeated TO	45	90
90	4.3e-11	-
109	4.2e-15	0.14

Competition = Presence	45	90
90	6.1e-14	-
109	<2e-16	0.012

Supplementary Table 2. Output of the multi-level model fitting for the variable log-transformed bacterial biomass measured via their GFP fluorescence, with chip as random effect and Angle, Turn order, and Competition as fixed factors. Each step performs an ANOVA and compares the model with the previous model.

Model	df	AIC	BIC	logLik	Test	L.Ratio	p-value
1	3	-840.1047	-826.9139	423.0524			
Angle	5	-988.4581	-966.4735	499.2291	152.35341	1vs2	<.0001
Turn order	6	-1019.0571	-992.6755	515.5285	32.59893	2vs3	<.0001
Competition	7	-1025.9199	-995.1414	519.9599	8.86280	3vs4	0.0029
Angle*Competition	9	-1051.1584	-1011.5861	534.5792	29.23858	4vs5	<.0001
Turn order*Competition	10	-1049.4017	-1005.4324	534.7008	0.24321	5vs6	0.6219
Angle*Turn order	12	-1015.8292	-1068.5924	546.2962	23.19071	6vs7	<.0001
Angle*Turn order*Competition	14	-1064.6408	-1003.0837	546.3204	0.04839	7vs8	0.9761

Supplementary Table 3. Contrasts of the multi-level model with the variable log-transformed bacterial biomass measured via their GFP fluorescence, with chip as random effect and Angle, Turn order, and Competition as fixed factors.

	Value	Std.Error	DF	t-value	p-value
(Intercept)	5.072999	0.033199	582	152.8039	0
Ang 45 – Ang 90	0.105983	0.016518	582	6.41606	0
Ang 109 - Ang 90	-0.01035	0.016518	582	-0.62646	0.5313
Alternated TO – Repeated TO	0.070932	0.015574	582	4.5546	0
Presence – Absence	-0.17115	0.046301	8	-3.69643	0.0061
Ang 45 – 90 (Pres-Abs)	0.065965	0.019074	582	3.45839	0.0006
Ang 109 – 90 (Pres – Abs)	-0.03847	0.019074	582	-2.01675	0.0442
Alternated TO – Repeated TO (Pres – Abs)	-0.00777	0.015574	582	-0.49879	0.6181
Ang 45 – 90 (Alternated TO – Repeated TO)	-0.072955	0.019074	582	-3.8249	0.0001
Ang109 – 90 (Alternated TO – Repeated TO)	0.012044	0.019074	582	0.63144	0.528

Supplementary Table 4. Output of the linear model with bacterial biomass (GFP fluorescence signal) as dependent variable and channel tortuosity as independent variable. Second and third panel indicate linear regression for bacterial biomass data in absence and presence of competitor respectively.

	Value	Std.Error	DF	t-value	p-value
(Intercept)	5.227055	0.040156	588	130.1694	<1E-10
Tortuosity	-0.163643	0.012562	588	-13.02687	<1E-10
Presence-Absence	0.035249	0.056789	8	0.6207	0.5521
Tor*Presence - Tor*Absence	0.081356	0.017765	588	4.57949	<1E-10
Absence					
(Intercept)	5.262304	0.046053	294	114.26531	<1E-10
Tortuosity (slope)	-0.082287	0.010905	294	-7.54597	<1E-10
Presence					
(Intercept)	5.227055	0.033227	294	157.31152	<1E-10
Tortuosity (slope)	-0.163643	0.014025	294	-11.66821	<1E-10

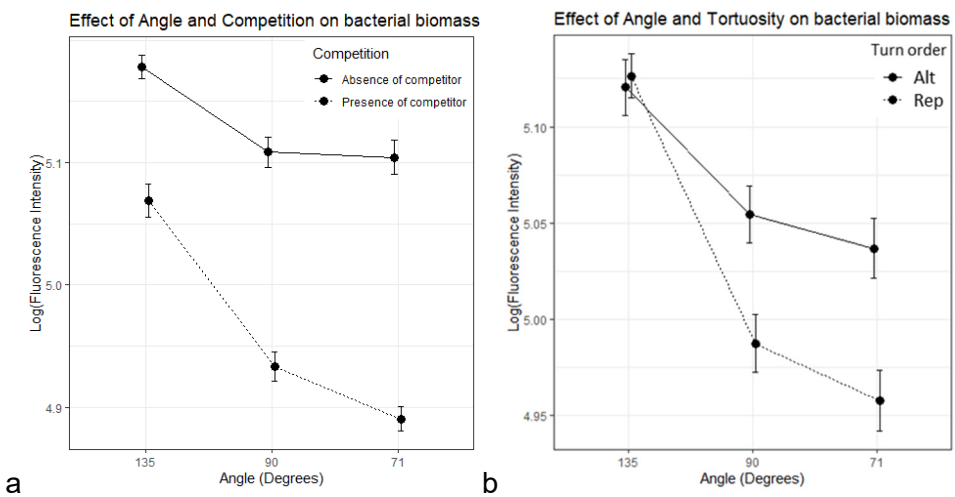

Supplementary Figure 3. Effect of interactions Angle-Competition (a) and Angle-Turn order (b) on the *Pseudomonas putida* biomass measured via their GFP fluorescent signal. The fluorescence data are log-transformed and presented for the alternated (continuous line) and for repeated turn order (doted line). The points represent the mean log-transformed fluorescence for each treatment and the error bars represent the ±standar error based on ANOVA for all the angles (*n*=50).

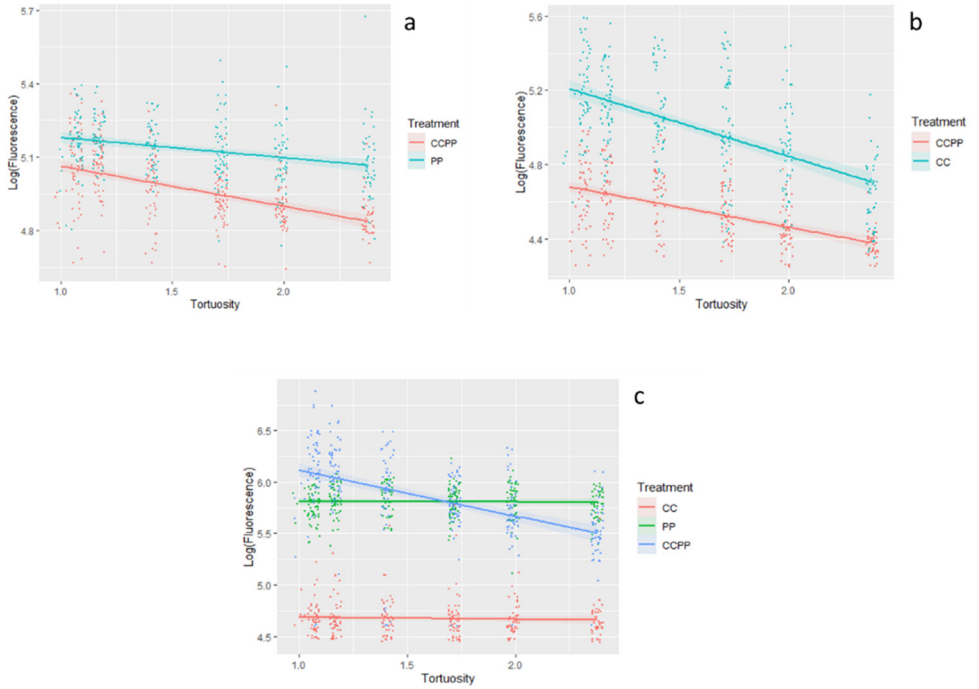

Supplementary Figure 4. The effect of tortuosity on bacterial biomass (a), fungal biomass (b) and substrate consumption (c), shown as linear correlations. The Y-axis shows the log transformed value of fluorescence intensity of GFP for bacteria, d-Tomato for fungi, and 4-methylcoumarin for the substrate. Different colours represent the experimental conditions: PP for bacteria only, CC for fungi only, and CCPP for bacteria and fungi growing together. The scattered points represent single measurements of fluorescence (*n*=50). Shaded areas represent confidence intervals.

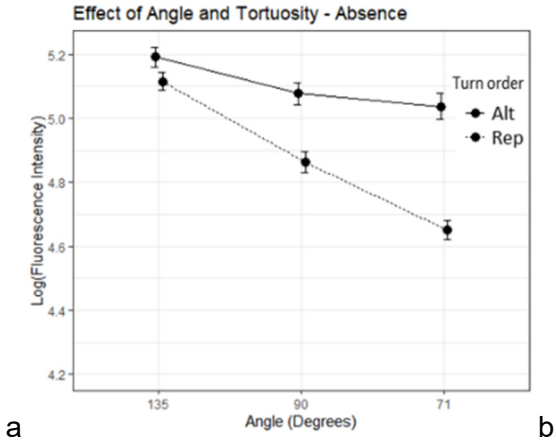

a b

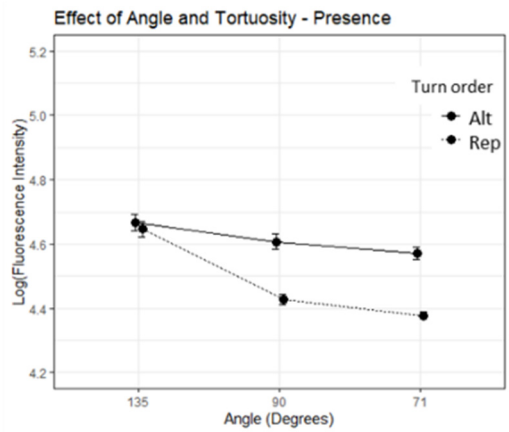

Supplementary Figure 5. Effect of interactions Angle-Turn order in absence of competitor (left) and in presence of competitor (right) on the *Coprinopsis cinerea* biomass measured with d-Tomato fluorescent signal. The fluorescence data are log-transformed and presented for the alternated (continuous line) and for the repeated turn order (doted line). The points represent the mean log-trasnformed fluorescence for each treatment and the error bars represent the ±standard error based on ANOVA for all the angle types (*n*=50).

Supplementary Table 5. Output of three-way ANOVA of the variable *Coprinopsis cinerea* log transformed biomass measured with d-Tomato fluorescence, with chip as random effect and Angle, Turn order, and Competition as fixed factors. Contrasts were analyzed separately using Dunn's method for multiple comparison of means. Pairwise comparisons were done with t-tests with p values adjusted using Holm corrections[45]. The significance of the three way interaction is likely to be produced because a similar interaction of angle and turn order in presence of bacteria could not be similar to the same interaction in absence of bacteria since fungal biomass levels are already showing a minimum growth, close to background levels.

	Sum of squares	Mean Square	Degrees of freedom	Density degrees of freedom	F value	P value	
Angle	6.236	3.118	2	580	148.188	<2.2e-16	***
Turn order	4.762	4.762	1	580	226.344	<2.2e-16	***
Competition	0.497	0.497	1	8	23.603	0.001	**
Angle*Turn order	1.484	0.742	2	580	35.254	3.55e-15	***
Angle*Competition	0.418	0.209	2	580	9.928	5.76e-15	***
Competition* Turn order	0.332	0.332	1	580	15.766	8.07e-05	***
Angle*Competition* Turn order	0.183	0.091	2	580	4.345	0.013	*
Competition							
Angle*Turn order @Presence	0.464	0.232	2	290	1.627	0.18963	
Angle*Turn order @Absence	1.202	0.601	2	290	4.209	0.00613	**
Competition = Absence							
Angle @ Turn order = Repeated	5.398	2.699	2	143	18.9	<1e-6	***
Angle @ Turn order = Alternated	0.641	0.321	2	143	2.245	0.07670	.
Competition = Presence							
Angle @ Turn order = Repeated	2.048	1.024	2	143	7.17	0.00634	***
Angle @ Turn order = Alternated	0.233	0.116	1	143	0.817	0.6641	

Pairwise comparisons:

Competition= Absence Turn order = Repeated TO	**45**	**90**
90	3.8e-8	-
45	<2e-16	1.7e-06

Competition = Presence	**45**	**90**
90	7.2e-9	-
45	1.3e-13	0.065

Supplementary Table 6. Output of the multi-level model fitting for the variable log-transformed fungal biomass measured with d-Tomato fluorescence, with chip as random effect and Angle, Turn order, and Competition as fixed factors. Each step performs an ANOVA and compares the model with the previous model.

	Model	df	AIC	BIC	logLik	Test	L.Ratio	p-value
1	1	3	-128.47	-115.28	67.23513			
Angle	2	5	-289.05	-267.066	149.5251	1 vs 2	164.5798	<.0001
Turn order	3	6	-453.421	-427.04	232.7106	2 vs 3	166.3711	<.0001
Competition	4	7	-465.159	-434.381	239.5797	3 vs 4	13.73815	0.0002
Angle*Competition	5	9	-478.266	-438.694	248.1331	4 vs 5	17.10689	0.0002
Turn order*Competition	6	10	-490.211	-446.242	255.1056	5 vs 6	13.9449	0.0002
Angle*Turn order	7	12	-552.955	-500.192	288.4775	6 vs 7	66.7438	<.0001
Angle*Turn order*Competition	8	14	-557.729	-496.172	292.8645	7 vs 8	8.77419	0.0124

Supplementary Table 7. Contrasts of the multi-level model with the variable log-transformed fungal biomass measured with d-Tomato fluorescence, with chip as random effect and Angle, Turn order, and Competition as fixed factors.

	Value	Std.Error	DF	t-value	p-value
(Intercept)	5.077005	0.060732	580	83.5974	0
Ang 45 – Ang 90	0.113564	0.029056	580	3.90849	0.0001
Ang 109 - Ang 90	-0.04097	0.029056	580	-1.41019	0.159
Alternated TO – Repeated TO	-0.21461	0.029056	580	-7.38624	0
Presence – Absence	-0.47	0.085887	8	-5.47231	0.0006
Ang 45 – 90 (Pres-Abs)	-0.05389	0.041091	580	-1.31138	0.1902
Ang 109 – 90 (Pres – Abs)	0.005047	0.041091	580	0.12282	0.9023
Alternated TO – Repeated TO (Pres – Abs)	0.034485	0.041091	580	0.83924	0.4017
Ang 45 – 90 (Alternated TO – Repeated TO)	0.13887	0.041091	580	3.37959	0.0008
Ang109 – 90 (Alternated TO – Repeated TO)	-0.17066	0.041091	580	-4.15322	0
Ang 45 – 90 (Alternated TO – Repeated TO) (Pres – Abs)	0.021144	0.058111	580	0.36385	0.7161
Ang109 – 90 (Alternated TO – Repeated TO) (Pres – Abs)	0.157559	0.058111	580	2.71134	0.0069

Supplementary Table 8. Output of the linear model with fungal biomass (d-Tomato fluorescence signal) as dependent variable and channel tortuosity as independent variable. Second and third panel indicate linear regression for fungal biomass data in absence and presence of competitor respectively.

	Value	Std.Error	DF	t-value	p-value
(Intercept)	5.572636	0.07139	588	78.05873	<1E-10
Tortuosity	-0.363774	0.019788	588	-18.38381	<1E-10
Presence-Absence	-0.6736	0.100961	8	-6.67188	2.00E-04
Tor*Presence - Tor*Absence	0.145963	0.027984	588	5.21595	<1E-10
Absence					
(Intercept)	5.572636	0.088027	294	63.30601	<1E-10
Tortuosity (slope)	-0.363774	0.02319	294	-15.68649	<1E-10
Presence					
(Intercept)	4.899036	0.049441	294	99.08868	<1E-10
Tortuosity (slope)	-0.21781	0.015663	294	-13.90632	<1E-10

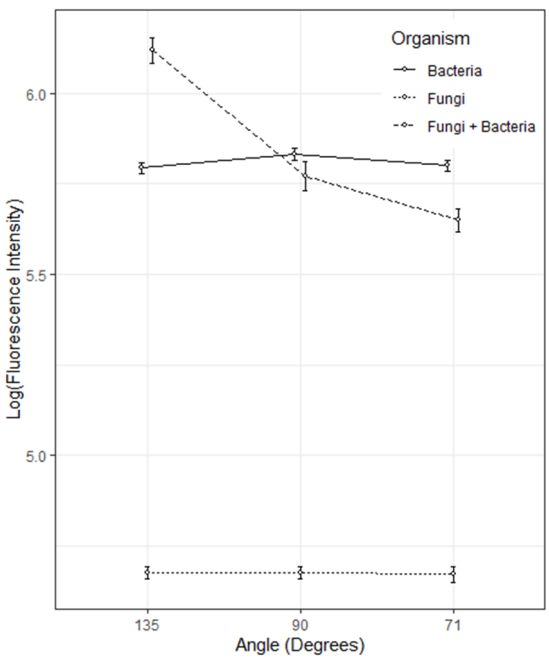

Supplementary Figure 6. Effect of the interaction between the factors Angle and Organism on the substrate consumption. The 4-methylcoumarin fluorescence data are presented for the bacterial *Pseudomonas putida* (continuous line), fungal *Coprinopsis cinerea* (doted line), and fungal-bacterial (dashed line) experiments. The points represent the mean fluorescence for each treatment and the error bars represent the ±standard error based on an ANOVA for all angle types (*n*=50).

Supplementary Table 9. Output of three-way ANOVA of the variable substrate consumption, measured with 4-Methylcoumarin fluorescence, with chip as random effect and Angle, Turn order, and Organisms as fixed factors. Contrasts were analyzed separately using the Dunn's method for multiple comparison of means. Pairwise comparisons were done with t-tests with p values adjusted using Holm corrections[45].

	Sum of squares	Mean Square	Degrees of freedom	Density degrees of freedom	F value	P value	
Angle	3.773	1.886	2	870	43.934	<2.2e-16	***
Turn order	0.788	0.788	1	870	18.351	2.04e-05	***
Organism	8.794	4.397	2	12	102.403	2.88e-08	***
Angle*Turn order	0.700	0.350	2	870	8.157	3.09e-04	***
Angle*Organism	8.243	2.061	4	870	47.993	<2.2e-16	***
Organism*Turn order	0.983	0.491	2	870	11.442	1.25e-05	***
Angle*Organism*Turn order	0.303	0.076	4	870	1.765	0.134	
Angle*Turn order							
Angle @Alternated	0.642	0.321	2	433	2.441	>0.05	
Angle @Repeated	3.831	1.916	2	433	14.53	<0.01	*
Angle*Organism							
Angle @Bacteria	0.081	0.041	2	293	0.309	>0.05	
Angle @Fungi	0.001	6.7e-4	2	293	5.12e-3	>0.05	
Angle @Bacteria + Fungi	11.932	5.966	2	293	45.39	<0.01	*
Turn order*Organism							
Turn order @Bacteria	8.4e-3	8.4e-3	1	294	0.064	>0.05	
Turn order @Fungi	0.015	0.015	1	294	0.117	>0.05	
Turn order @Bacteria + Fungi	1.747	1.747	1	294	13.28	<0.01	*

Pairwise comparison:

Turn order = Repeated	45	90
90	0.039	-
45	3.3e-03	0.348

Organism = Bacteria + fungi	45	90
90	1e-10	-
45	<2e-16	0.018

Supplementary Table 10. Output of the multi-level model fitting for the variable log-transformed substrate consumption measured with 4-Methylcoumarin fluorescence, with chip as random effect and Angle, Turn order, and Organism as fixed factors. Each step performs an ANOVA and compares the model with the previous model.

	Model	df	AIC	BIC	logLik	Test	L.Ratio	p-value
1	1	3	98.14038	112.5476	-46.0702			
Angle	2	5	35.67437	59.68634	-12.8372	1 vs 2	66.46601	<.0001
Turn order	3	6	23.14013	51.9545	-5.57007	2 vs 3	14.53424	0.0001
Organism	4	8	-16.2714	22.14778	16.13569	3 vs 4	43.41151	<.0001
Angle*Organism	5	12	-176.617	-118.988	100.3084	4 vs 5	168.3455	<.0001
Turn order*Organism	6	14	-195	-127.767	111.5002	5 vs 6	22.38354	<.0001
Angle*Turn order	7	16	-207.31	-130.472	119.6551	6 vs 7	16.30971	0.0003
Angle*Turn order*Organism	8	20	-206.461	-110.413	123.2304	7 vs 8	7.15064	0.1281

Supplementary Table 11. Contrasts of the multi-level model with the variable log-transformed substrate consumption measured with 4-Methylcoumarin fluorescence, with chip as random effect and Angle, Turn order, and Organism as fixed factors.

	Value	Std.Error	DF	t-value	p-value
(Intercept)	5.851698	0.063653	874	91.93076	0
Ang 45 – Ang 90	-0.09126	0.03395	874	-2.68804	0.0073
Ang 109 – Ang 90	-0.02163	0.03395	874	-0.63701	0.5243
Repeated TO – Alternated TO	-0.03984	0.030992	874	-1.28549	0.199
Fungi – Bacteria	-1.15348	0.088946	12	-12.9683	0
Fungi+Bacteria – Bacteria	0.010437	0.088946	12	0.11735	0.9085
Ang 45 – Ang 90 (Fungi – Bacteria)	0.035737	0.04158	874	0.85948	0.3903
Ang 109 – Ang 90 (Fungi -Bacteria)	0.026321	0.04158	874	0.63301	0.5269
Ang 45 – Ang 90 (Fungi+Bacteria – Bacteria)	0.386306	0.04158	874	9.29061	0
Ang 109 – Ang 90 (Fungi+bacteria – Bacteria)	-0.0905	0.04158	874	-2.17648	0.0298
Repeated TO – Alternated TO (Fungi – Bacteria)	-0.00368	0.03395	874	-0.10841	0.9137
Repeated TO – Alternated TO (Fungi+Bacteria – Bacteria)	-0.14198	0.03395	874	-4.18213	0
Ang 45 – Ang 90 (Repeated TO – Alternated TO)	0.107305	0.03395	874	3.16066	0.0016
Ang 109 – Ang 90 (Repeated TO – Alternated TO)	-0.01965	0.03395	874	-0.57869	0.5629

Supplementary Table 12. Output of the linear model with substrate consumption (4-methylcoumarin fluorescence signal) as dependent variable and organism present and channel tortuosity as independent variables.

	Value	Std.Error		DF	t-value	p-value
(Intercept)	4.705342	0.078689		882	59.79673	<1E-10
Bacteria – Fungi	1.11153	0.111283		12	9.98832	<1E-10
Bacteria + Fungi - Fungi	1.857722	0.111283		12	16.69367	<1E-10
Tortuosity	-0.019443		0.026835	882	-0.72454	0.4689
B:Tortuosity – F:Tortuosity	0.014389	0.03795		882	0.37917	0.7047
B+F:Tortuosity – F:Tortuosity	-0.426684	0.03795		882	-11.24339	<1E-10

Supplementary Table 13. Output of the linear model with substrate consumption (4-methylcoumarin fluorescence signal) as dependent variable and organism present and channel tortuosity as independent variables.

Turn Order	Alternated			Repeated		
Angle	45	90	109	45	90	109
Ratio Log(Substrate degradation fluorescence)/ Log (B GFP Fluorescence)	1.113	1.138	1.132	1.125	1.145	1.14

Paper III

Habitat complexity increases bacterial growth and enzymatic activity while reducing fungal growth in fractal maze model

Running Title:

Habitat connectivity affects microbial growth in fractal maze

Authors:

Carlos Gustavo Arellano Caicedo1,*

Pelle Ohlsson2

Martin Bengtsson2

Jason P. Beech3

Edith C. Hammer1, 4

Afiliations:

1. Department of Biology, Lund University, Lund, Sweden

2. Department of Biomedical Engineering, Lund University, Sweden

3. Division of Solid State Physics, Lund University, Sweden

4 Centre for Environmental and Climate Science, CEC, Lund University, Sweden

*Corresponding author. E-mail address: carlos.arellano@biol.lu.se

Abstract

The great variety of Earth's microorganisms and their functions is attributed to the heterogeneity of their habitats, but our understanding of the impact of those environmental conditions is limited, especially on the microscale. In the present study we tested how a gradient of habitat physical complexity in the form of increasing fractal order of a space filling maze influenced the growth, substrate degradation, and competition, of the bacterial strain *Pseudomonas putida* and the fungal strain *Coprinopsis cinerea*.

Bacteria and fungi responded to the habitat complexity in different ways: complex habitats strongly reduced fungal growth but in contrast increased the number of bacteria inside them. The substrate degradation also increased with habitat complexity, even more than the bacterial biomass. Detailed spatial analysis within the mazes showed that the maximal bacterial growth and substrate degradation occurred at intermediate depth into the mazes. Fungal hyphae did not reach far into the mazes but forced bacteria to mainly grow in the deeper regions. A likely reason for the increase of bacterial biomass and substrate degradation in more complex mazes and dead ends is the accumulation of enzymes and quorum sensing molecules leading to an onset of biofilm metabolism. These results suggest an increase in enzymatic activity in confined spaces and demonstrate the effect of spatial microstructures on microbial growth and substrate degradation which may add up to considerable differences in nutrient cycling when scaled up to macroscale.

Introduction

The habitats where microbes grow are far from homogeneous and static, but rather they tend to be patchy, and change over time. In human, plant and marine microbiomes, examples can be found of the characteristics of the habitat influencing not only the way microbes behave, but also the impact microbes they have in ecosystems. Heterogeneous microhabitats inside the human body, for instance, like crypts, mucus, or the appendix, can benefit microbial communities by serving as reservoirs for repopulation after stress, or as protection against external competitors, which they would not have in homogeneous environment (Donaldson et al. 2015). Another example is the skin microbiome, which exhibits a high diversity despite its exposure to harsh and variable conditions, thanks to the topographic characteristics of the skin which also determine in part the type of microbes that colonize it (Grice & Segre 2011).

The role of microhabitats is also crucial for biogeochemical processes occurring in marine and terrestrial environments. Microbial communities inside marine organic particles, for example, can influence the marine carbon dynamic differently depending on the inner chemical and physical structure of those particles (Carrias & Sime-Ngando 2009). A stronger effect is seen in soils, a far more heterogeneous environment, where the microscopic heterogeneity gives rise to a higher microbial density, genomic diversity, and substrate preservation, than any other microbial environment (Or et al. 2007; Lehmann & Kleber 2015; Rabbi et al. 2016). This last example is of special importance for climate change, for it can help to explain the high amount of easily degradable carbon sharing habitat with nutrient limited microorganisms in soils (Schmidt *et al.* 2011; Hobbie & Hobbie 2013).

The challenge when studying the effect of microhabitats on microbial communities is to be able to manipulate the characteristics of the environment on the relevant scale and to study the resulting behaviour. Microfluidic structures are ideal in this sense, and the use of microfluidic techniques opens up a wide range of possibilities to study microbial processes (Hol & Dekker 2014) . Microfluidics allow the building of environments with different physical or chemical characteristics at the micro scale, where processes such as bacterial attachment to surfaces (Gu et al. 2016), or bacterial biofilm formation (Nadell et al. 2017), can be studied. Microfluidic structures fabricated in PDMS are also transparent and provide a control of flows and nutrients, being therefore ideal for the microscopic study of microbial interactions and growth. Effects of habitat heterogeneity or spatial separation between bacterial communities in microfluidics have already shed light on crucial microbial processes that could not be studied before. It has been demonstrated, for instance, that otherwise mutually exclusive species can cohabit and even cooperate for mutual benefit when they are not in direct contact (Hyun et al. 2008), and that the predator-prey balance of a community can be reached in presence of physical complexity (Yawata et al. 2014; Hol et al. 2016).

In the present study we investigate how an increasing complexity of spatial microstructures affect growth, interactions, and substrate degradation patterns of the two major microorganism groups: fungi and bacteria. We designed structures in microfluidic devices that simulate different levels of spatial complexity via mazes of different fractal order. There we studied the effect of maze complexity on the growth of the fluorescently labeled soil bacterial strain *Pseudomonas putida* and the fungal strain *Coprinopsis cinerea*; both separately and when present in the microenvironment together. A fluorescent aminopeptidase substrate was used to quantify the spatially resolved enzymatic activity in the mazes. Bacterial and fungal biomass as well as substrate degradation inside the mazes were followed for 12 days using fluorescence microscopy. We hypothesized that increasing maze fractal order would reduce bacterial and fungal growth. When grown together, we expected an increased impact on bacterial biomass due to the additional complexity that fungal hyphae create. Because of the decreased biomass, we also expected the substrate to have lower degradation in high fractal order mazes. Our results showed, however, that bacteria and fungi were differently affected by maze complexity, resulting in an increase in bacterial biomass and a reduction of fungal biomass as mazes became more complex. The enzymatic activity of bacteria also increased as maze complexity increased, both in absolute values and proportional to bacterial biomass. We think that these results point towards a community behavior of bacteria versus the individual behavior of fungi. The increase in bacterial growth and nutrient degradation efficiency in complex mazes might thus be due to a decrease in competition between individuals which allowed a diverse, and more efficient, set of strategies to emerge and cohabit.

Materials and Methods

Device design

The design for the Fractal chip was written in AutoCad 2019 (Autodesk). The design consists of an inoculation area filled with pillars (100 µm diameter and 200 µm pitch) that allow the bacteria and fungi to grow across the width of the device and enter an array of treatment mazes (Figure 1). The treatments consist of dead-end mazes based on space filling Hilbert curves (Hilbert & Hilbert 1935) of four different fractal orders with a normalized internal volume. Four orders of the Hilbert curve were chosen for the experiments: zero, one, three and five (F0, F1, F3, F5, respectively; Figure 1). The “zero” fractal iteration consisted of a series of rectangular pillars that had one connection less with each other than the first iteration ones. The width of the channels within the mazes was 10 µm, and the height 12 µm so that we give enough space for hyphae and bacteria to grow. The mazes were randomly distributed along the chip (n=7/per chip).

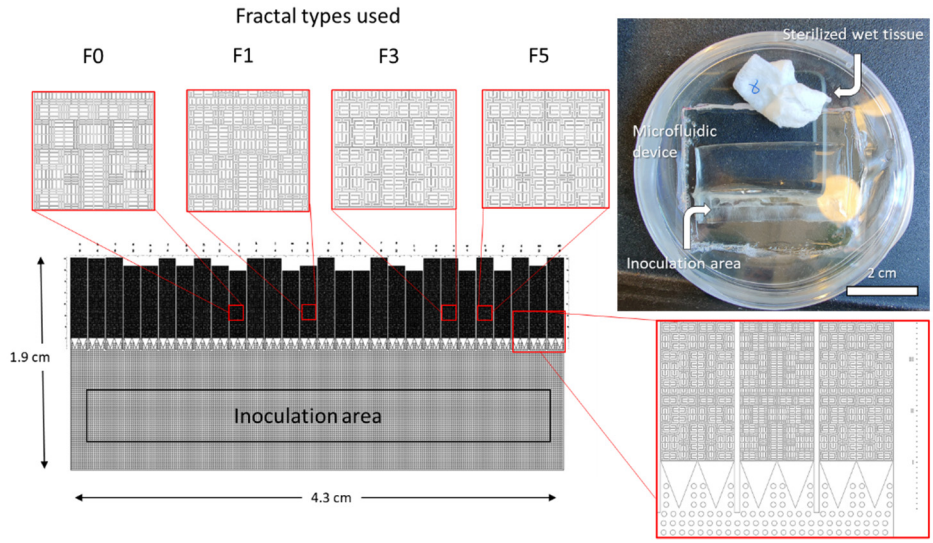

Figure 1. Microfluidic device designs containing 4 types of mazes of different fractal iteration: 0 iterations (F0), 1 iteration (F1), 3 iterations (F3), and 5 iterations (F5). The design contains 7 replicates of each type of maze with standardized internal volumes. The microfluidic device is molded in PDMS and bonded to a glass-bottom Petri dish. The device contains a pillar system serving as inoculation area in which an entrance is opened and filled with liquid inocula. A sterile wet tissue preserves humidity in the Petri dish during incubation.

Device fabrication

The Fractal chip was molded using polydimethylsiloxane (PDMS) on a master, previously made through UV photolithography using a photomask, and subsequently bonded to a glass bottom Petri dish (Aleklett *et al.* 2018). The photomask that was used to make the masters, was made from soda lime glass with a thin layer of chromium (Nanofilm, CA, USA) patterned with a dwl66+ mask writer (Heidelberg Instruments, Germany) where a NdYag laser with a wavelength of 532 nm was used to draw the designed patterns on a AZ1500 photoresist spray cotted with nanofilm. The patterns in the mask were afterwards developed in AZ 351B positive developer and the chromium etched in TechniEtchCr01 (Microchemicals GmbH, Ulm Germany).

The master was made by dispensing SU-8 2015 photoresist (MicroChem, Newton, MA, USA) on a heat dried (90˚C for 30 minutes) 3-inch silicon wafer (Siegert Wafer, Aachen, Germany) and spun at 4000 rpm to get a 12 µm thick layer. The wafer was soft-baked at 90 ˚C, after which the SU-8 on it was patterned with UV-light through the photomask using a contact mask aligner (Karl Suss MJB4 soft UV, Munich, Germany). After UV exposure and the post exposure-bake at 90 ˚C, the photoresist that was not crosslinked was removed through development (MrDev600) and the remaining structures were rinsed with isopropanol and hard-baked at 200 ˚C for 2 hours. To prevent PDMS from sticking to the mold in the microfluidic device fabrication, the wafer containing the structures was activated in

an oxygen plasma for 60 seconds (ZEPTO, Diener Plasma-Surface Technology, Germany) and then exposed overnight to a vapor of trichloro (1H,1H,2H,2H-perfluorooctyl) silane (PFOTS, Sigma Aldrich, Saint Louis, MO, USA) at 180˚C to obtain a monolayer. SYLGARD^{TM} 184 PDMS silicone was used for the microfluidic devices and it was prepared (Dow Chemicals Company, Midland, Michigan) by mixing the elastomer base with the curing agent in a proportion of 10:1 in mass, poured on top of the master, degassed at -15 kPa for one hour and finally polymerized in an oven at 60˚C for two hours.

The PDMS devices were cut out from the master and a rectangular portion of 4 cm x 0.5 cm was cut out in the middle of the pillar system, approximately 0.5 cm away from the entrance of every maze. This cut was made to create the reservoirs that served as entrance to the maze in the inoculation area (Figure 1). Using a plasma chamber, the PDMS mazes and a glass from a glass bottom Petri dish were activated and bonded. This activation consisted in treating the surfaces with a Zepto Plasma System (Diener Plasma Surface Technology, Germany) with these conditions: negative polarity; 1 min coating time for cover slips and 10 seconds for PDMS mazes. Directly after activation, the surfaces were put together, forming a tight irreversible bond (Mcdonald *et al.* 2000). Directly after bonding, 300 µl of the treatment medium was introduced through the reservoir.

Strains and growth conditions

Pseudomonas putida mt-2 carrying plasmid-borne msfGFP-reporter constructs were pre-cultured overnight in M9 minimal medium (12.8 g/L $NaHPO_4.7H_2O$, 3 g/L KH_2PO_4, 0.5 g/L NaCl, 100 mg/L NH_4Cl, 0.12 g/L $MgSO_4$, 4 g/L d-Glucose, 11.66 mg/L $CaCl_2$, 13.5 mg/L $FeCl_2$, 125 mg/L $MgCl_2.6H_2O$, 1 mg/L $MnCl_2.4H_2O$, 1.7mg of $ZnCl_2$, 0.43mg $CuCl_2.2H_2O$, 0.6 mg $CoCl_2.6H_2O$, 0.6mg $Na_2MoO_4.2H_2O$, pH 6.5) (Smith 1991) with pH 6.5 at 28°C and agitated at 150 rpm.

The experiments with *Pseudomonas putida* mt-2 were done as follows: 2 mL of overnight cultures were pelleted by centrifugation (5000 g for 10 min at 21 °C), and cells were resuspended in 0.5 ml of fresh M9 medium. L-Alanine 7-amido-4-methylcoumarin (AMC, 160 mg/L) was added to the medium to determine substrate consumption inside the chips. AMC is a fluorogenic substrate that becomes fluorescent when it is enzymatically hydrolyzed by aminopeptidase enzymes (Razavi *et al.* 2019). 1.5 µl of the bacterial suspension was added to the entrance of the chip to obtain a final optical density at 600 nm of 0.2 OD_{600} (Nicodème *et al.* 2005; Güll *et al.* 2009). This peptide can only be accessed by the bacterial, and not the fungal strain we used, and functions thus as an indicator of the bacterial enzymatic activity over the course of the experiment.

The fungal strain used for the experiment was *Coprinopsis cinerea* AmutBmut PMA412, expressing constitutively the cytoplasmic fluorescent dTomato protein (Burns *et al.* 2005). Pre-incubation was done in 1.5% agar plates of Yeast Malt

Glucose medium (Stanley *et al.* 2014), for 6 days at 28°C. A rectangular plug of the mycelium sized 1 mm x 25 mm was placed upside down (with the mycelia facing the inner part of the microfluidic device) in the reservoir inside the chip. Care was taken to separate the fungal mycelium from the top of the agar plug so that no extra nutrients would be added to the medium. The inner part of the maze was filled beforehand with 300 µL of M9 medium containing 160 mg AMC/L (pH 6.5) by capillary wetting directly after bonding. After 48 hours, once the hyphae had arrived at the entrance of the mazes, the medium from the reservoir was replaced with fresh M9 medium containing AMC. In the fungal-bacteria treatment, a 1.5 µL inoculum of *Pseudomonas putida* was introduced in the reservoir after the medium replacement to a final concentration of OD_{600} 0.2. Sterile wet tissues were placed inside the Petri dishes to preserve humidity. The plates were sealed with Parafilm (Bemis™ Parafilm™) to prevent water from evaporating and kept in the dark at room temperature (21 °C).

In total 12 chips were used for the experiment, 4 containing *Pseudomonas putida and* 4 with *Coprinopsis cinerea, (*absence of competitor)*,* and 4 containing both (presence of competitor).

Microscopy

Epifluorescence microscopy was used for visualization of *P. putida, C. cinerea,* and AMC using a fully motorized Nikon Ti2-E inverted microscope with PFS4 hardware autofocus, full 25 mm field-of-view, CoolLED pE300-White MB illumination connected via a 3 mm liquid light guide (LLG), and a Nikon Qi2 camera with 1x F-mount adapter. The filters used were LED-DAPI-A-2360A Semrock Filter Cube (Ex: 380-405 nm, Em: 413-480 nm), GFP-4050B Semrock Filter Cube (Ex: 444-488 nm, Em: 498-553 nm), mCherry-C Semrock Filter Cube (Ex: 520-585 nm, Em: 600-680 nm). Images for fluorescence quantification of the entire chip were captured using a (MRH00041) CFI Plan Fluor 4X, N.A. 0.13, W.D. 17.1 mm objective, with an exposure time of 20 ms for GFP, 100 ms for DAPI and 100 ms for mCherry. For high magnification pictures a (MRD31905) CFI Plan Apochromat DM Lambda 100X Oil N.A. 1.45, W.D. 0.13 mm and a (MRD30405) CFI Plan Apochromat DM Lambda 40X, N.A. 0.95, W.D. 0.21 mm objectives were used. NIS-Elements software was used for coordination of the multipoint imaging. Pictures were taken for every chip once a day for 12 days. The days selected for statistical analysis were the ones of maximum fluorescence signal for each treatment.

Image Analysis

The fluorescence intensity of each treatment was quantified using ImageJ 1.52n (Schindelin *et al.* 2012). Background was subtracted using the ImageJ rolling ball algorithm (Kneen & Annegarn 1996) using 7 pixels as radius of rolling ball for 4x objective images. The rolling ball radius was chosen based on the size of the largest

fluorescent object, which was the diameter of a PDMS channel in the images at the obtained resolution. After the subtraction, the total intensity was quantified inside each maze using the ROI manager tool.

The fluorescence spatial variation inside the mazes was quantified by measuring the fluorescence of the dead ends of the second portion of the F5 maze. The second portion was selected to minimize the edge effect produced in the first fractal due to its direct contact with the pillar system. The measurement was done in the 7 internal replicates of each maze type and in one chip per treatment.

Estimation of accessibility within mazes

The mean fluorescence of each dead-end path was compared to its accessibility defined as one minus the time required for a particle diffusion model to reach 50% of the asymptotic final concentration. The time was normalized so that 1 is the time required for the last dead end of the F5 maze to reach 50% of the final concentration, giving this point the accessibility 0 and the maze entrance accessibility 1. The diffusion was simulated using COMSOL Multiphysics® (Multiphysics & Multiphysics 2020).

Statistical Analysis

The experiment had a full-factorial design with fractal order (F0, F1, F3, F5) and competition (presence or absence of the other organism) as factors. Each device contained 7 copies of each type of maze, and four devices were used combinedly for each of the following inoculation conditions: 4 with bacteria (bacteria in absence of competitor), 4 with fungi (fungi in absence of competitor), and 4 with bacteria and fungi (presence of competitor). Multilevel model fitting correcting for random effects was used to test the influence of every variable. Random effects were attributed to each device as physical replicate of the experiment, to take into consideration the variation that existed between devices. For bacterial and fungal biomass, maze type and competition were considered as fixed factors. For substrate consumption, maze type and organism (Fungi, Bacteria, Fungi + Bacteria) were the fixed factors. For in-depth statistical analysis, the data from the day with maximum fluorescence was chosen for each maze type. The significance threshold used for all statistical tests was $p < 0.05$. When significant differences were found in the ANOVA, interactions were analyzed separately using the Dunn's method for multiple comparison of means (Dunn 1961). Pairwise comparisons were done with t-tests with p values adjusted using Holm corrections (Holm 1979). All statistical analysis was performed using R (Team 2019).

Results and discussion

The Fractal chip contained four different types of mazes. The mazes had different degrees of space filling fractal orders (Figure 1), namely, fractal order 0 (full

connectivity, F0), fractal order 1 (F1), fractal order 3 (F3), and fractal order 5 (F5). The bacterial (*Pseudomonas putida)* and the fungal (*Coprinopsis cinerea)* strains were inoculated together or separately inside the microfluidic devices and their biomass was measured as *GFP* and d-Tomato fluorescent signal, respectively. Also, the substrate degradation under the different treatments was followed using the fluorogenic substrate L-Alanine 7-amido-4-methylcoumarin trifluoroacetate salt. The experimented lasted 12 days in total, during which bacteria and fungi colonized all the mazes inside the microfluidic devices under all the studied conditions.

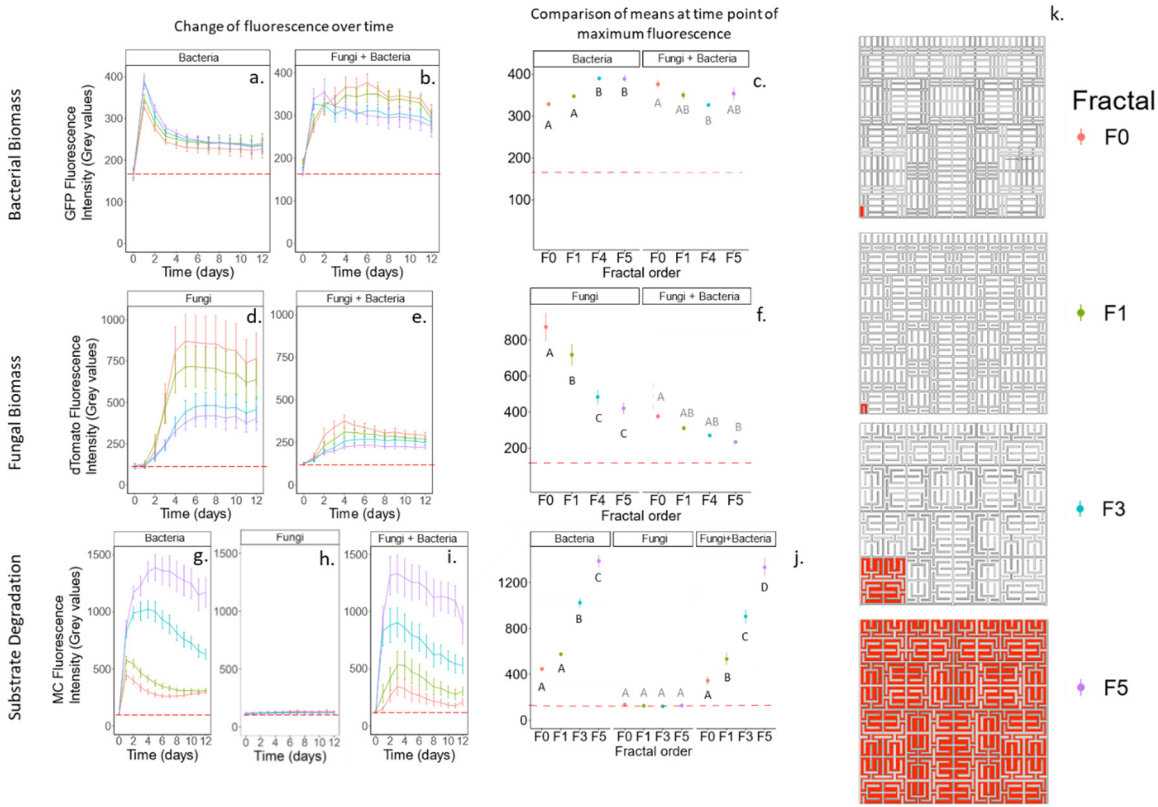

Figure 2. Fungal and bacterial biomass in time, with (a, d) and without competitor (b, e) and substrate consumption in bacterial (g), fungal (h), and bacteria + fungi treatment (i) for the four types of mazes tested (color coding of the curves is shown on the right side of the figure). Plots c, f, and j show the comparison of mean values for bacterial biomass, fungal biomass, and substrate consumption, respectively, between treatments on the day of maximum fluorescence. The capital letters under each mean value indicate weather significant difference was found between the different groups (p<0.05). The dashed red line indicates the background fluorescence level. The maze representation on the right side (k) with the connected structure that is repeated to form the maze in red. As the mazes increase in fractal order, the smallest connected building block of the maze increases in size, and the connectivity of the maze thus decreases.

Bacteria without competitor

During the experiment, all mazes were colonized by bacteria, however both the amount and timing of maximum bacterial growth differed significantly between maze fractal order and competition conditions (Figure 2, Supplementary videos 1-4). Even though we hypothesized that higher order mazes would result in lower bacterial biomass due to the large number of turns bacteria need to do (Arellano et.al. under review), bacteria in fact colonized and reproduced more in higher order mazes (F3 and F5 being higher than F0 and F1) (Figure 2). Substrate degradation followed the same principal pattern, meaning that it was higher in F3 and F5 compared to the simpler mazes F0 and F1.

To explore this further, we analyzed the spatial distribution of bacterial biomass within individual mazes at the day of maximum biomass. We used a diffusion model as a proxy for defining accessibility for randomly moving particles coming from the direction of the entry area. The level of accessibility of any region within the mazes was defined as one minus the time (normalized from 1 to 0 as the maximum in the F5 maze) needed for that region to reach half the final concentration of molecules. Thus, accessibility went from 0, given to the last region of the maze to reach half the final concentration of molecules, to 1, which was given to the first regions in the fractal that reached the desired concentration. In other words, an accessibility value of 1 would correspond to the most accessible regions, and 0 to the least accessible ones. Comparing the bacterial biomass with the accessibility within mazes revealed that in simple mazes (F0, F1) bacterial biomass was homogeneously distributed inside the maze. In complex mazes (F3, F5), on the other hand, bacterial cell density decreased towards the less accessible regions.

The reduced biomass in deeper regions of the mazes might be caused by the high number of 90˚ turns that bacteria need to make. Even though bacterial biomass in the deeper regions of these fractals stayed at similar or even lower levels than in the simple mazes (F0 and F1), the overall bacterial biomass was still higher in the complex mazes, F3 and F5, than in the simple ones, F0 and F1, due to the high bacterial biomass in the most accessible dead ends of F3 and F5.

Accumulation of bacteria in confined spaces has been shown before (Park *et al.* 2003; Hou *et al.* 2011), and could possibly be attributed to the tendency of bacteria to maximize their contact area with the surface (Mitik-Dineva *et al.* 2008; Hochbaum & Aizenberg 2010), although this seems to be species dependent (Chung *et al.* 2007). Dead end structures create a gradient of chemoattractant molecules both since cell mobility is reduced and since signal diffusion is only possible within the open space, attracting more bacteria. This has been observed to occur inside microfluidic devices (Long *et al.* 2017), and is likely present in the soil pore space and other microhabitats such as tumors or the appendix in the human microbiome. The bacterial biomass accumulation in mazes with more dead ends may be caused by quorum sensing where bacteria alter their gene regulation as response to cell

density, making them regulate their run and tumble frequency to follow a particular chemical cue coming from higher cell densities (Miller & Bassler 2001). When bacteria sense such a specific chemical cue or attractant, they regulate the duration (Baker *et al.* 2006) as well as the angle of their tumble (Saragosti *et al.* 2011) which directs their movement towards the chemical cue. In our case, the initial cue could be the nutrient gradient that attracts bacteria into the mazes. Nonetheless, the lower bacterial concentration in the less accessible dead ends of the mazes F3 and F5 suggests that the tortuosity and length of the path towards the dead end influences the number of bacteria that access it.

The fluorogenic substrate used in our study did not serve for measuring fungal enzymatic activity but only bacterial enzymatic activity, which enabled us to selectively know the effect of structures and interaction with fungi on bacterial enzymatic activity. Substrate consumption followed a similar trend as bacterial biomass in the different fractal order mazes. It was highest in the most complex maze (F5) and it decreased as maze fractal order decreased. High fractal order mazes (F3 and F5) reached the maximum substrate consumption on day 5 after inoculation which was later than the biomass peaked, while lower fractal order mazes (F0 and F1) reached their maximum values on day 1. Spatial analysis within the mazes showed that substrate consumption increased as accessibility decreased (Figure 3). However, in F5, substrate consumption increased only until a certain point, after which it decreased, in a similar pattern as for bacterial biomass. This pattern indicates an optimum accessibility point where substrate consumption is at its maximum, after which conditions seem to be suboptimal for enzymatic degradation, becoming thus proportional to the lowering of bacterial biomass in deeper regions. The increasing effect of higher fractal order on substrate degradation is stronger than on bacterial biomass, the ratio of AMC to GFP fluorescence being 1.36, 1.62, 2.59 and 3.56 for F0, F1, F3 and F5, respectively. These differences suggest that bacteria are becoming more efficient at degrading the substrate when the habitat is more complex. Such behavior can be the product of accumulation of enzymes in the confined spaces, and an emerging biofilm formation. It has been shown that *Pseudomonas putida* can form biofilms (Arevalo-Ferro *et al.* 2005) and that its properties can differ to a high degree from the properties of individual bacteria (Flemming *et al.* 2016). For instance, the capability of increased communal degradation of antibiotics (Park 2003) and contaminants (Breugelmans *et al.* 2008) is an emergent property of bacterial biofilms that is not present in single individuals of the same strain. In soils, the degradation of organic matter that requires the initial investment of enzymes, can be enhanced through bacterial biofilms, since the extracellular enzymes produced are functional for many hours and can become a common good for the bacterial population. It has been hypothesized that for this collective enzyme production to be efficient in soils, a certain enzyme to cell number ratio must be reached (Kaiser *et al.* 2015). Since confined spaces seem to favor biofilm-type metabolisms (Chu *et al.* 2018), it is possible that the confinement of the mazes in our design favors a biofilm formation that enhances and optimizes

enzyme production or metabolic exchange (Pande *et al.* 2016). Another reason for such increase in enzymatic activity might be the coexistence of bacteria with different metabolic strategies in complex environments. The heterogeneity of the landscape might allow different types of strategies to be adopted, such as fast, non-enzymatic degradation and slow, enzymatic degradation, which leads to an increased enzymatic production (Keymer *et al.* 2006).

Fungi without competitor

The overall effect of the maze structure on fungal growth was similar in presence or absence of bacteria: Fungal growth was strongly reduced as the fractal order of the mazes increased. Differences between mazes were stronger when fungi grew alone than when bacteria were present.

The day of maximum fungal growth occurred at different times among the maze types: At day 5 for F0 and F1, and at day 7 for F3 and F5. In the two simplest fractals (F0 and F1) fungal biomass distribution was unaffected by decreasing spatial accessibility inside the mazes (Figure 3). For the two complex and less connected mazes (F3 and F5), however, the fungal biomass decreased as accessibility decreased, with the strongest measured effect in the most complex maze type F5. The high magnification videos (Supplementary Videos 5-8) show the impact that structures had on fungi: The most connected maze (F0) allows fungi to forage and explore the spaces rather undisturbed via branching and anastomosis, and easily grow in a straight fashion without disrupted growth. In contrast, increasing structural complexity (F1, F3 and F5) impedes this advancement by forcing fungi to turn in order to advance through the maze, and the frequently occurring dead ends trap the lead hyphae, limiting the possible alternative paths for exploring the totality of the maze.

Supplementary videos 5 and 6 show how fungi branch in every turn of F0 and F1, optimizing the space they occupy. In contrast, in the complex mazes F3 and F5 (supplementary videos 7 and 8), only few possible passages allow access to the interior of the fractal (Figure 4). The efficient space exploration of the randomly branching hyphae is disturbed since the paths leading to access to the deeper parts of the maze are more limited. It has previously been shown that a colliding angle of 90° stops the hyphal growth or induces a branching event in *Neuraspora crassa* (Asenova *et al.* 2016), several basidiomycetes (Aleklett *et al.* 2021) and in *Coprinopsis cinerea* (Arellano-Caicedo et.al. *submitted*), and also in the present experiment, hyphal collision with the maze walls produces branching events (Supplementary Video 5-8). While such branching represents an increase in the exploratory ability of hyphae in F0 and F1, in the complex, less connected, mazes (F3 and F5), those branches often get trapped in dead ends reducing the advantage of branching in exploration under low spatial connectivity. This confirms the importance of pore connectivity for fungal colonization, which has earlier been pointed out based on modelled data (Kravchenko *et al.* 2011).

Despite the ability of fungi to keep an overall directionality (Asenova *et al.* 2016) and increase their rate of branching under confinement (Hanson *et al.* 2006), our results show that, due to the many turns and branching events needed (Figure 4, Supplementary video 5-8), the overall fungal colonization of the highest order mazes is lowered. Such patterns of colonization, being dependent on branching, anastomosis and apical growth rates, are very likely to differ between different fungal species, which differ in these parameters (Aleklett *et al.* 2021; Asenova *et al.* 2016).

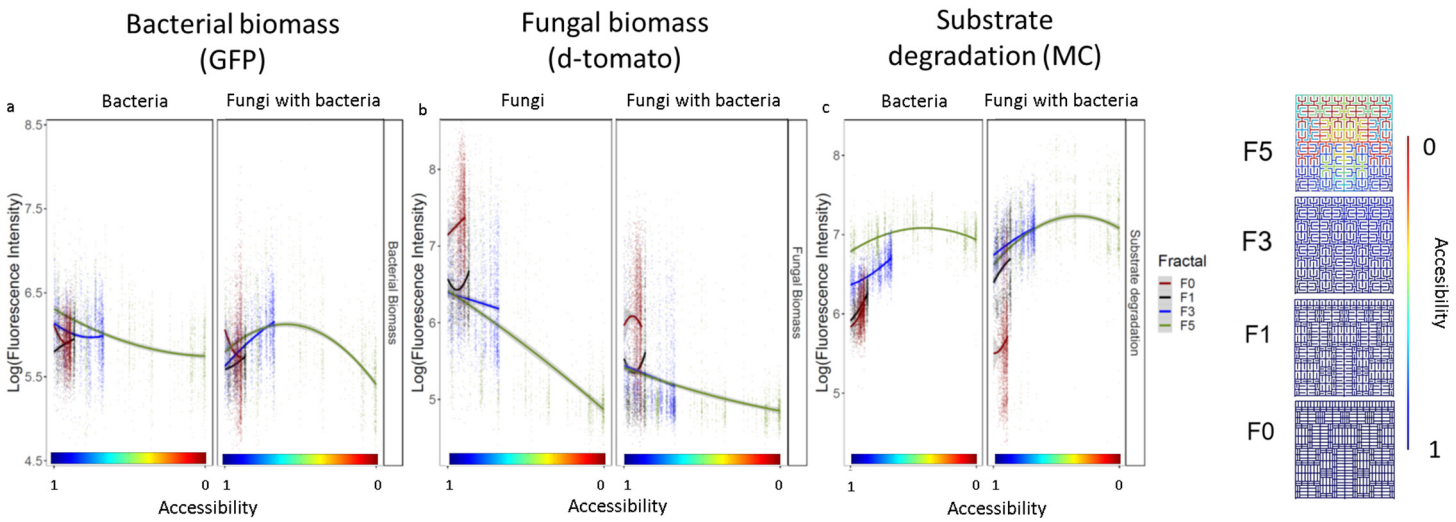

Figure 3. Spatial distribution of bacterial (a) and fungal biomass (b), as well as substrate degradation (c), along the different mazes measured as fluorescence intensity (GFP, d-tomato and MC fluorescence respectively). The space within the mazes is characterized as accesibility (d) and ranges from 1 to 0, where 1 is the most accesible region and 0 is the least accesible. Each dot corresponds to the mean fluorescence of a specific region within the middle region of the entire, which posses a certain accesibility calculated with the COMSOL diffusion model. The lines correspond to curve fitting using a quadratic model. The right pannels show the accesibility leves of each type of maze in relation to the whole studied accessibility range with the minimum at the most hidden dead-end in F5.

Bacterial-fungal interactions

When the bacteria grew together with the fungal competitor *Coprinopsis cinerea*, the peak of maximum bacterial biomass occurred at generally later but differing time points for each maze (Figure 2). While in the simple mazes, F0 and F1, bacterial growth peaked at day 6, in the complex ones, F3 and F5, it peaked already at day 1 and 2, respectively. F0 reached a higher maximal bacterial growth than the rest of the mazes (significant for F0 over F3, $p<0.001$). The spatial analysis of bacterial biomass distribution within the mazes in presence of the fungal competitor indicates that in the simplest maze (F0) the pattern of bacterial biomass was similar to the one in absence of competitor, namely, bacterial growth decreased in lower accessibility regions. In the rest of the maze types, however, bacterial biomass increased in lower accessibility regions, opposite to the distributions of bacteria growing alone (Figure 3). Initial dead ends, occupied by bacteria when those are growing alone, became in this case occupied by fungal hyphae that displaced bacterial accumulation (Figure 6). Thus, bacteria were forced to grow in the regions of the maze where fungi have difficulties to grow, namely the regions of lower accessibility, following a pattern of spatial niche partitioning. As mentioned before, spatial analysis of F5 shows that the increase in bacterial biomass in low accessibility regions occurs only until a certain accessibility level. After this critical point bacterial biomass starts decreasing, putatively due to the difficulty to access the deepest regions of the maze. High magnification images (Figure 6) show that the presence of bacteria and fungi in dead ends is mutually exclusive, meaning that bacteria accumulate when fungi are not present and vice versa. Hyphae have a strong protruding force that can penetrate strong structures and tissues (Lew 2011; Tayagui *et al.* 2017), which allows them to penetrate and easily disrupt the bacterial accumulations. The dead ends where bacteria could accumulate easily were the ones that were not accessible to fungi (Figure 3 and 5).

The data for bacterial biomass in presence and absence of fungi suggests that quorum sensing might determine the bacterial distribution in heterogeneous habitats when growing alone, but the presence of fungal hyphae can alter this spatio-temporal distribution by occupying the spaces where bacteria can grow. Thus it seems like fungi might constitute not only networks (Banitz *et al.* 2011), bridges (Furuno *et al.* 2010; Mafla Endara *et al.* under rev), highways (Kohlmeier *et al.* 2005), or food sources (Ballhausen *et al.* 2015) for bacteria, but also crucial modifiers of the microhabitat that bacteria inhabit. Since the antibiotics produced by *Coprinopsis cinerea* have been shown to affect gram positive bacteria exclusively (Essig *et al.* 2014), the effects of the fungi on the biomass patterns of the gram negative *Pseudomonas putida* are rather likely to be due to habitat modification by fungal hyphae and the nutrient competition between bacteria and fungi.

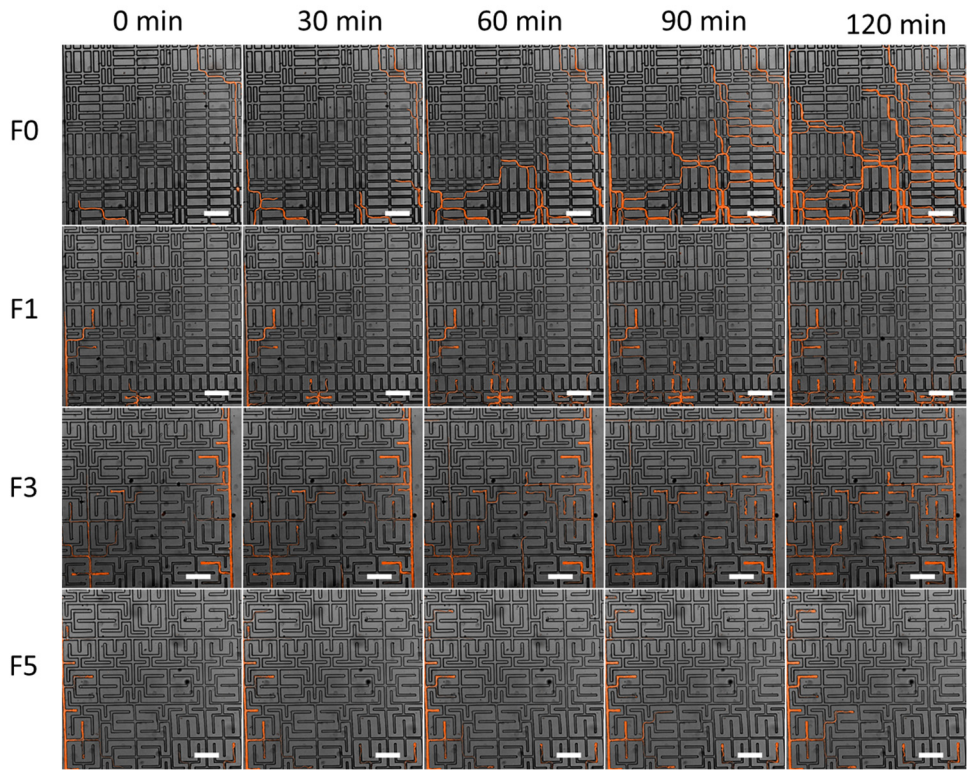

Figure 4. Time-lapses of fungal hyphae of *Coprinopsis cinerea* expressing d-tomato constitutively growing in the studied mazes. The images along the x axis have a time step of 30 minutes. The scale bars are 100 µm). The full time-lapses can be seen in Supplementary video 5 – 8.

The effect of maze structures on fungal biomass when growing together with the bacteria followed the same trend as when fungi grew alone, though overall fungal biomass was 88 % reduced. Fungal biomass decreased as complexity of the mazes increased, which can be seen especially when comparing the simplest maze (F0) with the most complex one (F5). Fungal biomass fluorescence reached its maximum on day 4 in the simplest mazes (F0 and F1), whereas on day 6 in F3 and F5; one day earlier compared to growth without competitor. Spatial analysis of the fungal biomass distribution within the mazes indicates a similar pattern as in absence of bacteria. Fungal biomass was homogeneously distributed for F0 and F1, whereas it decreases in F3 and F5 as accessibility decreases. These results suggest that, regardless of that bacteria grow faster than fungi and can thus colonize a habitat faster (Varma *et al.* 2008), we find no indications of a spatial priority effect in the spatial habitat as the fungus grows in similar patterns in the presence or absence of bacteria, confirmed by the high magnification time-lapse images on hyphal exploration patterns. There is apparently a competitive replacement in the higher accessible niches where fungi take over, while bacteria are displaced to the more

hidden spaces where they can grow undisturbed. Hence, the only impact that bacterial competitors seem to have on the hyphal exploration of the mazes is the magnitude and the speed at which it happens, which could be attributed to the decrease in nutrients along the channels due to bacterial growth.

The pattern of substrate consumption did not change when both organisms grew together in comparison to when bacteria was cultivated alone; however, less bacterial biomass developed, leading to an increased ratio of substrate degradation per bacterial biomass. Substrate consumption patterns showed a larger temporal variation across the maze types, as in the low order mazes it peaked later (day 3) than when bacteria grew alone (day 1), while it peaked earlier in high order mazes reached (day 3 and 2 for F3 and F5 respectively (Figure 2). Spatial analysis within mazes revealed a similar pattern of substrate consumption as when bacteria were cultivated without competitor, where substrate consumption increased with decreasing accessibility. The patterns of substrate consumption within the mazes in F5 reflected the pattern of the corresponding bacterial biomass distribution (Figure 3).

It is important to note that habitat complexity did reduce fungal growth, which means that fungal substrate consumption is likely reduced as well. This should, however, be tested in future experimentation for confirmation. For this purpose, a substrate that can only be targeted by fungi should be used, e.g. a substrate that demands enzymes produced by fungi only. This could show the effect of structure on the fate of nutrients acquired by fungi, leading to the idea that nutrient fate depends on where it is located in the soil matrix and what type of organism that can access it, spatially and metabolically. Our study points out the importance of studying multiple actors in an ecosystem simultaneously because feedback mechanisms may change or even reverse patterns, such as when the fungal growth changes the physical characteristics of the mazes, which also should be prioritized in future studies.

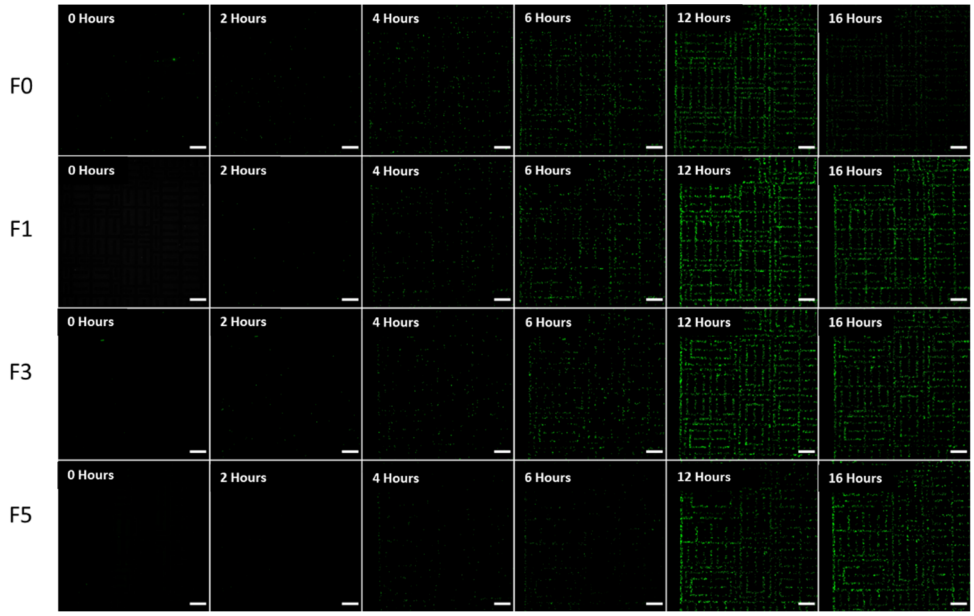

Figure 5. Time-lapses of the bacterial strain *Pseudomonas putida* expressing GFP constitutively growing in the studied mazes. The scale bars are 100 µm. The full time-lapses can be seen in Supplementary videos 1-4.

Earlier experiments in elongated channel-shaped pore spaces in microfluidic devices showed that also bacterial biomass and substrate degradation decreased with increasing spatial complexity. In that case, complexity was defined by the deviation from straight passage in increasingly sharper angles (Arellano *et al.* 202Xa under review). In contrast, the present study considers spatial complexity as an increase in fractal order of a maze like pore space, which is correlated to the connectivity of the space within it(decreasing with increasing fractal order), and to the length of individual channels and the number of dead ends (increasing with increasing fractal order). The angled channels require an increased amount of energy to move through increasingly sharper turns, as they require more turns for bacteria to find their way and, on the other hand, lead to increased branching for fungi. However, the angled channels likely do not differentially affect the level of interactions between individuals in a high degree, but the mazes with decreasing connectivity and increasing number of dead ends do, which could explain the different outcome of this study compared to Arellano et al. 202Xa. This isolating effect is even enhanced under fungal presence when hyphae take up and clog parts of the maze and, by this, decrease connectivity, where we in parallel see an increased substrate degradation efficiency.

These findings suggest confined microhabitats, like soil aggregates or gut microenvironments, increase enzymatic degradation efficiency of microbial communities that inhabit them. Other functions that might be affected by

confinement, such as resistance to disturbances, still need to be explored in future experiments. It is important to consider that microbes themselves also influence the spatial characteristics of microhabitats by occupying initially free spaces thus influencing long-term nutrient cycling by depositing new necromass at certain spatial locations. However, many more factors like air phases, differential chemical conditions and more complex biotic interactions will also influence these processes, and more research is needed to elucidate this.

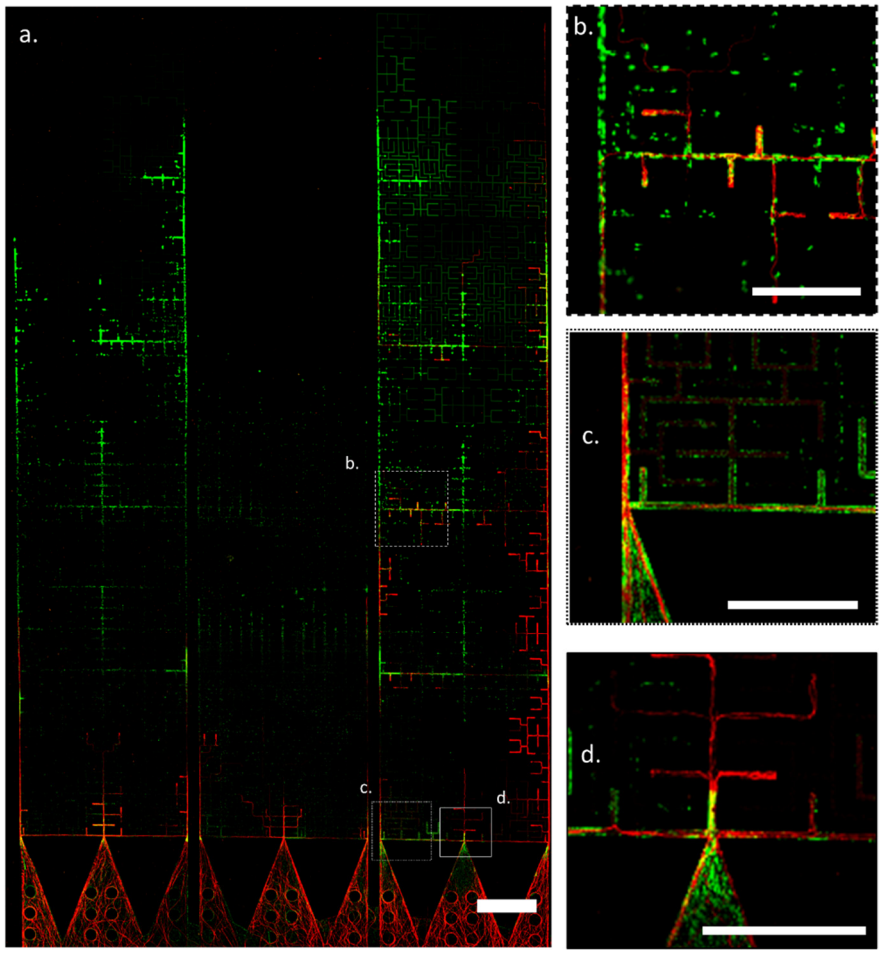

Figure 6. Example of mazes colonized by the fungal strain *Coprinopsis cinerea* (red) and the bacterial strain *Pseudomonas putida* (green), 24 hours after inoculation (a). Dead-ends being colonized alternatively by fungi or bacteria (b). Dead ends colonized mainly by bacteria (c). Dead-ends colonized mainly by fungi (d). The scale bar in a.is 500 µm, and in b. c. and d. is 250 µm.

Conclusion

Our initial hypothesis was that an increase in habitat physical complexity would lead to a reduction in bacterial and fungal biomass, along with a reduction in bacterial enzymatic activity, in line with what has earlier been seen in turning channels (Arellano et. Al. 202xa, submitted). However, our results showed that bacteria were positively affected by structures, increasing their biomass and their enzymatic activity as habitat complexity increased – at least until a certain level of spatial complexity. Fungi, on the other hand, followed the hypothesis and grew less as habitat complexity increased. Even though our study omits major parameters of natural microenvironments, such as gas-liquid interphases, pH and nutrient gradients, and a significantly higher diversity of microorganisms, we found a clear tendency of how the spatial complexity influences bacterial and fungal growth. Knowing the spatial distribution of the different microbial communities helps us better understand their ecological role in natural environments, from soil, to gut, sediments, and biofilms. The way microbes behave in nature depends strongly on the physical and chemical environment that surrounds them, but it can be methodologically challenging to study every aspect of their environment in isolation. Using microfluidic devices where we can control various physical parameters can teach us the way microbial communities grow, adapt, and interact in environments previously difficult to mimic.

References

Aleklett, K., Kiers, E.T., Ohlsson, P., Shimizu, T.S., Caldas, V.E. & Hammer, E.C. (2018). Build your own soil: Exploring microfluidics to create microbial habitat structures. *ISME J.*

Aleklett, K., Ohlsson, P., Bengtsson, M. & Hammer, E.C. (n.d.). Fungal foraging behaviour and hyphal space exploration in micro-structured Soil Chips. *ISME J.*, 1–12.

Arevalo-Ferro, C., Reil, G., Görg, A., Eberl, L. & Riedel, K. (2005). Biofilm formation of Pseudomonas putida IsoF: The role of quorum sensing as assessed by proteomics. *Syst. Appl. Microbiol.*, 28, 87–114.

Asenova, E., Lin, H.Y., Fu, E., Nicolau, D. V. & Nicolau, D. V. (2016). Optimal fungal space searching algorithms. *IEEE Trans. Nanobioscience*, 15, 613–618.

Baker, M.D., Wolanin, P.M. & Stock, J.B. (2006). Signal transduction in bacterial chemotaxis. *BioEssays*, 28, 9–22.

Ballhausen, M.B., Van Veen, J.A., Hundscheid, M.P.J. & De Boer, W. (2015). Methods for baiting and enriching fungus-feeding (Mycophagous) rhizosphere bacteria. *Front. Microbiol.*, 6, 1–11.

Banitz, T., Fetzer, I., Johst, K., Wick, L.Y., Harms, H. & Frank, K. (2011). Assessing biodegradation benefits from dispersal networks. *Ecol. Modell.*, 222, 2552–2560.

Breugelmans, P., Barken, K.B., Tolker-Nielsen, T., Hofkens, J., Dejonghe, W. & Springael, D. (2008). Architecture and spatial organization in a triple-species bacterial biofilm synergistically degrading the phenylurea herbicide linuron. *FEMS Microbiol. Ecol.*, 64, 271–282.

Burns, C., Gregory, K.E., Kirby, M., Cheung, M.K., Riquelme, M., Elliott, T.J., *et al.* (2005). Efficient GFP expression in the mushrooms Agaricus bisporus and Coprinus cinereus requires introns. *Fungal Genet. Biol.*

Carrias, J.F. & Sime-Ngando, T. (2009). Bacteria, Attached to Surfaces. In: *Encyclopedia of Inland Waters*.

Chu, E.K., Kilic, O., Cho, H., Groisman, A. & Levchenko, A. (2018). Self-induced mechanical stress can trigger biofilm formation in uropathogenic Escherichia coli. *Nat. Commun.*, 9.

Chung, K.K., Schumacher, J.F., Sampson, E.M., Burne, R.A., Antonelli, P.J. & Brennan, A.B. (2007). Impact of engineered surface microtopography on biofilm formation of Staphylococcus aureus . *Biointerphases*, 2, 89–94.

Donaldson, G.P., Lee, S.M. & Mazmanian, S.K. (2015). Gut biogeography of the bacterial microbiota. *Nat. Rev. Microbiol.*

Duffy, K.J. & Ford, R.M. (1997). Turn angle and run time distributions characterize swimming behavior for Pseudomonas putida. *J. Bacteriol.*, 179, 1428–1430.

Dunn, O.J. (1961). Multiple Comparisons Among Means. *J. Am. Stat. Assoc.*

Essig, A., Hofmann, D., Münch, D., Gayathri, S., Künzler, M., Kallio, P.T., *et al.* (2014). Copsin, a novel peptide-based fungal antibiotic interfering with the peptidoglycan synthesis. *J. Biol. Chem.*, 289, 34953–34964.

Falconer, R.E., Battaia, G., Schmidt, S., Baveye, P., Chenu, C. & Otten, W. (2015). Microscale Heterogeneity Explains Experimental Variability and Non-Linearity in Soil Organic Matter Mineralisation. *PLoS One*, 10, e0123774.

Flemming, H.C., Wingender, J., Szewzyk, U., Steinberg, P., Rice, S.A. & Kjelleberg, S. (2016). Biofilms: An emergent form of bacterial life. *Nat. Rev. Microbiol.*, 14, 563–575.

Furuno, S., Päzolt, K., Rabe, K., Neu, T.R., Harms, H. & Wick, L.Y. (2010). Fungal mycelia allow chemotactic dispersal of polycyclic aromatic hydrocarbon-degrading bacteria in water-unsaturated systems. *Environ. Microbiol.*, 12, 1391–1398.

Grice, E.A. & Segre, J.A. (2011). The skin microbiome. *Nat. Rev. Microbiol.*

Gu, H., Chen, A., Song, X., Brasch, M.E., Henderson, J.H. & Ren, D. (2016). How Escherichia coli lands and forms cell clusters on a surface: A new role of surface topography. *Sci. Rep.*

Güll, I., Alves, P.M., Gabor, F. & Wirth, M. (2009). Viability of the human adenocarcinoma cell line Caco-2: Influence of cryoprotectant, freezing rate, and storage temperature. *Sci. Pharm.*

Hanson, K.L., Nicolau, D. V., Filipponi, L., Wang, L., Lee, A.P. & Nicolau, D. V. (2006). Fungi use efficient algorithms for the exploration of microfluidic networks. *Small*, 2, 1212–1220.

Hilbert, D. & Hilbert, D. (1935). Über die stetige Abbildung einer Linie auf ein Flächenstück. *Dritter Band Anal. · Grundlagen der Math. · Phys. Verschied.*, 1–2.

Hobbie, J.E. & Hobbie, E.A. (2013). Microbes in nature are limited by carbon and energy: The starving-survival lifestyle in soil and consequences for estimating microbial rates. *Front. Microbiol.*, 4, 1–11.

Hochbaum, A.I. & Aizenberg, J. (2010). Bacteria pattern spontaneously on periodic nanostructure arrays. *Nano Lett.*, 10, 3717–3721.

Hol, F.J.H. & Dekker, C. (2014). Zooming in to see the bigger picture: Microfluidic and nanofabrication tools to study bacteria. *Science (80-.).*, 346.

Hol, F.J.H., Rotem, O., Jurkevitch, E., Dekker, C. & Koster, D.A. (2016). Bacterial Predator–prey dynamics in microscale patchy landscapes. *Proc. R. Soc. B Biol. Sci.*

Holm, S. (1979). A simple sequentially rejective multiple test procedure. *Scand. J. Stat.*

Hou, S., Gu, H., Smith, C. & Ren, D. (2011). Microtopographic patterns affect escherichia coli biofilm formation on poly(dimethylsiloxane) surfaces. *Langmuir*, 27, 2686–2691.

Hyun, J.K., Boedicker, J.Q., Jang, W.C. & Ismagilov, R.F. (2008). Defined spatial structure stabilizes a synthetic multispecies bacterial community. *Proc. Natl. Acad. Sci. U. S. A.*

Kaiser, C., Franklin, O., Richter, A. & Dieckmann, U. (2015). Social dynamics within decomposer communities lead to nitrogen retention and organic matter build-up in soils. *Nat. Commun.*

Keymer, J.E., Galajda, P., Muldoon, C., Park, S. & Austin, R.H. (2006). Bacterial metapopulations in nanofabricated landscapes. *Proc. Natl. Acad. Sci. U. S. A.*, 103, 17290–17295.

Kneen, M.A. & Annegarn, H.J. (1996). Algorithm for fitting XRF, SEM and PIXE X-ray spectra backgrounds. *Nucl. Instruments Methods Phys. Res. Sect. B Beam Interact. with Mater. Atoms*.

Kohlmeier, S., Smits, T.H.M., Ford, R.M., Keel, C., Harms, H. & Wick, L.Y. (2005). Taking the fungal highway: Mobilization of pollutant-degrading bacteria by fungi. *Environ. Sci. Technol.*, 39, 4640–4646.

Kravchenko, A., Falconer, R.E., Grinev, D. & Otten, W. (2011). Fungal colonization in soils with different management histories: Modeling growth in three-dimensional pore volumes. *Ecol. Appl.*, 21, 1202–1210.

Lehmann, J. & Kleber, M. (2015). The contentious nature of soil organic matter. *Nature*.

Lew, R.R. (2011). How does a hypha grow? the biophysics of pressurized growth in fungi. *Nat. Rev. Microbiol.*, 9, 509–518.

Long, Z., Quaife, B., Salman, H. & Oltvai, Z.N. (2017). Cell-cell communication enhances bacterial chemotaxis toward external attractants, 1–12.

Mcdonald, J.C., Duffy, D.C., Anderson, J.R. & Chiu, D.T. (2000). Review General Fabrication of microfluidic systems in poly (dimethylsiloxane). *Electrophoresis*, 21, 27–40.

Miller, M.B. & Bassler, B.L. (2001). Ensing in.

Mitik-Dineva, N., Wang, J., Mocanasu, R.C., Stoddart, P.R., Crawford, R.J. & Ivanova, E.P. (2008). Impact of nano-topography on bacterial attachment. *Biotechnol. J.*, 3, 536–544.

Multiphysics, C. & Multiphysics, C. (2020). COMSOL Multiphysics ® v.5.5. *COMSOL Multiphysics ® 5.5*.

Nadell, C.D., Ricaurte, D., Yan, J., Drescher, K. & Bassler, B.L. (2017). Flow environment and matrix structure interact to determine spatial competition in Pseudomonas aeruginosa biofilms. *Elife*.

Nejman, D., Livyatan, I., Fuks, G., Gavert, N., Zwang, Y., Geller, L.T., *et al.* (2020). The human tumor microbiome is composed of tumor type-specific intracellular bacteria. *Science (80-.).*

Nicodème, M., Grill, J.P., Humbert, G. & Gaillard, J.L. (2005). Extracellular protease activity of different Pseudomonas strains: Dependence of proteolytic activity on culture conditions. *J. Appl. Microbiol.*

Nottingham, A.T., Bååth, E., Reischke, S., Salinas, N. & Meir, P. (2019). Adaptation of soil microbial growth to temperature: Using a tropical elevation gradient to predict future changes. *Glob. Chang. Biol.*, 25, 827–838.

Or, D., Smets, B.F., Wraith, J.M., Dechesne, A. & Friedman, S.P. (2007). Physical constraints affecting bacterial habitats and activity in unsaturated porous media - a review. *Adv. Water Resour.*

Pande, S., Kaftan, F., Lang, S., Svato, A., Germerodt, S. & Kost, C. (2016). Privatization of cooperative benefits stabilizes mutualistic cross-feeding interactions in spatially structured environments. *ISME J.*, 10, 1413–1423.

Park, S. (2003). Motion to Form a Quorum. *Science (80-.).*, 301, 188–188.

Park, S., Wolanin, P.M., Yuzbashyan, E. a, Lin, H., Darnton, N.C., Stock, J.B., *et al.* (2003). Influence of topology on bacterial social interaction. *Proc. Natl. Acad. Sci. U. S. A.*, 100, 13910–13915.

Rabbi, S.M.F., Daniel, H., Lockwood, P. V., Macdonald, C., Pereg, L., Tighe, M., *et al.* (2016). Physical soil architectural traits are functionally linked to carbon decomposition and bacterial diversity. *Sci. Rep.*

Rath, K.M., Fierer, N., Murphy, D. V. & Rousk, J. (2019). Linking bacterial community composition to soil salinity along environmental gradients. *ISME J.*, 13, 836–846.

Razavi, B.S., Zhang, X., Bilyera, N., Guber, A. & Zarebanadkouki, M. (2019). Soil zymography: Simple and reliable? Review of current knowledge and optimization of the method. *Rhizosphere*, 11, 100161.

Rousk, J., Bååth, E., Brookes, P.C., Lauber, C.L., Lozupone, C., Caporaso, J.G., *et al.* (2010). Soil bacterial and fungal communities across a pH gradient in an arable soil. *ISME J.*

Saragosti, J., Calvez, V., Bournaveas, N., Perthame, B., Buguin, A. & Silberzan, P. (2011). Directional persistence of chemotactic bacteria in a traveling concentration wave. *Proc. Natl. Acad. Sci.*

Schindelin, J., Arganda-Carreras, I., Frise, E., Kaynig, V., Longair, M., Pietzsch, T., *et al.* (2012). Fiji: An open-source platform for biological-image analysis. *Nat. Methods*.

Schmidt, M.W.I., Torn, M.S., Abiven, S., Dittmar, T., Guggenberger, G., Janssens, I.A., *et al.* (2011). Persistence of soil organic matter as an ecosystem property. *Nature*.

Smith, M.C.M. (1991). Molecular biological methods for bacillus. *FEBS Lett.*

Stanley, C.E., Stöckli, M., Van Swaay, D., Sabotič, J., Kallio, P.T., Künzler, M., *et al.* (2014). Probing bacterial-fungal interactions at the single cell level. *Integr. Biol. (United Kingdom)*.

Tayagui, A., Sun, Y., Collings, D.A., Garrill, A. & Nock, V. (2017). An elastomeric micropillar platform for the study of protrusive forces in hyphal invasion. *Lab Chip*, 17, 3643–3653.

Team, R.C. (2019). R: A Language and Environment for Statistical Computing. *Vienna, Austria*.

Varma, A., Abbott, L., Werner, D. & Hampp, R. (2008). *Plant surface microbiology*. *Plant Surf. Microbiol.*

Yawata, Y., Cordero, O.X., Menolascina, F., Hehemann, J.H., Polz, M.F. & Stocker, R. (2014). Competition-dispersal tradeoff ecologically differentiates recently speciated marine bacterioplankton populations. *Proc. Natl. Acad. Sci. U. S. A.*

Supplementary material

Supplementary Table 1. Output of the multi-level model fitting for the variable mean fluorescence intensity of bacterial biomass measured via their GFP fluorescence, with device as random effect and fractal order and competition as fixed factors. Each step performs an ANOVA and compares the model with the previous model.

	Model	df	AIC	BIC	Log Lik	Test	L. Ratio	p-value
Baseline	1	3	2483.075	2493.310	-1238.537			
Fractal	2	6	2459.390	2479.860	-1223.695	1 vs 2	29.68515	<.0001
+ Organism	3	7	2431.675	2455.557	-1208.838	2 vs 3	29.71454	<.0001
+ Fractal*Organism	4	10	2423.213	2457.330	-1201.607	3 vs 4	14.46195	0.0023

Supplementary Table 2. Contrasts of the multi-level model with the variable mean bacterial biomass meassured with GFP fluorescence, with device as random effect and fractal orderd and organism as fixed factors.

	Value	Std.Error	DF	t-value	p-value
(Intercept)	329.0508	10.70607	210	30.734984	0.0000
F1 - F0	18.9404	13.93379	210	1.359311	0.1755
F4 - F0	61.5117	13.93379	210	4.414569	0.0000
F5 - F0	60.5800	13.93379	210	4.347707	0.0000
FB - B	-125.0832	15.14067	6	-8.261404	0.0002
F1 – F0: FB – B	-41.5140	19.70536	210	-2.106738	0.0363
F4 – F0: FB – B	-73.4469	19.70536	210	-3.727257	0.0002
F5 -F0: FB - B	-27.5075	19.70536	210	-1.395939	0.1642

Supplementary Table 3. Output of the comparisson of means bacterial biomass fluorescence values between groups using tukey method for comparing a family of 8 estimates.

contrast	estimate	SE	df	t.ratio	p.value
F0 B – F1 B	-18.940	13.9	210	-1.359	0.8744
F0 B – F4 B	-61.512	13.9	210	-4.415	0.0004
F0 B – F5 B	-60.580	13.9	210	-4.348	0.0006
F0 B – F0 FB	125.083	15.1	6	8.261	0.0020
F0 B – F1 FB	147.657	15.1	6	9.752	0.0008
F0 B – F4 FB	137.018	15.1	6	9.050	0.0012
F0 B – F5FB	92.011	15.1	6	6.077	0.0101
F1 B – F4 B	-42.571	13.9	210	-3.055	0.0509
F1 B – F5 B	-41.640	13.9	210	-2.988	0.0613
F1 B – F0 FB	144.024	15.1	6	9.512	0.0009
F1 B – F1 FB	166.597	15.1	6	11.003	0.0004
F1 B – F4 FB	155.959	15.1	6	10.301	0.0006
F1 B – F5 FB	110.951	15.1	6	7.328	0.0038
F4 B – F5 B	0.932	13.9	210	0.067	1.0000
F4 B – F0 FB	186.595	15.1	6	12.324	0.0002
F4 B – F1 FB	209.169	15.1	6	13.815	0.0001
F4 B – F4 FB	198.530	15.1	6	13.112	0.0002
F4 B – F5 FB	153.522	15.1	6	10.140	0.0006
F5 B – F0 FB	185.663	15.1	6	12.263	0.0002
F5 B – F1 FB	208.237	15.1	6	13.753	0.0001
F5 B – F4 FB	197.598	15.1	6	13.051	0.0002
F5 B – F5 FB	152.591	15.1	6	10.078	0.0007
F0 FB – F1 FB	22.574	13.9	210	1.620	0.7377
F0 FB – F4 FB	11.935	13.9	210	0.857	0.9894
F0 FB – F5 FB	-33.073	13.9	210	-2.374	0.2599
F1 FB – F4 FB	-10.638	13.9	210	-0.763	0.9947
F1 FB – F5 FB	-55.646	13.9	210	-3.994	0.0023
F4 FB – F5 FB	-45.008	13.9	210	-3.230	0.0306

Supplementary Table 4. Output of the multi-level model fitting for the variable mean fluorescence intensity of fungal biomass measured via their d-tomato fluorescence, with device as random effect and fractal order and competition as fixed factors. Each step performs an ANOVA and compares the model with the previous model.

	Model	df	AIC	BIC	logLik	Test	L.Ratio	p-value
Baseline	1	3	3026.371	3036.606	-1510.185			
Fractal	2	6	2928.914	2949.383	-1458.457	1vs2	103.4572	<.0001
+ Organism	3	7	2925.083	2948.965	-1455.542	2vs3	5.8304	0.0158
+ Fractal*Organism	4	10	2885.519	2919.635	-1432.759	3vs4	45.5641	<.0001

Supplementary Table 5. Contrasts of the multi-level model with the variable mean fungal biomass meassured with d-tomato fluorescence, with device as random effect and fractal orderd and organism as fixed factors.

	Value	Std.Error	DF	t-value	p-value
(Intercept)	870.4249	83.04410	210	10.481478	0.0000
F1-F0	-153.6034	37.01624	210	-4.149622	0.0000
F4-F0	-387.3626	37.01624	210	-10.464666	0.0000
F5-F0	-449.9701	37.01624	210	-12.156019	0.0000
FB-B	-494.2171	117.44209	6	-4.208177	0.0056
F1-F0: FB-B	87.7975	52.34886	210	1.677162	0.0950
F4-F0: FB-B	281.4306	52.34886	210	5.376060	0.0000
F5-F0: FB-B	307.6641	52.34886	210	5.877188	0.0000

Supplementary Table 6. Output of the multi-level model fitting for the variable mean fluorescence intensity of substrate degradation measured methyl coumarin fluorescence, with device as random effect and fractal order and competition as fixed factors. Each step performs an ANOVA and compares the model with the previous model.

	Model	df	AIC	BIC	logLik	Test	L.Ratio	pvalue
Baseline	1	3	4965.749	4977.201	-2479.875			
Fractal	2	6	4760.940	4783.843	-2374.470	1vs2	210.80929	<.0001
+ Organism	3	8	4734.558	4765.095	-2359.279	2vs3	30.38171	<.0001
+ Fractal*Org	4	14	4541.202	4594.642	- 2256.601	3vs4	205.35613	<.0001

Supplementary Table 7. Contrasts of the multi-level model with the variable mean substrate degradation meassured with methyl coumarin fluorescence intensity, with device as random effect and fractal orderd and organism as fixed factors.

	Value	Std.Error	DF	t-value	p-value
(Intercept)	447.5790	58.55928	315	7.643178	0.0000
F1 – F0	127.8715	52.51934	315	2.434751	0.0155
F4 – F0	576.4132	52.51934	315	10.975255	0.0000
F5 – F0	939.6686	52.51934	315	17.891859	0.0000
F – B	-311.1678	82.81533	9	-3.757369	0.0045
FB – B	-102.2334	82.81533	9	-1.234474	0.2483
F1 – F0: F – B	-138.0124	74.27356	315	-1.858163	0.0641
F4 – F0: F – B	-590.6654	74.27356	315	-7.952565	0.0000
F5 – F0: F – B	-947.1576	74.27356	315	-12.752284	0.0000
F1 – F0: FB – B	60.0165	74.27356	315	0.808046	0.4197
F4 – F0: FB – B	-16.8869	74.27356	315	-0.227360	0.8203
F5 – F0: FB – B	46.6460	74.27356	315	0.628029	0.5304

Paper IV

Microhabitat heterogeneity promotes substrate degradation by soil microbial community

Authors:

Carlos Arellano Caicedo[1,*]

Pelle Ohlsson[2]

Saleh Moradi[1]

Edith C. Hammer[1,4]

Afiliations:

[1.] Department of Biology, Lund University, Lund, Sweden

[2.] Department of Biomedical Engineering, Lund University, Sweden

[3.] Division of Solid State Physics, Lund University, Sweden

[4.] Centre for Environmental and Climate Science, CEC, Lund University, Sweden

*Corresponding author. E-mail address: carlos.arellano@biol.lu.se

Key words:

microhabitat, soil bacteria, organic matter stabilization, soil pore space, physical carbon stabilization, organic matter occlusion, microfluidics, micromodel.

Abstract

Soil pore space, considered the most complex biomaterial that exists, generates such a heterogeneous environment, that gives rise to a wide variety of properties, such as microbial diversity and carbon storage. Soils contain, at the same time, the largest carbon reservoir on earth, and an immense amount of nutrient limited microbial biomass. The reason why this carbon is not consumed by soil microbes is attributed to the heterogeneous nature of soil, which forms a labyrinth were carbon and microbes cannot be in direct contact. In the present study, by using microfluidics, we tested the effect of labyrinth-like structures of increasing complexity on the decomposing activity of soil microbial communities from a soil inoculum. The two parameters used to study the effect of microhabitat complexity were either the turning angle in an array of channel-like pore structures, or the fractal order in an array of maze-like pore structures. We found that in both cases, channels and mazes, an increased complexity produced a higher substrate degradation. When we analysed the degradation within the structures, we found that the majority of the activity is concentrated in the middle region of the structures. We think that the increased in degradation activity in complex mazes might be due to the reduced interactions within the microbial communities which leads to a reduction in competition. Lowered competition allows different communities with a wide range of metabolic strategies to co-habit in the structures, which resulted in a bulk increase of the substrate degradation.

Introduction

Heterogeneous habitats are responsible of the wide diversity of microbes in ecosystems (Whitman et al. 1998), ranging from marine ecosystems (Armeli Minicante et al. 2019), sea floors (Zeppilli et al. 2016), and gut microbiota (Lu et al. 2014) to the big array of microhabitats that are formed within soils (Crawford et al. 2005). In soils, a spatiotemporal fluctuating habitat gives rise to a patchy nutrient distribution, a fragmented aqueous interface, and a barrier to cells and molecules dispersion, which affect the distribution, functions, and diversity of microorganisms (Raynaud & Nunan 2014). This gives the soil emergent properties (Baveye et al. 2018), such as hosting a wide diversity of microorganisms in the bulk soil (Bach et al. 2018) cohabiting aggregates that may act as independent evolutionary incubators (Rillig et al. 2017). One of the most relevant emergent characteristics that arise from the unique nature of the soil pore space is its capacity to retain large amounts of carbon buried within its structure (IPCC 2007). The preservation of this carbon underground can last from minutes to decades, and it occurs even though soil microbial biomass is found in a constant state of starvation (Hobbie & Hobbie 2013). A tentative explanation to this paradox is that due to the physical complexity of the soil pore space, microbial decomposers, and their potential substrate, are not co-located in space and time and carbon consumption occurs only at short and specific times and locations (Kuzyakov & Blagodatskaya 2015).

To explore the way microhabitat characteristics, affect soil microorganisms, several approaches have been adopted, which range from studying intact soil aggregates to a simulation of the pore space in artificial microsystems. The study of intact soil structure is mainly conducted with help of microcomputed X-ray tomography, which registers the inner spatial properties of aggregates, revealing a maze-like matrix where microbial processes take place (Voltolini et al. 2017). From the images obtained, information such as distribution of air pockets, water interface, and particulate organic matter, can be derived. It have been detected that organic matter turn-over was linked to the connectivity and accessibility of the pores to the external part of the aggregate (Kravchenko et al. 2015), that there are correlations between pore size distribution and organic matter loss (Ananyeva *et al.* 2013; Toosi *et al.* 2017), and a link between the pore characteristics and the phylogenetic composition of microbial communities that they contain (Negassa et al. 2015). Limitations of this technique, nonetheless, arise when trying to have a controllable micro-environmental conditions, real time measurements of microbial communities, undisturbed sampling, and micrometre scale resolution (Rabot et al. 2018), which constrains the testable hypotheses.

The intrinsic characteristics of soil that limit an in-depth study of its nature can, however, be simulated using artificial models that mimic the inner pore space in a controlled way. An important approach is the use of microfluidics, which is defined as the manipulation of structures and fluids at the micro and nano scale (Beebe et

al. 2002), to test ecological questions. The use of microfluidics for microbial ecology has revealed mechanisms of chemotaxis (Mao et al. 2003; Ahmed & Stocker 2008; Ahmed et al. 2010; Saragosti et al. 2011), bacterial motility (Ahmed & Stocker 2008), effects of EPS in the resistance of pore spaces to drought (Deng et al. 2015), and the way fungi and bacteria interact at the cellular level (Stanley et al. 2014).

Previous microfluidic studies, focused on the influence of pore space physical parameters on microbial growth and their nutrient degradation, showed that fungi and bacteria are affected in different ways by turning angles in microchannels (Arellano-Caicedo et al. 202Xa, under review), and by the connectivity and fractal order of a pore space maze (Arellano-Caicedo et al._ 202Xb, submitted). The turning angle characteristics in long, non-connected microchannels increasingly deviating from straight passage reduced bacterial and fungal growth, as well as substrate degradation inside the channels. In contrast, when testing microhabitats of different fractal order in space-filling fractal mazes, fungal biomass was reduced, while bacterial biomass and substrate degradation increased as fractal order increased. The spatial patterns of substrate degradation inside the highest-order fractals indicated that the highest enzymatic activity occurred in regions of intermediate depth into the mazes, while in the deepest regions (i.e. the least connected, longest paths into the maze) enzymatic activity decreased again. This indicated that the different parameters defining spatial complexity, in the case of these two studies: channel turning angle, and maze fractal order, dissimilarly affect the microbial growth and substrate degradation.

These previous experiments (Arellano-Caicedo et. al 202Xa; b) were performed with the laboratory bacterial strain *Pseudomonas putida* and the fungal strain *Coprinopsis cinerea* under sterile laboratory conditions. It remained open whether these patterns would be generally true and thus similar in other microbial strains, or in a whole microbial community as from a natural inoculum. For this purpose, we aimed at testing the effect of these pore space physical parameters (turning angle and turning order in microchannels, and fractal order of a maze) on the microbial substrate degradation of a microbial inoculum extracted from a soil sample. With this approach we wanted to evaluate if (1) channel complexity would reduce substrate degradation as shown in Arellano-Caicedo et. al 202Xa, while (2) maze complexity would increase it (Arellano-Caicedo et al 202Xb). We also wanted to test (3) if the spatial pattern of nutrient degradation occurs in a way that it is higher at intermediate confined regions of the channels and mazes, while it is lower at their entrances, which was found in both studies.

Materials and Methods

Device design

The design of the microfluidic devices that we have named Channel device and Fractal device were made in AutoCad 2019 (Autodesk) and they consist of an experimental area with six and four treatments respectively, and a pillar system that served as entrance. The pillar system is formed by pillars of 100 micrometres in diameter, separated by 100 micrometres, which soil microbes to penetrate the full width of the device before entering the treatment areas.

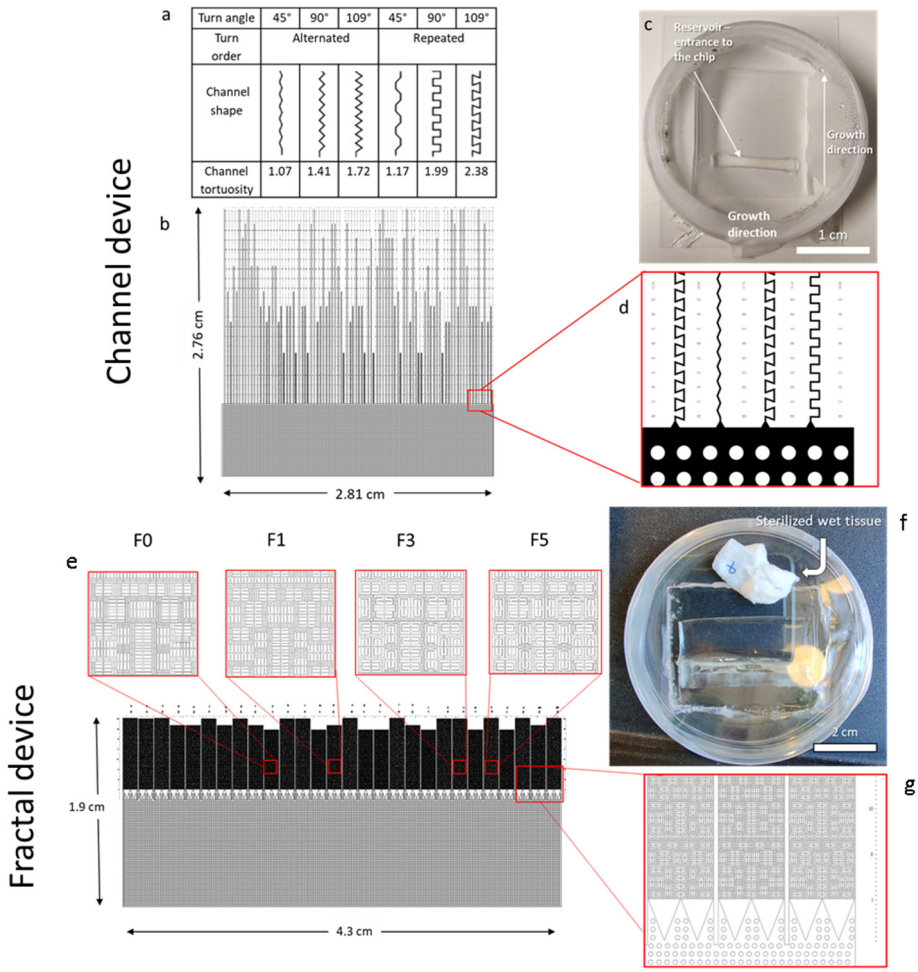

Figure 1 The two microfluidic devices used in the experiment containing different channels (a-d) and mazes (e-h) (Arellano-Caicedo 202X a; b). The channel device consists of channels with 6 different conditions: 3 angles (45°, 90°, and 109°) with two turning orders (alternated, repeated), which resulted in channels with different tortuosities (ratio between arc-chord ratio and the distance between the two ends of the channels). A pillar system connecting to the channels serves as inoculum area (a). The channel device contained 10 internal replicates of each treatment, with a

normalized volume, which were distributed randomly along the pillar system (b). The channel device was sterilized and bonded to a glass bottom Petri dish that contained a sterile wet tissue to prevent humidity losses during the experiment. A hole cut into the pillar system area served to enter the inoculum. (c). Detailed view of the entries with funnel-shaped connectors to different channels (d). The fractal device contained four different mazes of four fractal orders: 0, 1, 3, and 5, which were named respectively (F0, F1, F3, and F5). Five maze modules of each fractal order type of the size corresponding to the smallest entity of F5 (as shown in e red squares) are stacked to blocks that only internally connect to the pillar system. Seven replicate blocks of each maze type, with a normalized internal pore space volume, were randomly located along a pillar system (h). Once molded in PDMS and sterilized, the channel device was bonded to a glass bottom Petri dish that contained a sterile wet tissue to prevent humidity losses during the experiment, with an inoculation reservoir cut into the pillar system (f). Detailed view of the entries to the mazes with funnel-shaped connectors. Each maze block is accessible via three points from the pillar system, and internally connect to the following four maze modules, while a wall separates each block (g).

The Channel device consists of dead-end channels of six different geometries (n=10) with the same internal volume. The channels were randomly distributed in parallel orientation along the device. The parameters assigned to the channels were "Angle" and "Turn order". The angles used were 45˚, 90˚, and 109˚, measured as the deviation from a continued straight line and thus the turning angle an organism in this channel needs to perform (Figure 1). These angles were selected so that they could represent obtuse, right, and acute angles. Channels of each angle had two types of arrangements, one with an alternated turn order, and one with a repeated turn order. Channel types with alternated turn order followed a pattern of alternating right and left bends, while channels with repeated turn order followed a pattern of two right turns followed by two left turns. The channels dimensions were adjusted so that every type of channel would contain the same volume (2.42 nL) with a width of 10 µm and a height of 12 µm. Each channel segment was 50 µm long before the next turn. The tortuosity of the channels was is indicated in figure 1.

The Fractal device consists of an array of dead-end mazes constructed based on the space filling Hilbert curve (Hilbert & Hilbert 1935). Four orders of the Hilbert curve were chosen for the experiments: zero, one, three and five (Fig 1), with a normalized internal volume. The width of the channels within the labyrinths was 10 µm, and the height 12 µm. The labyrinths were randomly distributed along the device (n=7).

Device fabrication

The fabrication of the microfluidic devices was done according to previously described workflows (Aleklett *et al.* 2018). The photomask was made of soda lime glass covered with a thin layer of chromium (Nanofilm, CA, USA). The designed patterns were printed with a dwl66+ mask writer (Heidelberg Instruments, Germany). A NdYag laser, 532 nm, was used to print the patterns on a photoresist, AZ1500. The patterns were subsequently developed in AZ 351B positive developer and the chromium etched in TechniEtchCr01 (Microchemicals GmbH, Ulm Germany). For the masters fabrication, SU-8 2015 (MicroChem, Newton, MA, USA) was poured onto a heat dried (90 degrees 30 minutes) 3-inch silicon wafer (Siegert Wafer, Aachen, Germany) and then spun at 4000 rpm to get a 12 µm thick layer, which determined the height of the device structures. The wafer containing the SU-8 was exposed to UV-light in a contact mask aligner (Karl Suss MJB4 soft

UV, Munich, Germany). After UV exposure, the non-crosslinked photoresist was developed (MrDev600) and rinsed with isopropanol. To prevent PDMS from sticking to the mold, during the microfluidic device fabrication, the wafer was activated in oxygen plasma for 60 seconds (ZEPTO, Diener Plasma-Surface Technology, Germany) and exposed overnight to a vapor of trichloro (1H,1H,2H,2H-perfluorooctyl) silane (PFOTS, Sigma Aldrich, Saint Louis, MO, USA) at 180 degrees to obtain a monolayer over the structures. SYLGARD^{TM} 184 PDMS (Dow Chemicals Company, Midland, Michigan) for the microfluidic device fabrication, was made by mixing the elastomer base with the curing agent in a proportion of 10:1 in mass, then poured on top of the master that contained the structures, degassed at -15 kPa for one hour and finally polymerized in an oven at 60˚C for two hours.

The PDMS labyrinths were cut out from the master and a rectangular portion of 2.5 cm x 0.5 cm for the channel device, and 4 cm x 0.5 cm for the fractal device, was cut out in the middle of the pillar system, approximately 0.5 cm away from the entrance of every labyrinth. This cut was made to create the reservoir that served as entrance to the labyrinth (Figure 1). Using a plasma chamber, the PDMS labyrinths and a glass from a glass bottom petri dish were activated and bonded. This activation consisted in treating the surfaces with a Zepto Plasma System (Diener Plasma Surface Technology, Germany) with these conditions: polarity, negative; coating time, 1 min for cover slips and 10 seconds for PDMS labyrinths. Directly after activation, the surfaces were put together, forming a tight irreversible bonding (Mcdonald *et al.* 2000). Directly after bonding, 150 µl and 300 µl of the treatment medium were introduced through the reservoir of the Channel and the Fractal device respectively.

Soil inoculum and growth conditions

The soil used for the experiment was obtained from a grassland of pH 6.5 and a SOM content of 7.9% in weight, located outside the Ecology building of the Lund University, 55° 42′ 49.5″ N, 13° 12′ 32.5″ E. 1 gram of soil was mixed with 20 ml of distilled water and vortexed for 3 minutes at 3200 rpm (full speed). The mixture was allowed to sediment for 5 minutes to let sand and coarse silts collect at the bottom. 1.5 ml of the supernatant were collected and centrifuged for 10 minutes at 5000 RPM to concentrate the microbial extract. This strongly increases microbial cell numbers and diversity in the inoculum and thus decreases the risk of fast-growing species quickly outcompeting most others. The supernatant with the water solution was disposed and the pellet was resuspended with 100 µl of M9 minimal medium (12.8 g/L $NaHPO_4.7H_2O$, 3 g/L KH_2PO_4, 0.5 g/L NaCl, 100 mg/L NH_4Cl, 0.12 g/L $MgSO_4$, 4 g/L d-Glucose, 11.66 mg/L $CaCl_2$, 13.5 mg/L $FeCl_2$, 125 mg/L $MgCl_2.6H_2O$, 1 mg/L $MnCl_2.4H_2O$, 1.7mg of $ZnCl_2$, 0.43mg $CuCl_2.2H_2O$, 0.6 mg $CoCl_2.6H_2O$, 0.6mg $Na_2MoO_4.2H_2O$, pH 6.5) (Smith 1991) containing 160 mg/L of

L-Alanine 7-amido-4-methylcoumarin (AMC) to determine substrate consumption inside the devices.

The inner part of the microfluidic devices was filled beforehand with the same M9 medium containing 160 mg AMC/L (pH 6.5) by capillary forces directly after bonding. Directly after, 5 µl of the soil extract were pipetted into the reservoir of the devices. Sterile wet tissues were placed inside the Petri dishes to preserve humidity. The plates were sealed with Parafilm to prevent water from evaporating and kept in the dark at room temperature.

In total, 6 devices were used for the experiments, 3 of the Channel device and 3 of the Fractal device.

Microscopy

Epifluorescence microscopy was used for visualization of AMC degradation using a fully motorized Nikon Ti2-E inverted microscope with PFS4 hardware autofocus, full 25 mm field-of-view, CoolLED pE300-White MB illumination connected via a 3 mm liquid light guide (LLG), and a Nikon Qi2 camera with 1x F-mount adapter. The filter used was LED-DAPI-A-2360A Semrock Filter Cube (Ex: 380-405 nm, Em: 413-480 nm). Images for fluorescence quantification of the entire device were captured using a (MRH00041) CFI Plan Fluor 4X, N.A. 0.13, W.D. 17.1 mm objective, with an exposure time of 100. NIS Elements advanced research imaging software (Nikon) was used for coordination of the multipoint imaging. Pictures were taken for every device once a day for 12 days. The days selected for statistical analysis were the ones of maximum fluorescence signal for each treatment.

Image Analysis

The fluorescence intensity was quantified using ImageJ 1.52n (Schindelin *et al.* 2012). Background was subtracted with the ImageJ rolling ball algorithm (Kneen & Annegarn 1996) using 7 pixels as radius of rolling ball for 4x objective images. The rolling ball radius was given based on the size of the biggest fluorescent object, which was the diameter of a PDMS channel. After the subtraction, the total intensity was quantified inside each labyrinth using the ROI manager tool. For this, a ROI mask, which contained multiple rectangles of equal size that surrounded each channel or maze, was used to quantify the mean fluorescence intensity within each structure.

For comparison of the fractals of different order, replication consists of the pooled data of the area of each fractal block (n=10, 4 treatments), which equals the size of five connected modules of the F5 maze lined up after each other. It is inoculated via its connection to the entry pillar system only via the first module (Figure 1). The spatial variation of the fluorescence inside the fractal mazes was measured by quantifying the fluorescence of the channels at different regions inside the mazes. The spatial analysis was performed on the second module of each fractal block

counted from the pillar system, selected to minimize the edge effect produced in the first fractal due to its direct contact with the pillar system. The spatial analysis was done in all internal replicates of one microfluidic device.

Estimation of accessibility within Fractal mazes

The spatially resolved analysis of fluorescence at the dead ends or corresponding locations of all fractal order mazes was compared to their accessibility index which was calculated using COMSOL Multiphysics® (Multiphysics & Multiphysics 2020). The accessibility index is defined as the time required for a particle in a diffusion simulation to reach 50% of the final concentration and was compared between all dead end locations (n=324 dead ends per fractal module) of the maze order F5 or corresponding locations, second module from the pillar system.

Statistical Analysis

Both experiments with the respective microfluidic device type had full-factorial designs. The channel device experiment had *Angle* (45°, 90°, 109°) and *Turn order* (alternated or repeated) as fixed factors. Each device contained 10 channels of each type (with all the angle-turn order combinations), and three devices were analyzed. Multilevel model fitting correcting for random effects was used to test the influence of every factor on the variables.

A linear regression was performed to test the effect of channel tortuosity in the substrate degradation. Fluorescence intensity of AMC was regressed against the tortuosity of each type of channel considering the microfluidic device as a random variable.

The fractal device had fractal order (F0, F1, F3, F5) as fixed factors, each device had 7 mazes of each fractal order type, and three devices were included into the experiment. Multilevel model fitting correcting for random effects was used to test the influence of fractal order in fluorescence intensity. Random effects were attributed to each device as physical replicate of the experiment.

For in-depth statistical analysis in both experiments, the data from the day comprising maximum fluorescence for each fractal maze was chosen. The significance threshold used for all statistical tests was $p < 0.05$. When significant differences were found in the ANOVA, interactions were analyzed separately using the Dunn's method for multiple comparison of means (Dunn 1961). Pairwise comparisons between treatments (channel or maze type) were done with t-tests with p values adjusted using Holm corrections (Holm 1979). All statistical analysis was performed using R (Team 2019).

Results

During the run of the experiments, all the studied structures were colonized by microorganisms, mainly bacteria, confirmed by microscopy. Although there was no filtration process that would leave fungi excluded from the experiment, there were no hyphae observed within the structures during the first twelve days of measurements. In the later stage of the experiment, around day 14, several unicellular eukaryotes were observed to grow in both the pillar system and the experimental structures of the devices, for which reason data was only analysed up to day 12 where mainly bacteria, our intended study organisms, affected the measurements.

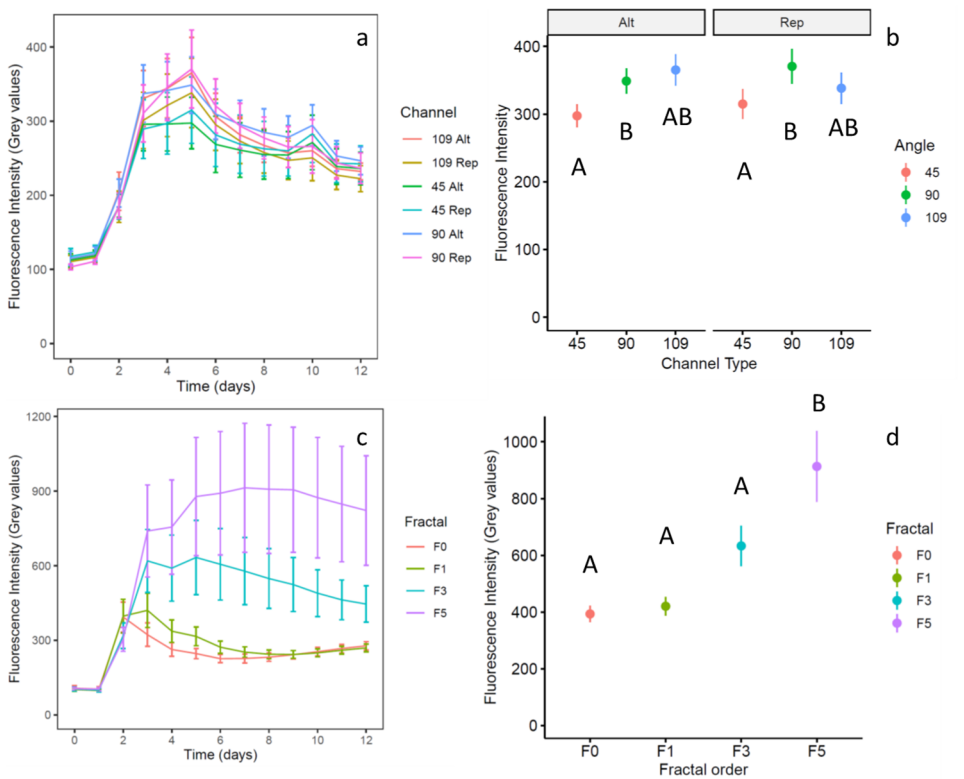

Figure 2 Fluorescence intensity indicating enzymatic activity in the channel (a,b) and the fractal (c,d) devices over time (a,c) and at the timepoint of maximum fluorescence signal (b,d). The fluorescence data over time for the channel device (a) is shown for the 6 studied treatments (45°, 90°, and 109°, with alternated or repeated turn order each one) with 30 total replicates (10 per device of a total of 3 devices used). The fluorescence means for the time points of highest mean fluorescence value for each treatment were compared considering fluorescence intensity as dependent variable and angle and turning order as independent variables (b). Fluorescence intensity data over time for the fractal device shown for the 4 fractal order treatments (fractal order 0,1,3, and 5) at normalized volume (c). Comparison of the fluorescence levels in the four maze types of increasing fractal order at the time points of their respective highest mean fluorescence (d). Mean comparisons were done with two- and one-way ANOVA for the channel and the fractal treatment, respectively. Error bars show standard error for n=30 and n=21 for the channel and the fractal condition, respectively. Different capital letters under mean values indicate statistically significant differences between the treatments derived from pairwise comparison using Sidak method for confident interval adjustment (b, d).

In device design 1 (Channel device), all studied channel types showed a measurable fluorescence signal starting from day 2 of the experiment (Figure 2, Figure 3). The fluorescence increased until it reached its maximum for all the channel types at day 5 after inoculation (Figure 2a). After 5 days, the fluorescence signal decreased until the end of the experiment on day 12. A comparison of the fluorescence between channel types at the day of maximum signal showed that as channel turn angle increased, the amount of substrate cleaved also increased (Figure 2b). The fluorescence increased, however, only from 45˚ angles to 90˚ angles, after which it did not change significantly, and turn order had no measurable effect. When the tortuosity of the channels was used as the independent variable to explain the fluorescence patterns in regression against fluorescence intensity, the results suggested a similar output: as tortuosity increased, the amount of cleaved substrate also increased (Figure 4, p=0.046, $R^2 = 0.017$).

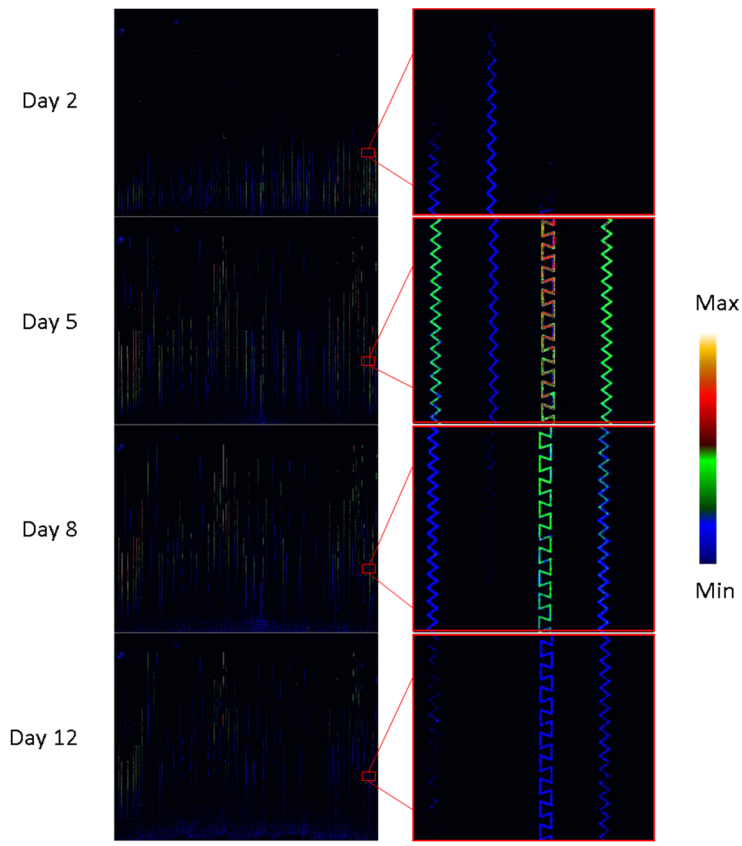

Figure 3 Example of the fluorescence intensity corresponding to enzymatic activity changing over time in the Channel device. Left panel images show the entire device and right panel images show a magnified part of the channel. The fluorescence intensity inside each channel is shown using the color coding placed on the right side of the figure. The selected days correspond to the days after inoculation where the first enzymatic activity is detected (day 2), when it reaches its maximum (day 5), when it starts decreasing (day 8), and when it reaches a lower plateau (day 12).

The fractal device also showed measurable fluorescence signals in each of its mazes from day 2 after inoculation (Figure 2, Figure 7). The maximal fluorescence was found at different time points, delayed with increasing fractal order of the mazes (Figure 2c): While F0 and F1 had their maximum fluorescent signal on day 2 and 3 respectively, F3 and F5 had it on day 5 and 7, respectively. The comparison between the maximum fluorescence values of each maze showed that as fractal order increased, fluorescent signal also increased (Figure 2d), highly significantly different from each other except for F0 and F1.

A spatial analysis of the fluorescence within the fractal modules indicates that the fluorescence distribution within the mazes depended on the fractal order (Figure 6). For simple fractals (F0 and F1), the enzymatic activity was higher towards the deeper parts of the maze, but as time passed the pattern was reverted and the fluorescence in the deeper parts of the maze decreases in comparison to the higher accessible regions. In the more complex fractals (F3 and F1), on the other hand, the pattern was the opposite (Figure 6). Fluorescence was higher in the most accessible areas compared to the deeper regions in the earlier stages of the experiment (day 2) but, as time passes (from day 3 on), the fluorescence reaches its maximum levels in the deeper regions of the maze. In the most complex fractal, F5, however, this increase was only until a certain point, after which lower fluorescence intensity were located.

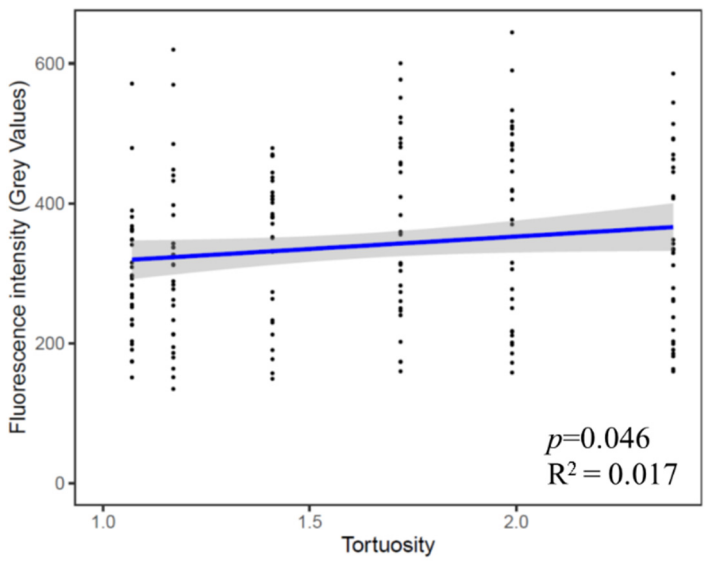

Figure 4 Linear regression of the fluorescence intensity corresponding to enzymatic activity measured in the different channel types of the Channel device as a function of the tortuosity of the channels, at the day of maximum fluorescence for each channel type.

Discussion

Our hypothesis stated that as spatial complexity of a microhabitat increases, the substrate cleaved by a natural inocculum would also decrese. This assumption was made based on previous perspective papers that have proposed the soil spatial microheterogeneity as a responsible factor for carbon stabilization (Baveye *et al.* 2018). The results obtained in this study show, however, the opposite pattern: as simulated habitat complexity increases, substrate degradation increases. We observed similar results to happen with a pure culture of the bacterial strain *Pseudomonas putida* in similar mazes of increasing fractal order (Arellano-Caicedo et. al. 202Xb) where higher fractal order mazes showed more bacterial biomass and nutrient degradation than low fractal order mazes.

There are two explanations to the increasing enzymatic activity observed as the spatial complexity in our experimental setting increases: one is that an increase in habitat complexity promotes a higher accumulation of bacteria due to quorum sensing, which leads to higher biomass and biofilm formation, which ends up in a higher nutrient acquisition efficiency. Bacterial strains such as *E. coli* have been shown to acumulate in dead ends of microfluidic mazes due to the action of quorum sensing molecules (Park *et al.* 2003). Quorum sensing can occur not only between bacterial individuals of the same strain, but also between organisms of different species (Willems *et al.* 2016), forming what is known as polymicrobial biofilms. These biofilms can have characteristics that differ to a great degree to the sum of characteristics of all the species that conform it (Flemming *et al.* 2016). One of the main difference is that enzymatic production can be shared between the different species, as exoenzymes can remain active for hours to days, and their products become available for all microbes in the vincinity, becoming in the long run more efficient at degrading substrates via a division of tasks (Hyun *et al.* 2008).

A complementary explanation is that an increase in habitat complexity reduces the interactions within the bacterial communities and individuals present in the mazes. A reduction of interaction reduces the competition stress in the different communities, allowing a higher diversity of species and metabolic functions to co-occur (Hyun *et al.* 2008). This means that species or individuals which show a preference for an enzymatic acquisition of nutrients, which is usually less efficient than a direct uptake of readily dissolved mineral elements, like carbon, nitrogen and phosphorous present as salts or sugars, are allowed to grow since potential interactions with fast growing competitors would be reduced. More connected, easibly accesible habitats reduce the fitness of the slow growers and favor communities of fast growers which are in a competitive advantage (MacLean & Gudelj 2006). Since such fast-grower communities have lower tendency to enzymatic nutrient acquisition, this could explain that the enzymatic activity is considerably lower than in less connected environments in our study. Having a physical separation allows otherwise slower growing bacteria to cooperate via

sharing metabolic pathways without being outcompeted by opportunists, as it has been seen to happen in pure cultures of bacteria (Hyun *et al.* 2008).

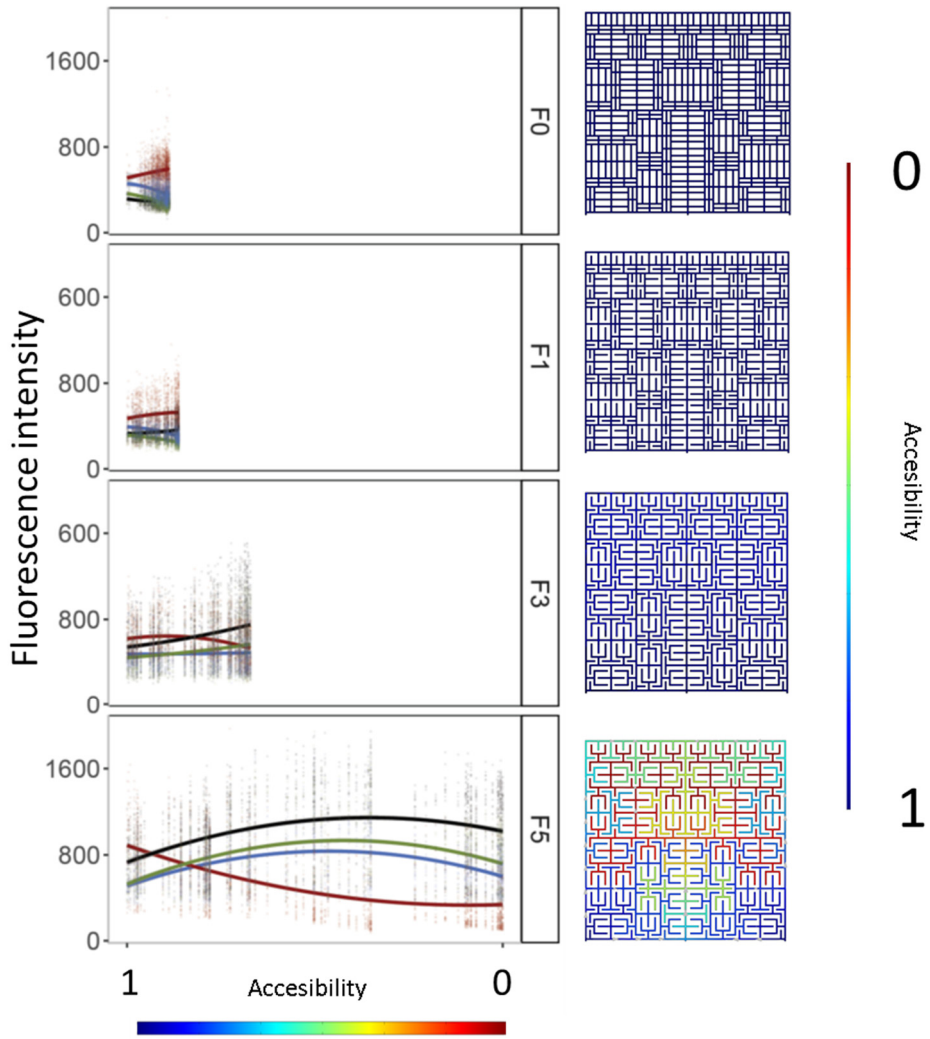

Figure 5 Spatial distribution of enzymatic activity within the different mazes measured via the fluorescence intensity of AMC. Accessibility of different spaces within the mazes are ranging from 1 to 0, determined via a COMSOL model simulation (right panel), where 1 is the most accesible region and 0 is the least accessible. All fractal order mazes are compared over the whole accessibility range for F5; comparison of the internal maximal variability of accessibility for each fractal order can be appreciated in the shorter curves of the rest of the fractal types compared to the F5 in the figure. Each dot in the regression plots (left panel) denote to the specific spatial accessibility of the COMSOL model and the measured mean fluorescence of that specific region, in all fractal order mazes corresponding to the dead-end locations within F5. The second fractal module of each block was used for analysis of seven internal replicates. The lines correspond to curve fitting using a quadratic model, the colors of the lines and the dots represent the timepoint they correspond to: day 2 (red), 5 (black), 8 (green), and 12 (blue).

This goes in line with the *species sorting* model that states that the variation of the populations is determined by the environmental characteristics of a particular habitat (Leibold & Chase 2017). In a heterogeneous habitat, the fitness landscape is more diverse, allowing several populations to grow with limited interactions with each other. Species sorting has been shown to be responsible of microbial community structures in aquatic environments (Staley *et al.* 2015; Souffreau *et al.* 2018), and might be responsible, at least in part, for the high microbial diversity found in soils. In this sense, trends in the population structure of the community should match those in the habitat structure, which can be partially confirmed with our results: the channels and mazes with the highes spatial complexity show a higher enzymatic activity, suggesting that populations exhibiting a higher substrate degradation efficiency have a better fitness than in more spatially homogeneous structures. We can not, however, show if the microbes in our system have a higher substrate degradation efficiency since we can not, with the methods used in this experiment, determine the microbial biomass for the distinct structures, nor determine their diversity. Nonetheless, and based on previous our studies with a bacterial lab strain that shows a substrate degradation uncoupled with the bacterial biomass (Arellano-Caicedo et al. 202Xb), we can speculate that in our case we also might have an increased substrate degradation efficiency in complex mazes and channels.

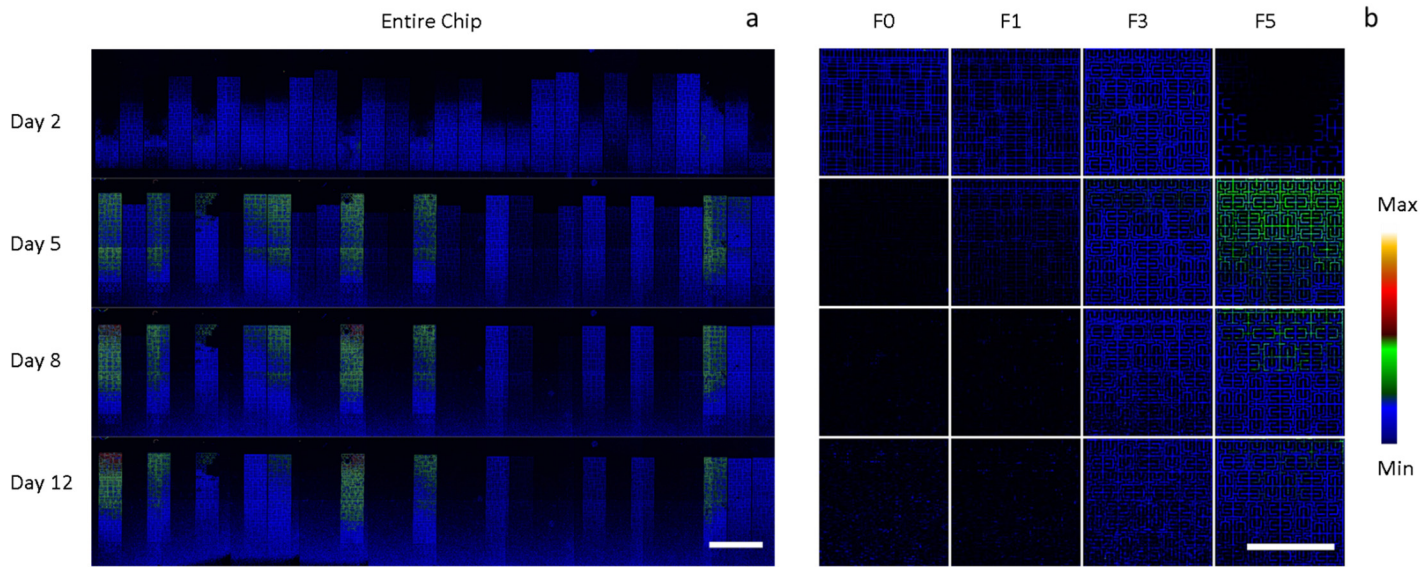

Figure 6 Example of fluorescence intensities recorded over time in the Fractal device. Left panel images show the entire device and right panel images show a high-magnitude excerpt of each maze type of the second module in each block. The fluorescence intensity within each maze is shown using the color coding to the right of the figure. The selected days correspond to the days after inoculation where the first enzymatic activity is detected (day 2), when it reaches its maximum (day 5), when it starts decreasing (day 8), and when it reaches a lower plateau (day 12).

In the present experiments we tested how spatial variation in a pore space structure affected the activity of peptidases, which presumably was used by the bacteria to complement their nitrogen demand. Other studies in soils have focused on how various enzymes for cleavage of different substrates act around plant roots. It has been shown that the ratios of enzymatic activities are different for each enzyme type, meaning that in regions where carbon specific enzymes are high, those needed to acquire nitrogen or phosphorous are low, and vice versa (Razavi *et al.* 2019). It would thus be interesting to investigate in future studies how the relationship of different enzyme activities is affected by spatial structures in controlable systems, by using a suite of different fluorogenic substrates. Even though our study was mainly focused on prokariotic nutrient degradation, which is the dominant community in the first 12 days of study, we know from previous experiments (Mafla Endara et al. 202X) that unicellular eucaryots also can grow within the devices. Thus, a study on how the onset of predation and trophic foodweb interactions acts on organic matter subtrate consumption in different microstructures can also be a step forward to our study.

We singled out spatial microstructures as the manipulated explanatory factor in our devices, while we had to disregard other variables that likely have a strong influence on OM dynamics in soils, such as the ratio and patchiness of gas/water saturation in the pores, or organo-mineral interactions that may immobilize organic molecules. Under such an increased complexity of physical components, an increased biological complexity including inter-kingdom interactions likely plays an even more important role, where e.g. fungi are the only organism group that easily bridge over air bubbles and can aid the dispersal of other organisms like bacteria and protists, which require water films for movement (Mafla Endara et al. 202X). Nevertheless, our approach was able to dempostrate the considerable effect that the 2-d spatial arrangement of a pore space can have on its microbial colonization and speed of nutrient cycling. This can in the long run lead to a better understanding of the role of pore space characteristics on soil functions and could lead to recommendations for land uses preserving soil structure and their related ecosystem functions.

References

Ahmed, T., Shimizu, T.S. & Stocker, R. (2010). Microfluidics for bacterial chemotaxis. *Integr. Biol.*

Ahmed, T. & Stocker, R. (2008). Experimental verification of the behavioral foundation of bacterial transport parameters using microfluidics. *Biophys. J.*

Aleklett, K., Kiers, E.T., Ohlsson, P., Shimizu, T.S., Caldas, V.E. & Hammer, E.C. (2018). Build your own soil: Exploring microfluidics to create microbial habitat structures. *ISME J.*

Ananyeva, K., Wang, W., Smucker, A.J.M., Rivers, M.L. & Kravchenko, A.N. (2013). Can intra-aggregate pore structures affect the aggregate's effectiveness in protecting carbon? *Soil Biol. Biochem.*

Armeli Minicante, S., Piredda, R., Quero, G.M., Finotto, S., Bernardi Aubry, F., Bastianini, M., *et al.* (2019). Habitat Heterogeneity and Connectivity: Effects on the Planktonic Protist Community Structure at Two Adjacent Coastal Sites (the Lagoon and the Gulf of Venice, Northern Adriatic Sea, Italy) Revealed by Metabarcoding. *Front. Microbiol.*, 10, 1–16.

Bach, E.M., Williams, R.J., Hargreaves, S.K., Yang, F. & Hofmockel, K.S. (2018). Greatest soil microbial diversity found in micro-habitats. *Soil Biol. Biochem.*, 118, 217–226.

Baveye, P.C., Otten, W., Kravchenko, A., Balseiro-Romero, M., Beckers, É., Chalhoub, M., *et al.* (2018). Emergent properties of microbial activity in heterogeneous soil microenvironments: Different research approaches are slowly converging, yet major challenges remain. *Front. Microbiol.*

Beebe, D.J., Mensing, G.A. & Walker, G.M. (2002). Physics and Applications of Microfluidics in Biology. *Annu. Rev. Biomed. Eng.*

Crawford, J.W., Harris, J.A., Ritz, K. & Young, I.M. (2005). Towards an evolutionary ecology of life in soil. *Trends Ecol. Evol.*, 20, 81–87.

Deng, J., Orner, E.P., Chau, J.F., Anderson, E.M., Kadilak, A.L., Rubinstein, R.L., *et al.* (2015). Synergistic effects of soil microstructure and bacterial EPS on drying rate in emulated soil micromodels. *Soil Biol. Biochem.*

Dunn, O.J. (1961). Multiple Comparisons Among Means. *J. Am. Stat. Assoc.*

Flemming, H.C., Wingender, J., Szewzyk, U., Steinberg, P., Rice, S.A. & Kjelleberg, S. (2016). Biofilms: An emergent form of bacterial life. *Nat. Rev. Microbiol.*, 14, 563–575.

Hilbert, D. & Hilbert, D. (1935). Über die stetige Abbildung einer Linie auf ein Flächenstück. *Dritter Band Anal. · Grundlagen der Math. · Phys. Verschied.*, 1–2.

Hobbie, J.E. & Hobbie, E.A. (2013). Microbes in nature are limited by carbon and energy: The starving-survival lifestyle in soil and consequences for estimating microbial rates. *Front. Microbiol.*, 4, 1–11.

Holm, S. (1979). A simple sequentially rejective multiple test procedure. *Scand. J. Stat.*

Hyun, J.K., Boedicker, J.Q., Jang, W.C. & Ismagilov, R.F. (2008). Defined spatial structure stabilizes a synthetic multispecies bacterial community. *Proc. Natl. Acad. Sci. U. S. A.*

IPCC. (2007). *Climate change 2007: the physical science basis*. *Contrib. Work. Gr. I to Fourth Assess. Rep. Intergov. Panel Clim. Chang. Publ. Intergov. Panel Clim. Chang.*

Kneen, M.A. & Annegarn, H.J. (1996). Algorithm for fitting XRF, SEM and PIXE X-ray spectra backgrounds. *Nucl. Instruments Methods Phys. Res. Sect. B Beam Interact. with Mater. Atoms*.

Kravchenko, A.N., Negassa, W.C., Guber, A.K. & Rivers, M.L. (2015). Protection of soil carbon within macro-aggregates depends on intra-aggregate pore characteristics. *Sci. Rep.*

Kuzyakov, Y. & Blagodatskaya, E. (2015). Microbial hotspots and hot moments in soil: Concept & review. *Soil Biol. Biochem.*, 83, 184–199.

LEIBOLD, M.A. & CHASE, J.M. (2017). *Metacommunity Ecology, Volume 59*. *Metacommunity Ecol. Vol. 59*.

Lu, H.P., Lai, Y.C., Huang, S.W., Chen, H.C., Hsieh, C.H. & Yu, H.T. (2014). Spatial heterogeneity of gut microbiota reveals multiple bacterial communities with distinct characteristics. *Sci. Rep.*

MacLean, R.C. & Gudelj, I. (2006). Resource competition and social conflict in experimental populations of yeast. *Nature*, 441, 498–501.

Mao, H., Cremer, P.S. & Manson, M.D. (2003). A sensitive, versatile microfluidic assay for bacterial chemotaxis. *Proc. Natl. Acad. Sci.*

Mcdonald, J.C., Duffy, D.C., Anderson, J.R. & Chiu, D.T. (2000). Review General Fabrication of microfluidic systems in poly (dimethylsiloxane). *Electrophoresis*, 21, 27–40.

Multiphysics, C. & Multiphysics, C. (2020). COMSOL Multiphysics ® v.5.5. *COMSOL Multiphysics ® 5.5*.

Negassa, W.C., Guber, A.K., Kravchenko, A.N., Marsh, T.L., Hildebrandt, B. & Rivers, M.L. (2015). Properties of soil pore space regulate pathways of plant residue decomposition and community structure of associated bacteria. *PLoS One*.

Park, S., Wolanin, P.M., Yuzbashyan, E. a, Lin, H., Darnton, N.C., Stock, J.B., *et al.* (2003). Influence of topology on bacterial social interaction. *Proc. Natl. Acad. Sci. U. S. A.*, 100, 13910–13915.

Quigley, M.Y., Negassa, W.C., Guber, A.K., Rivers, M.L. & Kravchenko, A.N. (2018). Influence of pore characteristics on the fate and distribution of newly added carbon. *Front. Environ. Sci.*, 6, 1–13.

Rabot, E., Wiesmeier, M., Schlüter, S. & Vogel, H.J. (2018). Soil structure as an indicator of soil functions: A review. *Geoderma*.

Raynaud, X. & Nunan, N. (2014). Spatial ecology of bacteria at the microscale in soil. *PLoS One*.

Razavi, B.S., Zhang, X., Bilyera, N., Guber, A. & Zarebanadkouki, M. (2019). Soil zymography: Simple and reliable? Review of current knowledge and optimization of the method. *Rhizosphere*, 11, 100161.

Rillig, M.C., Muller, L.A. & Lehmann, A. (2017). Soil aggregates as massively concurrent evolutionary incubators. *ISME J.*, 1–6.

Saragosti, J., Calvez, V., Bournaveas, N., Perthame, B., Buguin, A. & Silberzan, P. (2011). Directional persistence of chemotactic bacteria in a traveling concentration wave. *Proc. Natl. Acad. Sci.*

Schindelin, J., Arganda-Carreras, I., Frise, E., Kaynig, V., Longair, M., Pietzsch, T., *et al.* (2012). Fiji: An open-source platform for biological-image analysis. *Nat. Methods*.

Smith, M.C.M. (1991). Molecular biological methods for bacillus. *FEBS Lett.*

Souffreau, C., Busschaert, P., Denis, C., Van Wichelen, J., Lievens, B., Vyverman, W., *et al.* (2018). A comparative hierarchical analysis of bacterioplankton and biofilm metacommunity structure in an interconnected pond system. *Environ. Microbiol.*

Staley, C., Gould, T.J., Wang, P., Phillips, J., Cotner, J.B. & Sadowsky, M.J. (2015). Species sorting and seasonal dynamics primarily shape bacterial communities in the Upper Mississippi River. *Sci. Total Environ.*

Stanley, C.E., Stöckli, M., Van Swaay, D., Sabotič, J., Kallio, P.T., Künzler, M., *et al.* (2014). Probing bacterial-fungal interactions at the single cell level. *Integr. Biol. (United Kingdom)*.

Team, R.C. (2019). R: A Language and Environment for Statistical Computing. *Vienna, Austria*.

Toosi, E.R., Kravchenko, A.N., Mao, J., Quigley, M.Y. & Rivers, M.L. (2017). Effects of management and pore characteristics on organic matter composition of macroaggregates: evidence from characterization of organic matter and imaging. *Eur. J. Soil Sci.*, 68, 200–211.

Voltolini, M., Ta, N., Wang, S., Brodie, E.L. & Ajo-franklin, J.B. (2017). Geoderma Quantitative characterization of soil micro-aggregates : New opportunities from sub-micron resolution synchrotron X-ray microtomography, 305, 382–393.

Whitman, W.B., Coleman, D.C. & Wiebe, W.J. (1998). Prokaryotes: The unseen majority. *Proc. Natl. Acad. Sci. U. S. A.*, 95, 6578–6583.

Willems, H.M., Xu, Z. & Peters, B.M. (2016). Polymicrobial Biofilm Studies: from Basic Science to Biofilm Control. *Curr. Oral Heal. Reports*.

Zeppilli, D., Pusceddu, A., Trincardi, F. & Danovaro, R. (2016). Seafloor heterogeneity influences the biodiversity – ecosystem functioning relationships in the deep sea. *Nat. Publ. Gr.*, 1–12.

Supplementary material

Supplementary Table 1. Output of the multi-level model fitting for the variable mean fluorescence intensity measured with MC fluorescence, with device as random effect and Angle and Turn order as fixed factors. Each step performs an ANOVA and compares the model with the previous model.

	Model	df	AIC	BIC	Log Lik		Test	L. Ratio	p-value
baseline	1	3	2217.928	2227.507	-1105.964				
Angles	2	5	2213.556	2229.520	-1101.778	1	vs 2	8.372250	0.0152
Angles + T. Order	3	6	2215.492	2234.650	-1101.746	2	vs 3	0.063176	0.8015
Interaction	4	8	2217.613	2243.157	-1100.807	3	vs 4	1.879087	0.3908

Supplementary Table 21. Contrasts of the multi-level model with the variable mean fluorescence intensity measured with MC fluorescence, with device as random effect and angle and turn order as fixed factors, using the Sidak method for adjusting confidence interval.

contrast	estimate	SE	df	t.ratio	p.value
45 - 90	-53.41	19.9	175	-2.689	0.0213
45 - 109	-45.53	19.9	175	-2.293	0.0595
90 - 109	7.88	19.9	175	0.397	0.9169

Supplementary Table 3. Output of the multi-level model fitting for the variable mean fluorescence intensity measured with MC fluorescence, with device as random effect and maze type as fixed factor for the final model. Each step performs an ANOVA and compares the model with the previous model.

	Model	df	AIC	BIC	logLik	Test	L.Ratio	p-value
Baseline model	1	3	1242.339	1249.631	-618.1695			
Final Model	2	6	1215.864	1230.449	-601.9322	1vs2	32.47469	<.0001

Supplementary Table 42. Contrasts of the multi-level model with the variable mean fluorescence intensity measured with MC fluorescence, with device as random effect and maze type as fixed factor, using the Sidak method for adjusting confidence interval.

contrast	estimate	SE	df	t.ratio	p.value
F0 - F1	-27.1	95.5	78	-0.284	0.9920
F0 - F4	-239.7	95.5	78	-2.509	0.0663
F0 - F5	-519.7	95.5	78	-5.440	<.0001
F1 - F4	-212.6	95.5	78	-2.225	0.1254
F1 - F5	-492.6	95.5	78	-5.156	<.0001
F4 - F5	-280.0	95.5	78	-2.931	0.0225

Printed by Media-Tryck, Lund 2021 NORDIC SWAN ECOLABEL 3041 0903

The influence of soil structure on microbial processes in microfluidic models

The great variety of Earth's microorganisms and their functions is attributed to the heterogeneity of their habitats at the nano scale. Our understanding of the impact of those heterogeneous conditions on microbes is however still limited. In this project, we used microfluidic devices to simulate transparent microscale habitats for microbes. With this technology, we tested the effect of different physical characteristics of microhabitats on microbial interactions and functions.

LUND UNIVERSITY

Department of Biology
Faculty of Sciences
Lund University,
ISBN 978-91-7895-793-4 (print)
978-91-7895-794-1 (pdf)